



**NTNU – Trondheim**  
Norwegian University of  
Science and Technology

# Characterization of Corrosion patterns of Stainless Steel in Diethylenetriamine (DETA)-CO<sub>2</sub> and amine degradation products systems

**and an Introductory Modeling Approach**

**Ebenezer Hayfron-  
Benjamin**

Chemical Engineering

Submission date: July 2013

Supervisor: Hallvard Fjøsne Svendsen, IKP

Norwegian University of Science and Technology  
Department of Chemical Engineering



## **Preface**

This master's thesis with the course code -TKP4900 Kjemisk Prosesstekn Vår 2013- is a part of the fulfillment of the requirements for a Master of Science degree in the field of Chemical Engineering and which was undertaken during the spring of 2013.

The work was carried out at the CO<sub>2</sub> absorption research labs in the Environmental Engineering and Reactor Technology Group located at the Department of Chemical Engineering, at the Norwegian University of Science and Technology (NTNU) in Trondheim.

*I declare that this is an independent work according to the exam regulations of the Norwegian University of Science and Technology. All experimental set-ups, literature review, results and interpretations therein were solely done by the author and also the author adhered to the highest standards of ethics and integrity for scientific reporting.*

.....

Ebenezer Hayfron-Benjamin

Trondheim, July 4, 2013



## Acknowledgements

The successful completion of this work which spanned the duration of spring of 2013 wouldn't have been possible without the help of many individuals and professionals. Different people helped out in different times, some advice, some corrections, others lending me the use of scientific equipment and tools in order to further broaden the scope and depth of this work. I would like to take the time to express my deepest appreciations, respect and honor to all who helped in one way or the other. The list of thanksgiving in the paragraphs below is by no means exhaustive and for those not mentioned or seemingly forgotten, please all apologies are mine.

First of all I would like to say a big thank you to my supervisor, Professor Hallvard Svendsen, who was kind enough to have an "open door" policy whereby sometimes I could just walk into his office and try to clarify a confusing or sticking point in my work. Thanks again professor for giving me the freedom and latitude to run with this CO<sub>2</sub> corrosion topic. In addition you gave me opportunities to serve as your tutorial assistant in *Fluid Flow and Heat Transfer* for two different semesters and to top it all I was introduced to the CO<sub>2</sub> absorption group during my summer 2012 internship. The fundamentals of transport processes in chemical engineering were taught in a simple way by you in my first year and this helped me to solidify my understanding of unit processes of chemical engineering. For all of this and more I say *tusen takk for alt!*

Several friends at the department helped me, thanks to post-*doc*, Dr. Ardi Hartono, who was kind enough to explain to me a lot of about the seemingly new amine absorption solvent diethylenetriamine (DETA). *Doc* I want to say big thanks for letting me have some of the data on the characterization of DETA that was done by you. Extra appreciation goes to Yulia Flid in the analytical lab, thank you for teaching how to analyze for amine and CO<sub>2</sub> in solutions. Lisbeth Roel at the Department office deserves my thanks for all her help during my studies in NTNU.

From the Department of Materials, I would like to express my thanks to Kjell Røkke for letting me borrow the Potentiostat for my electrochemical test and Jools for teaching me how to use the scanning electron microscopy(SEM) and X-ray Diffraction( XRD) machines. At SINTEF, I say thanks to Ole Edvard Kongstein for lending me the Autoclave at such a short notice and helping me with the initial questions I had about how to go about using the equipment.

To Mr. Ebenezer Hayfron-Benjamin Sr., a civil engineer by profession thanks Dad for your belief in me during my trials and encouraging me to pursue my dream despite the odds. You also passed the engineering genes on to me, for that and more God continue to richly bless you! Extended warmth, love and thanks goes to my mother, Ms. Christiana Adu, for all here hard work in raising me at Abossey Okai and insisting that education was my only option, no more , no less. To Mrs Beatrice Afua Boakye, ‘*mama*’ “*medaase!*” You are my second mother, thanks to you and all the family.

And to those teachers of mine, who instilled a sense of discipline and pride, I would not be here if it were not your diligence, patience and words of wisdom when I needed it. To the following mentors of mine : Dr. Xu Maotian, Boakye, Dr Zhang Fu-Qiang, Dr. Zhou Xin Tao, and my primary school teacher ‘*teacher*’ Conduah. I hope one day you will read this report and be proud of your once little but stubborn student.

Finally to my family in Christ at Betel Church in Trondheim, I thank you for being a moral compass for me during my stay here. You have been a mighty blessing to me, thank you to Dr. Ugochukwu Edwin Aronu working also with CO<sub>2</sub> capture at SINTEF. Mighty thanks to Ernest Wilson, Esther and the family, Pastor Samuel Adjei and family, Pastor John Ganaah, Miriam and the family and most of all the head of the church Pastor Jean Alidor Mbuebue and Mama Esperence. God richly bless you.

Last but not least, from the bottom of my heart, I would like to thank soon-to-be mother-in-law Frau Marcelle Noé-Nordberg from Meires in Austria for opening your house to me anytime I came visiting and supporting me and Ursula Noé-Nordberg.

The two most important people in my life, I have dedicated the following pages to them, first to very my wife-to-be (Ursula Noé-Nordberg) and to my LORD and personal Savior Jesus Christ of Nazareth. I love you both! Amen.

## **Dedication to my beautiful Ushi**

Honey we made it finally! It has been a long time coming with all the up and down but hey at least we are there now! Also Vio is coming with us too wohooo!

"... aaa ma bre! yenko, yenko!, ushi medase pii!

Vielen Dank für das Glauben an uns und mir!

Thanks for your love, patience, guidance and wisdom.

Love you forever and will always do!



## **Dedication**

Dedicated to the LORD God Almighty, the Most High God, Elohim.

I dedicate this achievement to my LORD and personal Savior, who has seen me through life till this date. He promised to restore all the years that the locust has eaten and the successful completion of my education at the master's level for chemical engineering is an affirmation of His love, mercy and grace towards me. To this I say Lord, I thank You and with all my heart I declare myself as a proud bondservant of You. These scriptures are a tribute to my heavenly Father, my friend and Savior Jesus Christ and the Holy Ghost a comforter and source of wisdom in times of need.

## **Ancient of Days – Atik Yommin**

Daniel 7:13-14

13: הקרבוהי: וקדמוהי מטה יומיא עתיק ועד הוה אתה אנש כבר שמיא ענני עם וארו ליליא בחזוי הוית חזה

14: לא די ומלכותה יעדה לא די עלם שלטן שלטנה יפלחון לה ולשניא אמיא עממיא וכל ומלכו ויקר שלטן יהיב ולה תתחבל:

## **Jesus Christ of Nazareth**

Acts 10: 38 “how God anointed Jesus of Nazareth with the Holy Spirit and with power, who went about doing good and healing all who were oppressed by the devil, for God was with Him.”

## **The Holy Spirit**

Romans 8:26 “ωσαυτως δε και το πνευμα συναντιλαμβάνεται ταις ασθeneιας ημων το γαρ τι προσευξωμεθα καθο δει ουκ οίδαμεν αλλ αυτο το πνευμα υπερεντυγχανει υπερ ημων στεναγμοις αλαλητοις”



## Table of Contents

Abstract.....	xiii
List of Figures.....	xv
Nomenclature.....	xix
Chapter 1 Introduction and Background.....	1
1.0 Background.....	1
1.1 Problem Statement.....	5
1.2 Scope and Objectives.....	6
1.2.1 Objective of the Thesis.....	6
1.2.2 Scope.....	6
Chapter 2 Emissions, GHGs, CO <sub>2</sub> .....	10
2.0 Introduction.....	10
2.1 Types of emission and climate change.....	11
2.2 GHGs and sources.....	13
2.3 CO <sub>2</sub> and Power Plants.....	15
2.4 Carbon dioxide Capture and Storage Technology.....	18
Chapter 3 CCS technology and how it works.....	20
3.0 Introduction.....	20
3.1 Chemical Absorption Technologies.....	21
3.1.1 Process Overview.....	21
3.1.2 Chemistry.....	23
3.1.3 Advantages and Challenges.....	25
3.1.4 Environmental Impact.....	26
3.1.5 Innovations and the Future.....	27
3.2 Carbonate looping technology.....	28
3.3 Oxyfuel combustion technology.....	29
Chapter 4 CCS and Corrosion Challenges.....	31
4.0 Introduction.....	31
4.1 Corrosion and how amines play a role, special emphasis on MEA and DETA.....	32
4.2 Corrosion prevalent regions.....	35
4.3 Heat Stable Salts.....	38

4.4 Process Parameters leading to Corrosion.....	39
4.4.1 Effect of O <sub>2</sub> .....	39
4.4.2 Effect of CO <sub>2</sub> .....	40
4.4.3 Effect of Temperature .....	40
4.4.4 Effect of amine concentration .....	41
4.4.5 Effect of pH.....	41
4.4.6 Effect of amine solution conductivity .....	43
4.4.7 Effect of make up water .....	43
4.4.8 Effect of corrosion Inhibitors .....	43
Chapter 5 Theory .....	44
5.0 Introduction.....	44
5.1 Aqueous Corrosion Theory .....	44
5.1.1 Introduction.....	44
5.1.2 Thermodynamics- Potential-pH (Pourbaix) Diagrams .....	47
5.1.3 Kinetic Consideration .....	51
5.2 CO <sub>2</sub> Corrosion Mechanism .....	55
5.2.1 CO <sub>2</sub> -H <sub>2</sub> O-pH Chemistry.....	55
5.2.2 Anodic Reactions .....	57
5.3 DETA–CO <sub>2</sub> Absorption Mechanisms .....	60
5.3.1 Kinetics .....	60
5.4 DETA Degradation and Corrosion .....	64
5.4.1 Introduction.....	64
5.4.2 Heat Stable Salts (HSS) .....	67
5.5 Corrosion Inhibition.....	68
5.6 pH and Corrosivity.....	72
5.7 Corrosion Passivation films .....	74
Chapter 6 Methodology .....	77
6.1 Introduction.....	77
6.2 Experimental Procedure .....	78
6.2.1 Apparatus .....	79
6.2.2 Specimen.....	83
6.2.3 Surface Preparations (Before and After Testing).....	84
6.3 Calculating Corrosion Rate.....	84

6.3.1 Weight loss- based .....	84
6.3.2 Electrochemical testing .....	85
6.4 Surface Investigation .....	86
6.5 Solution Analysis Methods .....	90
6.5.1 Titration.....	90
6.5.2 Corrosion Solution analysis by ICP-MS .....	93
6.6 Parameters for Testing .....	94
Chapter 7 Experimental Set-up .....	95
7.0 Introduction.....	95
7.1 Swagelok® Cylinder Apparatus.....	95
7.2 EC-Autoclave (1L) Apparatus .....	97
7.3 Stainless Steel 316L Chemical Composition .....	97
7.4 Specimen Dimensions and Surface preparation.....	98
7.4.1 Dimensions .....	98
7.4.2 Surface preparation .....	99
7.5 Solution preparation and calculations .....	100
7.5.1 Preparation .....	100
7.5.2 CO <sub>2</sub> loading and Analysis .....	101
7.5.3 Acid loadings .....	102
7.6 Experimental Procedure.....	103
7.6.1 Swagelok® 1.0.....	103
7.6.2 Swagelok® 2.0.....	105
7.6.3 EC- Autoclave.....	105
7.6.4 After the Test .....	107
Chapter 8 Results and Discussion.....	109
8.0 Introduction.....	109
8.1 Coupon weight- loss Tests .....	109
8.1.1 Swagelok® 1.0.....	109
8.1.2 Swagelok® 2.0.....	124
8.2 Solution Analysis .....	126
8.2.1 ICP-MS .....	126
8.3 Amine and CO <sub>2</sub> analysis .....	134
8.4 SEM and EDS Analysis .....	135

8.4.1 SEM .....	135
8.4.2 EDS .....	142
8.5 EC-Autoclave Analysis.....	143
8.5.1 Tafel Plot Technique.....	145
8.5.3 Pourbaix Diagrams.....	161
8.6 Uncertainties in the Result.....	164
Chapter 9 Introductory Modeling Approach.....	165
9.0 Introduction.....	165
9.1 Chemistry of Corrosion.....	165
9.1.1 Thermodynamic equilibrium Considerations.....	165
9.1.2 Electrochemical Reactions.....	169
9.1.3 Transport Processes.....	174
9.2. Conclusion .....	176
Chapter 10 Conclusion and Recommendations .....	177
10.1 Summary .....	177
10.2 Recommendations and Future works.....	180
Bibliography .....	182
Appendices.....	198

## Abstract

Diethylenetriamine (DETA) which has three amine functional groups and touted to be potential CO<sub>2</sub> mitigation solvent has been shown to have high loading capacity, faster absorption rates, lower activation energy than the benchmark solvent monoethanolamine (MEA). The main drawback in using DETA and other amines is in the area of plant equipment corrosion, a significant capital investment loss in the event of excessive and uncontrolled corrosion. Corrosion dent on global investment in Carbon Capture and Storage (CCS) technologies can run into the hundreds of billions of US dollars. These mitigating drawbacks will need to be fully addressed before commercial scale plants based on these amines are established. From a pure capital expense point of view stainless steel will likely be preferred as a construction material to carbon steel in critical parts of an absorption such rich-amine piping, cross exchanger tubes and internals of the reboiler and stripper. The premise for this work was thus focused on an important aspect of the value chain of CCS technology development: corrosion of stainless steel materials in a diethylenetriamine-CO<sub>2</sub>- degradation products environment and an introductory modeling approach. The methodology used for investigating corrosion were: weight-loss of stainless steel coupons and electrochemical tests(Tafel plot polarization and Linear Polarization Resistance), Inductively coupled plasma mass spectrometry(ICP-MS) for corrosion solution analysis, and scanning electron microscopy(SEM) and energy dispersive X-ray spectroscopy(EDS) for the surface morphologies. A diethylenetriamine concentration of 2.5M , loaded with CO<sub>2</sub> with two ratios of mole CO<sub>2</sub> to mole DETA (i.e.  $\alpha = 1.2$  and max) , 1-2wt% of heat stable salts(HSS) being formate, acetate and oxalate, temperatures of 135°C and 80°C, and a time period of one(1) to five(5) weeks were the parameters for testing. The results indicated that CO<sub>2</sub> pre-loaded diethylenetriamine caused extensive corrosion of stainless steel, corrosion was enhanced in the presence of HSS species in the order [DETA + acetate] > [DETA + oxalate] > [DETA + formate], [DETA]. Tafel plot analysis showed that the oxalate systems were the most corrosive in the DETA-CO<sub>2</sub> environment with a high of 26.52 mm /yr. , with a relatively high current density  $i_{corr} = 2.0719095 \text{ mA/cm}^2$  after only 13 hours on stream.

Furthermore, the effect of the operating temperature has a significant impact on the corrosion rates. Faster kinetics at higher temperatures results in the quick transport of corrosion species and hence higher corrosion rates. For example DETA containing no acid system, at 80°C has corrosion rate of only 4.587E-06 mm/yr compared to 0.872 mm/yr at 135°C. ICP-MS revealed that the phenomenon of selective corrosion of the elements contained in stainless steel were not present. Surface morphology of the stainless steel specimen done with the scanning electron microscopy (SEM) showed the following types of surface features: flaky, porous, flowery and layers of corrosion products, fine plates typical of lepidocrocite, cotton ball shaped features typical of goethites, and severe pitting at the edges of the sample(cover picture). Finally a review of simple mechanistic model was introduced that can be applicable to DETA corrosion and covered key reactions in corrosion of stainless steel in deithlenetriamine-CO<sub>2</sub>- H<sub>2</sub>O medium. The key reactions being : electrochemical reactions at the steel surface, diffusion of species to and from the bulk including diffusion through porous surface films, migration due to potential (electric field) gradients, surface film precipitations and the accompanying fluxes.

## List of Figures

Figure 1-1. Common Amines used in CO <sub>2</sub> Capture .....	3
Figure 1-2. Chemical structure of DETA .....	4
Figure 2-1. Change in atmospheric concentration of CO <sub>2</sub> over the last thousand years (Jones 2011) .....	12
Figure 2-2. Trending of jump in CO <sub>2</sub> emissions (Rogner, D. Zhou et al. 2007) .....	13
Figure 2-3. Annual greenhouse gas emissions per sector (EEA 2000).....	14
Figure 2-4. USA GHGs emission pie chart (EPA 2012) .....	14
Figure 2-5. Breakdown in generation by energy source (Armor and Preston 1996).....	16
Figure 2-6. Integrated Gasification Combined Cycle Power Plant(DOE 2004).....	17
Figure 3-1. CO <sub>2</sub> amine absorption process flow sheet diagram.....	22
Figure 3-2. TCM CO <sub>2</sub> Capture Plant at Mongstad, Norway(AkerCleanCarbon 2012; Svendsen 2012) .....	23
Figure 3-3. Post-combustion carbonate looping(J. Blamey, N. H. Florin et al. 2009; MacDowell, Florin et al. 2010).....	28
Figure 3-4. Schematic of Oxyfuel combustion plant(MacDowell, Florin et al. 2010).....	29
Figure 4-1. Corrosion rates at 50° C on stainless steel A316 (Tavera-Valero and Svendsen 2011) .....	34
Figure 4-2. Schematic materials selection for Post-combustion capture on a coal power plant(Billingham, Lee et al. 2011) .....	37
Figure 4-3. Legend for Materials Selection Diagrams (stripes indicate lined/clad materials)(Billingham, Lee et al. 2011) .....	37
Figure 4-4. Corrosion rates and pH correlation (Rooney, DuPart et al. 1997) .....	42
Figure 5-1. Schematic of model description of electrochemical nature of corrosion of process (Roberge 2000) .....	45
Figure 5-2. Rust layers found on corroded metal surfaces .....	47
Figure 5-3. E-pH stability diagram of water at 25°C (Roberge 2000).....	48
Figure 5-4. Thermodynamic boundaries of the types of corrosion observed on steel (Roberge 2000) .....	50

Figure 5-5. Observed corrosion behavior of Iron in water and pH correlation (Roberge 2000) ..	51
Figure 5-6. Graphical Representation of the processes occurring at an electrochemical interface (Roberge 2000) .....	53
Figure 5-7. Tafel Plot from polarization technique (Roberge 2000) .....	54
Figure 5-8. Semi-batch thermal distillation process applied to remove Heat Stable Salts (Wonder, Balke R.J. et al. 1959).....	65
Figure 5-9. Structure of thermal degradation product of DETA .....	66
Figure 5-10. Imidazoline structure.....	68
Figure 5-11. Inhibition Mechanisms (Duda, Govea-Rueda et al. 2005).....	70
Figure 5-12. Simplified schematic diagram of oxide corrosion film on the surface of a metal (DepartmentofEnergy 1993) .....	75
Figure 6-1. Picture of sample in the cylinder, showing also the Teflon cover at the tip of the metal specimen.....	80
Figure 6-2. The relative size of the cylinders used as compared to a 30cm ruler.....	80
Figure 6-3. Schematic of the experimental test cell (Nesic, Postlethwaite et al. 1996).....	82
Figure 6-4. Two surface pictures showing pitting on the specimen caused by acetic acid after 165 hrs of exposure at 135°C. (Hayfron-Benjamin 2012).....	88
Figure 6-5. SEM images showing different phases and forms of corrosion products (S.W. Dean, D. Knotkova et al. 2010; de la Fuente, Díaz et al. 2011).....	89
Figure 6-6. SEM/EDS identification image (S.W. Dean, D. Knotkova et al. 2010; de la Fuente, Díaz et al. 2011).....	89
Figure 7-1. Cross-section view of cylinders for coupon testing .....	96
Figure 7-2. A Memmert® 600 thermostat chamber at 135°C ready to be used for the experiment .....	96
Figure 7-3. Schematic of coupon showing dimensions .....	99
Figure 7-4. Schematic of Teflon cover for metal specimens .....	99
Figure 7-5. The inside of the Memmert ®600 thermostat chamber at 135°C with the containers for the 5 different weeks of exposure shown. ....	104
Figure 7-6. E-C Autoclave with the potentiostat and data processing unit .....	106
Figure 8-1. Corrosion rates as a function of time (weeks).....	111

Figure 8-2. Week 2 corrosion rates and various systems- A = DETA, B = formate, C = oxalate, D = acetate .....	113
Figure 8-3. Week 4 corrosion rates and various systems- A = DETA, B = formate, C = oxalate, D = acetate .....	113
Figure 8-4. Week 5 corrosion rates and various systems- A = DETA, B = formate, C = oxalate, D = acetate .....	114
Figure 8-5. Corrosion trend for all systems for 5-week time period .....	118
Figure 8-6. Baseline (DETA) % change in corrosion rates comparison.....	119
Figure 8-7. Relative corrosion rates, compared to DETA system .....	120
Figure 8-8. Snapshot of corrosion rates of all systems including parallel samples. A, B = DETA; C, D = formate; E, F = oxalate; G, H = acetate .....	122
Figure 8-9. MEA and DETA acetic acid system corrosion rates comparison .....	124
Figure 8-10. MEA and DETA corrosion rates.....	124
Figure 8-11. ICP-MS absolute values (mg/L) of ions in corrosion solution for Week 1 .....	129
Figure 8-12. ICP-MS absolute values (mg/L) of ions in corrosion solution for Week 2 .....	129
Figure 8-13. ICP-MS absolute values (mg/L) of ions in corrosion solution for Week 3 .....	130
Figure 8-14. ICP-MS absolute values (mg/L) of ions in corrosion solution for Week 4 .....	130
Figure 8-15. ICP-MS absolute values (mg/L) of ions in corrosion solution for Week 5 .....	131
Figure 8-16. Overall ICP results composition wt% of various ions for whole 5 week period ...	131
Figure 8-17. Composition wt% compared to nominal values (system 1 = DETA, system 2 = oxalate, system 3 = formate, system 4 = acetate) .....	132
Figure 8-18. Fe spectrum as obtained by (HR-ICPMS) .....	133
Figure 8-19. Total spectra of all ions as-obtained via -(HR-ICPMS).....	133
Figure 8-20. Contrast between optical microscope image (to the left) and the SEM image (to the right) showing deposition of corrosion products .....	136
Figure 8-21. SEM images showing features on specimens (grinding marks, cracks, pits and deposition of corrosion products) .....	137
Figure 8-22. Oxalate system features after 236 hours as obtained by SEM.....	138
Figure 8-23. SEM image of DETA systems after 405 hours looking like a human skull .....	138
Figure 8-24. SEM revealing severe pitting on the edges of specimen.....	140
Figure 8-25. Lepidocrocite phase feature of corrosion products via SEM.....	140

Figure 8-26. SEM showing typical goethite phase of corrosion product .....	141
Figure 8-27. Flaky, porous and layers on metal surface as revealed by SEM.....	141
Figure 8-28. SEM images of corrosion on iron obtained in a different work found in the open literature (de la Fuente, Díaz et al. 2011).....	142
Figure 8-29. EDS image of a corrosion section showing the elemental map spectrum .....	143
Figure 8-30. Tafel Plot extrapolation for DETA system .....	151
Figure 8-31. Tafel Plot extrapolation for DETA + 2wt% formate system .....	151
Figure 8-32. Tafel plot extrapolation for DETA + 2 wt% oxalate.....	152
Figure 8-33. Tafel plot extrapolation for DETA + 2wt% acetate system.....	152
Figure 8-34. Corrosion rates, time and potential of DETA system .....	154
Figure 8-35. Corrosion rates, time and potential of DETA + 2 wt% formate system .....	154
Figure 8-36. Corrosion rates, time and potential of DETA + 2wt% oxalate system .....	154
Figure 8-37. Corrosion rates, time and potential of DETA + 2wt% acetate system.....	155
Figure 8-38. End of experiment overall corrosion rates comparisons .....	155
Figure 8-39. Superimposed potentiodynamic graph of all systems in Tafel polarization experiment.....	156
Figure 8-40. Tafel plot for 80° C experiment for DETA system.....	157
Figure 8-41. Tafel plot for 80° C experiment of DETA + 2wt% oxalate system.....	157
Figure 8-42. Tafel plot for 80° C experiment of DETA + 2wt% formate system .....	158
Figure 8-43. Tafel plot for 80° C experiment of DETA + 2wt% acetate system .....	158
Figure 8-44. Overall Tafel plot for 80° C experiments.....	159
Figure 8-45. Linear polarization line for DETA + 2 wt% oxalate at 135° C.....	159
Figure 8-46. Comparing LPR and Tafel Polarization results for oxalate system at 135° C.....	160
Figure 8-47. LPR corrosion rates trend over time for oxalate system.....	160
Figure 8-48. Schematic Pourbaix diagram with regions of corrosion, immunity and passivity (uobabylon 2013).....	161
Figure 8-49. Pourbaix diagram for Iron in water at ambient conditions (uobabylon 2013).....	162
Figure 8-50. Pourbaix diagram for Cr in salt solution at ambient conditions (Kongstein 2010)	163
Figure 8-51. Pourbaix diagram for Nickel in solution at ambient conditions (CORWIKI 2008)	163

## Nomenclature

### Abbreviations

AE	Auxiliary electrode
AEEA	2-(2-aminomethyl-amino)ethanol
AMP	2-amino-2-methyl-1-propanol
ASTM	American Society for Testing and Materials
CCS	Carbon dioxide capture and storage
CO <sub>2</sub>	Carbon Dioxide
COS	Carbon Oxy Sulfide
CS	Carbon Steel
<i>C. R</i>	Corrosion rate
DEA	Diethanolamine
DETA	Diethylenetriamine
DIPA	Diisopropanolamine
DM	Deshmukh-Mather
DGA	Diglycolamine
EC	Electrochemical
EDA	Ethylenediamine
EDS	Energy Dispersive X-ray Spectroscopy
<i>EW</i>	Equivalent weight
GHG	Greenhouse gas
<i>HAc</i>	Acetic acid
HSS	Heat stable salts
H <sub>2</sub> O	Water
H <sub>2</sub> SO <sub>4</sub>	Sulfuric acid
IR	Infrared
ICP-MS	Inductively Coupled Plasma Mass Spectrometry
LPR	Linear Polarization Resistance
MEA	Monoethanolamine
NACE	National Association of Corrosion Engineers
N <sub>2</sub>	Nitrogen
NH <sub>3</sub>	Ammonia
NMR	Nuclear Magnetic Resonance
NRTL	Non Random Two Liquid
Pz	Piperazine
RE	Reference electrode
SEM	Scanning Electron Microscopy
SHE	standard hydrogen electrode
SINTEF	Stiftelsen for industriell og teknisk forskning

Swagelok® 1.0 and 2.0	Weight-loss experiments in a metal cylinder
VLE	Vapor-Liquid Equilibria
XRD	X- ray diffraction Spectroscopy
SS	Stainless Steel
WE	Working Electrode

***Abbreviation for this Thesis and legend in graphs***

NO	DETA system containing <i>no</i> degraded acid products
FA	DETA system containing <i>formic acid</i>
OA	DETA system containing <i>oxalic acid</i>
AA	DETA system containing <i>acetic acid</i>

***Upper Latin letters***

<i>A</i>	surface area of the steel in $m^2$ , constant in the Arrhenius-type equation
<i>C</i>	Concentration ( $mol/l$ )
$D_j$	diffusion coefficient of species <i>j</i> in $m^2/s$
<i>E</i>	Activation energy ( $J \times mol^{-1}$ ); Enhancement factor, potential (V)
$E_{corr}$	corrosion (open circuit) potential in mV
<i>F</i>	Faraday's constant (96,485 C/mole)
<i>G</i>	Gibb free energy ( $J$ )
<i>H</i>	Henry's law constant ( $Pa \times m^3 \times mol^{-1}$ )
<i>I</i>	Ionic strength in $kmol/m^3$
$I_a$	anodic current (mA)
$I_c$	cathodic current (mA)
<i>K</i>	Equilibrium constant
$K_{spFeCO_3}$	solubility product constant for ferrous carbonate in $(kmol/m^3)^2$
<i>Me</i>	Metal species
<i>N</i>	Flux ( $mol \times m^2 \times s^{-1}$ ); Number of component
$N_A$	Avogadro's number ( $6.022 \times 10^{23} mol^{-1}$ )
<i>Ox</i>	Oxidized species
<i>V</i>	Volume (l)
<i>P</i>	Total pressure ( $Pa$ )
$P_o$	Vapor pressure ( $Pa$ )
<i>R</i>	Universal gas constant ( $8.314 J \times mol^{-1} \times K^{-1}$ )

$R_p$	Polarization resistance ( $\Omega \cdot \text{cm}^2$ )
Re	Reynolds number ( $\rho \cdot v \cdot d \cdot \mu^{-1}$ )
Red	Reduced species
$S$	supersaturation factor
$Sc$	Schmidt number ( $\mu \cdot \rho \cdot D^{-1}$ )
$Sh$	Sherwood number ( $k_m \times d \times D^{-1}$ )
$T$	Temperature ( $K/^\circ C$ )
$T_f$	Temperature in Fahrenheit

### ***Lower Latin letters***

$e$	Electronic charge ( $1.602 \times 10^{-19} C$ )
$i$	current density in $\text{mA}/\text{cm}^2$
$i_{corr}$	corrosion current density in $\text{mA}/\text{cm}^2$
$k_m$	Mass transfer coefficient ( $m/s$ )
$k$	Reaction rate constant for $\text{CO}_2$ hydration at infinite dilution ( $s^{-1}$ )
$m$	Mass ( $kg$ ) ;
$n$	Number of mol ( $mol$ ); Number of equivalent
$p$	Partial pressure ( $Pa$ )
$pH$	negative logarithmic of hydronium ions
$pKa$	Dissociation constant
wt%	composition weight percentage
$z_j$	species charge of various aqueous species

### ***Greek symbols***

$\alpha$	$\text{CO}_2$ loading ( $\text{mol CO}_2/\text{mole amine}$ )
$\beta$	Stern-Geary Constant ( $\text{mV}/\text{decade}$ )
$\beta_a$	Tafel slope in the anodic controlled region ( $\text{mV}/\text{decade}$ )
$\beta_c$	Tafel slope in the cathodic controlled region ( $\text{mV}/\text{decade}$ )
$\varepsilon$	porosity
$\mathcal{K}$	surface permeability
$u_j$	mobility of species $j$
$v$	characteristic velocity ( $m/s$ )
$\emptyset$	electric potential in the solution
$\mathfrak{R}$	electrochemical reaction rate in $\text{kmol}/(\text{m}^2 \text{ s})$

### ***Subscripts***

<i>Ab</i>	Absorbed
<i>Am</i>	adsorbed
<i>ad</i>	Amine
<i>aq</i>	aqueous
<i>calc</i>	Calculated
<i>exp</i>	Experimental
<i>g</i>	Gas phase
<i>i</i>	Interface; Species <i>i</i>
<i>j</i>	Reaction <i>j</i> ; Species <i>j</i>
<i>k</i>	Species <i>k</i>
<i>l</i>	Liquid phase
<i>s</i>	Solid phase
-	Negative charge
+	Positive charge
±	Mean charge

### ***Units***

Gt	giga-tons ( $10^9$ )
kW h	kilowatts hours (power)
MPa	Mega Pascal ( $10^6$ Pa)
mpy	milli inch per year
mmpy	millimeters per year
$\mu\text{m}/\text{yr}$	micrometers ( $10^{-6}$ ) per year

## **Chapter 1 Introduction and Background**

Carbon dioxide capture and storage (CCS) technology usage has seen a surge in the processing and power generation industry. The surge has been aided by the awareness of the negative effects of emissions to the atmosphere and their consequences of climate change among other known side effects. Carbon capture using varying blends of aqueous amines is a matured technology and can be found in the power generation, oil and gas processing industries. The drawback in using amines is in the area of plant equipment corrosion, a significant capital investment loss in the event of excessive and uncontrolled corrosion. For examples it has been stated that corrosion has a vast impact on the global and domestic economy, and currently incurs losses of nearly \$300 billion annually (2006 dollar figure) to the U.S. economy alone (Steven J. Suess 2006). This development has prompted an interest into the research of corrosion of plant equipment in CCS technology. The premise for this work is thus focused on an important aspect of the value chain of CCS technology development: corrosion of stainless steel materials. With the aid of a number of different types of experimental designs for corrosion studies, a better, broader and fundamental understanding of corrosion mechanisms in aqueous amines is developed.

### **1.0 Background**

Human needs and industrial processes need energy and this supply of energy is derived from the abundant supply of fossil fuels such as coal, oil and gas. These fossil fuels account for a far greater proportion of commonly used energy sources but the combustion of these fuels has led to a rise in the emission of carbon related compounds into the ecological system. The resulting shift from equilibrium of the carbon cycle (caused by the rise in emissions especially CO<sub>2</sub>) has given rise to the concept of greenhouse gases (GHGs), climate change. This point is reiterated in a report which states that “the world runs on a carbon cycle which has been in approximate equilibrium for thousands of years” (Jones 2011), however since the time of the Industrial revolutions, anthropogenic sources of carbon emitted has seen a steady rise, leading to concepts of greenhouse gases and global climate change.

More about the concepts of GHGs, CO<sub>2</sub> emissions and climate change will be covered in Chapter 2.

Emission challenges as briefly highlighted above then presents an opportunity in the form of CCS technology development. The key question lies in the fact that the processes (power, oil and gas processing unit operations) responsible for CO<sub>2</sub> emissions are vital for industrial and economic growth of any society and as such can not be done away with. So how do we solve this challenge? Carbon capture and storage (CCS) might be the answer and in chapter 3 of this thesis, it will be shown why chemical absorption CCS using amines (such as monoethanolamine (MEA), N-(2-aminoethyl)ethane-1,2-diamine(DETA)) is the most matured technology among the others for CO<sub>2</sub> emission abatement.

Chemical absorption using amines in post-combustion CO<sub>2</sub> capture consists of a chemical absorption process that involves exposing a flue gas stream (containing the CO<sub>2</sub>) to an aqueous amine solution (Stangeland September 2009). Soluble carbamate salts formed are then heated in a stripper and the reverse reaction takes place releasing the captured CO<sub>2</sub>. Most commonly used amines are monoethanolamine (MEA), methyldiethanolamine (MDEA), 2-Amino-2-methylpropanol (AMP), Piperazine (PIPA), diglycolamine (DGA), diethanolamine (DEA), and di-isopropanolamine (DIPA) and their formulas shown in figure 1-1 below (Stangeland September 2009), (Hayfron-Benjamin 2012).

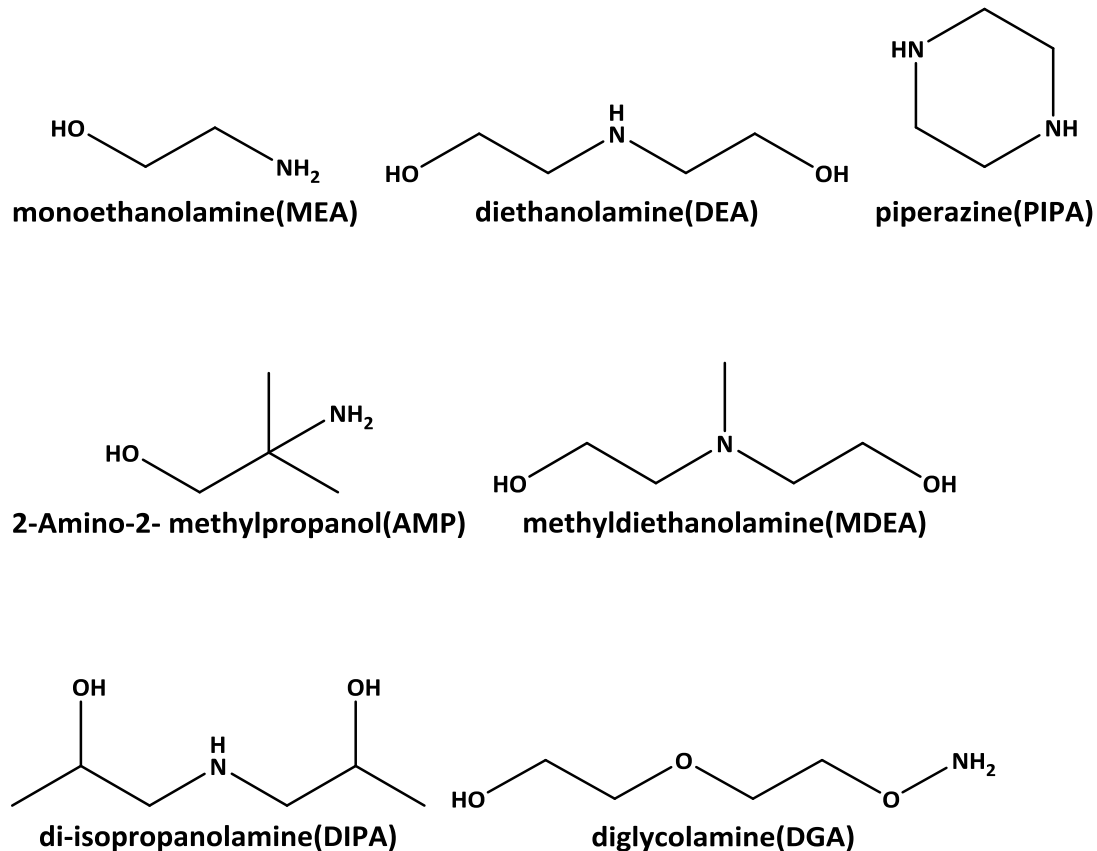


**Figure 1-1.** Common Amines used in CO<sub>2</sub> Capture

The choice of which amine to be used in a particular task will be based on a variety of factors such as solvent capacity, stability towards degradation, energy requirements to name a few. Experience in the industry has shown that MEA has been the accepted benchmark solvent for CO<sub>2</sub> capture because it is reported to have “highest alkalinity and highest volume of acid-gas removal at the fastest rate” (Saiwan, Supap et al. 2011), this however does not distract from its disadvantages like high energy consumption required for CO<sub>2</sub> regeneration and high vapor pressure, leading to considerable vaporization and solvent loss”. (Saiwan, Supap et al. 2011). But of most importance as far as this work is concerned is the fact that MEA has been reported to be the most corrosive of the commonly used amines because of oxidative and thermal degradation, leading to the formation of corrosive agents and consequently cause equipment corrosion in the absorption plant (DuPart 1993; A.L. Kohl 1997). The order of corrosiveness of benchmark amines has been reported by DuPart, Bacon and Edwards to be of the order of MEA > DEA > MDEA (DuPart 1993). In an earlier work (Hayfron-Benjamin 2012) comparable corrosion rates (compared to

other works like Dupart, Bacon and Edwards) (DuPart 1993) on stainless steel 316 by MEA was determined.

In a related development, new amine solvent designs are underway in various world class labs around the world including the labs of the CO<sub>2</sub> capture research group at the chemical engineering department of the Norwegian University of Science and Technology (NTNU). One of the reported promising candidate solvent for CO<sub>2</sub> capture is N-(2-aminoethyl) ethane-1,2-diamine or commonly known as diethylenetriamine (DETA). A full characterization of the DETA was undertaken by Ardi Hartono (Hartono 2009) and in that report and other published papers (Hartono, da Silva et al. 2006; Hartono, Juliussen et al. 2008; Hartono, da Silva et al. 2009; Hartono and Svendsen 2009; Hartono and Svendsen 2009) DETA (with three amine functional groups) was shown to have high loading capacity and faster absorption rates than mono amine functionality like MEA. Most of the data in this work about diethylenetriamine is taken from the work of Ardi Hartono. The main source of information about DETA was taken from Ardi Hartono (Hartono 2009) because there is a lack of general information about DETA in the open literature. The DETA structure is shown in figure 1-2 below.

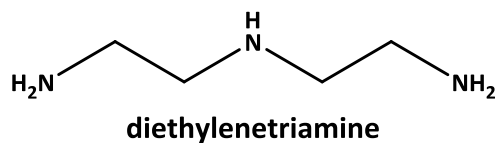


**Figure 1-2.** Chemical structure of DETA

The problem with DETA and other amines that are used in CCS chemical absorption technique is that, there are several mitigating drawbacks that will need to be fully addressed before commercial scale plants based on these amines are established. One of the major challenges lies in the corrosive behavior of the aqueous amines used in the absorption of CO<sub>2</sub> in plants. DETA for all its high superiority to MEA in absorption, is however very corrosive. In one example, DETA was used in a trial campaign in a pilot plant in NTNU and was reported to have etched a sizeable portion of the stainless steel regenerator plant equipment (Svendsen 2013). Corrosion is an important facet of the value chain of the CCS technology development because if left

unattended or poorly managed in gas treatment plants, they can result in unscheduled downtime, production losses, reduced equipment life and even injury or death” (DuPart 1993). The focus of the project is thus on the corrosion characterization of stainless steel 316L in diethylenetriamine-CO<sub>2</sub> environments and briefly a look at the modeling of such systems for corrosion prediction programs. It should be noted that the choice of project was based in the fact that, in the open literature, there are few or next to nothing on DETA corrosion. This lack of information can be reasoned along the lines that until now, MEA unlike DETA has been the benchmark solvent, with lots of experimental and theoretical body of works to support the CO<sub>2</sub> absorption mechanisms. DETA on the other hand is yet to be fully characterized in both experimental and theoretical works. With that said, it is believed that by laying down the fundamentals of experimental works on how DETA corrodes plant equipment such as stainless steel, an innovative and pioneering foundation can thus be created for future considerations such as at the design stage of CCS commercial plants, where material selection is a major portion of the capital investment decisions. All the brief introduction given above leads to the formulation of the problem statement for the thesis and from thus how to go about contributing a meaningful solution to the underlining theme of corrosion in amine plant equipment.

## **1.1 Problem Statement**

Corrosion poses a major challenge to the implementation of Carbon Capture and Storage (CCS) Technology for carbon capture. This results in downtime, lost production and poses health and safety risk to personnel. Proper characterization of corrosion of stainless steel, a likely construction material for CCS plants, will improve the overall feasibility of adopting CCS technology on an industrial scale.

This thesis work will seek to examine the corrosion behavior of stainless steel 316L in a corrosive diethylenetriamine (DETA)-CO<sub>2</sub> and degradation systems.

## 1.2 Scope and Objectives

The main areas of focus for this body of work is the characterization of corrosion patterns of stainless steel in diethylenetriamine (DETA)-CO<sub>2</sub> and amine degradation products systems. This will be achieved by designing an experimental program around a set of parameters, which are commonly used in corrosion experiments.

The scope and objectives include:

### 1.2.1 Objective of the Thesis

- The thesis will seek to examine the corrosion behavior of stainless steel 316L in a corrosive. This will be achieved by carrying out experimental programs based on industrial wide accepted standards such as the American Standards for Testing of Materials (ASTM). Two main distinctions will be made: weight loss concept and electrochemical testing. By performing tests on stainless steel specimens under controlled environment, the resultant corrosion rates will be used to assess how the material will fare in a conceptual plant application such as those found in CCS technology pilot plants.

### 1.2.2 Scope

- **Corrosive Solution and concentration and CO<sub>2</sub> loading**

To achieve the above objective experiments with the following parameters and scope will be defined. The corrosion medium mentioned in section 1.2.1 above is diethylenetriamine (DETA), a three functional group amine known for its high absorption capacity and faster kinetics. A diethylenetriamine concentration of 2.5M shall be used in all cases and loaded with CO<sub>2</sub> with two ratios of mole CO<sub>2</sub> to mole DETA (ie.  $\alpha = 1.2$  and  $1.5$ ). In addition to the CO<sub>2</sub> preloading, small wt% of degradation products will be added to the prepared solutions.

- **Degradation Products**

The degradation products to be used in all experiments are: Oxalic, Formic and Acetic acid. These acids have been found to be responsible for most of the reported corrosion. The sources of these acids lie in the thermal and oxidative degradation of amines under absorption and regeneration conditions in typical carbon capture plants.

- **Simulating Process Conditions**

In order to simulate process conditions, stripper conditions at 135 °C, and absorber temperature of 80°C will be the chosen thermal conditions for the electrochemical and weight loss experiments.

- **Length of Experiments and Apparatus**

Total length of the testing will vary between 1-5 weeks for the weight loss concepts and 8 days for the electrochemical testing. Because the EC (electrochemical) testing takes less time, many parameters will be varied leading to multiple testing programs. Details for this variation are clearly stated in the methodology of this work. The weight loss experiments were carried out in stainless steel Swagelok<sup>®</sup> cylinders, which contained an injected preloaded solution of the corrosive medium, DETA. The electrochemical testing was carried out in a 1L Electrochemical (EC) Autoclave cell, which is fitted with a thermocouple (for temperature control) and pressure valves and gauges (for pressure monitoring). The limit of the Autoclave in terms of pressure was in the region of 3-4 bars, but since the highest temperatures encountered were within 120°C – 135°, the upper limit of the pressure was never reached and the safety integrity of the Autoclave was also never breached.

- **Corrosion Solution Analysis**

With the aid of solution analysis technique like Inductive Coupled Plasma- Mass Spectrometry (ICP-MS) a full quantitative and qualitative characterization of the type of corroded metal ions in solutions will be attained. Furthermore simple amine and CO<sub>2</sub> analysis of solutions will shed some light on the speciation of the DETA-H<sub>2</sub>O-CO<sub>2</sub> systems.

- **Surface Morphology**

Surface Metallography analysis: Optical and Scanning Electron Microscopy (SEM). In order to account for surface morphology of corroded stainless steel 316L surfaces, optical and SEM microscopy is employed. The aim is to give further insight into the plausible mechanism for the corrosion as seen on the specimen surfaces.

- **Reproducibility**

This work will try to improve the accuracy on reproducibility compared to a previous project which was based on MEA.

- **Modeling Predict and characterize the corrosion behavior of stainless steel in Amine systems used in post-combustion CO<sub>2</sub> Capture**

The theory governing the establishment of a sound theoretical model for amine-CO<sub>2</sub> corrosion will be briefly looked at. This should include the physicochemical model of CO<sub>2</sub> corrosion of steel, in other words the chemical and electrochemical reactions occurring at the surfaces of steel will be established. Then the rate and equilibrium constants will need to be defined. Once the reaction framework is formulated, the transport processes of the ions in the corrosion process need to be also established. This should naturally lead to a mathematical model which can then be solved by means of numerical methods. Eventually, time permitting the verification of any model could be measured against the experimental data for corrosion rates of stainless steel in diethylenetriamine (DETA). The starting point for the modeling will come from an open source which will be properly referenced and defined in the section dealing with the models.

In the subsequent chapters (chapter 2, 3 and 4) background information about CCS technology, emissions and corrosion challenges is introduced to the reader. These chapters all include summary of the literature works of other authors on the subject of amines and corrosions. Basic terms or corrosion and other chemical reactions as found in the rest of the work will be explained and the rest found in the corrosion related terms glossary(Roberge 2000) in the appendix.

The justification for the chosen parameters outlined above is explained in Chapter 6 which covers the methodology chosen for the work. The concepts of corrosion, its mechanisms and effects on materials are covered in the theory portion in chapter 5. In the theory, the reader is introduced to all relevant terms of corrosion, what kind of amine is diethylenetriamine (DETA), the science behind all the techniques used in this work such as titration (for amine and CO<sub>2</sub> analysis), SEM, ICP-MS etc. The experimental section, in chapter 7 covers a description of all procedures followed. All methods are a standardized corrosion procedure which ensures that the data achieved in this work can be reproduced in any laboratory in the world provided that the stated conditions are adhered to. A thorough and rigorous analysis of the volume of data (weight loss and electrochemical potential data) is done in the results and discussion in chapter 8. In that

chapter for the weight loss experiments corrosion rates (mm/year) will be tabulated and the different systems will have their rates compared. This should give an idea of the extent of corrosion of each type of system (be it only DETA or DETA+ formic acid, or DETA+ acetic acid or DETA+ oxalic acid). With regards to the electrochemical testing data, analysis should explain the form of the curves and discuss features like active dissolution, passivation, transpassivity or pitting.

The last chapter of this work will be the conclusion, which will summarize the works done, answer the problem statement and objectives and recommend further works in the area of characterization of corrosion patterns of stainless steel in diethylenetriamine (DETA)-CO<sub>2</sub> and amine degradation products systems, especially in the field of modeling of systems for predicting corrosion in DETA medium as used in the process industry.

## **Chapter 2 Emissions, GHGs, CO<sub>2</sub>**

### **2.0 Introduction**

The concept of global climate change which has been in the forefront of scientific and political debates for quite sometime can trace its genesis to the United Nations Framework Convention on Climate Change (UNFCCC) which was adopted in May 1992 in New York and opened for signature at the ‘Rio Earth Summit’ in Rio de Janeiro a month later. The convention was effective in March 1994 and has achieved near universal ratification with ratification by 189 countries of the 194 UN member states (December 2006) (Rogner, D. Zhou et al. 2007). Article 2 of the convention spells out the objective which among other things included “stabilization of greenhouse gas concentrations in the atmosphere at a level that would prevent dangerous anthropogenic interference with the climate system. Such a level should be achieved within a time frame sufficient to allow ecosystems to adapt naturally to climate change, to ensure that food production is not threatened and to enable economic development to proceed in a sustainable manner” (Rogner, D. Zhou et al. 2007). Sustainable development being defined as “the development that meets the needs of the present without compromising the ability of future generations to meet their own needs and does not imply in any way encroachment upon national sovereignty (Annex II to decision 15/2 of the 15th session of the UNEP Governing Council. Nairobi, May 1989).

It is universally accepted that the world runs on a carbon cycle which has been in approximate equilibrium for thousands of years (Hayfron-Benjamin 2012), however since the time of the Industrial revolution, anthropogenic sources of carbon emitted has seen a steady rise, leading to concepts of greenhouse gases and global climate (Hayfron-Benjamin 2012). This naturally leads to the question about what greenhouse gases are and what exactly is climate change and the causes. The rest of this chapter tackles such basic yet fundamentally important concepts. These concepts should be understood in order to grasp the concept of carbon capture and sequestration (CCS) technology and the challenges such as corrosion facing the deployment of CCS on a commercial basis worldwide.

## 2.1 Types of emission and climate change

Greenhouse gas (GHG) collectively refer to a number of atmospheric gases which are responsible for trapping solar radiation (Hayfron-Benjamin 2012) and thereby changing the pattern of how radiation is reflected back from the earth, this leads to general warming of the climate. In precise definition it refers to those gaseous constituents of the atmosphere, both natural and anthropogenic, that absorb and emit radiation at specific wavelengths within the spectrum of thermal infrared radiation emitted by the Earth's surface, the atmosphere itself, and by clouds (Knuutila 2012). The concept of the ensuing climate change is known as the greenhouse effect. The main constituents of GHGs are water vapor (H<sub>2</sub>O) carbon dioxide (CO<sub>2</sub>) methane (CH<sub>4</sub>) nitrous oxide (N<sub>2</sub>O) and ozone (O<sub>3</sub>) and the kyoto protocol included the following compounds: sulphur hexafluoride (SF<sub>6</sub>), hydrofluorocarbons (HFCs) perfluorocarbons (PFCs). Of these constituents, it is widely acknowledged though, that the most abundant greenhouse gas in the atmosphere is water causing approximately two-thirds (~2/3) of the greenhouse effect. The result of increasing concentrations of GHGs that cause the other approximately a third (~ 1/3) is referred to as the “enhanced greenhouse effect”, or, since it is primarily the result of human activities, the “anthropogenic greenhouse effect” (R.T. Watson, H.Rodhe et al. 1990; John and Jacobsen 1993).

Climate change therefore can be defined as per IPCC definition as “a change in the state of the climate that can be identified by changes in the mean and/or the variability of its properties, and that persists for an extended period, typically decades or longer”. It refers to any change in climate over time, whether due to natural variability or as a result of human activity.

From the view of global climate change, the most important GHG of concern and that which will be the focus in this subject is CO<sub>2</sub>. As previously stated, the concentration of CO<sub>2</sub> in the atmosphere has grown since pre-industrial times, with an increase of 70% between 1970 and 2004 (Rogner, D. Zhou et al. 2007) *and of this* increasing emissions of *attributed to* human activities.

Figure 2-1 shows the claim in change in atmospheric concentration of CO<sub>2</sub> over the last thousand years (Hayfron-Benjamin 2012). Atmospheric CO<sub>2</sub> concentrations have increased by almost 100 ppm since their pre-industrial level, reaching 379 ppm in 2005, with mean annual

growth rates in the 2000-2005 period higher than in the 1990s (Rogner, D. Zhou et al. 2007) and still projected to increase if no mitigation efforts are undertaken.

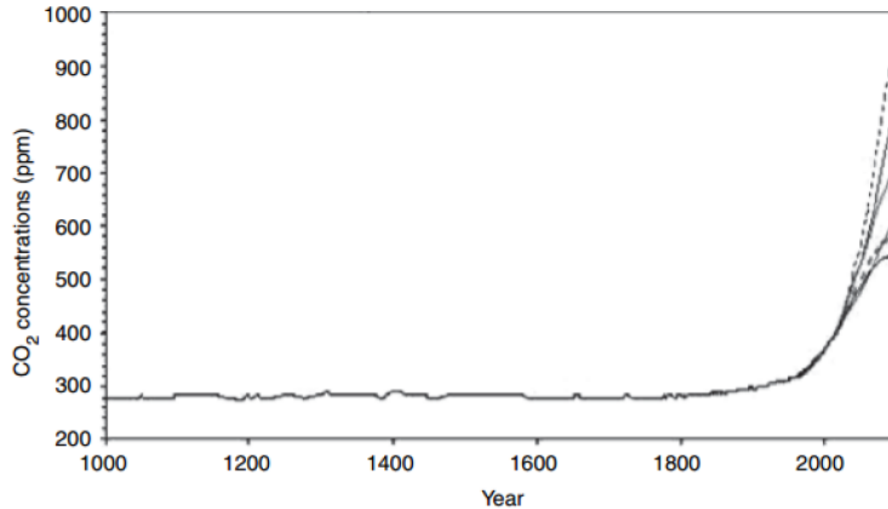


**Figure 2-1.** Change in atmospheric concentration of CO<sub>2</sub> over the last thousand years (Jones 2011)

A more definite data that shows that Emissions of the GHGs covered by the Kyoto Protocol increased by about 70% (from 28.7 to 49.0 GtCO<sub>2</sub>-equivalent ) from 1970–2004 (by 24% from 1990–2004), with carbon dioxide (CO<sub>2</sub>) being the largest source (Rogner, D. Zhou et al. 2007). This jump in CO<sub>2</sub> emissions is illustrated in figure 2-2 in the following page.

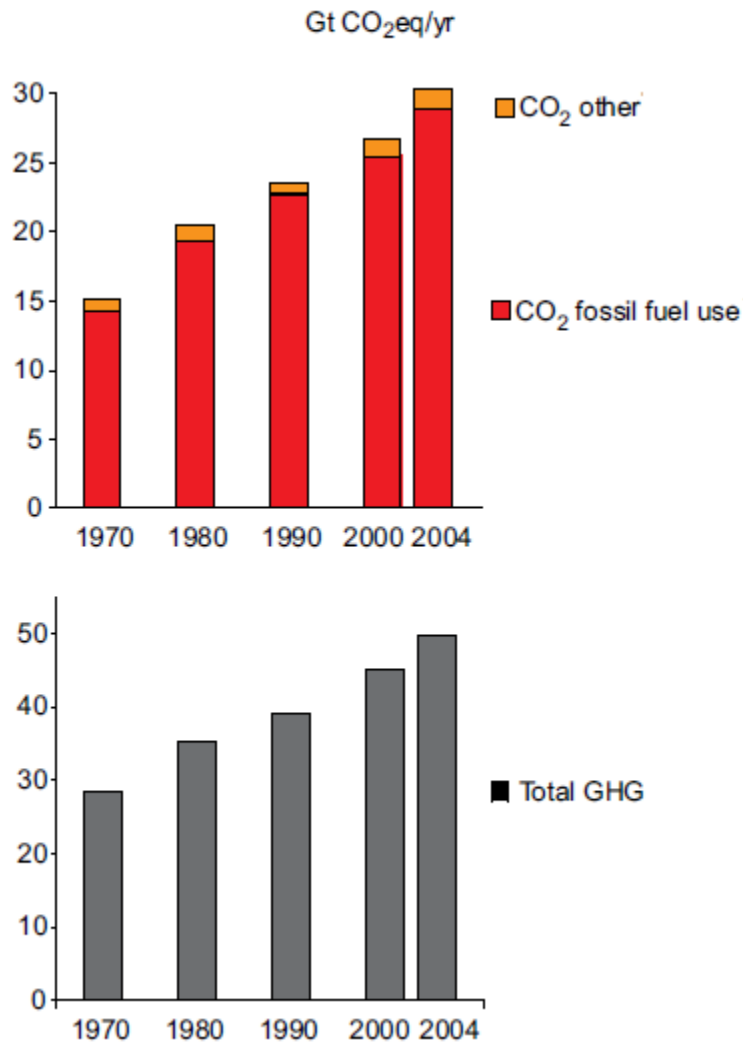


**Figure 2-2.** Trending of jump in CO<sub>2</sub> emissions (Rogner, D. Zhou et al. 2007)

## 2.2 GHGs and sources

Depending on what are the energy consumption patterns of a country, there are diverse sources where greenhouse gases are constantly emitted. The main sources of GHGs are in the sectors of: industry processes, transportation fuels, power stations, agriculture, land use and biomass burning, and residential, commercial sources. Of these sectors, power stations (energy supply) and industrial processes account for nearly 40% of all emissions and of the all GHGs emissions CO<sub>2</sub> accounts for 70% of the total with the rest being methane and nitrous oxide. A division of the emissions by sector basis for the year is shown in figure 2-3.

### Annual Greenhouse Gas Emissions by Sector

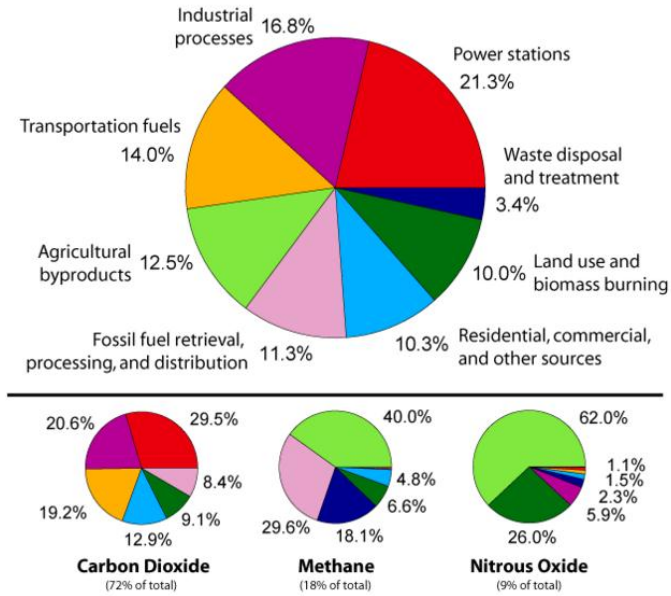


Figure 2-3. Annual greenhouse gas emissions per sector (EEA 2000)

### U.S. Greenhouse Gas Emissions by Sector 2010

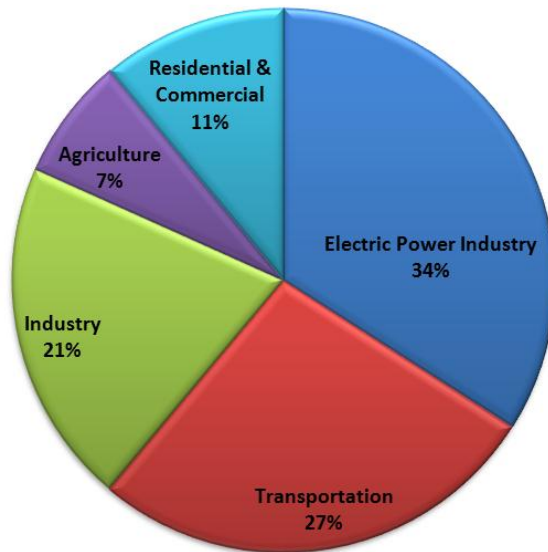


Figure 2-4. USA GHGs emission pie chart (EPA 2012)

CO<sub>2</sub> emission mainly comes from burning of fossil fuels, and they play a role in offsetting the carbon cycle thereby making CO<sub>2</sub> the most important greenhouse gas to date. The offsetting of the carbon cycle is explained by the claim that “carbon has been locked away millions of years and is suddenly released to the atmosphere” (Jones 2011) thereby the natural balance is offset. It is estimated that annually as much as 25-30 billion (Svendsen, Hessen et al. 2011) tons of CO<sub>2</sub> is emitted and as much as 750 Gt of carbon in the form of CO<sub>2</sub> is stored in the atmosphere (Jones 2011). Compare that to late 1980s, early 1990s data where only as much 6 Gt were emitted (R.T. Watson, L.G.Meira Filho et al. 1992), thus representing close to an increase of nearly 80% in emissions. The stored and emitted CO<sub>2</sub> causes changes in the partial pressures in the atmosphere thereby leading to observed climate change associated with greenhouse gas emissions. Factor in the other sources of CO<sub>2</sub> emissions such as deforestation such as in the Amazon in Brazil, agriculture and land use, transportation, waste and power production and one gets to understand the magnitude of the problem at hand. It is the latter, power production which is of interest to chemical engineers from the point of view of CO<sub>2</sub> sequestration. A brief overview is written in the subsequent sub-section.

### **2.3 CO<sub>2</sub> and Power Plants**

Previously in the text, it has been stated, that a majority of the CO<sub>2</sub> emissions are from fossil fuels and in particular a large fraction is from combustion of fuel at power plants with an estimated fraction in total CO<sub>2</sub> emissions being 35–36% (INER RAS. -M. 2001). Depending on the source of fuel used and the inherent efficiency of the power plant, CO<sub>2</sub> emissions scenarios vary. For example Russia is reported to have a fuel balance in the power sector of the following ratios: 63% gas, 10% of heavy oil and 27% of coal and other fossils; and by 2050 the gas fraction might decrease up to 34% and the coal fraction might increase up to 64%. Coal is widely used in most power plants to generate electricity, for example in 1996 coal provided fuel for about 57% of the electricity utilized in the U.S but it is being slowly replaced with natural gas in areas where the environmental awareness of pollution is high, such as Europe and the US which has seen a boom in gas production and subsequently for power production. Figure 2-5 below shows the forecasted power sources by the US Department of Energy. To further show the contrast between coal-fired and gas-fired plants, Hiroki Hondo did a life cycle analysis of various power

generation plants and concluded that for coal-fired plants the life cycle analysis resulted in 975.2 g-CO<sub>2</sub>/kWh generated whereas for gas based it resulted in 518.8 g-CO<sub>2</sub>/kWh power (Armor and Preston 1996).

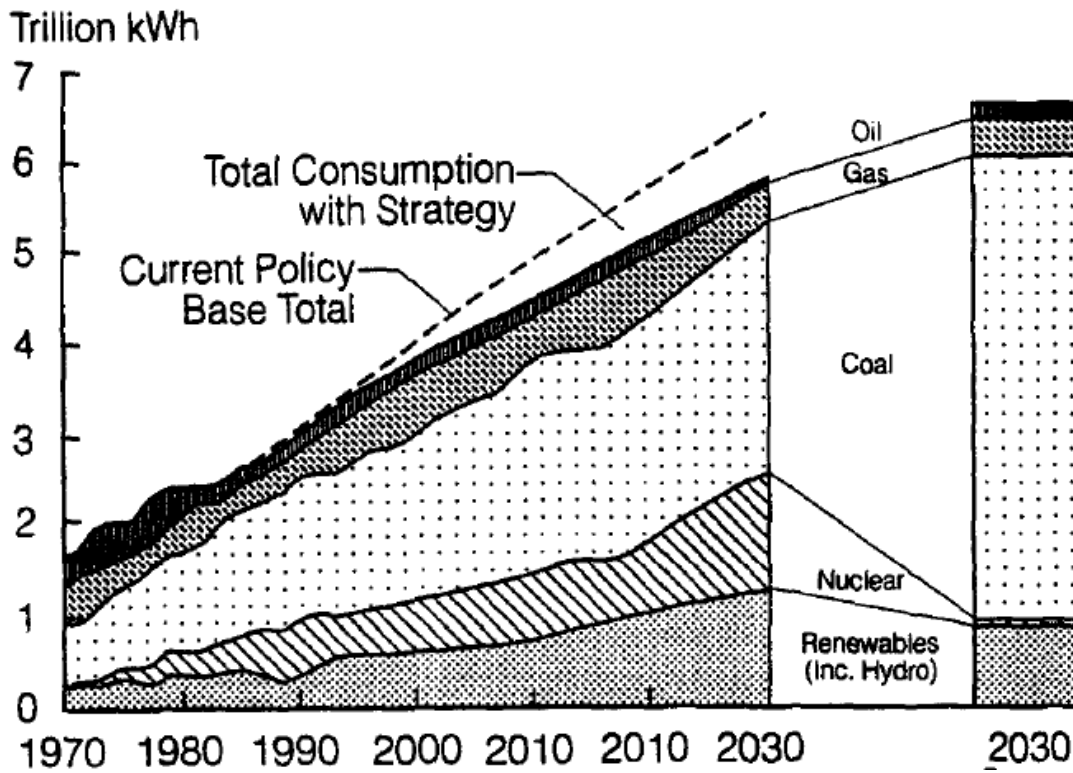


Figure 2-5. Breakdown in generation by energy source (Armor and Preston 1996)

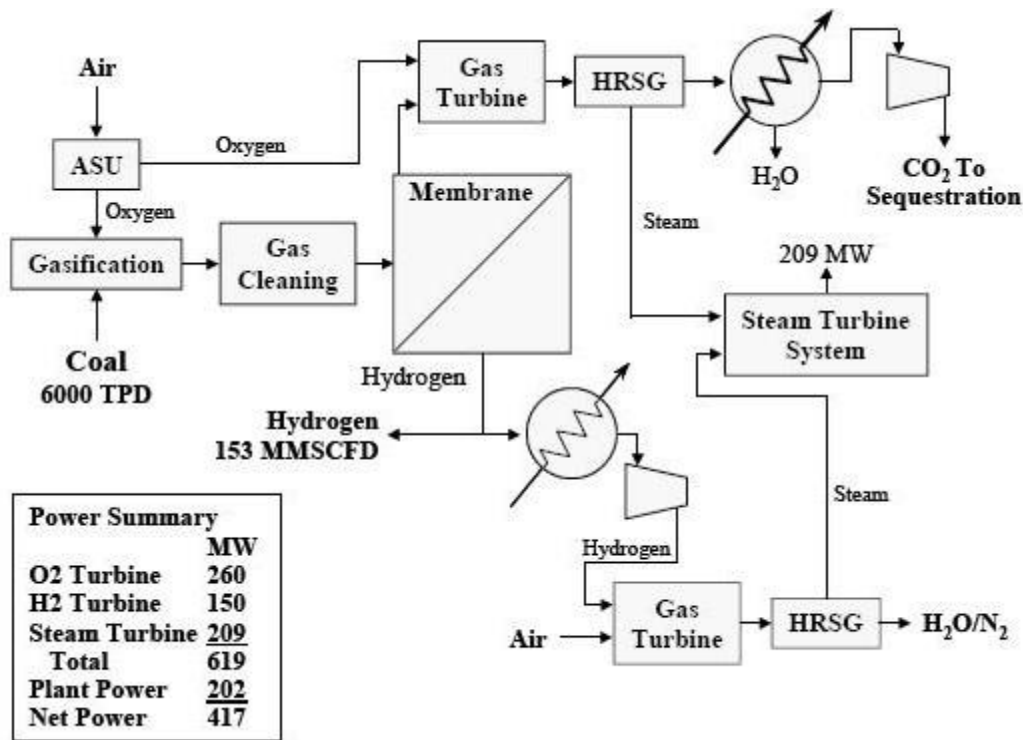


Figure 2-6. Integrated Gasification Combined Cycle Power Plant(DOE 2004)

Natural gas is known to burn cleanly and efficiently compared to coal. Efficiency of most type of power plants such, as integrated gasification combined cycle (IGCC) which employs high temperature gas turbines and with a reported thermal efficiency up to 60%, are largely based on combined Rankine and Brayton cycles. Such combined cycles, fired by gas, result in significantly higher efficiency (Armor and Preston 1996). Thermal efficiency is of high significance in the energy industry because by burning less fuel per kW generated, emissions such as CO<sub>2</sub>, SO<sub>2</sub>, NO<sub>x</sub> and particulates can be reduced. A typical IGCC plant is shown below in figure 2.5 and shows where the exhaust CO<sub>2</sub> emissions are released. It should be noted that efficiency talked about here is based on the gross heating value (GHV) of the fuel. However the abundance of coal in countries such as China will always present a problem of what to do with the post-combustion CO<sub>2</sub>.

There are some suggested methods for improving efficiency of power generation plants and reducing their CO<sub>2</sub> emissions. Examples include fuel substitution – coal to natural gas – fossil fuels to renewable fuels such as biofuels, wind, Sun, Geothermal, Efficiency improvement,

Nuclear power and Carbon capture and storage. Of all the listed methods CCS has attracted and continue to attract the most interest due to the level of maturity of the technology and the technical and economical feasibility of the technology in mitigating post-combustion CO<sub>2</sub> capture from mainly power plants.

Naturally, the discussion leads to the question the definition of CCS and how to address challenges to CCS technology such as corrosion reported in various pilot plants and bench-scale testing?

## **2.4 Carbon dioxide Capture and Storage Technology**

Carbon dioxide capture and storage (CCS) is an umbrella of technologies used to store CO<sub>2</sub> emitted from various combustion sources in different industries and then the stored high pressure CO<sub>2</sub> is transported in pipelines to safe storage sites such as geological features. In essence carbon dioxide capture and sequestration (CCS) technologies, involve capturing the CO<sub>2</sub> from large point sources such as power plants and putting it away in various storage facilities like underground aquifers. The first part of the CCS, which is the capture part, has much different type of techniques used: chilled ammonia technology, amine technology, both of which fall under chemical absorption. In this work, the role of alkanolamines and to be precise diethylenetriamine (DETA) is examined and how the use of such substances in post-combustion CO<sub>2</sub> capture has been reported to created corrosion in the absorption plants.

Native to most if not all CCS technology is the intensive energy requirements, the overall reduction of thermal efficiency, degradation of absorbents in the case of chemical absorption-based techniques and the concept of corrosion as has been reported extensively by different authors (Danckwerts PV 1967; Danckwerts 1979; Sekine and Senoo 1984; Kohl 1985; Mattsson 1989; Tontiwachwuthikul, Meisen et al. 1992; DuPart 1993; Veawab, Tontiwachwuthikul et al. 1999; Wiersma and Mickalonis 2008; Kladkaew, Idem et al. 2009; Saiwan, Supap et al. 2011; Svendsen, Hessen et al. 2011; Tavera-Valero and Svendsen 2011; Gao, Wang et al. 2012; Hayfron-Benjamin 2012; Martin, Lepaumier et al. 2012; Svendsen 2013; Stangeland September 2009). For example commercial processes such as the Fluor Econamine and Econamine Plus, GAS/SPEC FT by Dow chemicals, Amine Guard FS system by UOP all based on MEA

processes has advantages such as High loading capacity on the basis of solvent weight, Faster rate of reaction, Possibility of simultaneous dehydration (Svendsen 2012). But even with such obvious advantage challenges such as process incompatibility with contaminants e.g. COS, CS<sub>2</sub>, Corrosive and degradation of MEA, limitation of loading on mole basis and a high heat of reaction and high vapour pressure is commonly reported (Svendsen 2012). The Fluor Econamine is known to have an energy requirement (3.7-4.2 MJ/kg CO<sub>2</sub>) which can be challenging to say the least.

In Chapter 3 we delve into what the process of CCS entails, the different kinds on the market and the readiness of such technology. From the point of view of this thesis, the most interesting is the issue of corrosion, so after establishing a strong basis for what the technology used in amine-based CO<sub>2</sub> capture plants, the characterization of the relatively new solvent DETA and the theory of the corrosion caused by it will be dealt with in the rest of the work.

## Chapter 3 CCS technology and how it works

### 3.0 Introduction

The concept of global climate change has now been established by notable expert bodies such as the Intergovernmental Panel on Climate Change (IPCC). Climate change can be attributed to natural causes or man-made. Therefore concerns due to anthropogenically forced climate change because of emissions of CO<sub>2</sub> have resulted in a number of initiatives to reduce CO<sub>2</sub> emissions (MacDowell, Florin et al. 2010). In this chapter of the work, we examine the leading options for large scale CO<sub>2</sub> capture – from the technology to the level of maturity of that technology and assess any problems that might hinder large-scale implementation of that technology.

It has been reported that, worldwide, there are more than 8000 large stationary CO<sub>2</sub> emission sources whose cumulative emissions in 2005 lie within an estimate of 13 466 megatons of CO<sub>2</sub> per year (Mt/yr) (B. Metz, O.Davidson et al. 2006). Most of these point sources are mainly but not limited to power plant stations (coal and natural gas-based) and industrial processes which together accounts for almost half of all CO<sub>2</sub> emissions from anthropogenic sources.

Carbon capture and storage (CCS) technologies offer a hope for significant reduction targets for CO<sub>2</sub> emissions, with some of these technologies achieving emission reduction targets of 80-90% of CO<sub>2</sub> emissions from fixed sources. For example the Kerr-McGee/ABB Lummus amine process which uses a chemical solvent 15-20 wt% MEA without inhibitors has claimed the process can capture more than 96% of the CO<sub>2</sub> in the flue gases (John. Marion, Nsakala. ya Nsakala et al. 2001; Svendsen 2012). But one should note that such claims often come with many disadvantages such as high energy penalties and capitals costs. The subject of this literature review is with regards to post-combustion CO<sub>2</sub>.

The overall challenge is therefore to have an optimal CCS method in terms of capital and operating costs and relatively harmless effect to the environment. The most relevant technologies that could be used in post-combustion CO<sub>2</sub> capture are: amine solvents systems, oxyfuel combustions and calcium looping. These are what some experts call matured technologies ready to be deployed in the near to medium term (MacDowell, Florin et al. 2010).

## 3.1 Chemical Absorption Technologies

### 3.1.1 Process Overview

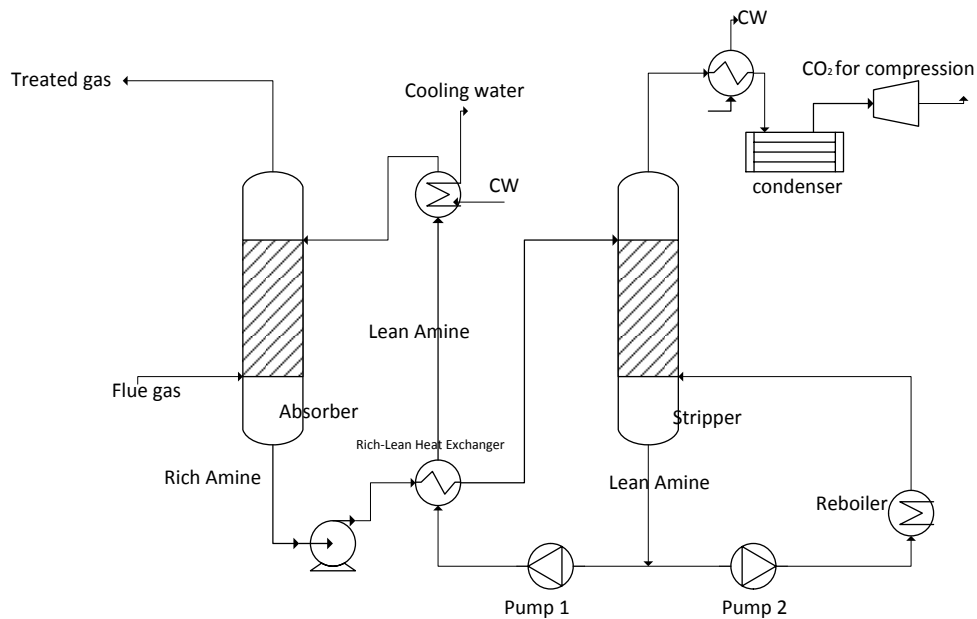
Amine absorption and Chilled Ammonia process are the two main known technologies that fall under chemical absorption. This brief review looks at the former, which is more commonly deployed in pilot plants worldwide.

Chemical absorption for CO<sub>2</sub> refers to the process where by gas and liquid make contact and are separated in different equipment. The gas and liquid streams flow in a counter-current manner inside a vertical column containing horizontal trays or packing material (either random or structured) which allows for sufficient mixing and contact times. Structured packing material has been because of availability and also because they have large specific area (area per unit volume) which will lead to reduction in equipment size and hence lower capital expenditure (de Brito, von Stockar et al. 1994; MacDowell, Florin et al. 2010). From the flow-sheet in figure 3-1 below, it can be seen that the process consists of mainly two unit operations pieces – absorber and stripper. In the absorber, where absorption of CO<sub>2</sub> takes place in the solvent, in this case, amine-based solvents such as MEA, DETA, MDEA. The CO<sub>2</sub> from the flue gases is introduced from the bottom of the absorber, whereas a lean solvent flows vertically down the absorber over the packing material. Lean solvent in the sense that the stream introduced contains little or no of the components in the gas phase (CO<sub>2</sub>). After counter-current flow down the vertical column over the packing material, the solvent becomes rich in the CO<sub>2</sub> molecules, which means that the mole fraction of the gas is high in the liquid phase. Typical process conditions encountered in the absorber are temperatures of 45-80°C and pressures of the order 100kPa (Svendsen 2012). The rich solvent is then fed to the top of the stripper from where the solvent is regenerated. The second process occurring in the desorber essentially separates the CO<sub>2</sub> from the solvent. This unit has auxiliary components like the reboiler at the bottom and condenser at the top. The condenser provides a reflux liquid stream and at the same time ensuring that the top-product stream (CO<sub>2</sub>) is as pure as possible (Martin, Lepaumier et al. 2012). The reboiler supplies stripping fluid and heat to the rich solvent to raise its temperature in order to aid in breaking the chemical bonds formed between the gas and liquid molecules. Because of the energy intensive nature of the solvent regeneration process, it is the area where energy considerations are important in any CCS venture. Parameters such as the total steam requirement (kJ/mol CO<sub>2</sub>

captured), sensible and stripping heat requirements are needed to determine what the optimal lean loading the process needs. Optimization and details of the process is beyond the scope of this work and thus the interested party can find such details elsewhere in the literature (Jassim and Rochelle 2005; Ho, Allinson et al. 2008; Agarwal, Biegler et al. 2009; Bhattacharyya, Turton et al. 2010; Lin, Pan et al. 2010; Geers, van de Runstraat et al. 2011; Freeman and Rochelle 2012; Han and Lee 2012; Hasan, Baliban et al. 2012; Hasan, Baliban et al. 2012; Liu, Wang et al. 2012).

The most important key performance indicators for chemisorption technologies are (Martin, Lepaumier et al. 2012):

- (a) the operating cost, (b) the amount of CO<sub>2</sub> emitted in the cleaned flue gas, (c) the capital cost and (d) fugitive emissions of volatile organic compounds (VOC).



NTNU Department of Chemical Engineering CO <sub>2</sub> Absorption Group	Amine Treating Plant for CO <sub>2</sub> Absorption			
	«Corrosion Effect on Stainless Steel A316 by Amines and Degradation Products»			
EBENEZER HAYFRON-BENJAMIN	SIZE	FSCM NO	DWG NO 1	REV Final
MSc(Chem. Eng)	SCALE 1:1		SHEET	1 OF 1

**Figure 3-1.** CO<sub>2</sub> amine absorption process flow sheet diagram

An example of a CO<sub>2</sub> capture plant which has received world-wide attention is that of TCM at Mongstad and picture of the plant under construction is shown in figure 3-2 below.



**Figure 3-2.** TCM CO<sub>2</sub> Capture Plant at Mongstad, Norway(AkerCleanCarbon 2012; Svendsen 2012)

### 3.1.2 Chemistry

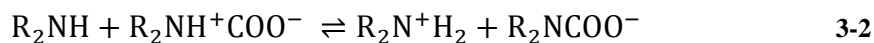
Reactivity of aqueous amine solutions with CO<sub>2</sub> is the main attraction for their use as chemisorption solvents. Mechanisms and reaction pathways for the reaction between amines and CO<sub>2</sub> have been proposed over the years and the two main schools of thoughts are the zwitterion mechanisms and lately the termolecular mechanisms. For the zwitterion mechanisms, the exact details of the reaction mechanisms and kinetics has been reported to vary widely but the most common reaction pathway for both primary amines (monoethanolamine, MEA) and secondary amines such as diethanolamine (DEA), has been proposed by Laddha and Danckwerts who published experimental results for aqueous MEA and DEA that seem to support the proposed mechanism (Danckwerts 1979; Haimour, Bidarian et al. 1987; Littel, Van Swaij et al. 1990;

Littel, Versteeg et al. 1992; Tontiwachwuthikul, Meisen et al. 1992; Suda, Iijima et al. 1997) shown here: (Hsu Ch Fau - Chu, Chu H Fau - Cho et al.).

Zwitterion formation:



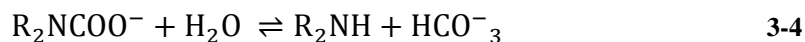
Zwitterion deprotonation or carbamate formation:



Protonated amine formation:



Bicarbonate formation:



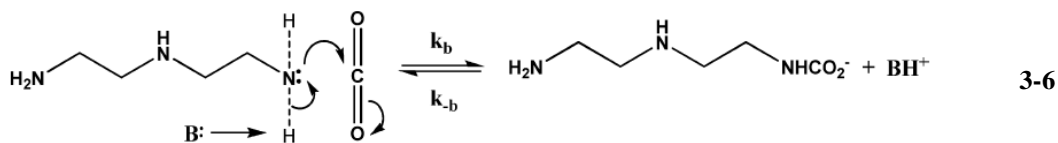
In essence the principle reaction involves the reaction of aqueous primary or secondary amines solutions and  $\text{CO}_2$ , with the formation of carbamate via sequence of zwitterion formation, base-catalyzed deprotonation as shown above.

Reaction mechanisms for tertiary amines differ from that of the other amine types (primary and secondary) in that tertiary amines do not react directly with  $\text{CO}_2$ , rather they act as a base, catalyzing the hydration of  $\text{CO}_2$  (Edali, Aboudheir et al. 2009). The reaction is as shown



Termolecular mechanism originally proposed by Crooks and Donnellan (1989) (Crooks and Donnellan 1989) and later reviewed by da Silva and Svendsen (2004) (da Silva and Svendsen 2004) suggests that the amine bonding to  $\text{CO}_2$  and the proton transfer take place simultaneously. The initial product is not a zwitterion, but a loosely bound encounter complex. Most of these

complexes break up to give reagent molecules again but a few react with a second molecule of amine, or a water molecule, to give an ionic product. Bond formation and charge separation occur only in the second step as shown below (Hartono 2009).



Depending on the amine type used (primary, secondary, tertiary or sterically hindered) there are implications for the chemistry involved. Primary amines are known to form stable carbamate, react fast, high reaction energy but their loading capacity  $\alpha$  is restricted to 0.5., secondary amines on the other hand have carbamates which are not stable, and finally tertiary amines do not form carbamate, has slow kinetics react, relatively low reaction energy but a high  $\alpha$  which can go upwards to 1.0 (Svendsen 2012). Then we have the special groups of amines such as sterically hindered amines (AMP) that do not form stable carbamates although primary in nature, react slower, relatively low reaction energy. Finally polyamines such as DETA, containing more than one amine group (3 amine groups in DETA) which can form carbamate (varies), has fast kinetics, high reaction energy and uniquely the loading not restricted but can exceed 1, maybe 1.5. The complicated implications of the chemistry give a window into the complexity of implementing a standardized chemisorption-based CCS technology.

### 3.1.3 Advantages and Challenges

Amine-based CCS technology has the advantage of being flexible in its use to the existing power plants either as a retrofit or a new build. This is because the adoption of this particular technology will not unduly affect the flexibility of operation demanded of existing plants (Chalmers and Gibbins 2007). Additional advantages includes the fact that CO<sub>2</sub> is separated at low pressures (becomes a challenge owing to the low CO<sub>2</sub> partial pressure in the inlet flue gas, relatively high solvent flow rates are required to achieve a high rate of CO<sub>2</sub> capture), and high amount of gas can be treated. But the glaring disadvantage relates to their intensive energy requirements especially in the reboiler sections. This leads to increases in both capital expenditure (CAPEX) and operational expenditure (OPEX). Either as retrofits to existing power

plants or newly built, amine-based processes have been known to reduce the thermal efficiency of a modern power plant from approximately 45% to approximately 35% (Herzog 1993; MacDowell, Florin et al. 2010). This drop in efficiency will increase the costs of solvent regeneration (approximately 4 GJ/ton of CO<sub>2</sub> captured) (Alie, Backham et al. 2005; MacDowell, Florin et al. 2010). Other notable disadvantage is the cost of CO<sub>2</sub> compression, transport of the sequestered gas and storage options available.

Additionally the tendencies of amines to undergo thermal and oxidative degradation increases the cost of replacing the solvents. These processes are expected to consume between 0.35 and 2.0 kg of solvent per tonne of CO<sub>2</sub> captured (Bailey and Feron 2005; MacDowell, Florin et al. 2010).

The process conditions at the outlet- regeneration stage are approximately 120°C and 0.2 MPa. Such low pressures will necessitate ramping up of pressures using compressors to bring the pressures of the CO<sub>2</sub> sequestered in-line with gas pipeline specifications.

### **3.1.4 Environmental Impact**

The environmental impact assessment of CCS has been extensively reported by the Bellona Foundation (Stangeland September 2009). In their report, the authors raised a number of concerns about how amines could impact the environment. It is reported that an amine based capture plant will in general have several positive impacts on the environment. An amine plant will not only remove 85 to 90 percent of the CO<sub>2</sub>, but considerable amount of other polluting components such as ashes, NO<sub>x</sub> and SO<sub>2</sub> will also be removed due to required pre-treatment of the flue gas (Stangeland September 2009). With this said, however, amines are known to pose some health risks to human and animal and aquatic ecosystems. To what extent and in what concentrations that amines will pose significant risk is yet not fully understood. This is so because of the current gap in knowledge of the full extent of reaction mechanisms and degradability of amines. Available literature shows that some amines and amines degradation products can have negative effects on human health (irritation, sensitization, carcinogenicity, genotoxicity). The amines can also be toxic to animals and aquatic organisms, and eutrophication and acidification in marine environments are also possible (Stangeland September 2009) but these side effects are worst case scenarios. The most commonly used amine MEA has been

known to have high biodegradability and till date not reported to have any health risk on humans and other organisms. For the other types of amines such as DETA, the literature is lacking in information and hence the judgment on the environmental impact is still yet to be known.

### **3.1.5 Innovations and the Future**

Chemical absorption technology is a mature process widely used in various parts of the world. This means we are not likely to see a revolutionary set of innovations with respect to the basic process of absorption and solvent regeneration and column internals. What is agreed upon by many experts is that there is still room for improvement in the solvent design stage of the process. Any improvements in the solvent design will impact heavily on the costs associated with the process. It is also the solvent which lies at the heart of the limits of kinetics and thermodynamics.

The benchmark solvent used is primary alkanolamine, monoethanolamine (MEA) and other compounds used include sterically hindered 2 – amino-2-methyl -1- propanol (AMP), diethanolamine (DEA) and of more concern to this work is diethylenetriamine (DETA) which was used in a trial campaign in a pilot plant at the Norwegian University of Science and Technology (NTNU). The DETA used however presented a huge challenge of corrosion of stainless steel materials of the process and hence triggering the need for this work.

Commercially patented process abound in the world, examples include but not limited to; The Fluor Econamine Process, Mitsubishi Heavy Industries (MHI) KS-1 amine process, Kerr-McGee/ABB Lummus amine process. All the known commercial processes comes with an in-house proprietary solvent, claims of CO<sub>2</sub> absorption capture capacity, energy requirements, solvent stability to degradation among other parameters. All the claims can not be independently verified.

Another major challenge for the industry lies in the area of solvent degradation and induced corrosion of equipment. This aspect of the CCS technology will be fully tackled in the subsequent chapters of this body of work.

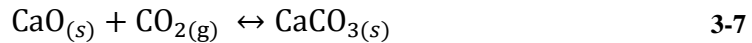
In conclusion, by having a better understanding of the chemistry in both theoretical and experimental aspects, key limitations such as degradations of amines, environmental impact will

help in advancing the scale of CCS from the present limited pilot-basis scale to more commercial basis and this will ultimately impact on global emission reduction targets.

### 3.2 Carbonate looping technology

CO<sub>2</sub> capture using solid sorbents like calcium oxide (CaO) is not as widespread as the amine based technology. Nevertheless for the purposes of elucidation, the highlights are summarized below for the reader to make a contrast with the more matured technology of amines.

In Carbonate looping, the CO<sub>2</sub> is absorbed by the CaO in a solid-liquid reversible reaction at relatively high temperatures of about 650°C.



A simplified flow sheet is shown in figure 3-3 below.

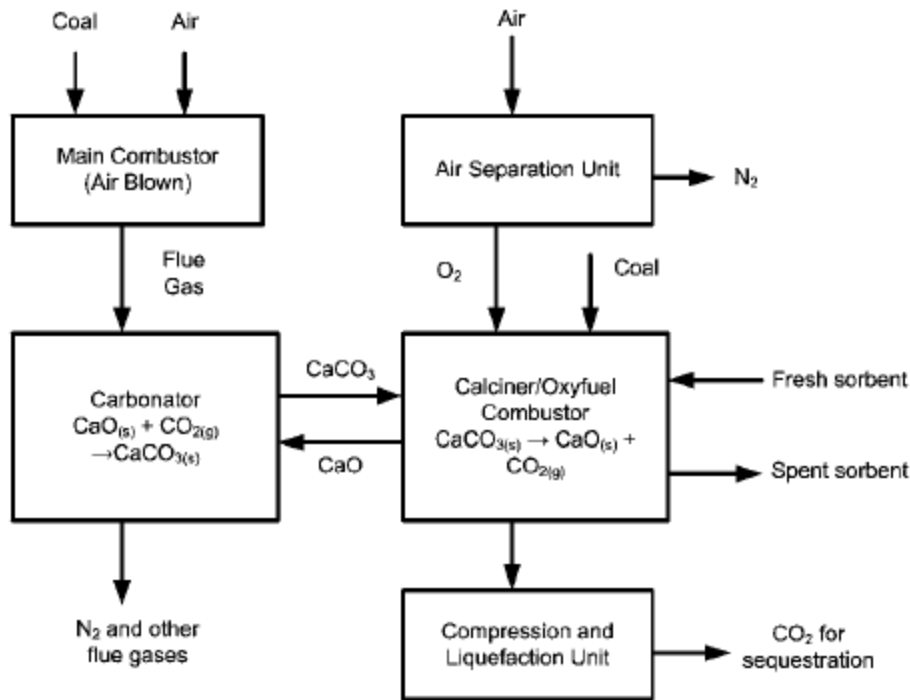


Figure 3-3. Post-combustion carbonate looping(J. Blamey, N. H. Florin et al. 2009; MacDowell, Florin et al. 2010)

In the first reactor known as the carbonator, the reaction shown above takes place, later it is transferred to another vessel the calciner, where the reverse reaction takes from where the CaO is regenerated and the CO<sub>2</sub> absorbed is released. In all the vessels, a circulating fluid bed reactor is used because of the very good gas-solid contacting and temperature uniformity across the reactor bed (MacDowell, Florin et al. 2010). The cheap raw material used, CaO obtained from natural limestone makes this process attractive compared to MEA based processes, this notion is supported by the fact that on year 2000 basis, limestone was priced at 0.0015USD/mole compared to 0.544USD/mole for MEA (MacDowell, Florin et al. 2010). This will inherently reduce the operating expenses. The carbonate looping technology is also well suited for cement factories because used sorbents can be used in the cement productions and this will also help in reducing CO<sub>2</sub> emissions from such plants.

Further detailed process descriptions and limitations are beyond the scope of this project and the interested reader can refer to the literature (MacDowell, Florin et al. 2010).

### 3.3 Oxyfuel combustion technology

Oxyfuel combustion is the combustion of the fuel in a mixture of CO<sub>2</sub> (from reactor exit) and pure O<sub>2</sub>. The process is shown in the figure 3-4 below. Even though pure or close to pure CO<sub>2</sub> leaves the boiler, separation of O<sub>2</sub> from air is expensive. In addition it requires new design for gas, turbines, boilers and burners. Detailed description can also be found in MacDowell et al. (MacDowell, Florin et al. 2010).

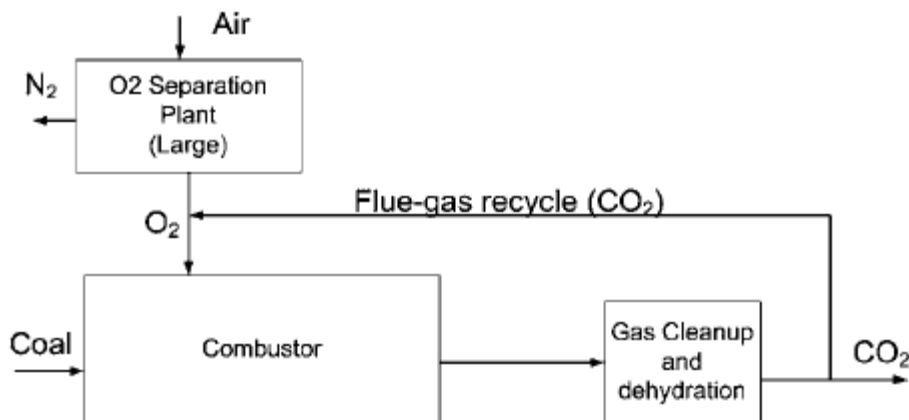


Figure 3-4. Schematic of Oxyfuel combustion plant(MacDowell, Florin et al. 2010)

To conclude, based on current technology, CCS is expected to be commercially available in the near to medium term range. However issues like thermal efficiency reduction, operating and capitals expenses will all need to be addressed and brought down to make the technology feasible and economical and among all the technology available, it is the amine-based CCS which looks promising. But even then it is facing the issue of corrosion for which extensive studies have been taken to help in the selection of materials for the design stage when the technology is deployed on a commercial basis. The subsequent chapter looks at corrosion and amines from the point of view of carbon capture and storage process.

## Chapter 4 CCS and Corrosion Challenges

### 4.0 Introduction

Fossil fuel such as coal or natural gas is widely employed in the generation of power and electricity. This leads to the effect of emissions of GHGs and of a particular interest is CO<sub>2</sub>, which as been previously in this work stated to be a major concern to the concept of global climate change. Post –combustion CO<sub>2</sub> needs somehow to be captured to prevent a variety of problems like: enhanced GHG effect, CO<sub>2</sub> tax in some locations world wide such as Norway. CO<sub>2</sub> capture method can be either retrofitted to existing power plants or built as an additional unit, all depends on the economics. Chemical absorption process suitable for low-pressure flue streams is the closest thing to technological maturity on the market now, as explained in chapter 3 under the broad CCS technologies overview. With that said, it should be mentioned that “corrosion in alkanolamine gas treatment plants can result in unscheduled downtime, production losses, reduced equipment life and even injury or death”, increase in production costs in an era where everyone is trying to come up with an economically feasible CCS technology (DuPart 1993). Further more “these challenges faced in the post-CO<sub>2</sub> capture Industry has necessitated the need for a thorough understanding” of the mechanism by which industrial grade metals such as stainless steel are degraded in process conditions in the industry (Hayfron-Benjamin 2012). In essence the drawback of corrosion prevents the amine process from achieving its highest efficiency (Saiwan, Supap et al. 2011) with the exact reduction in CO<sub>2</sub>-capture caused by corrosion being a gray area needing further research.

So, designers of CCS plants will need to examine various parameters such as amine concentration, CO<sub>2</sub> loading, process, type of metals (stainless steel vs. carbon steel), temperature, pH, degradations products in the form of heat stable salts, amongst others which will need to be taken into account in the overall analysis and criteria for material selection, solvent design and plant construction. The purpose of this part of the work is to introduce the reader to these critical parameters that affect corrosion and how to optimize such in the plant operation.

## 4.1 Corrosion and how amines play a role, special emphasis on MEA and DETA

Corrosion can be defined as an electrochemical reaction (redox) that involves transfer of electrons eventually leading to the degradation of the metal in question. This degradation condition is the preferred thermodynamic state of most metals such as iron which are found as ores in nature.

The simple mechanism of metal corrosion can be represented by the following reactions (Hayfron-Benjamin 2012):

Anode reaction:



Cathode reaction:



Overall reaction:



From the above reaction it can be deduced that the presence of an oxidizing agent (which is then reduced) needs to be present for corrosion to occur. Usually it is dissolved oxygen which plays the role of oxidizing agent, or in some cases acidic media in the form of protons ( $\text{H}^+$ ).

Since the 1930s, regenerative processes have used alkanolamines for  $\text{CO}_2$  and  $\text{H}_2\text{S}$  removal (DuPart 1993) but this use is mitigated by the constant solvent attack on plant equipment mainly because of the presence of the acid gas causing corrosion and also fouling of heat exchanger surface area and contact equipment (Veldman 2000). Design engineers therefore need to have an adequate but fundamentally sound understanding of the mechanisms and implications of the effects of corrosion in order to efficiently run an amine plant, CCS plant being no exception. The type of amine used, the metal (carbon steel or stainless steel) and a host of other parameters go a long way to determine the extent corrosion rates expected in any plant using amine-based solvents.

The more prevalent solvents used in CCS are the amine based solvents like MEA, DEA, PIPA and lately DETA has attracted some attention due to its fast kinetics, high reaction energy and high CO<sub>2</sub> loading. The literature has stated that MEA, even though it is benchmark solvent for CCS, is the most corrosive of the amines in the presence of CO<sub>2</sub> as reported in the order of MEA > DEA > MDEA (DuPart 1993; Hayfron-Benjamin 2012). MEA is known to be even more corrosive than the blend of MEA/PZ solutions (DuPart 1993; Stangeland September 2009). In addition MEA corrosion rates also increase with CO<sub>2</sub> loading (L.D. Polderman, C.P. Dillon et al. 1955).

Another dimension of amines and corrosion is in the area of solvent degradation. It is a fact that amines have been known to degrade (both oxidative and thermal degradation), forming products that are corrosive agents and consequently cause equipment corrosion in the absorption plant (DuPart 1993; A.L. Kohl 1997). For example from an earlier project done by this author, it was reported that in the presence of solvent degradation products such as oxalates, formates, acetates in MEA-CO<sub>2</sub>- systems, corrosion high corrosion rates recorded for oxalic acid for 330 hours on exposure, with a rate of 0.0429 mm/yr (Hayfron-Benjamin 2012). Further examples include Svendsen and Tavera, (Tavera-Valero and Svendsen 2011) who investigated the “effects of degradation products on the corrosion of stainless steel in an aqueous MEA-CO<sub>2</sub>-air environment”, (Tavera-Valero and Svendsen 2011) and came to the conclusion that localized corrosion such as pitting and stress corrosion cracking are more prevalent in “equipment constructed of stainless steel in amine-based CO<sub>2</sub> capture plants”. (Sekine and Senoo 1984; Veawab, Tontiwachwuthikul et al. 1999; Kittel, Idem et al. 2009; Kladkaew, Idem et al. 2009; Kladkaew, Idem et al. 2009; Tavera-Valero and Svendsen 2011; Gao, Wang et al. 2012; Hayfron-Benjamin 2012) and this assertion is illustrated by figure 4-1 as shown below for a test done on A316 Stainless steel.

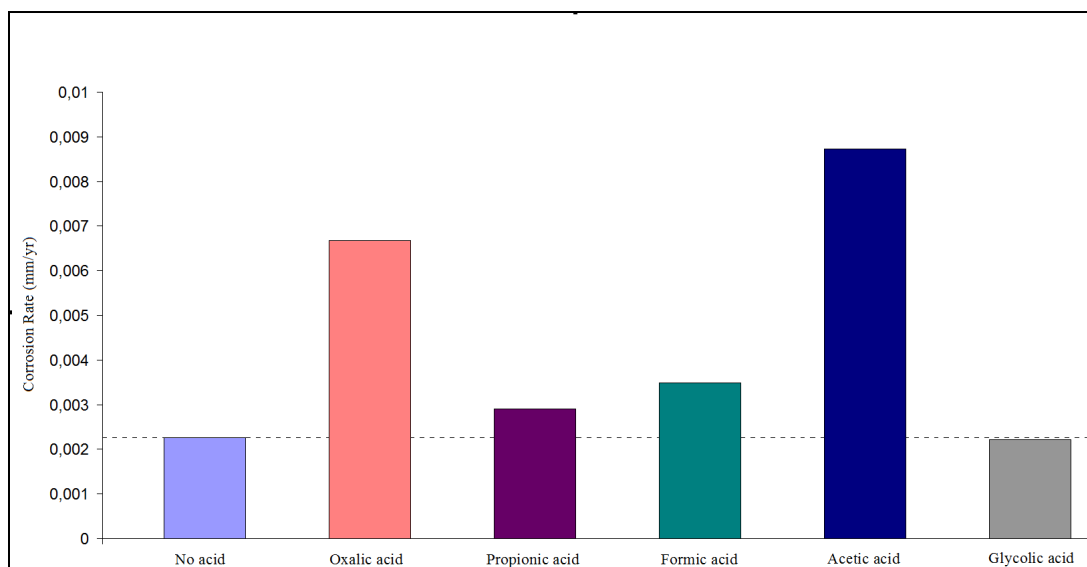


**Figure 4-1.** Corrosion rates at 50° C on stainless steel A316 (Tavera-Valero and Svendsen 2011)

The table below shows a compilation of some corrosion works done mainly involving MEA and other benchmark solvents used in CO<sub>2</sub> capture.

**Table 4-1.** Corrosion review in the open literature

Type of Amine	T/°C	Metal Type	CO <sub>2</sub> loading( $\alpha$ )	O <sub>2</sub> concentration/ Partial Pressures(kPa)	HSS species	Methodology	Corrosion result	Ref.
MEA and Piperazine	40, 80	CS 1018, SS 430	0.20-0.68	0 -10.13	acetate, formate, oxalate, thiosulfate	potentiodynamic polarization	formate most corrosive	(Nainar and Veawab 2009)
MDEA and DEA	88	carbon steel	0.03 - 0.50	N/A	N/A	weight loss weight loss and Electrochemical techniques	MDEA > DEA	(Veldman 2000)
3wt% NaCl aqueous solution	22- 80	mild steel	N/A	free	acetic acid	Electrochemical techniques	acetic acid enhances corrosion	(George and Nešić 2007)
MEA	135	SS 316L	0.4	free	acetate, formate, oxalate	weight loss	oxalate most corrosive	(Hayfron-Benjamin 2012)
MEA, MDEA, AMP, DEA	30-80	Carbon steel	0 - 0.4	free - 10% feed gas	N/A	Electrochemical techniques weight loss and Electrochemical techniques	AMP > DEA,MEA	(Veawab, Tontiwach wuthikul et al. 1999)
DETA	80, 135	SS 316L	1.2 - 1.5	free	acetate, formate, oxalate	Electrochemical techniques	acetate, formate, oxalate?	This work (Gao, Wang et al. 2012)
Proprietary amine-based	40 - 120	Carbon steel	0.05 - 99%(captured gas)	industrial pilot conditions, 18 vol%	N/A	weight loss in Pilot Plant	coupons at absorber bottom and outlet of the rich-lean exchanger shows a higher corrosion	(Gao, Wang et al. 2012)

Diethylenetriamine (DETA) on the other hand, even though it has been used in some trial pilot plants (at NTNU, Trondheim) and found to be excessively corrosive, few to none extensive data is found in the open literature. To the best of my knowledge, the only work on DETA corrosion was carried out by Ole Edvard (Kongstein 2010) from SINTEF, Norway who characterized DETA-CO<sub>2</sub> corrosion systems and concluded that in the presence of diethylenetriamine and CO<sub>2</sub>,

only uniform corrosion of 316 Steel was observed. The dearth of information on DETA-CO<sub>2</sub> system can be partly explained by the fact that not many authors save a few (Davis 2009; Hartono 2009; Kongstein 2010) have written extensively about DETA and only Ardi Hartono (Hartono 2009) has done an extensive characterization of this potential CO<sub>2</sub> capture solvent.

## **4.2 Corrosion prevalent regions**

The construction of the process plant required for carbon capture in power generation and also other industrial processes is expected to be among the most significant capital investments of the next 20-30 years (Billingham, Lee et al. 2011). Choosing the right materials for piping, vessels and all types of equipment will be vital in ensuring the long-term performance, safety and high operational availability of the capture plants through their lifetime (Billingham, Lee et al. 2011). This makes the problem of material degradation and corrosion of process equipment in CCS plants vital and by further examining corrosion issues like this work does, it helps make material selection issues at the front-end- engineering design (feed) much simpler.

In carbon capture process environment, the high levels of CO<sub>2</sub>, high temperatures, wet conditions and amine degradation products leads to a combination of both oxidizing and acidic environment, causing high corrosion rates for equipment materials like carbon and stainless steel. All the major types of corrosion such as: general and localized corrosion, metal dusting, erosion corrosion have been reported to have occurred in amine gas treating plants which is similar to potential carbon capture plants. In addition corrosion has been reported in mainly the cross exchanger's rich side, rich-amine piping after the cross exchanger, the still and the reboiler, where the free acid gas and high temperatures are the main driving forces for corrosion (DuPart 1993). Dupart, Bacon and Edward and Rooney have done extensive work on this and the interested reader can refer to their work for further details (DuPart 1993; Rooney, DuPart et al. 1997).

Focusing on the specific areas of carbon capture plants where corrosion can occur, it must be recognized that low pressure, large volume flows are common at the front end of the capture plants and will be handled by ducting rather than piping similar to the outlet end of FGD plant (Billingham, Lee et al. 2011). Hence mixtures of different grade of metals are commonly

employed such as carbon steel and stainless steel. For example steel trays in either the absorption or regenerator columns are known to suffer from some form of galvanic corrosion because if the tray is made from stainless steel but held together by bolts of carbon steel the electrochemical potential arising because of dissimilar metals and also the presence of an electrolyte (DETA) leads to corrosion. Also previous experience in gas removal processes such as Flue gas desulphurization (FGD) can provide a guide for predicting how corrosion will occur in CCS plants. Billingham et. al (Billingham, Lee et al. 2011) claims that “materials performance in flue gas desulphurisation (FGD) plant is very relevant to similar acid oxidizing conditions in carbon capture plant: the inlet for the capture plants in post-combustion and oxy-fuel scenarios when using coal firing would be from an FGD unit.” But the presence of the oxidizing acid species  $\text{NO}_x$  and  $\text{SO}_x$  in the flue gas stream (even though it is thought to be removed, traces will remain), can lead to acidic corrosion. For example with the right conditions of dew point, acidity (pH), temperature, halide,  $\text{SO}_2$  condensation (leading to concentrated sulfuric acid) can lead to crevice corrosion amongst other types.

Figure 4-2 below shows a schematic diagram of a typical post-combustion  $\text{CO}_2$  capture with the type of materials likely to be employed.

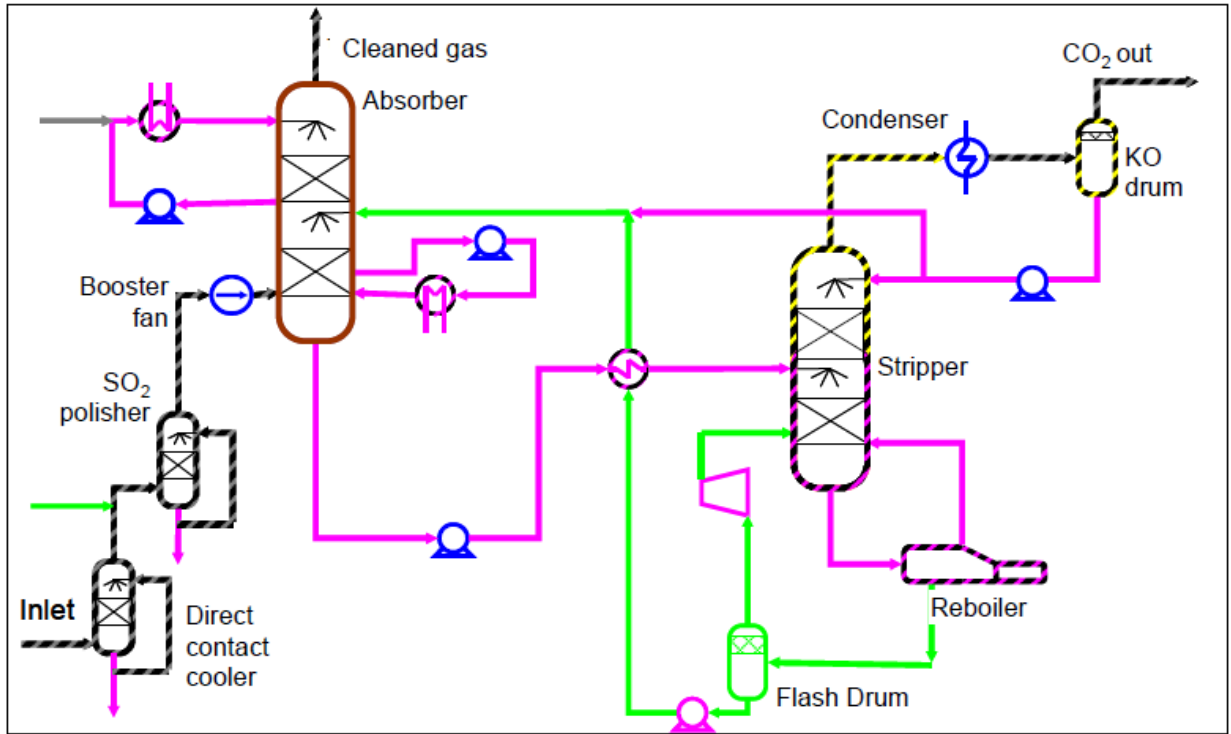


**Figure 4-2.** Schematic materials selection for Post-combustion capture on a coal power plant(Billingham, Lee et al. 2011)

	Carbon / low alloy steels		Martensitic stainless steel
	Carbon / low alloy steels + corrosion allowance		Non metallic (flake glass/GRP/FRP/PP)
	Duplex stainless steel		Nickel alloys
	Austenitic stainless steel		Cement and tiling
	Special austenitic stainless steel		Aluminium, other specified materials

**Figure 4-3.** Legend for Materials Selection Diagrams (stripes indicate lined/clad materials)(Billingham, Lee et al. 2011)

From a pure capital expense point of view, carbon steel will be ideal, because it is cheap but factor in corrosion leading to downtime, production losses, stainless steel is needed in parts of the plant like rich-amine piping, cross exchanger tubes and internals of the reboiler and stripper as can be seen in the figure above. Typical the absorber vessel in the amine system requires special consideration because of its size, estimated at 15 -20 m diameter and 50 m height and

runs at just over atmospheric pressure (Billingham, Lee et al. 2011). Because this is not strictly considered a pressure vessel, cement and tiling materials are leading candidates for absorber columns, but then again the internals as shown in the figure 4-2 and 4-3 is made up of a mixture of both carbon and stainless steel.

The stripper on the other hand can be considered a pressure-vessel and appropriate materials like stainless steel are used for the structure and internals. It is also an area, because of the mixture of high temperatures, pressure, amine degradation ions oxidizing and acidic, causes equipment failures brought about by corrosion of material.

Areas such as flow in piping and vessels, control valves etc. all need extensive attention to material selection criteria and suggested process conditions as has been reported by Dupart et al. (DuPart 1993).

To conclude, identifying where corrosion occurs in a potential process carbon capture plant will help in the choice of materials, increase options for construction for what is often very large scale plant, and the costs and practicality of maintenance or replacement (DuPart 1993). A technical solution with regards to corrosion and material selection will take into account balance between capital and operating costs, initial cost, service life, expected down-time and maintenance intervals (DuPart 1993), and detailed studies are required and this work seeks to fulfill part of that.

### **4.3 Heat Stable Salts**

One of the key objectives of this work is to investigate what kind of corrosion can be caused by a combination of DETA-CO<sub>2</sub> systems and that of a range of amine degradation products. The fundamental question here is what are these degradation products and how do they lead to the observed corrosion as reported in an earlier work (Hayfron-Benjamin 2012)? There are two well known phenomenon associated with amine loss via thermal and oxidative degradation. The details of the mechanism for the interested reader will be covered in chapter 5 covering the plausible paths for DETA thermal and oxidative degradation. Many authors have reported extensively on mainly MEA degradation and mechanism (Davis and Rochelle 2009; Supap, Idem et al. 2009; Epp, Fahlenkamp et al. 2011; Vevelstad, Eide-Haugmo et al. 2011) but DETA

has received some attention lately (Davis 2009). The degradation products such as oxalic, formic and carboxylic acids reacts with the amine solvent and forms what is known as heat stable salts (HSS). These are called heat stable because they are not regenerated in the amine stripping section and as such present degrees of corrosion issues with plant operation. For example, the literature abound with specific cases where HSS have been reported to cause great rates of corrosion. In an earlier project using stainless steel oxalate species were reported to have a high rate of 0.045 mm/yr after 330 hours on stream in a 30 wt% MEA-CO<sub>2</sub> ( $\alpha = 0.4$ ) system (Hayfron-Benjamin 2012). Others have also reported on HSS and their negative effects (DuPart 1993; Rooney, DuPart et al. 1997; Tanthapanichakoon and Veawab 2003; Meng, Zhang et al. 2008; Verma and Verma 2009; Saiwan, Supap et al. 2011; Supap, Idem et al. 2011). To recap, the literature has little information on HSS and DETA corrosion correlation and that is a major reason for this work, to provide a reference for future works.

#### **4.4 Process Parameters leading to Corrosion**

Possible CCS plant process conditions are the keys to understanding and effectively having a better corrosion control. Plants typically operate in high temperatures, low pressures, large volume flows conditions. The state of the amine solvent such as the concentration of DETA, the CO<sub>2</sub> loading, oxygen content and what kind of HSS in solution and other impurities will together constitute a range of process parameters that will affect the plant corrosion. SO<sub>2</sub> content in the flue gas composition, no matter how small it is on vol% basis also can have corrosive effects.

##### **4.4.1 Effect of O<sub>2</sub>**

Depending on the source of the flue gas and its composition O<sub>2</sub> content in the flue gas can be expected, especially in coal-fired power plants which are known to also contain CO<sub>2</sub>, N<sub>2</sub>, O<sub>2</sub>, SO<sub>2</sub> and NO<sub>2</sub>. In the presence of dissolved O<sub>2</sub> and the high temperatures high corrosion rates have been reported in parts of capture plants such as the heat exchanger, stripper and reboiler, reclaimers (S.F Bosen and Bedell 2004; Saiwan, Supap et al. 2011). It is understood that O<sub>2</sub> leads to oxidative degradation of amines, DETA, MEA and others, which forms HSS in solution and hence causes corrosion in those parts of the plant where the conditions are ripe for corrosion. It does not mean that without O<sub>2</sub> in the flue gas feed oxidative degradation cannot take place as

proved by Bello and Idem (Bello and Idem 2005; Saiwan, Supap et al. 2011). In general increasing the O<sub>2</sub> partial pressures lead to an increase in solubility and increase in O<sub>2</sub> concentration leads to a higher corrosion rate. For example Kladev, Idem and co-workers (Kladkaew, Idem et al. 2009; Kladkaew, Idem et al. 2009; Saiwan, Supap et al. 2011) reported in their work for carbon steel, that in 1-7 kmol/m<sup>3</sup> MEA, 0-100% feed gas O<sub>2</sub>, 0-204ppm SO<sub>2</sub>, 0-0.5 CO<sub>2</sub> and 30-80°C, a correlation which showed that by increasing the O<sub>2</sub> concentration, it leads to a higher corrosion rate. The correlation is as shown below (Saiwan, Supap et al. 2011).

$$corrosion\ rate = 1.77 \times 10^9 \left\{ \exp \left[ \frac{-5995}{T} \right] \right\} \times \{ [SO_2]^{0.0011} [O_2]^{0.0006} [CO_2]^{0.9} [MEA]^{0.0001} \} \quad 4-4$$

#### 4.4.2 Effect of CO<sub>2</sub>

High CO<sub>2</sub> absorption capacity of an amine solvent is ideal. Diethylenetriamine(DETA) has been reported by Ardi Hartono (Hartono 2009) to have a high loading as high as  $\alpha = 1.5$ . This loading capacity should lead to a decrease in in operating costs in CCS plants but with it comes an increase of ions in solution which leads to increased corrosion. High CO<sub>2</sub> in solution means that both H<sup>+</sup>/RNH<sup>+</sup> and bicarbonate HCO<sub>3</sub><sup>-</sup> will increase in concentration (Saiwan, Supap et al. 2011) and as will be shown in the theory of corrosion section in chapter 5, these species leads to the formation of corrosion products such as FeCO<sub>3</sub>.

#### 4.4.3 Effect of Temperature

Temperature is an essential parameter in kinetics. By altering the kinetics, temperature can shift the direction of many equilibrium reactions to favor CO<sub>2</sub> absorption, carbamate formation, hydrolysis of carbamate, pH of the solution (Saiwan, Supap et al. 2011) and solubility in general. The just mentioned reaction formations lead to corrosion and as such increasing solution temperatures increases corrosion rates. Examples abound in the literature, such as by comparing the corrosion rates on Stainless steel 316 of the an MEA-CO<sub>2</sub>( $\alpha = 0.4$ ) system at different temperatures, an earlier work showed higher rates than that of Nuria and Hallvard (Tavera-Valero and Svendsen 2011). This is because my earlier work was done at the elevated temperatures of 135 °C but Nuria and Hallvard (Tavera-Valero and Svendsen 2011) did theirs at 50°C.

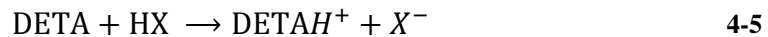
The fact that high temperatures causes higher corrosion rates is supported by the report that shows that the most corrosive part of a carbon capture plant is located at the hottest parts being, the cross exchanger's rich side, the reboiler and stripper sections and this was confirmed by the works of Gao et al. (Gao, Wang et al. 2012) who investigated areas in a pilot plant where corrosion rates are high and concluded that high corrosion rates occurs at the cross exchanger's side and the rich amine section coming out of the bottom of the absorber.

#### 4.4.4 Effect of amine concentration

As the concentration of the amine in solution increases, the corrosivity also should increase. This assertion is supported by data from earlier alkanolamine based treating gas plants (DuPart 1993) which are similar in process to carbon capture plants. In theory too, it can be explained by the fact that higher amine concentrations should mean that more CO<sub>2</sub> is absorbed (not on  $\alpha$  basis but just in pure numbers), leading to a greater amount of HCO<sub>3</sub><sup>-</sup> and CO<sub>3</sub><sup>2-</sup> which is responsible for the iron dissolution and hence corrosion (Kladkaew, Idem et al. 2009; Kladkaew, Idem et al. 2009).

#### 4.4.5 Effect of pH

In the presence of degradation products such as oxalic, carboxylic and formic acid, the pH of the DETA system will invariably change according to the reaction due to the changes in concentration of protons H<sup>+</sup>



Where HX represents a weak acid as listed above.

From the acid-base theory, should the pKa of the weak acid be much less than the solution pH, the acid in question will behave as a strong acid leading to all the protons of the acid reacting with the DETA to form heat stable salts and increasing the corrosion rates. The formula below shows the link between pKa and pH:

$$pH = pKa - \log \frac{[\text{DETAH}^+]}{[\text{DETA}]} \quad 4-6$$

[DETAH<sup>+</sup>] refers to the added acid concentration (diprotic acids such as oxalic acid have twice the number of protons as monoprotic acids like acetic and formic acid). It should be noted that at room temperature, pH depends solely on the total acid concentration regardless of the degree of protons in the acid. For higher temperatures the correlation of pH from the equation above becomes complicated due to different equilibrium equations, and much higher solution ionic strengths (Rooney, DuPart et al. 1997).

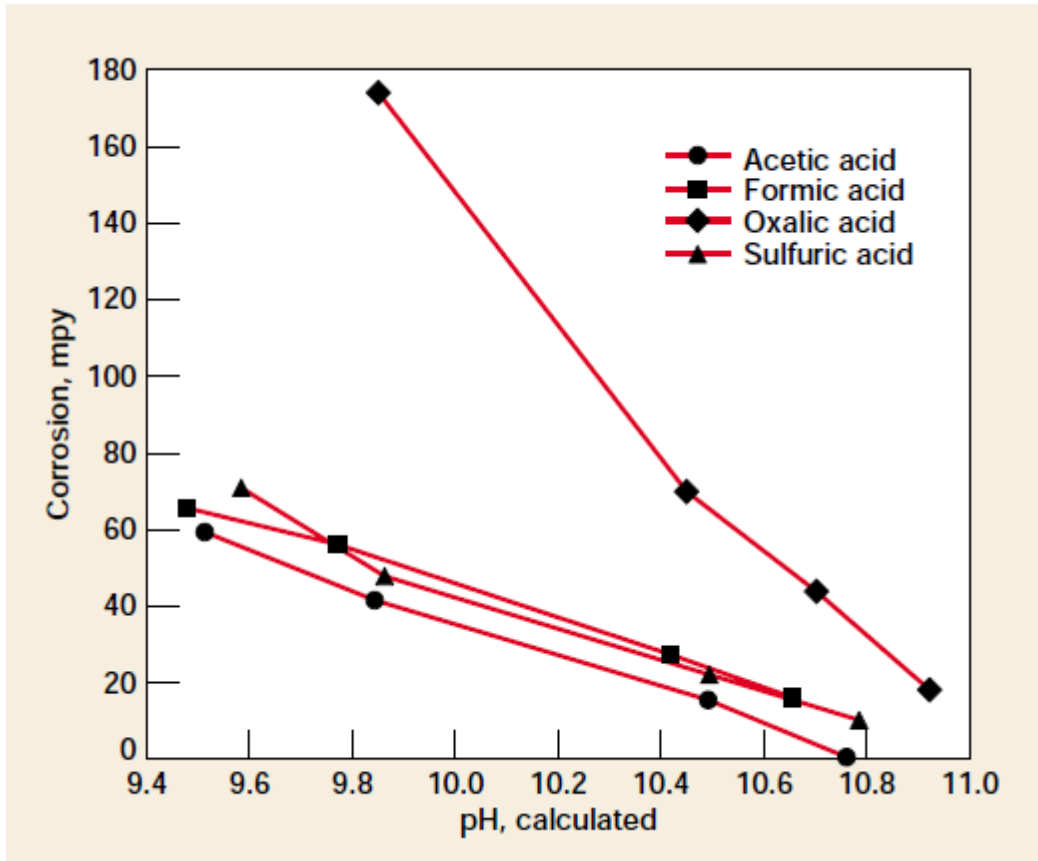


Figure 4-4. Corrosion rates and pH correlation (Rooney, DuPart et al. 1997)

For a particular temperature, corrosivity decreases with increasing pH as shown in figure 4-4 for a test done for carbon steel at 120°C typical stripper conditions and in MDEA solution (Rooney, DuPart et al. 1997).

This work will correlate the pH of the DETA-CO<sub>2</sub> systems and from a diagram known as Pourbaix, conclusions can be drawn. It will be the first work in the open literature as far as I know.

#### **4.4.6 Effect of amine solution conductivity**

Contrary to the perception that amine solutions with higher conductivity might result in higher measured corrosion rates (corrosion is an electrochemical process), it is however proven that there exists little correlation of conductivity and corrosion. Rooney et.al gave a detailed analysis on this subject (Rooney, DuPart et al. 1997).

#### **4.4.7 Effect of make up water**

The presence of chlorides and other ions in solution leads to corrosion, so the type and source of process make-up water is vital to preclude the aforementioned ions. Generally it is recommend that deionized water be used in capture plants (DuPart 1993).

#### **4.4.8 Effect of corrosion Inhibitors**

If the possible carbon capture plant process employs the use of corrosion inhibitors, research has shown that the earlier generation heavy metal based inhibitors such as arsenic and vanadium are not benign to the environment. In addition newer inhibitors based on amine film formed structures are also not stable and can lead to further corrosion (DuPart 1993).

## **Chapter 5 Theory**

### **5.0 Introduction**

This chapter will seek to explain the fundamental principles underlining corrosion in aqueous carbon dioxide (CO<sub>2</sub>) and amine environment. More importantly what are the basic thermodynamic and kinetic principles underpinning metal corrosion which in fact is an electrochemical reaction. The use of thermodynamic tools such as the Pourbaix diagrams and kinetic data diagrams like the Tafel plots are introduced to the reader. These tools will be used to analyze the data collected in the experimental section of this work. Also it will be used to interpret the electrochemical data and answer the basic question of what the extent of corrosion of stainless steel 316L is.

### **5.1 Aqueous Corrosion Theory**

#### **5.1.1 Introduction**

The ability to fully define what environment corrosion takes place is a key step in understanding the fundamental mechanisms by which the process proceeds. Water-based systems are used in most chemical processes such as carbon, capture and storage. For example different amounts of reagent grade water is used to prepare amine solutions for testing in the laboratory. In this work 25wt% (based on water as solvent) of diethylenetriamine solutions were used in all the experimental runs. Hence corrosion of metals in a water based system will aptly describe what is observed in this work.

The theory of aqueous corrosion is best understood in two broad concepts: thermodynamics and kinetics. In corrosion science, thermodynamics in the form of Pourbaix or E-pH diagrams, are used to evaluate the theoretical activity of a given metal or alloy. The investigation, it must be pointed out, should include realistic corrosive environment for the metal because an experiment is useless for life-time prediction and integrity of materials, if it only investigates nominal conditions without consideration of local effects such as flow, pH cells, deposits and galvanic effect (Roberge 2000). The inclusion of a realistic corrosion medium is even more important

when the modeling and prediction of corrosion comes into play as will be explained in the corrosion modeling section (chapter 9).

Corrosion by definition is the metal ions dissolution at the anode of an electrochemical cell at a rate chemically equivalent to the reaction at the cathodic areas. For iron(Fe)-based alloys such as stainless steel 316L as used in this project, a schematic of the corrosion process is shown in figure 5-1 as well as the electrochemical redox reactions in equations 5-1 to 5-6 below:

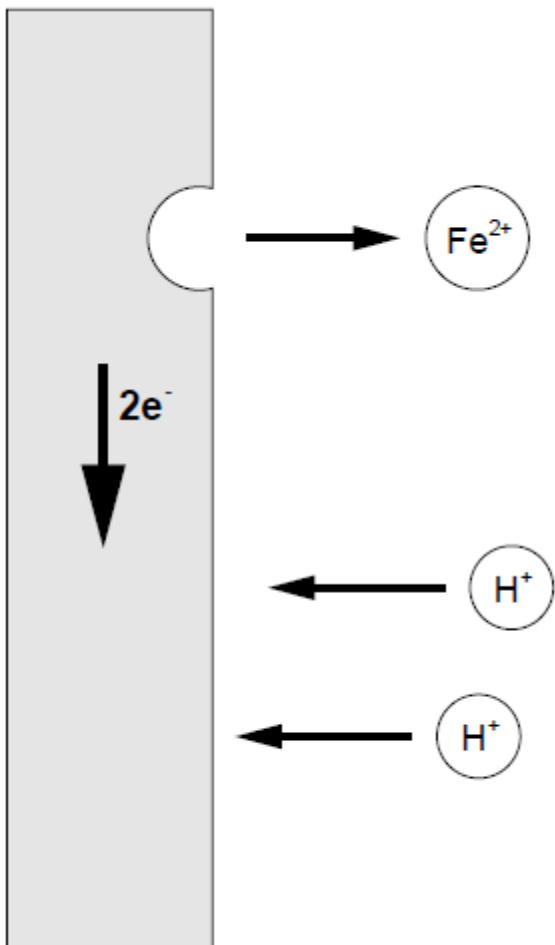


**Figure 5-1.** Schematic of model description of electrochemical nature of corrosion of process (Roberge 2000)

Anode oxidation reaction:

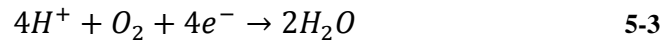


In the absence of oxygen O<sub>2</sub> (deaeration), cathode reaction:

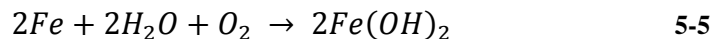


The reaction shown above is controlled by the cathodic reaction (i.e. cathode reaction is slower than the anode reaction), hence the cathode reaction is the rate determining step.

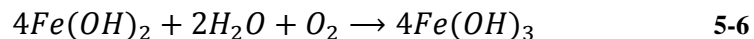
The cathodic reaction is obviously faster in acidic medium than neutral or alkaline medium. This is simply due to the presence of protons in acidic environments. The cathodic reaction is also further accelerated via reduction of dissolved O<sub>2</sub> in a process called depolarization:



Adding the above equations: (5-1) + (5-3) + (5-4) yields:



The ferrous hydroxide Fe(OH)<sub>2</sub> or FeO.nH<sub>2</sub>O species shown above is green to greenish black in appearance on corroded Iron metal surfaces. This same species acts like a diffusion barrier layer and is an important factor in kinetic considerations of corrosion theory. Upon further oxide film reaction with H<sub>2</sub>O/O<sub>2</sub> a new rust layer is formed:



The ferric hydroxide ( $\text{Fe}(\text{OH})_3$ ), orange to red-brown in color, thus formed undergoes a number of phase transformations and one of the phase structures is  $\alpha - \text{Fe}_2\text{O}_3$  (hematite, a non-magnetic species).

In conclusion in aqueous solutions, corrosion of Fe based metals results in a three layer of iron oxides in different states of oxidation as schematically shown in figure 5-2 below:

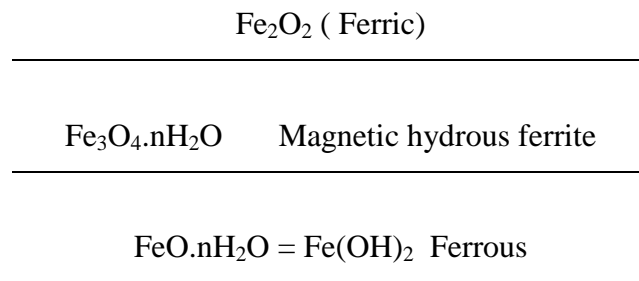


**Figure 5-2.** Rust layers found on corroded metal surfaces

### 5.1.2 Thermodynamics- Potential-pH (Pourbaix) Diagrams

Two fundamental parameters, pH and corrosion potential can be derived from corrosion in aqueous medium and these parameters provide little information about the kinetics but much about the thermodynamic boundaries for important corrosion species and reactions. A representation of potential versus pH is a common tool in electrochemical corrosion studies and these types of diagrams are known as Pourbaix.

In order to understand how thermodynamic information is gleaned from a typical E-pH diagrams, a look at figures 5-3 , 5-4, 5-5 (Roberge 2000) below is used to explain what the different thermodynamic boundaries means for corrosion of steels.

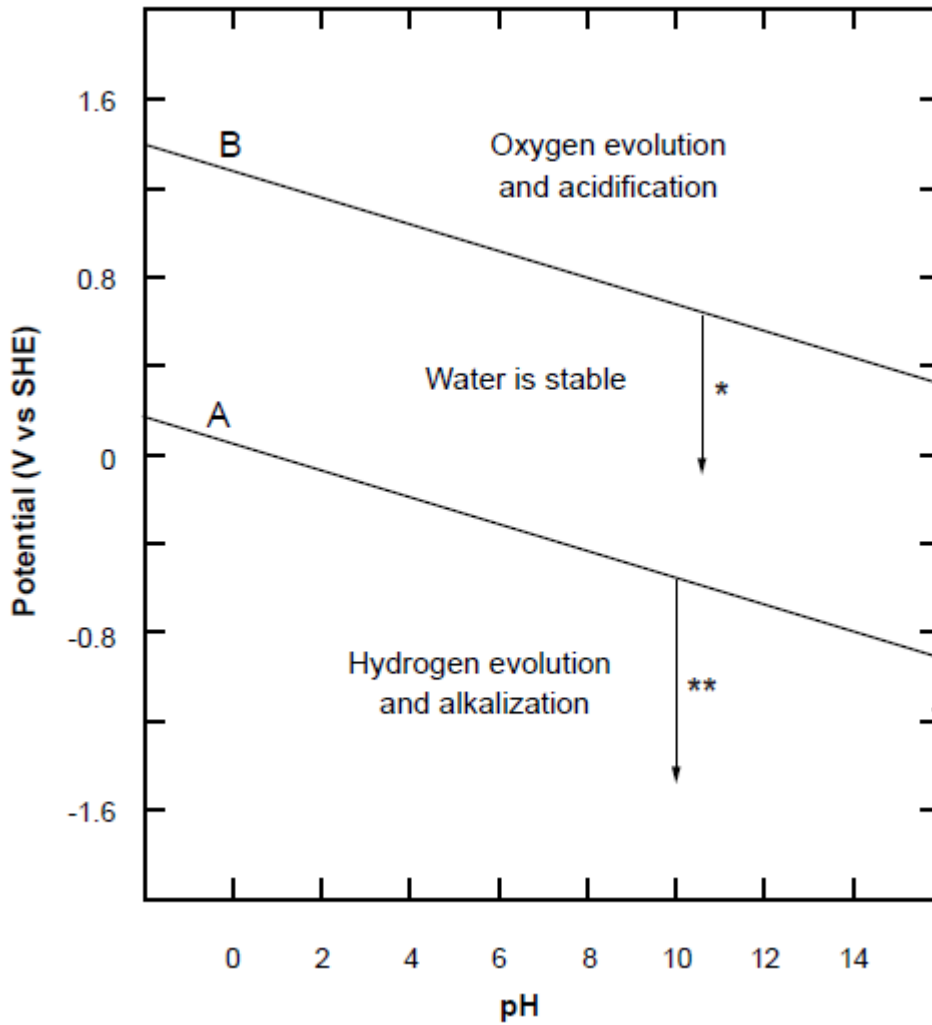
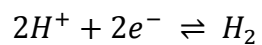


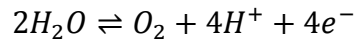
**Figure 5-3.** E-pH stability diagram of water at 25°C (Roberge 2000)

In figure 5-3 it shows the thermodynamic stability of oxygen, water and hydrogen, all three species that take part in corrosion electrochemical reactions in aqueous medium as explained earlier. Equilibrium line A represents the cathodic reaction



5-7

whereas equilibrium line B represents:



5-8

Also from the figure in question, by decreasing the potential (in the direction of the arrows and \* shown) pushes the systems towards an increasing thermodynamic driving force first for cathodic oxygen reduction (\* as potential falls below equilibrium line B) and then for cathodic hydrogen evolution (\*\* as potential falls below equilibrium line A).

In essence by having such diagrams, observed corrosion behavior (i.e. measuring the changing potentials and p-H of alloys such as stainless steel 316L in aqueous medium) can be superimposed on a Pourbaix diagram and then important thermodynamic boundaries can be established for the key corrosion species and reaction. In this light, by carrying out polarization resistance testing on steel for example, resulting superimposed figure looks like figure 5-4 below. In this figure important features of corrosion such as uniform corrosion, severe and mild pitting and passivation are clearly demarcated. This then gives the engineer a thermodynamic information about which boundaries the material (steel) can used in a process situation to avoid loss and degradation of material and hence a dent in capital expenditure.

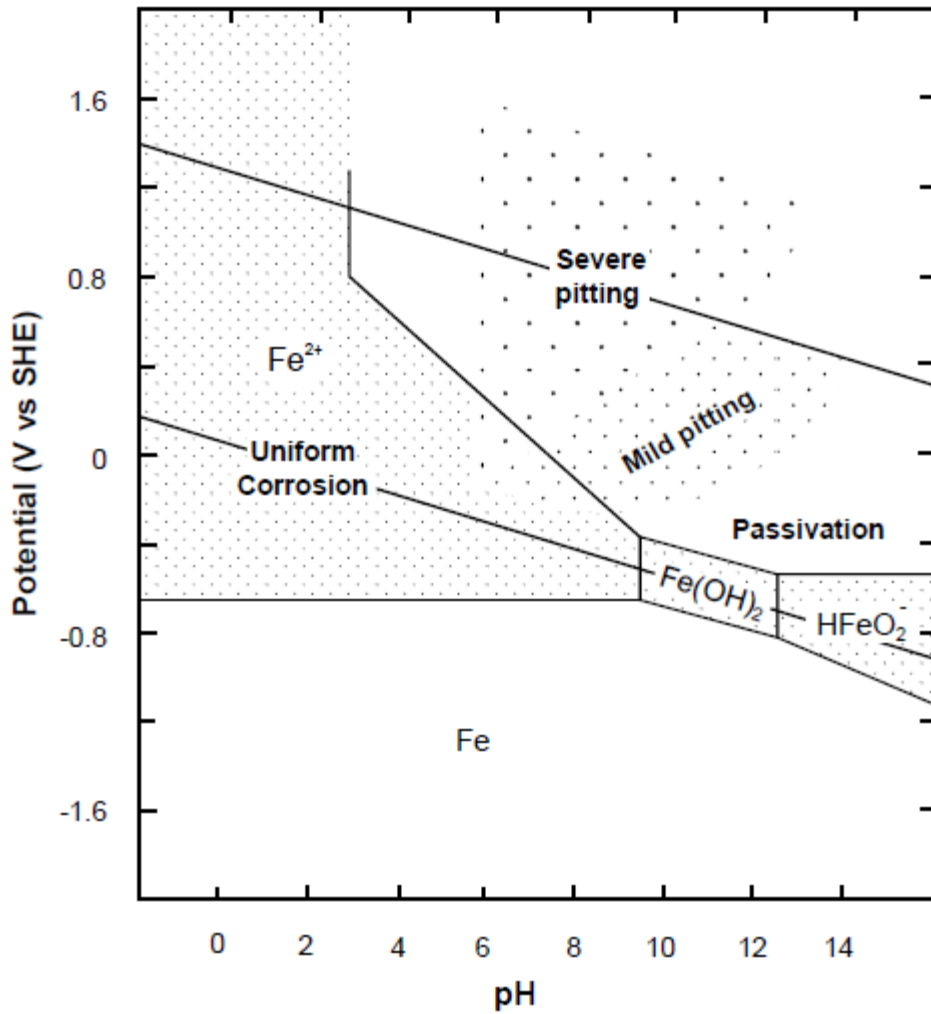


**Figure 5-4.** Thermodynamic boundaries of the types of corrosion observed on steel (Roberge 2000)

Finally Pourbaix diagrams in combination with kinetic data can be used to illustrate how corrosion rates are related to the measured potentials and p-H of steel. In figure 5-5 both kinetic (corrosion rates) and thermodynamic are used to paint a clear picture of what takes place in corrosion. How the kinetic data is obtained is tackled in the next section.

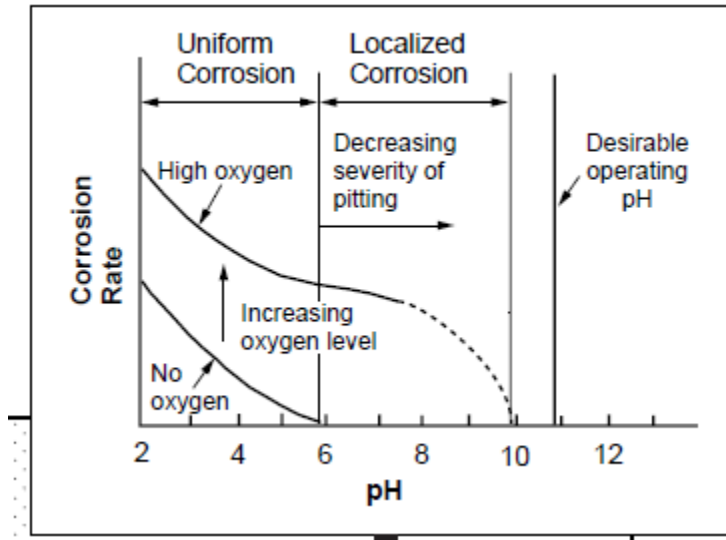


**Figure 5-5.** Observed corrosion behavior of Iron in water and pH correlation (Roberge 2000)

### 5.1.3 Kinetic Consideration

Thermodynamic principles can be used to explain observed corrosion process in terms of the stability of chemical species and reactions associated with the process. But thermodynamic calculation are limited with regards to prediction of corrosion rates. Electrode kinetic principles are thus used to predict corrosion rates and hence quantify the observed corrosion. This is another important piece of the corrosion puzzle.

From kinetics observed at equilibrium, a fundamental parameter known as the exchange current  $I_0$ , which is a characteristic of electrode behavior must be defined. The exchange current is defined as the rate of oxidation or reduction at equilibrium electrode expressed in terms of current (Roberge 2000).

From the reversible equilibrium reactions at the anode:



At equilibrium

$$I_a + I_c = 0 \quad 5-11$$

$$I_a = -I_c = I_o \quad 5-12$$

Where the exchange current  $I_o$  is determined experimentally. In practice a normalization of  $I_o$  is preferred resulting in current density where:

$i$  = current density (normalized exchange current),

$$i = \frac{I_o}{\text{surface area}} \quad 5-13$$

$$i = f(\text{Electrode, conc. (DETA), surface roughness, impurities}) \quad 5-14$$

### **5.1.3.1 Kinetics under polarization**

Quite often to be able to generate current in order to measure the exchange current  $I_o$  as described earlier on, a technique known as polarization is undertaken. Polarization is basically the deviation of electrode potential from its equilibrium potential. The applied deviation potential causes current to flow from the electrodes and thus exchange current can be quantified. Details of polarization are given in the methodology section (chapter 6). The magnitude of polarization is represented by the parameter  $\eta$  (positive for anodic polarization and negative for the cathode side). In anodic polarization the metal surface is driven towards the anodic side of the electrochemical reaction and loses electrons (Saiwan, Supap et al. 2011). The graphical picture of the processes occurring during polarization is shown in figure 5-6 below:

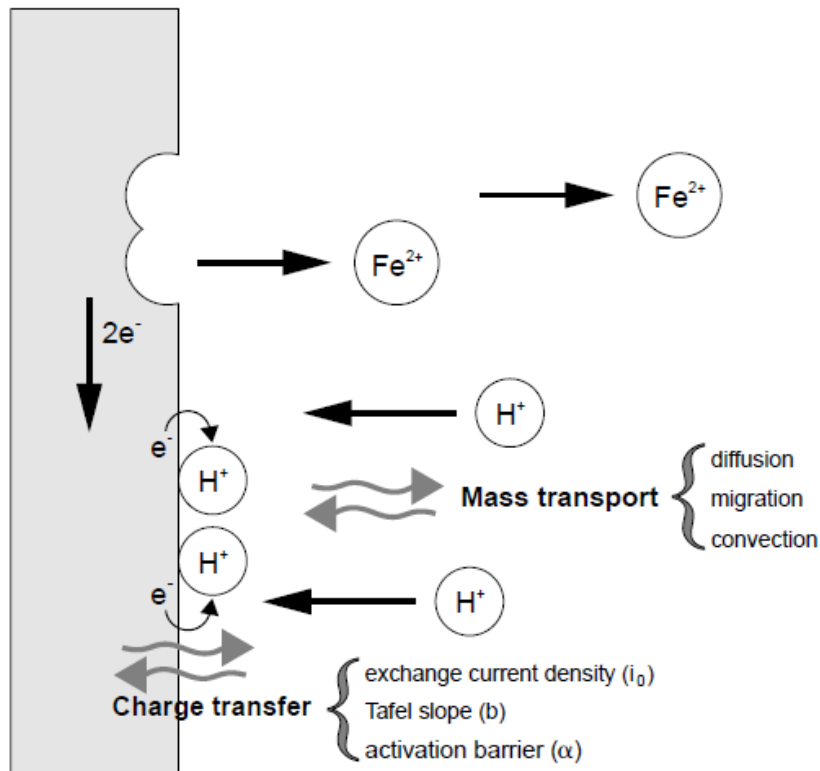


**Figure 5-6.** Graphical Representation of the processes occurring at an electrochemical interface (Roberge 2000)

In the figure above mass transport as per related to the corrosion process, charge transfer and metal dissolution are graphically represented. Details of governing equations and mass transport to the metal surface limitation regions can be found in Roberge's Handbook of corrosion engineering (Roberge 2000).

Once the kinetic data is obtained, it can be represented in the form of informative graphical forms known as Evans diagram or polarization diagrams or mixed-potential diagrams or Tafel plots. In the electrochemical part of the experimental section of this work, numerous such figures were obtained and their interpretation per related to corrosion rates calculation are given in the results and discussion section (chapter 8).

From a typical ideal Tafel plot like figure 5-7 below, there are two regions of interest: the anodic and cathodic processes, each represented by a straight line of opposite signs (positive for the anode and negative slope for the cathode). The intersection of the two slopes gives both the

corrosion potential ( $E_{corr}$ ) also sometimes known as rest potential and corrosion current  $i$ . Hence to calculate the corrosion rate (C.R) the following equations (Roberge 2000) are used:

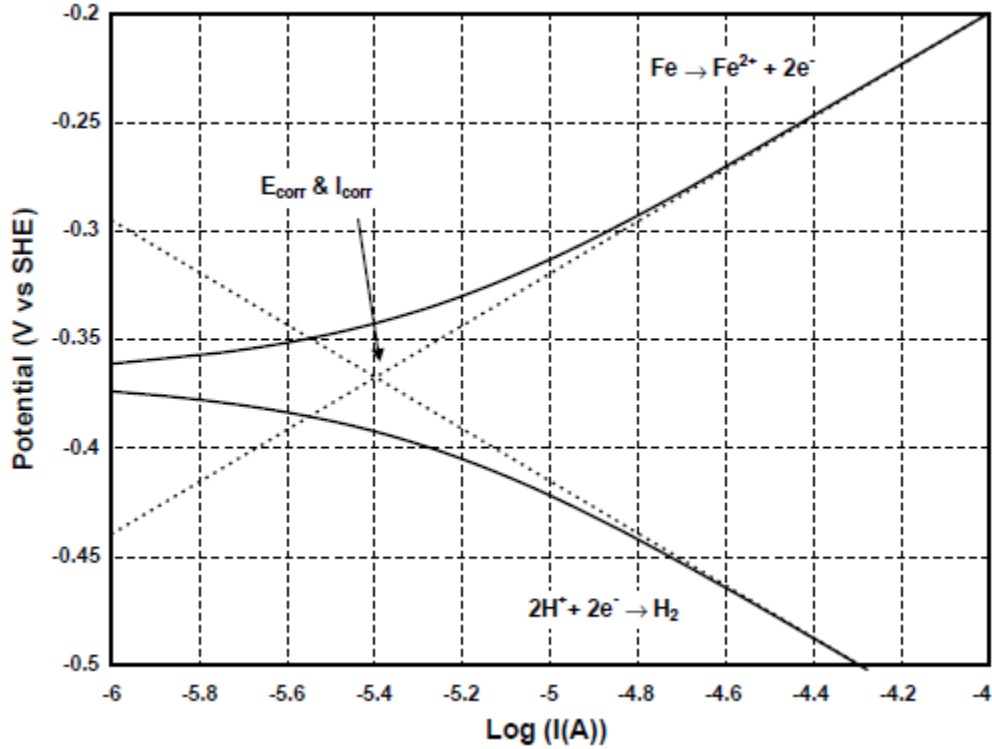


Figure 5-7. Tafel Plot from polarization technique (Roberge 2000)

$$C.R = \frac{0.13(i_{corr} * EW)}{d} \quad 5-15$$

where C.R = corrosion rate (mils per year),  $i_{corr}$  = current density( $\mu\text{A}/\text{cm}^2$ ), EW = equivalent weight (M(molecular weight))/(charge(Z)), d = density

Faraday's law (linear relationship) between metal dissolution rate or corrosion rate and the corrosion current  $i_{corr}$  can also be used to estimate corrosion rates (MetrohmAutoLab)

$$C.R = \frac{M * i_{corr}}{n.F.d} \quad 5-16$$

where C.R=corrosion rate (mm/yr),  $i_{corr}$  = current density ( $\mu\text{A}/\text{cm}^2$ ), F = Faraday's constant = 96.485 C/mol, d = density, M/n = equivalent weight, where n represents the number of electrons exchanged in the dissolution reaction.

Corrosion currents can be estimated using Tafel slope analysis as will be shown in the discussion part of the work.

One should note that the size of the anodic area is often inversely related to the severity of corrosion problems. That is the smaller the anodic area (corresponds to low corrosion rates) or higher ratio of cathode area/ anode area will often lead to low corrosion rates but high incidents of localized corrosion like pitting.

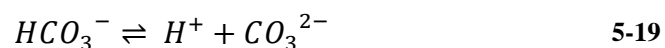
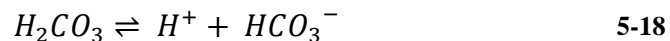
## 5.2 CO<sub>2</sub> Corrosion Mechanism

### 5.2.1 CO<sub>2</sub>-H<sub>2</sub>O-pH Chemistry

CO<sub>2</sub> dissolves in water and becomes partly hydrated according to the equation:

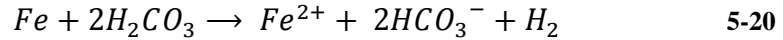


Diprotic dissociation (Hartono, da Silva et al. 2006)

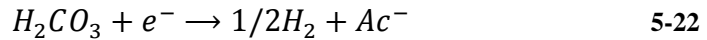


Changes in pH as a result of the presence of  $\text{HCO}_3^-$  and  $\text{CO}_3^{2-}$  is a function of the CO<sub>2</sub> partial pressures ( $P_{\text{CO}_2}$ ) and hence pH increasingly becomes acidic with increasing  $P_{\text{CO}_2}$  leading to more dissolution of iron at higher partial pressures of CO<sub>2</sub>.

The presence of the above species influences corrosion according to the overall equation:



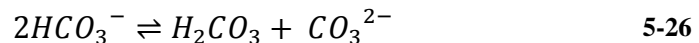
The overall equation can be explained in terms of electrochemical reactions at the surface of the metal. In the presence of CO<sub>2</sub>, 3 main cathodic reactions occur:



H<sub>2</sub>CO<sub>3</sub> has been identified as the main cathodic reactant in CO<sub>2</sub> corrosion (Nesic, Postlethwaite et al. 1996; Pletcher and Garsany 2003; Sun, George et al. 2003; Dugstad 2006). In addition “the presence of CO<sup>2</sup> affects cathodic reactions by altering the proton [H<sup>+</sup>] concentration and amount of H<sub>2</sub>CO<sub>3</sub> undissolved” (Dugstad 2006). Furthermore at low P<sub>CO2</sub> partial pressures and high pH (Delahay 1952; Ogundele and White 1987; L. G. S. Gray, B. G. Anderson et al. 1990; Nesic, Postlethwaite et al. 1996) further additional reactions are observed to be important:



In situation where corrosion rates (currents) are observed at pH > 6, that could be due to regeneration of H<sub>2</sub>CO<sub>3</sub> by the bicarbonate reduction (S. Turgoose, and et al.):

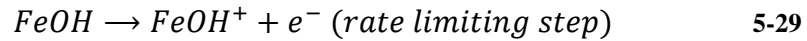
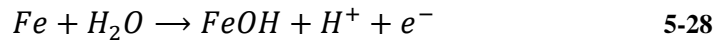


### 5.2.2 Anodic Reactions

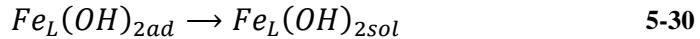
Iron dissolution at the anode as previously mentioned is given by the equation:



The above anode reaction is strongly pH dependent and for low pH (strong acids, which is applicable to CO<sub>2</sub> corrosion) the following mechanism has been suggested by Brockris et al. (Bockris, Drazic et al. 1961):

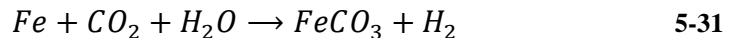


For pH < 4,



The only drawback to the above proposed mechanism is that qualitative determination of some of the intermediate species is yet to be determined. This inconclusive affirmation of aqueous-CO<sub>2</sub> systems corrosion of steel points to a yet-to-be understood mechanisms. That is the mechanisms involved are still being debated in various research groups around the world.

However the fundamental aspects of CO<sub>2</sub> corrosion have been confirmed by various authors such as Riesenfeld and Blohm (F.C. Risenfeld and Blohm 1950; Kladkaew, Idem et al. 2009) who were the first to recognize CO<sub>2</sub> as a primary cause of steel corrosion. For amine solutions, they suggested that the corrosion was associated with an evolution of CO<sub>2</sub> from the rich amine solution, hence the observed high corrosion rates in the stripper section of an amine absorption plant, where rich amine is readily found. They proposed the following:



This pH dependency corrosion reaction decreased rapidly with increasing pH (S.Nesic 2004). For example reaction order with respect to OH<sup>-</sup> (as represented in the kinetic equation 5-33 below) was 2 at low pH but progressively decreases to 1 and eventually 0 at pH > 4 (Nesic, Drazic et al. 1996).

Iron dissolution current density (Nesic, Drazic et al. 1996):

$$i_a = k[OH^-]^{a_1} P_{CO_2}^{a_2} 10^{\frac{E}{b_a}} \quad 5-33$$

Where (Dugstad 2006)

pH < 4    a<sub>1</sub> = 2, b<sub>a</sub> = 0.03V per decade

4 < pH < 5    a<sub>1</sub> = 2-0    b<sub>a</sub> = 0.03-0.12 V per decade

pH > 5    a<sub>1</sub> = 0.12V per decade

P<sub>CO<sub>2</sub></sub> < 10<sup>-2</sup> bar    a<sub>2</sub> = 0

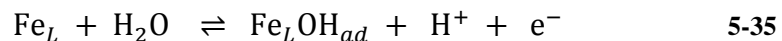
10<sup>-2</sup> < P<sub>CO<sub>2</sub></sub> < 1bar    a<sub>2</sub> = 1

P<sub>CO<sub>2</sub></sub> > 1 bar    a<sub>2</sub> = 0

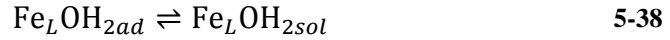
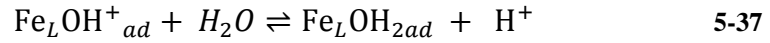
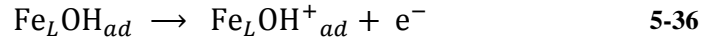
Another dimension using surface mechanisms has been proposed by (Dugstad 2006) for corrosion (corrosion currents) above pH > 5. In that mechanism, corrosion occurs via a series of surface reaction involving adsorbed species and more:



where Fe<sub>L</sub> is the adsorbed species, Fe-CO<sub>2</sub> at the electrode surface that catalyzes the dissolution of the iron.



The rate limiting step, ie. slowest step:



It is easily seen that the above mechanisms (equations 5-24 to 5-39) are akin to the major steps in catalysis i.e. the species are adsorbed on the surface, they react to form products on the surface, the products desorb from the surface and the catalyst return to their original state.

In other works for proposed mechanisms by which CO<sub>2</sub> corrosion occurs, by using mechanistic models, Amornvadee and Aroowilas (Veawab and Aroonwilas 2002) postulated that HCO<sub>3</sub><sup>-</sup> and H<sub>2</sub>O were the primary oxidizing agents with HCO<sub>3</sub><sup>-</sup> contributing to significant corrosion because of its high rate of reduction as previously stated under the cathodic reactions in this this section.

To conclude the section, the question that arises is that of the relationship between the observed corrosion in DETA-H<sub>2</sub>O-CO<sub>2</sub> systems as investigated in this work and that of the various mechanisms postulated in the literature. This question is relevant because as stated in the introduction chapter, diethylenetriamine (DETA) for CO<sub>2</sub> absorption is not yet widely used and in addition information about the amine speciation and other characterizations are lacking (at least those pertaining to corrosion). Therefore in order to give a fundamental and plausible mechanisms for DETA-H<sub>2</sub>O-CO<sub>2</sub> corrosion as experimentally observed in this work and others (Kongstein 2010), it is key to be able to use techniques to identify species in the DETA-H<sub>2</sub>O-CO<sub>2</sub> system. By thus identifying the species, we can fit the observed species into existing corrosion models as described also in this section. The answer to the above posed question can be found in the work of Ardi Hartono et. al (Hartono, da Silva et al. 2006), which is one of the few works in the literature on DETA. In that work they used Nuclear Magnetic Resonance (NMR) technique to determine which species are formed in a DETA-H<sub>2</sub>O-CO<sub>2</sub> solution. The

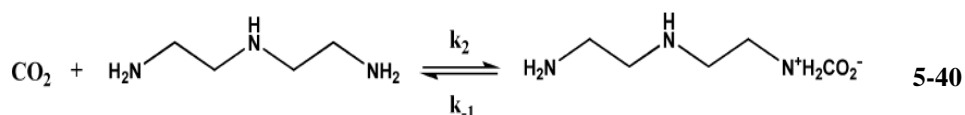
objective of that work is special in the sense that “determination of the species formed is a first step to understanding the chemistry of the systems and this a needed stage in the development of a thermodynamic model” (Hartono, da Silva et al. 2006). In the aforementioned NMR work,  $^{13}\text{C}$  NMR spectroscopic investigations was carried out on aqueous solutions of diethylenetriamine(DETA) and carbon dioxide with loadings ( $\alpha = 0 - 1.69$ ), the conclusion of the work revealed that 24 potential species were accounted for and the dominating species were suggested to be carbamate, dicarbamate and  $\text{HCO}_3^-/\text{CO}_3^{2-}$  species (Hartono, da Silva et al. 2006). The dominating presence of  $\text{HCO}_3^-/\text{CO}_3^{2-}$  will thus give credence and fit into the existing corrosion mechanisms postulated by the various authors as has been outlined in this chapter and section.

### 5.3 DETA–CO<sub>2</sub> Absorption Mechanisms

#### 5.3.1 Kinetics

There are two well established mechanisms for the absorption of CO<sub>2</sub> in aqueous amine solutions (Hartono 2009). These two are the zwitterion (named after the German word for double (second) ion) and termolecular mechanisms, all named after the type of ion formed.

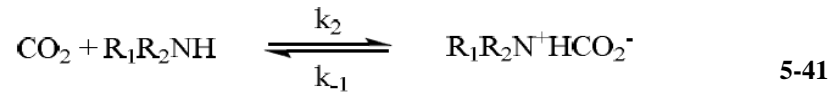
Zwitterion mechanism:



##### 5.3.1.1 Zwitterion mechanism

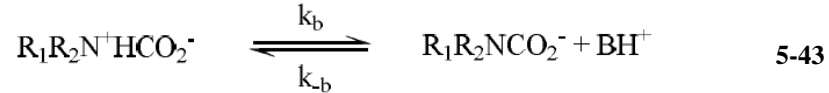
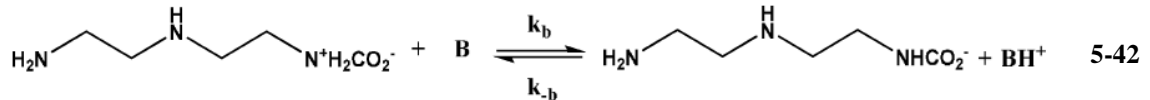
The zwitterion mechanism as per proposed by Caplow (1968) and Danckwerts (1979) (Caplow 1968; Danckwerts 1979; Hartono 2009) consists of two steps (Hartono, da Silva et al. 2009).

First the formation of the zwitterion:



Where for DETA,  $\text{R}_1, \text{R}_2$  depending on the position of the amino groups could be -  $\text{CH}_2(\text{NH})\text{C}_2\text{H}_4(\text{NH}_2)$ , - H respectively and in that case be considered a primary DETA. For secondary DETA, the respective amine groups are  $\text{R}_1 = -\text{C}_2\text{H}_4(\text{NH}_2)$  and  $\text{R}_2 = -\text{C}_2\text{H}_4(\text{NH}_2)$ .

The second step of the zwitterion mechanism involves the deprotonation of the formed zwitterion by a base species. Here the base could be either water ( $\text{H}_2\text{O}$ ) or another molecule of DETA acting as a base.



In addition, depending on which reaction is rate determining step, a mixture of first-order dependency and broken-order kinetic equations with respect to amine and  $\text{H}_2\text{O}$  has been reported as shown in equation 5-44 below (Hartono 2009; Hartono, da Silva et al. 2009):

$$-r_{\text{CO}_2}^z = k_2 [\text{DETA}][\text{CO}_2] \quad 5-44$$

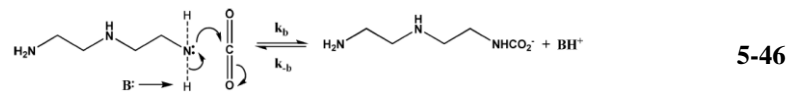
And for broken order kinetics:

$$-r_{\text{CO}_2}^z = \{k_{\text{DETA}}^z [\text{DETA}] + k_{\text{H}_2\text{O}}^z [\text{H}_2\text{O}][\text{DETA}][\text{CO}_2]\} \quad 5-45$$

Further kinetic details of amines such as DETA is found in the work of Ardi Hartono (Hartono 2009)

### 5.3.1.2 Termolecular Mechanism

This CO<sub>2</sub> amine absorption mechanism was originally put forward by Crook and Donnellan (1989) (Crooks and Donnellan 1989; Hartono 2009) and in this mechanism a loosely bound complex is formed by the simultaneous events of amine-CO<sub>2</sub> bonding and proton transfer (Hartono 2009). The complex formed subsequently undergoes charge separation. The Termolecular mechanism has been confirmed by da Silva and Svendsen (2004) (da Silva and Svendsen 2004; Hartono, da Silva et al. 2009) from first principle calculations and solvation modelling. The complex carbamate formation is shown in equation 5-46 below:



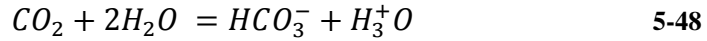
The proposed rate equation (Hartono 2009; Hartono, da Silva et al. 2009) has been assigned to this mechanism and with simplifying assumption can be written as shown in equation 5-47:

$$(-r_{\text{CO}_2}^T) = \{k_{\text{DETA}}^T[\text{DETA}] + k_{\text{H}_2\text{O}}^T[\text{H}_2\text{O}]\}[\text{DETA}][\text{CO}_2] \quad 5-47$$

So in essence, by having a fundamental understanding of the kinetics of any compound (DETA in this case), a better grasp of the observed effects or phenomenon (such as corrosion, mass transfer etc.) of amine in plants can be well accounted for. For example in corrosion characterization via electrochemical techniques as explained in section 5.1.3, showed that kinetics play a big factor in determining the magnitude and understanding of corrosion current ( $i_{\text{corr}}$ ). This parameter ( $i_{\text{corr}}$ ) is used to calculate the corrosion rates. Hence the relevance of having better kinetics fundamentals of an amine such as DETA can not be underscored. Sadly DETA characterization information in the open literature is scarce.

The reported additional reactions that occur in DETA-H<sub>2</sub>O-CO<sub>2</sub> systems include the hydration of CO<sub>2</sub> and bicarbonate formation (Hartono, da Silva et al. 2009).

CO<sub>2</sub> hydration:



Bicarbonate formation:



The ions HCO<sub>3</sub><sup>-</sup>, OH<sup>-</sup>, H<sub>3</sub><sup>+</sup>O all play a part in stainless steel corrosion and has been thoroughly explained in the corrosion theory section (chapter 5) and the reader is referred to that section for further explanation.

From the conclusion drawn by the work of Ardi et al. (Hartono, da Silva et al. 2009) it was reported that for a polyamine such as DETA, it has the fastest rate of reaction among amines (exception being Piperizine). For example as compared to MEA (Hartono, da Silva et al. 2009):  $k_{obs}^{MEA} = 5.3 * 10^{-4} /s$  and  $k_{obs}^{DETA} = 17 * 10^{-4} /s$ . So DETA is almost three times faster in kinetics than MEA. DETA also has the lowest reported activation energy ( $\Delta E$ ). Again comparison with the benchmark solvent MEA paints a contrasting and clear picture:  $\Delta E_{MEA} = 36.6kJ/mol$  (Aboudheir, Tontiwachwuthikul et al. 2003) and  $\Delta E_{DETA} = 32.2kJ/mol$  (Hartono 2009; Hartono, da Silva et al. 2009) coupled with the high absorption rates, which increases with increasing temperatures, has made diethylenetriamine (DETA) a promising solvent for CO<sub>2</sub> capture (Hartono, da Silva et al. 2009) but with such promise comes the major drawback of corrosion of plant material like stainless steel. This assertion that DETA highly corrodes can be on qualitative terms be understood by viewing the high absorption rates of DETA as a source of corrosive agents like HCO<sub>3</sub><sup>-</sup>, OH<sup>-</sup>, H<sub>3</sub><sup>+</sup>O. All these agents have been mentioned in the theory of steel corrosion in CO<sub>2</sub>-amine environment.

## 5.4 DETA Degradation and Corrosion

### 5.4.1 Introduction

Amine degradation which can be divided into oxidative and thermal degradation are common occurrences in CO<sub>2</sub> capture amine plants. Oxidative degradation, due to the presence of dissolved oxygen (O<sub>2</sub>) occurs in the absorber and thermal degradation occurs in heat critical locations like the cross-exchange and stripper. Oxidative degradation results in the oxidation and fragmentation of the amine molecule, which then forms heat stable salts (HSS), these salts acting as precursors of corrosive agents for plant equipment corrosion. It should be mentioned that oxidative degradation is not normally present in current applications of amine absorption and stripping such as natural gas treating and hydrogen production since significant O<sub>2</sub> is not present (Davis 2009).

Three quarters of thermal degradation in the stripper occurs in the reboiler due to the elevated temperatures and long residence times which offset the decrease in CO<sub>2</sub> concentration compared to the packing (Davis 2009). Among amines, thermal degradation has a particular order, depending on the type of amine structure. Degradation increases in the order: cyclic amines with no side chains (PZ) < long chain alkanolamines (AEEA) < alkanol amines with steric hindrance (AMP) < tertiary amines (MDEA) < MEA < straight chain di and triamines (DETA, EDA). From the list it is no wonder that diethylenetriamine (DETA), a straight chain triamine, has over 90% loss (6% remaining) at 135°C for just a period of only 4 weeks on stream (Davis 2009).

Thermal degradation due to high temperatures proceed via carbamate polymerization resulting in higher molecular weight products being formed (Davis 2009) (1-(2-aminoethyl)imidazole). In the experimental section in this work, after corrosion testing at 135°C, the viscosity of DETA was visibly increased as compared to MEA under the same conditions.

To minimize the effects of HSS on process dynamics and corrosion, sometimes a semi-batch thermal distillation process is applied to remove these HSS as shown in figure 5-8 (Wonder, Balke R.J. et al. 1959; Davis 2009).

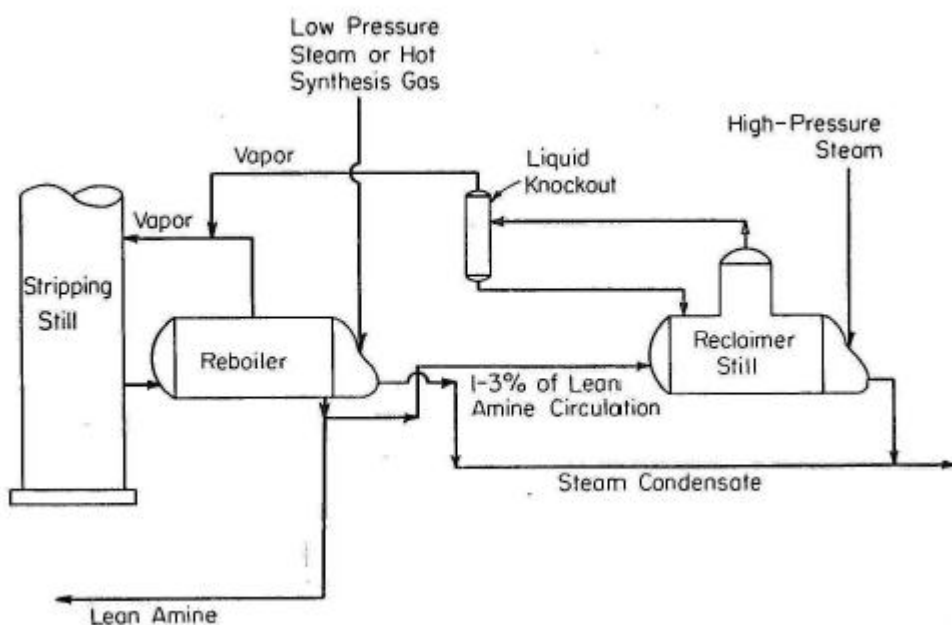


**Figure 5-8.** Semi-batch thermal distillation process applied to remove Heat Stable Salts (Wonder, Balke R.J. et al. 1959)

In this process of reclaiming the heat stable salts which are mostly found in the stripper, a feed stream from the “stripper bottoms is fed to a distillation vessel and concentrated until the concentration of MEA in the vapor phase is equivalent to the amount in the feed stream. The pressure of the unit is matched to the stripper pressure and the overheads are returned to the stripper” (Davis 2009). The bottoms contain degradation products in high concentrations but at elevated temperatures in the region of 150°C, these HSS products start to co-distill with the MEA and water.

“The feed to the unit is halted and caustic solution and water are then added to the still to break the heat stable salts in solution. The bottoms are then batch distilled to recover as much MEA as possible” (Davis 2009). The waste containing the HSS is disposed off as hazardous waste.

DETA thermal degradation has been reported in the literature albeit few sources like Davis (Davis 2009) and from that work Davis was able to identify (identification done by IC/MS analysis) some thermal degradation products like 1-(2-aminoethyl)imidazole which was found to be the largest degradation product in DETA thermal degradation. This product is also similar to HEIA. The imidazole type intermediate of DETA degradation product explains why in certain

concentration DETA has been used as a corrosion inhibitor for a long time and details of this inhibition behavior will be covered in section 5.5 in this chapter.

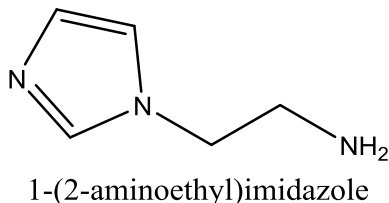


**Figure 5-9.** Structure of thermal degradation product of DETA

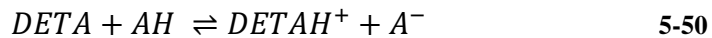
From the work of Davis (Davis 2009) he also reported that diethylenetriamine undergoes quick thermal degradation with a high limit of 94% loss of amine after just 4 weeks on stream at typical stripper temperatures of 135°C.

The reason for this high DETA thermal degradation is because by forming the intermediate 1-(2-aminoethyl)imidazole, the internal urea (the ring structure) deactivates two-thirds (2/3) of the active nitrogen groups available for CO<sub>2</sub> absorption (Davis 2009), hence rendering the solvent-diethylenetriamine, useless for CO<sub>2</sub> absorption and accounting for the observed fast thermal degradation. The conclusion therefore is that straight chain polyamines should be avoided in CO<sub>2</sub> solvent design due to their high thermal degradation rate but this is one side of the matrix in solvent design and does not take into account some of DETA superior qualities like faster kinetics, low activation energy, low energy requirements.

Thermal degradation in the industry is reduced by running the process at lower pressures (meaning low stripper temperatures, which can be a drawback since this will result in high work for the CO<sub>2</sub> compression leaving the units), solutions with elevated CO<sub>2</sub> partial pressures (P<sub>CO<sub>2</sub></sub>) which is achieved by high amine concentrations; high lean loadings thereby decreasing reboiler temperatures and finally by reducing the residence times of the lean amine in the reboiler (because the rate of thermal degradation is three (3) times faster in the reboiler than in the packing or cross exchange (Davis 2009)).

### 5.4.2 Heat Stable Salts (HSS)

Heat stable salts (HSS) are the products of the reaction between weak organic acids (derived from thermal and oxidative degradation of amines) and the amine itself. HSS in amine solution consume the solvent and leads to corrosion (Veldman 2000). Observed corroded (pitting corrosion) areas in amine absorption units include the reboiler tube bundle, reboiler piping, lower trays of the regenerator and the hot lean inlet side of the cross-exchanger (Veldman 2000). The most commonly found HSS are formate, acetate, oxalate and these have been reported to be found in DETA pilot plant (Svendsen 2013). The respective weak acids of the aforementioned heat stable salts (formic, acetic and oxalic acids) were used in this work to evaluate how they react and to what extent they corrode stainless steel 316L. The observed high corrosion rates due to the presence of HSS species can be explained by the fact that, these acids react with the amine by proton transfer (Veldman 2000) according to the following chemical equations:



And the corrosion reaction (A.L. Kohl 1997; Mariz, DeHart et al. 1999):



The fact is that amine pH is greater than the pKa of the HSS organic acids as well as the fact that in concentration terms (DETA = 26 wt% and those of the organic acids are typically in the range of 1 and 2wt%), the amines concentration far exceeds those of the acids. The consequence is that equilibrium (equation 5-51) shifts to the right and the acids stay in the neutralized heat stable form (Veldman 2000). Therefore by increasing CO<sub>2</sub> loadings, pH is decreased and in addition under thermal regeneration of amines in the stripper, the acids in the heat stable form becomes volatile. This volatility coupled with hot temperatures, aqueous environment leads to very corrosive conditions.

In a previous work (Hayfron-Benjamin 2012), it was shown that the presence of the acids of the HSS results in significantly high corrosion rates of stainless steel 316L as compared to the corrosive effect of only amine solutions.

## 5.5 Corrosion Inhibition

Corrosion as a phenomenon is known to be a major industrial setback in terms of how much damage it causes materials and, has had considerable economic losses on process plants. To combat this phenomenon of losses in the process industry, substances that act to decrease the rate of corrosion processes is employed. These substances are collectively known as corrosion inhibitors (C.I) and are widely used especially in the crude oil extraction and process industries (Roberge 2000). The specific process areas are those experiencing acid-alkaline sectors of the oil and gas industry, namely the atmospheric distillation plants, pipelines, vacuum vessels, hydrodesulphurization plants, and catalytic reactors (Ehmke 1975; Gutzeit and Johnson 1993; Duda, Govea-Rueda et al. 2005).

By definition, a corrosion inhibitor is a chemical substance that when added in small concentration to an environment, effectively decreases the corrosion rates (Roberge 2000). To illustrate examples of corrosion inhibitor, a close look needs to be taken at the precursor agents used in producing the CI. Depending on the precursors, inhibitors can be classified along the lines of: inorganic (examples chromate, phosphate, molybdate etc.), organic anionic (sodium sulfonates, phosphonates or mercapto benzotriazole (MBT) or organic cationic (imidazole-IM). A typical structure of imidazoline molecule widely used as an inhibitor is shown in figure 5-10 below:

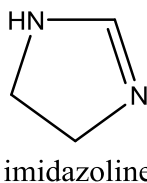


**Figure 5-10.** Imidazoline structure

A closer look at the above molecular structure of imidazoline reveals that it bears a striking resemblance to one of the main thermal degradation products of DETA (1-(2-aminoethyl)imidazole) as we mentioned earlier this work. The core resemblance will explain why DETA can be considered to have a dual role in corrosion of metallic surfaces.

The effectiveness of any corrosion inhibitor is measured by its efficiency which is defined below.

The efficiency of the CI is defined as:

$$\text{Inhibitor efficiency(\%)} = 100 \frac{(CR_{uninhibited} - CR_{inhibited})}{CR_{uninhibited}} \quad 5-52$$

Where  $CR_{uninhibited}$  = corrosion rate of the uninhibited system,  $CR_{inhibited}$  = corrosion rate of the inhibited system.

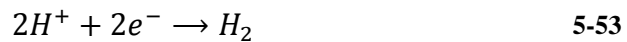
DETA, the CO<sub>2</sub> capture solvent which is used in this work, has often times been used as a corrosion inhibitor. In fact since the late 1940's, patents (Charles M. Blair Jr 1949) were granted for the application of DETA-related compounds as corrosion inhibitors. These CIs when used in certain concentrations and mixtures with other compounds makes it an effective corrosion inhibitor. In one such instance, a patent filed for "the design of process for preventing corrosion and corrosion inhibitors (Charles M. Blair Jr 1949)", the patent stated that "basic amides of polyamines containing two or more amino nitrogen atoms are particularly effective as corrosion inhibitors" (Charles M. Blair Jr 1949). It must be noted that the said polyamines included diethylenetriamine (DETA).

There remains yet the question as to how DETA can be effectively used as a corrosion inhibitor on one hand and from this work and others (Grimstvedt and He 2008; Kongstein 2010) how can DETA also act as a corrosive agent? Does it mean DETA has a dual role, both as a corrosion inhibitor and corrosion agent? The answers to the questions posed will only be revealed by properly assessing corrosion inhibition mechanism and thermal degradation of DETA.

Corrosion inhibition proceeds by the CIs adsorbing themselves onto the metallic surfaces, thereby protecting the surface by forming a film (Roberge 2000). Thus forming a passivating film layer, the corrosion process is slowed by an increasing electrochemical polarization (corresponding to steep Tafel slope) reduction of diffusion activity of ions to the surface and increasing the electrical resistance at the metallic surface (Roberge 2000).

For typical acidic medium encountered in CO<sub>2</sub>- corrosion, the corrosion inhibition mechanism starts by the adsorption of corrosion inhibitors onto the metallic surface and this step is controlled by the fraction of the surface coverage  $\theta$  covered by the inhibitor. The adsorbed species (usually the functional moiety) then forms strong coordination bonds with the metallic surface. The layer of adsorbed species then acts as a diffusion barrier to restrict the movement of anodic and cathodic ions which are necessary for the corrosion process. With high diffusion barrier comes increasing polarization of both the anode and cathode points and as has been mentioned under the electrochemical section of corrosion theory, increasing polarization corresponds to decreasing corrosion rates.

In short, the adsorption of ions at the cathodic planes creates a positive potential displacement, which retards the discharge of the positively charged hydrogen atom (H<sup>+</sup>) (Roberge 2000).



Since the cathode is polarized with positive potential and resistance is increased, a small corrosion current ( $i_{corr}$ ) will imply low corrosion rates. Further detailed explanation for the mechanism can be found in the literature (Charles M. Blair Jr 1949; Gutzeit and Johnson 1993; Jovancicevic, Prince et al. 1998; Roberge 2000; Schmitt and Saleh 2000; Veldman 2000; Zhang, Wang et al. 2001; Duda, Govea-Rueda et al. 2005; Liu, Chen et al. 2006).

Diethylenetriamine (DETA) when it reacts with carboxylic acid (as seen in figure 5-11 below) can result in the formation of an imidazole-type corrosion inhibitor and has been reported to have corrosion inhibition efficiency (IE%) in the range 22%-99% (Duda, Govea-Rueda et al. 2005).

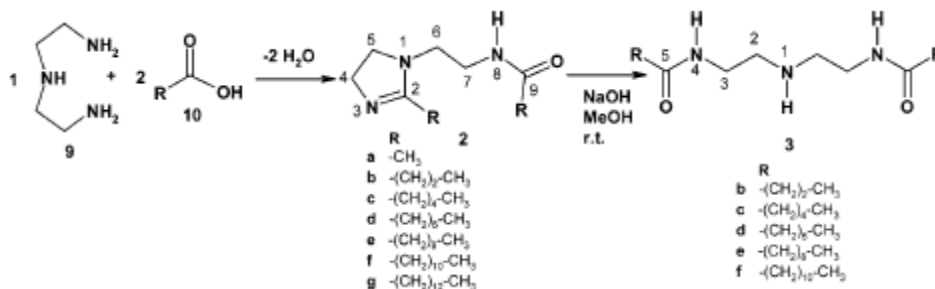


**Figure 5-11.** Inhibition Mechanisms (Duda, Govea-Rueda et al. 2005)

From the above chemical reaction, relevant features of the imidazole as far as corrosion inhibition is concerned are the:

- a) five membered ring, which is responsible for the strong bonding on metallic surfaces;
- b) a long hydrocarbon chain R1, reported by some authors (Pebere, Duprat et al. 1988; Jovancicevic, Prince et al. 1998), to play a key role in the inhibitive behavior;
- c) a pedant side chain with an active functional group R2. This part was investigated via quantum chemical calculations by Wang et.al. (Zhang, Wang et al. 2001) and was found to be conjugated with the five-membered ring, thereby improving inhibition efficiency.

Naturally with all that has been written about corrosion inhibition and the role of DETA, one will expect that DETA as a potential CO<sub>2</sub>-capture solvent will be ideal, at least from the point of view of corrosion of process equipment. However, the key point in understanding this dichotomy, seemingly contradictory role of DETA lies in the concentration of DETA applied. In the design of corrosion inhibitors, low concentrations (0.008wt% or 1000ppm) (Roberge 2000) are routinely encountered. But in CO<sub>2</sub>-capture processes relatively high concentrations are needed such as 2.5M (~25.56wt%) which was used in a trial pilot plant (Svendsen 2013) and also this work.

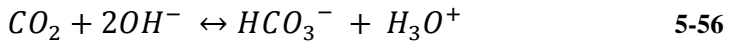
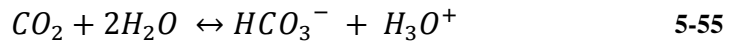
In conclusion for this section, for a fact diethylenetriamine (DETA) can be considered to have a dual role: first decreasing corrosion and second, increasing corrosion rates. These two fundamental reasoning are indeed mutually exclusive (the occurrence of one precludes the occurrence of the other) and one does not contradict the other, so far as a proper understanding of the level of applied DETA concentration is taken into account.

## 5.6 pH and Corrosivity

The pH of a solution is defined as the negative logarithm of the hydrogen concentration, represented as  $[H^+]$  in moles/liter. It measures the acidity of solution.

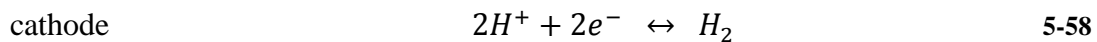
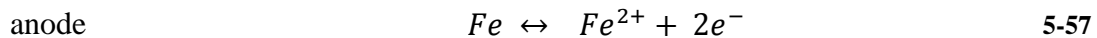
$$pH = -\log[H^+] \quad 5-54$$

The presence of  $CO_2$  in say a DETA- $CO_2$ - $H_2O$  system is related to the acidification of the medium. This is shown by the reaction of aqueous amine solution the hydration of  $CO_2$  leading to an increase in protonated species ( $H_3O^+$ ) and also the formation of the important corrosion causing agent bicarbonate species  $HCO_3^-$ : The presence of  $H_3O^+$  is responsible for changes in pH.



By using Nuclear Magnetic resonance (NMR) technique, Hartono (Hartono, da Silva et al. 2006) was able to confirm the presence of the species shown above such as  $H_2O$ ,  $OH^-$ ,  $H_3O^+$ ,  $HCO_3^-$  and  $CO_3^{2-}$  in DETA- $CO_2$ - $H_2O$ . In addition, it was confirmed in the same work that at higher loadings ( $>1.0$ ), dicarbamate and  $HCO_3^-$  and  $CO_3^{2-}$  are dominating in the DETA system. The same thus, can be concluded that in this work, such species will dominate and the postulation for the correlation between pH and corrosion to hold.

Corrosion of iron either in stainless steel or carbon steel can be represented by the two electrochemical reactions:



The H<sub>2</sub> as represented in the cathodic reaction is normally first adsorbed on the surface of the metal as atomic H (later in deaeration conditions, combines to be evolved as H<sub>2</sub> gas). The cathode reaction based on thermodynamic considerations is considered to be the controlling step and as such rate of corrosion depends on this reaction. The layer of adsorbed atomic hydrogen causes what is known as cathodic polarization resulting in a decrease the net oxidation-reduction reaction and hence lower corrosion rate (DepartmentofEnergy 1993) by virtue of the fact that the adsorbed atomic H block the metal active site preventing it from undergoing the reduction that leads to dissolution and corrosion.

The dependence of corrosion rates on pH is a complex subject but it has been reported (DepartmentofEnergy 1993; Moiseeva and Rashevskaya 2002) that the subject can be broadly divided into three major areas of the pH scale. The acidic range where corrosion generally increases sharply with decreasing pH (or conversely decreases sharply with increasing pH), the range where the rate is independent of the pH and in the more alkaline range where corrosion rate is retarded by increasing pH values.

For pH values below 4.0, ferrous oxide FeO a corrosion product (in addition to Fe<sub>2</sub>O<sub>3</sub> and Fe<sub>3</sub>O<sub>4</sub>) is soluble, so as it formed the oxide dissolves rather than depositing on the metal surface to form a film (DepartmentofEnergy 1993) thereby causing passivation which might retard corrosion rates. Furthermore in the absence of the protective oxide film, the metal surface is in direct contact with the acid solution, and the corrosion reaction proceeds at a greater rate than it does at higher pH values (DepartmentofEnergy 1993).

So in acidic medium, with pH low and high hydronium ions (H<sub>3</sub>O<sup>+</sup>) concentration, the cathodic reaction as seen in equation 5-58 above proceeds at a faster rate, leading to the evolution of H<sub>2</sub> gas and thus the overall redox corrosion reaction increases and thus corrosion rate increases.

For high pH values , (pH ≥ 7) Moiseeva and Rashevskaya (Moiseeva and Rashevskaya 2002) reported that an additional cathode process becomes important:



With the accumulation of the hydroxide ions and thus increasing the pH, favorable conditions are produced for the formation of carbonate ions by the reaction:



The produced carbonate ions  $CO_3^{2-}$  reacts with the Iron (Fe) to form a protective siderite layer  $FeCO_3$ . It is the formation of the passivating layer which is largely responsible for observed corrosion rates at high pH. But it should be pointed out that it is only the general corrosion that decreases in this case but local corrosion such as pitting will not be affected in the same manner due to local acidification the affected areas (Moiseeva and Rashevskaya 2002).

In summary, corrosion should increase with decreasing pH values of the DETA solution and also the presence of HSS in the form of thermal and oxidative degradation products like oxalic, formic, and acetic acid, should decrease the pH of the amine and as such increase the corrosion rates as has been observed in the field and in a previous work (Hayfron-Benjamin 2012).

### **5.7 Corrosion Passivation films**

It was observed in a previous work (Hayfron-Benjamin 2012) that after sometime on exposure, stainless steel in MEA-CO<sub>2</sub>( $\alpha=0.4$ )- degradation product systems experienced a gradually decreasing corrosion rate after hitting a high in the previous time on stream. This phenomenon is linked to the formation of corrosive film layer on the steel. The process of forming the protective film in corrosion is known as passivation which is the condition where a naturally active metal corrodes at a very low rate, probably due to an oxide coating or an absorbed layer of oxygen. This feature offers stainless steel an outstanding corrosion resistance and the thickness of the film has been estimated to be in the range 1-3nm thick (Olsson and Landolt 2003) and this estimation is done by using in-situ and ex-situ characterization tools. Passivity is caused by the buildup of a stable, tenacious layer of metal oxide on the surface of a clean metal surface (DepartmentofEnergy 1993). The formed film acts as a diffusion control regime, retarding the diffusion of reactants and hence “corrosion either decreases markedly or stops” (DepartmentofEnergy 1993).

Passive films are formed during an exposure of the bare metal surface to an oxidizing environment. Once a film is formed, the reaction rate between the metal and the environment will be several orders of magnitude lower (Olsson and Landolt 2003). The film is not static but changes with the environment (Olsson and Landolt 2003). The characterization of passive films has been done with the aid of surface analysis tools such as, X-ray photoelectron spectroscopy (XPS), Auger electron spectroscopy (AES) and recently X-ray absorption near edge structure (XANES), which acquires in-situ chemical information. Researchers have developed a three-layer model for passive films formed on austenitic stainless steel such as 316L used in this work. In this model, the metal forms the base, on top of which is an oxide layer consisting of various ferritic oxides like FeO, Fe<sub>2</sub>O<sub>3</sub> and Fe<sub>3</sub>O<sub>4</sub>. It is this oxide layer that offers resistance to further corrosion. The top of the three-layer model consists of a ferrous hydroxide (rust) Fe(OH)<sub>2</sub> film. The three-layer model is schematically shown in figure 5-12 below.

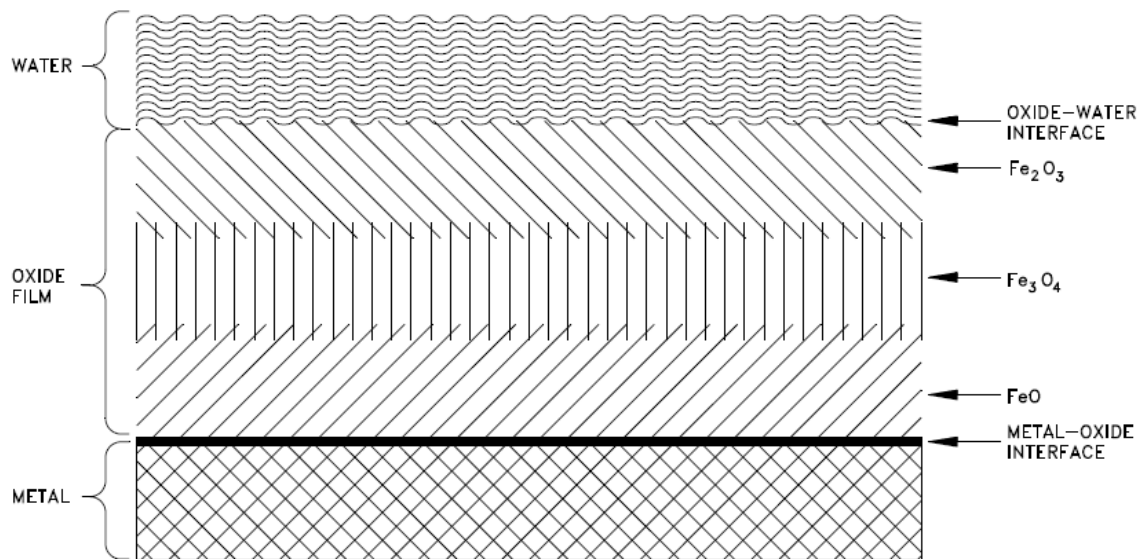


**Figure 5-12.** Simplified schematic diagram of oxide corrosion film on the surface of a metal (Department of Energy 1993)

Factors affecting the growth of the passive film on the stainless steel and which could be of importance in analyzing the trends obtained in the DETA-CO<sub>2</sub> stainless steel corrosion include but not limited to: pH, potential and temperature. Maurice et al. (Maurice, Yang et al. 1998) investigated the development of passive film with changes in potential and the interested reader can refer to that paper. Temperature on the other hand has little or no effect on the thickness of

the passive film and in one work by Wegrelius and Olefjord using XPS (L. Wegrelius and Olefjord 1993; Wegrelius, Falkenberg et al. 1999) it was found that only a difference of 2 Å<sup>o</sup> thicker film was recorded for the higher temperature.

The pH dependency is essentially that an increased pH leads to a lower dissolution of Iron as we proved in the pH section (section 5.6). This decrease in corrosion rate will lead to a thicker passive film and a larger fraction of iron in the film, as iron oxides are more stable in basic solutions (Olsson and Landolt 2003). The effect of pH on the passive layer of Fe and Cr alloys have also been studied by Strehblow et al. (Hoppe, Haupt et al. 1994; Haupt and Strehblow 1995) and they found out that the films were thicker in basic solutions. In addition, there was a marked increase of the amount of Fe(III) oxide. Armed with this information, in this DETA-corrosion of stainless steel 316L work, we expect that periods where corrosion is recorded to have slowed should correspond to higher pH of the aqueous amine solution.

## Chapter 6 Methodology

### 6.1 Introduction

The development of a fundamentally sound methodology for corrosion monitoring is one of the keys to properly assessing and controlling the damaging effects on industrial plants caused by the presence of heat stable salts in amines.

It is from this designed methodology that, systems could be designed for detecting, measuring, and predicting corrosion damage.

The basis for the design of a particular method has been framed around a couple of standard considerations as reported by (Lloyd and Lipow 1984; Roberge 2000):

- (i) What are the objectives of the test?
- (ii) How should the results be interpreted?
- (iii) How can the information be integrated with earlier results?
- (iv) What parameters are to be included in the tests?
- (v) Correlation between different parameters?
- (vi) How representative is the sample?
- (vii) What types of data are to be measured?
- (viii) Are the tests destructive to the sample?
- (ix) How expensive are the tests and/or specimens?
- (x) How much control is there over the testing?
- (xi) The role of human errors, aliasing, biasing and all forms of statistical error that could be introduced.
- (xii) What apparatus is to be used?

The answers to some of the above design considerations will be clear by the end of this work. For example answer to (i) is found in the introduction section of this thesis (chapter 1), answers to (ii), (iii), (vi), (xi), (xii), the reader is referred to the results and discussion part (chapter 8). In that chapter thorough analyses of all the data collected is done. Concerning the type of parameters to be used, a brief explanation will be covered in this chapter but further light has been shed on this subject in the theory portion (chapter 5). Finally the answer to which specimen

to use and how representative will that sample be, will be shortly covered in the ensuing sections of this chapter.

Thus the aim of the methodology chapter is to introduce the reader to the justification behind the chosen apparatus, metal specimen, solvent design (responsible corrosive medium-diethylenetriamine (DETA)), and the role of the relevant standards developed in the industry such as those issued by ASTM and NACE. The standards are needed to ensure reproducibility of results by corrosion specialists both in the industry and laboratory.

ASTM standard G31-72 (ASTM 2004) explains why standardization is essential by stating that “expansion of the test program in the future or correlating the results with tests of other investigators will be possible only if all pertinent information is properly recorded”.

Each phase of the methodology is thoroughly explained and the reasons behind each choice are given in the following section.

The aim of having a well-defined methodology in a corrosion investigation is so because it helps (Mattsson 1989; E. Heitz 1992): a) develop new materials that are resistant to corrosion, b) with selection of construction materials, c) quality control of materials, d) explanation of corrosion reactions and corrosion mechanisms and e) corrosion monitoring.

In this section we describe the apparatus used in the experimental section (see chapter 7), the type of corrosion test chosen and detailed breakdown of how the corrosion parameters are to be measured. In all of this the choice of a particular methodology is justified based on the needs, scope and objectives of this project. The main point is that the type of media, size of test piece, test conditions and duration of the test are particularly relevant (E. Heitz 1992).

## **6.2 Experimental Procedure**

In general, corrosion test can either be classified into two main categories: field testing and laboratory testing. In field testing, the approach is that the conditions as experienced in the Industry are closely matched and the subsequent corrosion effects measured. However this method tend to be expensive and parameters such as temperatures, pH are difficult to control, control of parameters being a key issue to ensure accurate results. The other approach which is used in this project is laboratory testing and this basically tends to simulate service conditions

like those encountered in the industry. In laboratory testing, a multi-technique approach is usually recommended (Roberge 2000) because it helps to increase confidence in the results that will be obtained. Thus immersion techniques (long-term corrosion coupon testing) and electrochemical techniques (a brief given in this section) are going to be the preferred methodology for “Characterization of corrosion patterns of stainless steel 316L in DETA-CO<sub>2</sub> and amine degradation product systems”.

For this work, the methodology was based on these standards from ASTM; G1-03 and G31-72, G5-13, G46-94 (ASTM 2004; ASTM 2005; ASTM 2011; ASTM 2013)

## **6.2.1 Apparatus**

### ***6.2.1.0 Coupon Testing***

This type of immersion testing simply consists of exposing small section of the specimen under investigation, to the test medium for a period of time and the accompanying weight loss measured. From this weight loss, the corrosion rates can be calculated as shall be shortly shown. This approach of testing has the advantage of simplicity, low cost, detailed analysis of corrosion solution (Roberge 2000). With that said, coupon testing has some drawbacks because for example the effects of heat transfer cannot be adequately accounted for. It is also labor intensive because of the many steps involved; cleaning, weighing, and microscopic examination. An overall judgment has to be made, and by all accounts in the literature (Veawab, Tontiwachwuthikul et al. 1999; Kongstein 2010; Tavera-Valero and Svendsen 2011; Gao, Wang et al. 2012) coupon testing is scientifically sound-based methodology and hence the choice for this work.

#### ***6.2.1.1 Swagelok® 1.0 and 2.0***

The recommended apparatus per and ASTM G31-72 (ASTM 2004) is described as one that is versatile, and convenient and that the choice of apparatus is limited only by the judgment and ingenuity of the investigator. On this basis we choose for each test specimen, a metal cylinder constructed from 316 stainless steel tubes with an outer diameter of ½ inch and equipped with Swagelok® end caps (Eide-Haugmo 2011). A picture of the apparatus with stainless steel specimen is shown in figure 6-1 and 6-2 below.



**Figure 6-1.** Picture of sample in the cylinder, showing also the Teflon cover at the tip of the metal specimen



**Figure 6-2.** The relative size of the cylinders used as compared to a 30cm ruler

Inside these cylinders, stainless steel A316 metal coupons of dimensions (88 x 6 x 2 mm for Swagelok 1.0 and 35 x 6 x 1 mm for Swagelok 2.0) fitted with Teflon<sup>®</sup> covering the tips of the metal are placed. There is an opening in the Teflon through which the corrosive medium (CO<sub>2</sub> loaded DETA and degradation products) are introduced. The volume of cylinders is approximately 11 ml and takes about 7 ml of solution to completely surround metal coupons in the cylinder. Also as a further insurance against any possible leakage, the cylinders will be held in an upright position in the metal containers which had been marked, properly identified and stored in a Memmert<sup>®</sup> 600 thermostat chamber at 135° C. On an additional note, for Swagelok<sup>®</sup>

2.0, extra torqueing will be applied to both ends of the cylinder caps to deal with the issue of solution loss and evaporation in such a high pressure and high temperature (135°C) environment, which was encountered in the earlier run (Swagelok® 1.0). The second batch of coupon testing (Swagelok® 2.0) design of the metal specimen is less thick, shorter length-wise and has a smaller area of specimen/volume of test solution ratio. This should increase the amount of corrosive medium (DETA) that the specimen is exposed to, and thereby that should also improve reproducibility of results. The dimension of the new design also has the benefits of ease of surface grinding and in addition eliminate the need for using separate Swagelok® cylinders for parallel samples. This will undoubtedly save time and less cylinders will be used. These types of immersion testing and apparatus set-up can be described as high temperature and/or high pressure static tests. It seeks to recreate the high temperatures and pressures encountered in commercial or industrial processes such as CCS plants (Roberge 2000). The only form of agitation of the solution, though, comes from the convection of heated DETA-CO<sub>2</sub> solution.

#### **6.2.1.2 Electrochemical Apparatus**

For the electrochemical testing, 1 L autoclave apparatus, together with a heating plate and coupled with an ACM® instruments Potentiostat will be used. The EC-autoclave consists of an outer metal cylinder, and an inner 1 L glass cylinder. The DETA– CO<sub>2</sub>- degradation products were put into the inner glass cylinder. This apparatus was chosen to meet the standards per ASTM G5-13(ASTM 2013) “*Standard Reference Test Method for Making Potentiodynamic Anodic Polarization Measurements*”. This standard states that the apparatus designed for polarization tests should aim to provide repeatable potentiodynamic polarization measurements that can be reproduced by others at other times in other laboratory. Specifically according to section 4.1 of this same standard, the test cell “should be constructed to allow the following items to be inserted into the solution chamber: the test electrode, two auxiliary electrodes, a Luggin capillary with salt bridge connection to the reference electrode, inlet and outlet for an inert gas and a thermometer”. In addition the test cell materials should not corrode, deteriorate or otherwise contaminate the test solution.

So, based on the specifications of ASTM G5-13, section 4 (ASTM 2013), a 1L EC-Autoclave cell supplied by SINTEF will be the test cell used for this work. The electrochemical cell set-up is complete with the electrodes systems, consisting of platinum electrodes, which should be connected to the test specimen, 316L SS and this electrode will act as the working electrode (WE). Options for an auxiliary electrode (AE) can also be made. The most important feature of the apparatus is the reference electrode system, which consists of a silver/silver chloride (Ag/AgCl) reference system. The details about connection of electrodes and data processing will be covered in chapter 7 under experimental procedure. A schematic of the chosen electrochemical cell is as shown in figure 6-3.

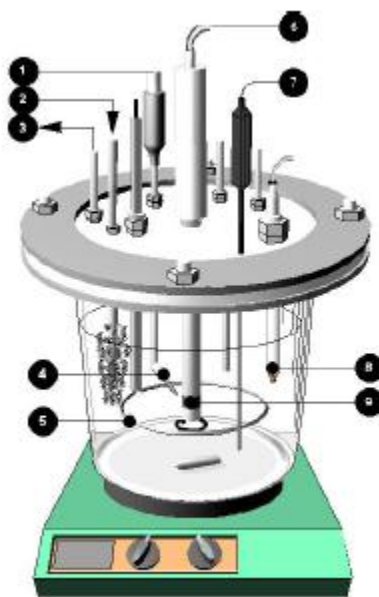


**Figure 6-3.** Schematic of the experimental test cell (Nesic, Postlethwaite et al. 1996)

1-reference electrode, 2-gas in, 3- gas out, 4-Luggin capillary, 5-platinum counter electrode, 6-rotating cylinder, 7- temperature probe, 8-pH electrode, 9-working electrode.

As shown in the figure 6-3 above, the counter electrode is made from platinum wires, the reference electrode being an external saturated silver/silver chloride (Ag/AgCl) reference electrode connected from the external to the cell (electrolyte-DETA-CO<sub>2</sub> - degradation products system) via a Luggin capillary and a porous wooden plug. The reference electrode actually consists of a silver wire (Ag) coated with a thin layer of molten silver chloride (AgCl). The

working electrode consists of the specimen (stainless steel 316L) connected to an external ACM<sup>®</sup> instruments potentiostat, via platinum wires and BNC electrode cables with gold-plated crocodile clips. Temperatures in the cell are controlled jointly by a IKA<sup>®</sup> RCT basic hot plate and a thermocouple. To measure pressures, a pressure gauge is also installed and typical pressures encountered are in the range of 1-5 bars. Whatever electrochemical process that takes place in the EC-Autoclave, the data generated must be processed and converted into high value information. The ACM<sup>®</sup> Gill AC 780 Potentiostat does the job data collection and transformation.

The potentiostat should be able to maintain an electrode potential within  $\pm 1$  mV according to ASTM G5-13 standards (ASTM 2013). The other standard specifications needed to have a measurable and reproducible result will thus be applied in this work. Further details of such specifications is found in the ASTM G5-13 section 4.2 (ASTM 2013).

The electrochemical cell described above has a gas inlet and outlet and for corrosion characterization of 316L in DETA-CO<sub>2</sub> environment, these inlet and outlet are not utilized, because the amines are prepared as pre-loaded and also the effect of CO<sub>2</sub> partial pressures is not being investigated.

Therefore, having an autoclave as an electrochemical cell where corrosion takes place, and couple that with a potentiostat, the desired measurements can be adequately done and the results reasonably interpreted based on sound basic electrochemistry principles.

### **6.2.2 Specimen**

Stainless steel is the choice of metal that will be used to imitate the likely construction material in a potential absorption plant (absorber and regenerator) process units in a CCS project (Billingham, Lee et al. 2011). The type of stainless steel to be used belongs to the Austenitic family of alloys characterized by 17% Cr and 11 % Ni content among other elements. Stainless steel 316L of composition wt%: Max C(0.06), Cr(17.0), Ni(11.0), Mo(2.2) and Fe(balance); is used as the test specimen for this body of work. The “L” in 316L indicates a low carbon content which improves the material properties. The dimensions of these specimens will be measured with the aid of digital calipers. In order to improve accuracy in the data for corrosion rates, duplicate specimen to ensure that statistically reliable results can be obtained (Mattsson 1989).

### 6.2.3 Surface Preparations (Before and After Testing)

The method of preparing the metal specimen is crucial for reporting test results to help other investigators to interpret the results. ASTM standards G1-03 and G31-72 (ASTM 2004; ASTM 2011) spells out two procedures: Before the test is done and one for after the test. A procedure known as wet-grinding is applied for specimens like stainless steel and chemical cleaning where, reagent grade solutions are used to remove corrosion products and then the weight loss is used. The detailed descriptions of these processes are presented in the experimental section of the next chapter.

## 6.3 Calculating Corrosion Rate

### 6.3.1 Weight loss- based

The corrosion rate in (mm/yr) is calculated using the mass loss obtained from a number of cleaning cycle procedure as described in detail in ASTM G1-03. (ASTM 2011)

From the weight loss obtained the average corrosion rate is given by the formula

$$\text{Corrosion rate} = \frac{K * W}{A * T * D} \quad \mathbf{6-1}$$

Where:

$K$  = a constant (depending on the units to be used),

$T$  = time of exposure in hours,

$A$  = area in  $\text{cm}^2$ ,

$W$  = mass loss in grams, and

$D$  = Density in  $\text{g/cm}^3$

Depending on the units used, the constant  $K$  varies and in this experiment, we will report some in mm/yr, as hence the ASTM G1-03 (ASTM 2011) recommends value of  $K = 8.76 \times 10^4$ . The aforementioned standard also gives a density of  $D = 7.98 \text{ g/cm}^3$  for stainless steel 316. Therefore, by determining the weight loss  $W$ , and knowing the time of exposure and knowing the dimensions of the steel coupons we will be able to calculate the corrosion rate and that is what is done in the results section of this report.

### 6.3.2 Electrochemical testing

Two electrochemical techniques Tafel plot and linear polarization resistance will be the chosen methodology for investigating corrosion from an electrochemical point of view. Each technique has specific parameter choice, which will ultimately guide the type of results obtained. For the both methods, a suitable scan rate between 12mV/min to 50mv/min is the recommended practice. Any number outside this range makes the polarization methods either too fast or too slow. The purpose for choosing these methods is to help measure the corrosion current and from which the corrosion rate can be estimated.

For the Tafel plots, extrapolation of the E-log  $i_{corr}$  and calculation of the Tafel slopes are then used to estimate the corrosion rates according to the following equations:

$$corrosion\ rate\left(\frac{mm}{year}\right) = \frac{3.3 * i_{corr} * E.W}{\rho} \quad 6-2$$

Where E.W = equivalent weight of test coupons

P = density of stainless steel 316L ( $g/cm^3$ )

$i_{corr}$  = corrosion current density( $mAcm^{-2}$ )

For the linear polarization resistance, the following equations are used to compute the corrosion current and the equation 6-2 above is used to estimate the penetration rates.

$$i_{corr} = \frac{\beta}{R_p} \quad 6-3$$

$$\beta = \frac{\beta_a \beta_c}{2.3(\beta_a + \beta_c)} \quad 6-4$$

$$R_p = \frac{\Delta E}{\Delta i} \quad 6-5$$

Where  $\beta$  = Stern and Geary Constant,

$\beta_a \beta_c$  = tafel slopes in the anodic and cathodic regions respectively

$i_{corr}$  = corrosion current density

$R_p$  = polarization resistance

$\Delta E$  = change in potential on the LPR diagram

$\Delta i$  = change in the current density on the LPR diagram.

## 6.4 Surface Investigation

The impact of corrosion is mainly a surface phenomenon and as such it will make sense to apply techniques that can study the surface effects of corrosion. Surface analysis involves the use of microscopic, chemical and physical probes that give information about the surface of a region of interest of the test specimen (Roberge 2000). The choice of a particular surface technique for corrosion work is ultimately based on what type of corrosion effect will be expected. Effects include dealloying, exfoliation, cracking or intergranular attack. For this work, uniform corrosion with pockets of localized corrosion, caused by diethylenetriamine and CO<sub>2</sub> and acids, is mainly suspected. Based on the needs of the work (scope), time and resources, the option of simple microscopy and SEM was chosen.

It is a recommended practice to use surface investigative techniques as per ASTM G1-03 (ASTM 2011) in order to characterize corrosion products on the surfaces of metals in general, stainless steel 316L included. Metallography is the study of the microscopic structure of metals and alloys using optical metallographs, electron microscopes or other surface analysis equipment (PaceTechnologies 2013). Microstructural analysis is an important feature of quality control and product reliability. In the case of this work, stainless steel, corrosion on its surfaces will only be properly characterized by the appropriate metallography and as such a better correlation between the steel structure and the properties can be understood.

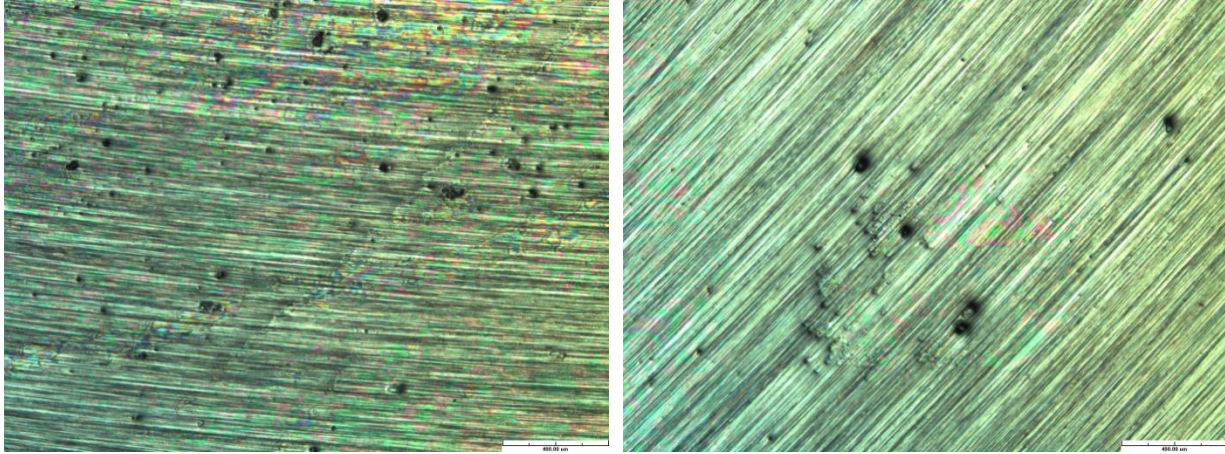
The use of microscopy can be divided into three main categories; the first, optical microscopy, consists of examination of metal surfaces using visible light to provide magnified image of the micro- and macrostructure (M.R. Louthan 1986). The second is the scanning electron microscopy (SEM) in which a focused beam of electrons is used to produce a high resolution

image of the metal surface revealing the topology and composition. Lastly, transmission electron microscopy (TEM) consisting of transmitted beam of electrons and used for structural analysis. Of the three mentioned, SEM and Optical microscopy has found popularity in usage in corrosion studies (Steven J. Suess 2006; Cindra Fonseca, Bastos et al. 2007; Z.F. Yin, X.Z. Wang et al. 2010; Hayfron-Benjamin 2012) mainly because the technology is established and easily accessible in most labs. Microstructural examination of which SEM belongs involves magnifications of 50X and higher and for the SEM, magnification of 5000X- 20000X (Steven J. Suess 2006) and resolutions of up to 1 *nanometer* is achievable. Simple optical microscopy which belongs to the class of macro structural examination, with a magnification of 50X or lower is a major constraint because it has limited depth of focus.

Characterization of corrosion surfaces reveals the metal structure in terms of grain boundaries, phase boundaries, determination of the extent and form of the corrosive attack and differentiating the type of corrosion: pitting, uniform, crevice, and erosion corrosion (M.R. Louthan 1986).

In essence, corrosion morphology characterisation has traditionally been performed using techniques such as optical microscopy, polarized light microscopy, SEM, and electron probe micro-analysis (EPMA) (de la Fuente, Díaz et al. 2011).

Additional tools like Energy Dispersive X-ray Spectroscopy (EDS) in conjunction with SEM are used for morphology and composition of the coupon surface and cross-section. XRD (X-ray Diffraction), Raman spectrometry can be used to identify what are the chemical constituents of the corrosion layers. The question that needs answering is which of the above described surface tool will then be appropriate for this work? (DETA-CO<sub>2</sub>- degradation products, stainless steel system). The answer lies in a review of a number of related works in the field of CO<sub>2</sub> corrosion of metals. For example in the previous work (Hayfron-Benjamin 2012) the surface morphology of stainless steel A316 was investigated in a corrosive medium of MEA-CO<sub>2</sub> - plus various degradation products and with the aid of an optical microscope, definite presence of localized corrosion in the form of pits were noted. Figure 6-4 below shows the details of the surface morphology of that work.



**Figure 6-4.** Two surface pictures showing pitting on the specimen caused by acetic acid after 165 hrs of exposure at 135°C. (Hayfron-Benjamin 2012)

One glaring drawback of the simple use of the lower power microscope is the fact that it lacks incisive deductions compared to all the other metallography tools. Simple microscopy is in fact the most basic tool, and as such for more advanced analysis, SEM, XRD is recommended by the experts (Mattsson 1989).

Now, turning to advanced surface technique such as SEM and XRD combination, Gao et al. (Gao, Wang et al. 2012) investigated the corrosion behavior of carbon steel in a CO<sub>2</sub> pilot plant using MEA. With the aid of Scanning electron microscopy and energy dispersive X-ray spectroscopy, X-ray diffraction and Raman spectroscopy, they (Gao, Wang et al. 2012) were able to analyze the morphology and compositions of the coupon surface and cross section. The conclusion was that the corrosion products on the sample's surface and cross section were analyzed and found to consist of an inner layer of mainly hematite ( $\alpha$ -Fe<sub>2</sub>O<sub>3</sub>) and magnetite (Fe<sub>3</sub>O<sub>4</sub>) with traces of goethite ( $\alpha$ -FeOOH), while the outer layer mainly consists of siderite (FeCO<sub>3</sub>). In some works by other authors (A. Razvan and Raman. 1986; Raman, Razvan et al. 1986; A. Raman, S. Nasrazadani et al. 1987; A. Raman, S. Nasrazadani et al. 1987; Raman, Nasrazadani et al. 1989; Yamashita, Miyuki et al. 1994; Kamimura, Yamashita et al. 2001; de la Fuente, Díaz et al. 2011), the rust morphology of found on corroded steels were investigated using a combination of the above mentioned advanced tools. It was found out that composition of the rust layer, contain (A. Razvan and Raman. 1986; Raman, Razvan et al. 1986; A. Raman, S. Nasrazadani et al. 1987; A. Raman, S. Nasrazadani et al. 1987; Raman, Nasrazadani et al.

1989; Yamashita, Miyuki et al. 1994; Kamimura, Yamashita et al. 2001; de la Fuente, Díaz et al. 2011)  $\alpha$ -FeOOH (goethite),  $\beta$ -FeOOH (akaganeite),  $\gamma$ -FeOOH (lepidocrocite), magnetite. These phases most frequently appear as small crystalline globules or flowery plates ( $\gamma$ -FeOOH-lepidocrocite), semi-crystalline (goethite) and as cotton balls (akaganeite) (A. Razvan and Raman. 1986; Raman, Razvan et al. 1986; A. Raman, S. Nasrazadani et al. 1987; A. Raman, S. Nasrazadani et al. 1987; Raman, Nasrazadani et al. 1989; Yamashita, Miyuki et al. 1994; Kamimura, Yamashita et al. 2001; de la Fuente, Díaz et al. 2011). A sample of these phases is shown in figure 6-5 (S.W. Dean, D. Knotkova et al. 2010; de la Fuente, Díaz et al. 2011).

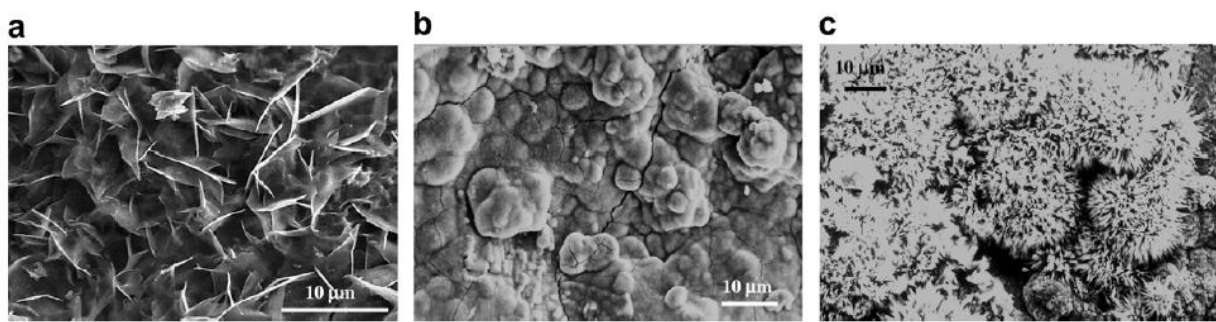


**Figure 6-5.** SEM images showing different phases and forms of corrosion products (S.W. Dean, D. Knotkova et al. 2010; de la Fuente, Díaz et al. 2011)

Figure 6-6 shows a combination of SEM/EDS images highlighting the corrosion layers and identification obtained by a cross-section of the steel sample.

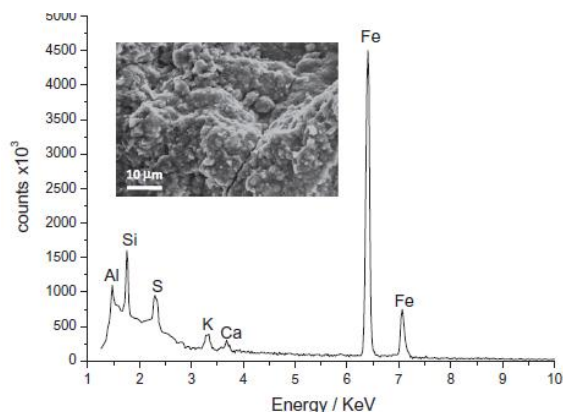


**Figure 6-6.** SEM/EDS identification image (S.W. Dean, D. Knotkova et al. 2010; de la Fuente, Díaz et al. 2011)

These incredible high resolutions of publication quality can only be achieved by using advanced surface metallography tools such as SEM, XRD, and the rest. Thus one of the aims of this thesis

is to be able to use theoretical and experimental techniques to properly characterize what corrosion products can be found in stainless steel 316L, when it is exposed to DETA-CO<sub>2</sub>-degradation products environment. Also the use of the ASTM G46 (ASTM 2005) Standard Guide for the “*Examination and Evaluation of Pitting Corrosion*” can be used to accurately characterize and model pitting corrosion. In summary properly accounting for the corrosion observed by means of the weight loss method, will only enhance the body of work in the field of DETA corrosion, which is especially lacking in the current literature.

## **6.5 Solution Analysis Methods**

In order to properly account for the types of species in solution (speciation) in the DETA-CO<sub>2</sub> – degradation products systems, accurate solution analysis is needed and the choice of analytical method goes a long way to establish the accuracy and interpretation of the results of this work. To identify the accurate CO<sub>2</sub> loadings and amine concentration, basic titration method (described shortly) will be employed. This method is used for both pre and post experiment solution analysis. After the corrosion experiments, some of the metal ions go into solution and to quantify these ions, an advanced method of inductively coupled plasma mass spectrometry (ICP-MS) will be used. The purpose of this section is to justify why ICP-MS was chosen for the elemental determination of corrosion systems in DETA-CO<sub>2</sub>- degraded product systems. The ultimate purpose of knowing what corroded elements are in solution is to be able to draw a conclusion about whether selective alloying corrosion of stainless steel 316L occurs in DETA-CO<sub>2</sub>- degraded product systems. In other words if we know the elemental composition of the 316L SS before the experimental and we compare the elemental composition after corrosion, then a contrast can be drawn, if it indeed exists. The solution analysis methods are described in the ensuing sections.

### **6.5.1 Titration**

Titration is a convenient analytical tool for analyte concentration quantification in solutions. The theory of titration is based on the reaction between the analyte (in this work, DETA) and a reagent (titrant) of known concentration which is added to the sample. For example after CO<sub>2</sub> loading of DETA solution, in order to determine the exact CO<sub>2</sub> solubility in amine solution, and the total amine concentration, the Metrohm Titrand 836/Mettler Toledo barium chloride and

acid-base back-titration methods respectively will be employed. For total amine analysis for CO<sub>2</sub> loaded solutions the titrant used is a 0.2N H<sub>2</sub>SO<sub>4</sub> solution and for the CO<sub>2</sub> determination, 0.1N NaOH and 0.2N H<sub>2</sub>SO<sub>4</sub> are also used. The titrant is added until the reaction is complete and depending on the characteristics of the titrant and the ensuing reaction, monitoring of the end point is done via potentiometry (potential measurement with a sensor measuring changes in the pH of the reaction solution or in other words the concentration-dependent potential (mV) of the solution is measured against a reference potential) or with colour indicators (MettlerToledo 2013). By thus measuring the dispensed titrant volume, the exact concentration of the analyte content based on the stoichiometry of the chemical reaction will be determined. The use of titration is done because of the inherent advantages such as it being an established analytical technique, fast and accurate.

The procedure for amine analysis involves adding a sample (about 2ml) of the amine to be tested (DETA) to 50 ml of deionized water and using the Mettler Toledo<sup>®</sup> titrator which uses 0.2N H<sub>2</sub>SO<sub>4</sub> and titration is done until the pH = 2.5, which indicates the end-point which is the point is identified where analyte and reagent are present in equivalent amounts. For this work, detailed titration curves and reports are attached to the appendix.

The amine (mol/liter) is thus calculated from the formula

$$Amine \left( \frac{mol}{litre} \right) = \frac{H_2SO_4(ml) * 0.2N}{DETA \ sample(ml)} \quad 6-6$$

$$Amine \left( \frac{mole}{kg} \right) = \frac{Amine \left( \frac{mole}{liter} \right)}{\rho_{DETA sol} \left( \frac{kg}{liter} \right)} \quad 6-7$$

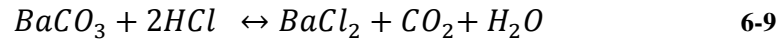
For dissolved CO<sub>2</sub> analysis, the procedure involves quite a bit of analytical work. It uses a blank sample to account for atmospheric CO<sub>2</sub> which might interfere with the results. Thus the correct total carbon dioxide is adjusted using the results from the blank sample analysis. The barium chloride method uses 1.0 N BaCl<sub>2</sub> in addition to 0.1 N sodium hydroxide NaOH to displacing the

dissolved carbon dioxide (CO<sub>2</sub>) in the diethylenetriamine (DETA) system according to the following equation :



The precipitation as seen in the reaction above is normally achieved after boiling the solution for about four (4) minutes and then cooling it.

The solid precipitate BaCO<sub>3</sub> is then reacted with 0.1N HCl in order to liberate (dissolve) the CO<sub>2</sub> for the titration to be accurately performed. To dissolve the precipitation, a Magnetic Mix control<sup>®</sup> stirrer is used. The liberation reaction is as shown



The dissolved BaCO<sub>3</sub> is hence titrated again 0.1N NaOH until an end- point pH = 5.2 is obtained.

The CO<sub>2</sub> content is obtained from the equations 6-10 & 6-11 shown below.

$$CO_2 \left( \frac{mol}{kg} \right) = \frac{1}{20} \cdot \frac{HCl(g) - NaOH(ml) - [Blank HCl(g) - Blank NaOH(ml)]}{DETA\ sample(g)} \quad \mathbf{6-10}$$

$$CO_2 \left( \frac{mole}{liter} \right) = CO_2 \left( \frac{mole}{kg} \right) \cdot \rho_{DETA\ sol} \left( \frac{kg}{liter} \right) \quad \mathbf{6-11}$$

All titrations and measurements will be performed at ambient temperature and pressure.

### 6.5.2 Corrosion Solution analysis by ICP-MS

In order to determine and quantify corrosion accurately, the use of precise and powerful analytical techniques is required. In the solution of the DETA-CO<sub>2</sub>- degraded products systems, after corrosion has occurred for a time period, some ions of elements such as Fe, Cr, Mn are naturally expected to be in the solution. These elements are the alloying composition of stainless steel 316 as shown in table 7-1 in the experimental section of this work. To determine and quantify these ions in solution, the choice of a powerful analytical technique, the Inductively Coupled Mass Spectrometry (ICP-MS) is used for elemental determinations.

Inductively Coupled Plasma Mass Spectrometry or ICP-MS is an analytical technique used for elemental determinations and has been around for close to 30 years (Jenna Worley and Kvech. ; Wolf 2005). The ICP-MS is a tool that combines the quick analysis (using a high temperature) of the ICP technology and the accurate and low detection limits of a mass spectrometer (Jenna Worley and Kvech.) with as low detection levels as parts per trillion (ppt) achieved. This tool is used in many applications including drinking water, wastewater, natural water systems/hydrogeology, geology and soil science, mining/metallurgy, food sciences, and medicine (Jenna Worley and Kvech.).

The ICP technology is similar to the same principles used in atomic emission spectrometry i.e. decompose species using high temperature argon plasma and then separating ions on mass to charge ratio (m/e) basis but with added advantages such as greater detection limits, higher throughput, better ability to handle simple and complex matrices with minimum matrix interference and also the ability to obtain isotopic information (Wolf 2005).

The ICP-MS process occurs in mainly three major areas: sample preparation and introduction stage, the ICP-plasma generation and ionization and mass/charge separation and detection stages. Details of the working nature and a schematic can be found in the open literature.

The typical ICP-MS resolutions are in the range of 0.7- 1.0 amu (atomic mass unit) but it is widely known that resolution power is influenced by specific matrix interferences and such correction is made for the resolution thus obtained.

In general by using the ICP-MS technique, high precision and accurate quantification of corrosion elements can be achieved and as such an important conclusion regarding selective alloying corrosion (dealloying corrosion) can be reached. The detailed ICP-MS analysis and

discussion will be tackled in chapter 8 and some of the spectra results from the ICP-MS lab are attached in this report.

## 6.6 Parameters for Testing

The following parameters were chosen based on a number of factors such as the standard representations of process conditions in the field. For the CO<sub>2</sub> loading a range of  $\alpha$  (1.2 – 1.5) was suggested but based on advice from the supervisor on tests done with DETA in a pilot plant, the extreme values were selected (i.e.  $\alpha = 1.2$  and  $\alpha = 1.5$ ). A DETA concentration (2.5M) which corresponded to approximately 26 wt% was selected. From the literature, typical acid (oxalic, formic, acetic) loadings are in the range of 500 ppm to 50,000ppm. These values are to mimic industrial conditions of heat stable salts in amine solvents used in CO<sub>2</sub> capture. Different acid loadings (1wt%, 2wt%) were chosen and this fell in the range of accepted values as seen in the industry. Temperatures of 80°C, 135°C were chosen because they represent the high end of absorber/cross exchanger and the stripper (reboiler) temperatures respectively. These parameters are varied and observed over a time span of 5 weeks (weigh loss experiments) and one (1) to two (2) days for the electrochemical testing technique. At the end of each test, the requisite observable change in properties such as weight loss and corrosion current are measured and the corrosion rates calculated according the fitting formula.

All test solutions will be prepared from reagent grade chemicals, deionized water was used in all cases. This procedure of using reagent grade materials is recommended per ASTM G31-72, section 8.5 (ASTM 2004). Test conditions are carefully controlled, an example being the accurate amine and CO<sub>2</sub> analysis determination of the diethylenetriamine-carbon dioxide systems, before and after testing. Also the temperature of test solution in the electrochemical experiments is controlled within  $\pm 3^{\circ}\text{C}$  by means of an IKA<sup>®</sup> RCT basic heater plate and a thermocouple.

To conclude this chapter, the particular methodology for going about characterizing corrosion patterns of stainless steel in DETA systems has been clearly explained and the scientific principles behind each methodology has also be thoroughly tackled. The subsequent chapter illustrates all relevant experimental procedure and the recording of key data.

## Chapter 7 Experimental Set-up

### 7.0 Introduction

The experimental stage consisted of two runs, each with a different apparatus. Each batch of experiment had a set of parameters that was varied, as mentioned in the methodology section (chapter 6). The first type consisted of stainless steel cylinders which has been named Swagelok<sup>®</sup> 1.0 and 2.0. The second type of apparatus is the EC-Autoclave(1L). The Swagelok<sup>®</sup> cylinder type of experiment was similar to an earlier project (Hayfron-Benjamin 2012) and the ensuing description applies for both Swagelok<sup>®</sup> 1.0 and 2.0, with the minor difference of having different acid loadings (1wt% for Swagelok<sup>®</sup> 1.0 and 1wt% & 2wt% for Swagelok<sup>®</sup> 2.0).

### 7.1 Swagelok<sup>®</sup> Cylinder Apparatus

The experiments were carried out in a metal cylinder constructed from 316 stainless steel tubes with an outer diameter of ½ inch and equipped with Swagelok<sup>®</sup> end caps. The experimental set-up consists of the above mentioned steel cylinder, into which the metal specimen (stainless steel 316) is inserted. The specimen was fitted at the ends with a Teflon, which has a small opening, through which the corrosive medium (CO<sub>2</sub> loaded DETA and degradation products-oxalic, formic and acetic acids) are introduced. The volume of cylinders is approximately 11ml and takes about 7ml of solution to completely surround metal coupons in the cylinder. After filling the cylinders with the appropriate solution, the ends are tightly screwed to prevent leakage. Also as a further insurance against any possible leakage, the cylinders were held in an upright position in the metal containers which had been marked, properly identified and stored in a Memmert<sup>®</sup> 600 thermostat chamber at 135°C. On an additional note, for Swagelok<sup>®</sup> 2.0, extra torquing was applied to both ends of the cylinder caps to deal with; the issue of solution loss and evaporation in such a high pressure and high temperature(135°C) environment, which was recorded in the earlier run (Swagelok<sup>®</sup> 1.0).

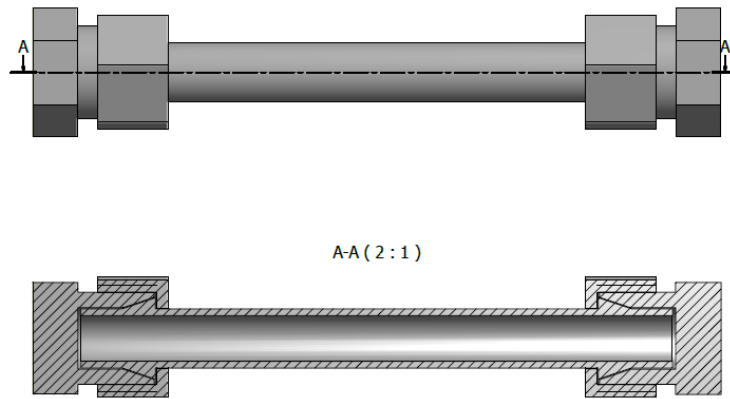


**Figure 7-1.** Cross-section view of cylinders for coupon testing



**Figure 7-2.** A Memmert® 600 thermostat chamber at 135°C ready to be used for the experiment

## 7.2 EC-Autoclave (1L) Apparatus

For the electrochemical testing, 1L autoclave apparatus, together with a heating plate and coupled with an ACM<sup>®</sup> instruments Potentiostat was used. The EC-autoclave, which was in-house assembled, consists of an outer metal cylinder, and an inner 1 L glass cylinder. The DETA-CO<sub>2</sub>- degradation products were put into the inner glass cylinder. The electrochemical cell set-up is complete with the electrodes systems, consisting of platinum electrodes, which could be connected to the test specimen, 316L SS and this electrode will act as the working electrode (WE). Options for an auxiliary electrode (AE) can also be made. The most important feature is the reference electrode system which has already been described and this consists of a silver/silver chloride (Ag/AgCl) reference system. After inserting the test specimen to the right electrode (WE) and the proper connection is established, the potentiostat is connected to an external computer for data processing.

## 7.3 Stainless Steel 316L Chemical Composition

The test specimen all the corrosion tests carried out (both Electrochemical and Swagelok cylinder experiments) were constructed out of stainless steel 316L. A total of 88 stainless steel coupons of various dimensions were used. In accordance with the ASTM standard G1-03 section 9, which deals with the standard format of reporting corrosion experiments, the chemical composition of the stainless steel 316 L is as shown in Table 7-1 below.

**Table 7-1.** Stainless Steel Chemical Composition

element	C	Si	Mn	Cr	Ni	Mo	Fe
weight(%)	0.06	0.47	1.74	17.0	11.0	2.2	balance

---

## 7.4 Specimen Dimensions and Surface preparation

### 7.4.1 Dimensions

It has been mentioned earlier in this report, that different dimensions were chosen for the different types of experiments (be it Swagelok<sup>®</sup> 1.0 or 2.0 or the EC-Autoclave). In this chapter the dimensions are reported and a brief mention of the instrument and accuracy used in the measurement.

The specimens as obtained were in rectangular strips, the dimensions were measured with the aid of digital vernier calipers. The dimensions were taken after surface preparation of test specimen had been thoroughly done and its dimension was determined to the third significant figures as per ASTM G1-03 (ASTM 2011) recommendations. Please refer to **Appendix A1** for detailed measurements of all specimens.

#### *Swagelok<sup>®</sup> 1.0*

average size of the specimens(mm): 88 x 6 x 2

#### *Swagelok<sup>®</sup> 2.0*

average size of the specimens(mm): 35 x 6 x 1 with a hole diameter of 1.80mm

#### *EC- Autoclave*

average size of the specimens(mm): 80 x 20 x 1 with a hole diameter of 1.80mm

A schematic of the different types of specimens used with the dimensions and also the Teflon cover for introducing the preloaded DETA solution into the cylinders, are shown in figures 7-3 and 7-4 below.

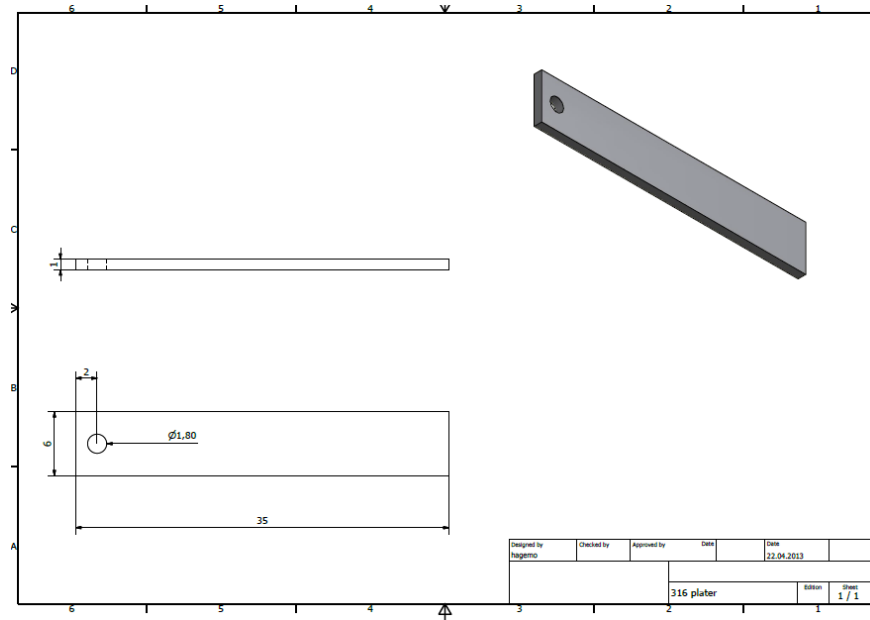


Figure 7-3. Schematic of coupon showing dimensions

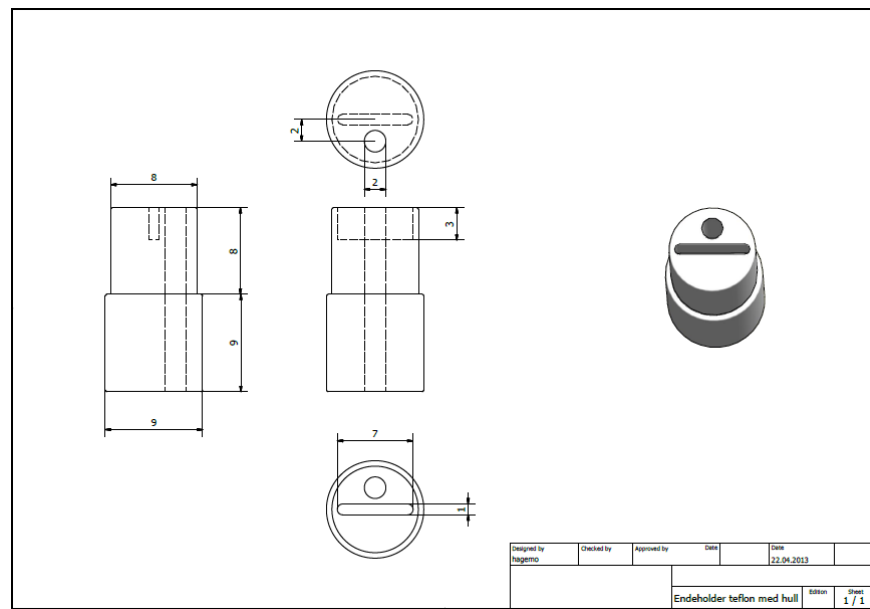


Figure 7-4. Schematic of Teflon cover for metal specimens

## 7.4.2 Surface preparation

Prior to the tests, surfaces of all the specimens were prepared by following the guidelines ASTM G1-03 – “*Preparing, Cleaning, and Evaluating Corrosion Test Specimens*” (ASTM 2011). The surface wet grinding as well as chemical cleaning were used (grinding for Swagelok<sup>®</sup> 2.0 and EC–Autoclave experiments and chemical cleaning for Swagelok<sup>®</sup> 1.0). The ultimate goal of

surface preparation is to remove the usual passive oxide film on stainless steel specimens and accelerate corrosion effects. By so doing a measurable corrosion rate can be obtained and surface investigation microscopy can be effectively used. The procedure for each specimen is as follows: first wet grinding with 320 grit paper for 10 minutes followed by another wet grinding with finer grit paper 500 grit for an additional 5 minutes. Both surfaces of the metal strip are subjected to this wet-grinding procedure. Then degrease surface of the specimens with acetone to remove carbide particles (from the grit paper). Next the specimens were washed with 96% ethanol by means of ultrasonic cleaning. The cleaning takes 15 minutes. Finally the samples were dried with hot air and the clean, dry specimens were weighted (to 5 significant figures) and stored in a desiccator in the Lab until they were used in experiment.

The chemical pickling consists of first washing with specimens with soap water and deionized water in order to remove the usual grease found on steel specimens (source: mechanics shop) and then preparing 15 wt% hydrochloric (HCl) acid at room temperature. The washed 316L SS was then placed in the HCl solution for a period of 5-10 minutes. Following the acid bath, there is the washing in deionized water and acetone in that order. Samples were dried with hot air and the clean, dry specimens were weighted (to 5 significant figures) and stored in a desiccator in the Lab until they were used in experiment.

## **7.5 Solution preparation and calculations**

### **7.5.1 Preparation**

The aqueous solutions of 2.5 M DETA with CO<sub>2</sub> loading of  $\alpha = 1.2$  (0.4 per amine group in DETA molecule) were prepared using chemical reagents of industrial grade obtained from Sigma – Aldrich with concentrations and purity more than 99%. The solutions are prepared by diluting a weighted quantity of the pure solvent (diethylenetriamine) with deionized water as per described in the ASTM standards (ASTM 2004; ASTM 2011).

DETA solution involved a multistage exact concentration determination. The meaning being that because of the heat of solution, when DI water was added to the solvent (DETA) in for example 1L flask, the volume recorded on the flask was not the exact volume required. By allowing the

solution to cool and stir overnight, a make-up water can be accordingly added (i.e the volume decreased and as such make up DI water was needed).

After, the prepared solution was put on a magnetic stirrer to achieve a well-mixed and uniform solution.

Regarding experiment type Swagelok<sup>®</sup> 2.0 and EC-Autoclave, a higher CO<sub>2</sub> loading of  $\alpha = 1.5$  (0.5 per amine group in DETA molecule) were employed.

Please find a detailed step by step procedure in Appendix A2, including the make-up water that was added as described above.

The following sections in the rest of the chapter describes briefly how the CO<sub>2</sub> and amine analysis were conducted as well as the acid loading contents (1wt% and 2wt%).

### 7.5.2 CO<sub>2</sub> loading and Analysis

A careful inspection of the structure of diethylenetriamine (DETA) reveals that it has three amine groups- 2 primary and a secondary group. The result is that the CO<sub>2</sub> loading is calculated slightly different from other benchmark solvents like MEA. Unlike MEA,  $\alpha$  for DETA can be specified on two basis: mol CO<sub>2</sub>/mol amine or mol CO<sub>2</sub>/mole total alkalinity. So typically if  $\alpha = 0.4$  (on per amine basis), then for total alkalinity one multiplies it by 3 to get  $\alpha = 1.2$  (on total alkalinity basis).

For CO<sub>2</sub> loading to  $\alpha = 1.2$  ( alkalinity basis, Swagelok<sup>®</sup> 1.0) and  $\alpha = 1.5$  (alkalinity basis, Swagelok<sup>®</sup> 2.0), the prepared 2.5 M DETA solution (corresponding to ~ 25.5 wt% basis) was contacted and bubbled through with a CO<sub>2</sub> gas stream (purity > 99.9 mol % from AGA Gas GmbH) for a period of about 30 minutes. The time for the gas-solvent contact is needed in order to obtain the desired amount of CO<sub>2</sub> that is needed to be absorbed in the amine. The loading was determined from the weight change of the solution after the CO<sub>2</sub> bubbling. The exact amount of CO<sub>2</sub> required was calculated from the simple formula shown below (on total alkalinity basis, please notice the multiplication by 1/3 equation 7-1):

$$\text{DETA CO}_2 \text{ loading} \quad \alpha = \frac{\text{mole CO}_2}{\text{mole DETA} * (1/3)} \quad 7-1$$

$$\text{Mole DETA} = \frac{\text{mass 25.5wt\% DETA Solution(g)}}{\text{molecular weight}(103.17 \frac{\text{g}}{\text{ml}})} \quad 7-2$$

$$\text{Mass CO}_2 \text{ needed} \quad m_{\text{CO}_2} = \text{mol DETA} * \alpha * \text{molar mass of CO}_2 \left( \frac{44.01\text{g}}{\text{mol}} \right) \quad 7-3$$

After the loading, the exact amount of CO<sub>2</sub> was determined by the barium chloride method, total amine concentration was determined by acid-base back-titration both methods using the Metrohm Titrando 836. The equations for the barium chloride CO<sub>2</sub> determination method is found in the titration section in the methodology chapter 6. To account for uncertainty repeated samples were used for the titrations and, the standard deviation for repeated measurements was in the range ±0.065. All titrations and measurements were performed at ambient temperatures and pressures.

All detailed calculations can be found in the excel file supporting information in Appendix A2.

### 7.5.3 Acid loadings

The various experiments had different varying parameters and as has been mentioned in the methodology, for the acid loadings, 1wt% - 2wt% were used. These degradation products (oxalic acid, acetic acid and formic acid) solutions were prepared from reagent grade (Sigma Aldrich) and high purity (>99%) samples. Deionized water was used to prepare all solutions. For a typical wt% acid loading, the basis of calculation was on the unloaded CO<sub>2</sub> DETA solution. To clearly illustrate this point a sample calculation (based on a round number like 100g solution) is shown below, the rest can be found in the supporting information in Appendix A2.

Amount of 2.5M, 22.0 wt% DETA ( $\alpha = 0.4$ ) loaded solution = 100 g

DETA in 100g loaded solution = 22 g

$$\text{Mole DETA} = \frac{22\text{g}}{103.17\text{g/mol}} = 0.213 \text{ mols} \quad 7-4$$

$$\text{mol CO}_2 = (\alpha = 0.4) * \text{mol DETA}(0.213) \quad 7-5$$

$$\begin{aligned} \text{Mass CO}_2 \\ \text{in solution} \end{aligned} = (\alpha = 0.4) * \text{mol MEA}(0.213) * \frac{44.01\text{g}}{\text{mol}} = 3.749 \text{ g} \quad 7-6$$

So this means that if we want to know the amount of DETA unloaded in our loaded sample

$$\begin{aligned} \text{DETA unloaded} &= \text{DETA solution} - \text{mass CO}_2 \text{ in solution} \\ &= 96.251\text{g} \end{aligned} \quad 7-7$$

Therefore 1 wt% of acid (oxalic, formic and acetic) is calculated based on the above DETA unloaded solution weight of acid needed.

$$= \left(\frac{1}{100}\right) * 96.251 \text{ g} = 0.96251\text{g} \quad 7-8$$

After putting in the 1 wt% (or 2wt%) samples, the DETA solutions, were placed on a magnetic stirrer for uniform mixing and appropriately labeled for the experiment.

## 7.6 Experimental Procedure

### 7.6.1 Swagelok<sup>®</sup> 1.0

This experimental procedure was similar to an earlier project based on MEA (Hayfron-Benjamin 2012). In total the experiment was planned for 5 weeks, and at the end of each week a set of samples are taken for examination.

The experiment starts by weighing and recording all the surface prepared metal specimens (as described in the prior surface methods and this includes dimensions taken). Next the specimens

are fitted into the metal cylinder constructed from 316 stainless steel tubes with an outer diameter of ½ inch and equipped with Swagelok<sup>®</sup> end caps. For each week, 8 test specimens were chosen for the four different corrosive medium–loaded DETA solution containing the following: no degradation acid, oxalic, formic and acetic acid. For each medium duplicate metal specimen are included to ensure that results can be reproducible within certain range of deviation (recommended practice  $\pm 10\%$ ).

After placing the specimen in the cylinders, an average of 7ml of solution is injected with the aid of syringe and needle through the opening in the Teflon into the metal cylinders to completely immerse the test specimen in the particular corrosive medium. The cylinder which by now would be full with the test specimen and DETA solution was then tightly sealed, weighed and placed in an upright position in a marked container. To check for leakage, the cylinders including solutions were all weighed before and after incubation. The containers, one for each week: 1, 2, 3, 4 and 5, were all stored in a thermostat; Memmert<sup>®</sup> Oven (model 600) from GmBH<sup>+</sup> Co and heated at 135°C which is representative of the classical conditions in a stripper (Eirik F. da Silva). The time of incubation in the thermostat was noted in the Lab logbook.



**Figure 7-5.** The inside of the Memmert<sup>®</sup>600 thermostat chamber at 135°C with the containers for the 5 different weeks of exposure shown.

### 7.6.2 Swagelok<sup>®</sup> 2.0

The procedure for the second type of experiment was similar in all way to the earlier one described (Swagelok<sup>®</sup> 1.0), with the notable exception of the following: specimens are of different designs and dimensions, time of incubation was 1-2 weeks instead of the 5 week period in the earlier one and the pH of all the solutions involved was taken before the start of the experiments. In addition, torquing was applied to the cylinders in Swagelok<sup>®</sup> 2.0 to combat the issue of leakage that plagued Swagelok<sup>®</sup> 1.0.

Swagelok<sup>®</sup> 2.0 involved fewer samples and duplicates were all in the same cylinder under the same conditions, so reproducibility was expected to be much better than Swagelok<sup>®</sup> 1.0.

Finally the experiments were conducted in the same oven and under the same temperature conditions of 135°C.

### 7.6.3 EC- Autoclave

The electrochemical experiments were slightly different from the weight loss ones. In the EC-Autoclave set-up, the as prepared metal specimen (grinded on the surface, dimensions and weight recording done) was connected to the working platinum electrode (WE) as shown in the schematic of the electrochemical cell (figure 7-6). For each experiment about 400 ml (known and recorded pH) of a different type of DETA solutions (no acid, oxalic, formic and acetic acid) was poured into the cell. The cell was tightly closed (to ensure pressurization and hence the detection of reference electrode, Ag/AgCl was made possible with the aid of the metal enclosures of the EC-Autoclave as shown in the picture figure 7-6). The EC-Autoclave was placed on a heating plate (IKA<sup>®</sup> RCT basic), which has a temperature control button (temperatures chosen 135°C and 80°C). This plate slowly heats up the solution in the metallic EC-Autoclave. The correct electrode wiring (Working-WE, auxiliary-AE and reference electrodes-RE) was connected (via a number of color-code wires with a BNC connector and a gold-plated crocodile clips) to the ACM<sup>®</sup> Instruments Potentiostat and hooked to the computer (data processing). After a stable temperature has been reached for quite sometime (10 minutes stability) and next depending on what was being measured (LPR, Potentodynamic or EIS) the appropriate technique was selected from Sequencer<sup>®</sup> and Core<sup>®</sup>. According to ASTM standard G5-13 for “*Standard Reference Test Method for Making Potentiodynamic Anodic Polarization Measurements*” (ASTM 2013), it is recommended that the corrosion potential  $E_{\text{corr}}$  (rest potential) should be in equilibrium and as such the open-circuit specimen potential, that is, the corrosion potential, was measured after

about 55 min immersion of the reference electrode in the DETA solutions in the cell. So in total after 1 hour of setting up, measurements begins. For the LPR, 2 measurements were made (each at 15minutes apart), with a sweep range of -20mv to + 20mv. Furthermore a scanning rate of 12 mv/min was chosen. A slow scan rate gave better results. The LPR technique allowed the linear polarization resistance to be determined and from it the corrosion current ( $I_{corr}$ ) can be calculated from the Stern-Geary equation. The potentiodynamic (cyclic) sweep was started from -180mv to + 100mv about the rest potential. A scan rate of 50mv/min, a half cycle, cell settle time (to give the working electrode, WE, a moment to adjust to the initial polarization) were entered in the parameters for the cycle sweep interface. Typically each sweep took, 5 minutes but repeated measurements (3-5 times) were made to improve reproducibility.

Finally, once selected the potentiostat is activated (core runner starts the logging sequences) and begins measuring the corrosion and relevant potentials of the stainless steel 316 specimen placed in the DETA solution. The Tafel constants and the polarization resistances are accordingly determined. The electrochemical testing was repeated a number of times, mostly over the span of 1-2 days and the data as produced was recorded and interpreted for the corrosion rates and characterization.

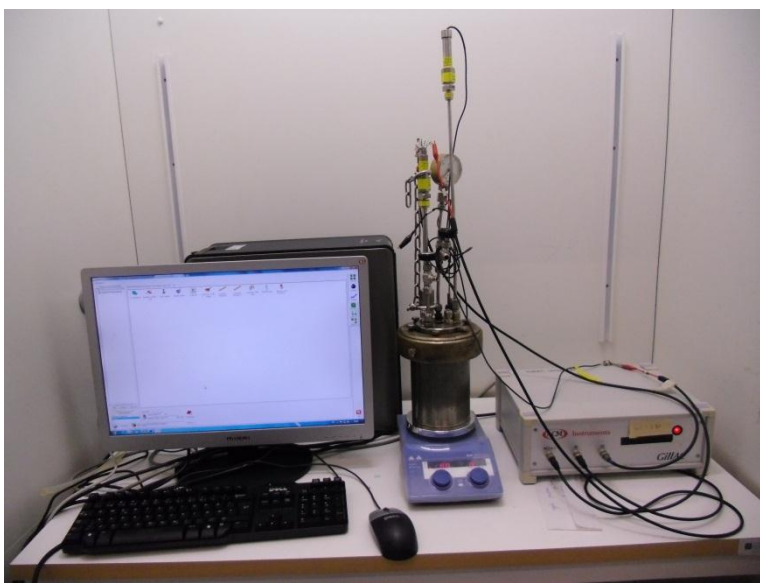


**Figure 7-6.** E-C Autoclave with the potentiostat and data processing unit

## **7.6.4 After the Test**

### ***7.6.4.1 Swagelok® 1.0 & Swagelok® 2.0***

During regular intervals- once a week- a marked container is taken out of the Thermostat, the time noted, and it is allowed to cool for about 2 hours. The specimens in the stainless steel metal cylinders were cleaned according to ASTM G1-03 (ASTM 2011) which prescribes a chemical cleaning procedure for stainless steel method. The method involved cleaning test specimens in 15 wt% di-ammonium citrate ( $(\text{NH}_4)_2\text{HC}_6\text{H}_5\text{O}_7$ ) solution at 70°C, prepared with reagent grade chemical (obtained from Merck®) and deionized water. Test specimen were placed in this chemical for an average of 10 minutes, and then later rinsed with deionized water and dried with hot air and finally weighted to determine the weight loss. The procedure was repeated for about 4 cycles for each test specimen until all corroded material on the surface of the test specimens were removed. Cleaning of specimens is vital in corrosion experiments because if not done properly misleading results can occur.

The mass loss was determined and the cleaned and weighted samples were then investigated for any surface defects caused by corrosion. It should be noted that for some of the samples, before they were cleaned their appearance was observed and recorded with the aid of an optical microscopy (magnification 50X-100X) in order to help with "location of deposits, variations in types of deposits or variation in corrosion products which defines what type of localized corrosion that might have happened such as pitting and concentration attack" (ASTM 2004). Scanning electron microscopy (SEM) was performed for Swagelok® 2.0 samples to help with further surface characterization. Some of the images obtained in using both tools (SEM and Optical Microscope) can be seen in discussion part (chapter 8).

### ***7.6.4.2 EC- Autoclave***

The after- testing procedure involved the sample being removed from the platinum electrode wiring, the surface cleaned as per the weight loss method and weighing of corroded specimen were additionally done. The weighing was not necessary, since the EC-Autoclave experiments were electrochemical in nature and as such weight loss becomes redundant but to have greater spread in data, the additional corrosion rate obtained from weight loss was done. Surface

morphology was done for the specimens using a simple microscopy with magnifications of 500x, 100x and 10x. pH of corrosive solutions were also taken after the testing and duly recorded. The interpretation of the data will be covered in the discussion portion of this work in the next chapter.

## Chapter 8 Results and Discussion

### 8.0 Introduction

In accordance with the experimental set-ups as described in the previous chapter, the results and discussion part of this chapter will be headed under the three main types of experiments that were done: Swagelok<sup>®</sup> 1.0, Swagelok<sup>®</sup> 2.0 and the EC-Autoclave experiments. Also the surface morphology using the simple optical microscope (Microfibre Optronics<sup>®</sup>) and the scanning electron microscopy (SEM- Hitachi S-3400N<sup>®</sup>) will ensue. Eventually how the experimental values measures up against models in the literature will also be looked at in this chapter.

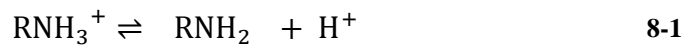
### 8.1 Coupon weight- loss Tests

#### 8.1.1 Swagelok<sup>®</sup> 1.0

The effect of corrosion on the stainless steel 316L material in the presence of previously CO<sub>2</sub> loaded ( $\alpha = 1.2$ ) diethylenetriamine and a combination of heat stable salts were investigated. The heat stable salt anions like acetate, formate and oxalate were introduced by dissolving the respective acid forms as described in the experimental section in the previous chapter. A total of four different corrosive mediums set-ups: only diethylenetriamine, diethylenetriamine + oxalic acid(1wt%), diethylenetriamine + formic acid(1wt%), and diethylenetriamine + acetic acid(1wt%); were allowed to be on stream in Memert<sup>®</sup> oven thermostat at a constant temperature of 135°C for approximate periods of 168, 360, 530, 670 and 750 hours. This represented a corrosion monitoring over a period a 5-week period with intermittent corrosion results obtained after each week. Results obtained showed some familiar and interesting trends such as the fact that acetic acid set-ups were the most corrosive, followed closely by the likes of oxalic and formic acid and that of diethylenetriamine in that order. It can be mentioned that at a higher temperatures of 135°C, corrosion rates is much higher than for similar set-ups at lower temperatures. In the literature, for MEA corrosion of stainless steel 316L was carried out by Nuria and Hallvard (Tavera-Valero and Svendsen 2011) at an absorber reactor-like temperatures of 50°C and the results as compared to this work is less than one hundredth of millimeter.

The differences between the rates from this work and that of Nuria and Hallvard (Tavera-Valero and Svendsen 2011) can be attributed to the higher temperatures at which this work was conducted. This led to a considerable acceleration of corrosion rates. This phenomenon of increased corrosion rates with temperature could be explained by examining the two equations taking place in amine-CO<sub>2</sub> systems as shown below and this is equally applicable to a polyamine like diethylenetriamine (C<sub>4</sub>H<sub>13</sub>N<sub>3</sub>) the mechanisms described by Veawab and co-workers (Veawab, Tontiwachwuthikul et al. 1999).

Dissociation of protonated amine:



Dissociation of bicarbonate ion:



Since temperature is an essential kinetic parameter in all absorption systems, CCS systems included, an increase in temperature shifts the above equilibrium reactions resulting in greater amounts of H<sup>+</sup> and HCO<sub>3</sub><sup>-</sup> as explained by Rochelle and co-workers. (Austgen, Rochelle et al. 1989). The increase in the above mentioned species (shown in equations 8-1 and 8-2 above) results in more importantly disturbing the equilibrium of the metal dissolution and oxidizer reduction reactions which are the key reactions for corrosion and rust formation. So to restore equilibrium, more metal (iron) dissolves, generating more electrons for the cathodic reaction, which enhances the corrosion rate (Hayfron-Benjamin 2012).

Another angle for looking at corrosion rates of DETA unlike other amines (MEA, DEA etc.) is from the view of the thermal degradation profile of DETA. It was observed that after 530 hours of specimen on stream, negligible weight loss were obtained, this corresponds to very unusual low corrosion rates of stainless steel by diethylenetriamine. Not surprisingly from the works of Jason Davis (Davis 2009) who studied thermal degradation of different amines diethylenetriamine included and concluded that that for diethylenetriamine (DETA), a straight chain triamine, it experienced over 90% amine loss (6% remaining) at 135°C for just a period of

only 4 weeks on stream. This observation has been corroborated by Ingvild Eide-Haugmo (Eide-Haugmo 2011). In light of these observations, a plausible reason for the observed low corrosion rates can be the fact that significant diethylenetriamine was not present during these periods. Figure 8-1 below shows a snapshot of the various corrosion rates and the varying systems

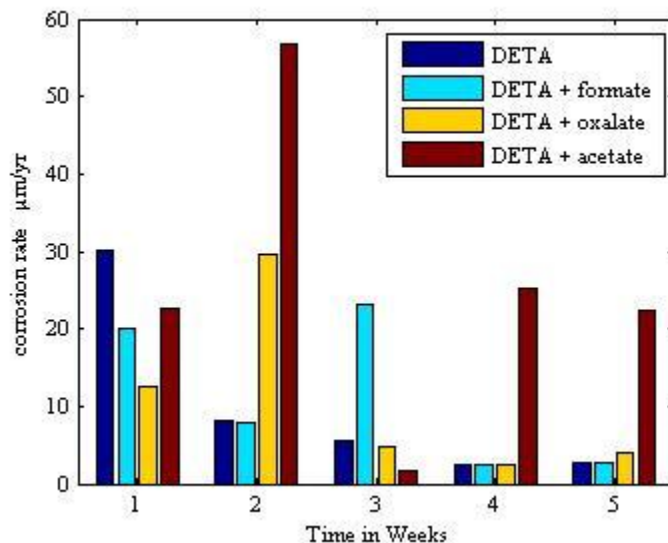


**Figure 8-1.** Corrosion rates as a function of time (weeks)

From the diagram above one can see that acetic acid has had the consistent higher rates of corrosion, with formate and oxalate following in no particular order and then the plain diethylenetriamine systems. The trend for each system will be duly analyzed in the following paragraphs.

For the first week on stream, that is after roughly 170 hours in the heated cabinet: [DETA], [DETA + 1 wt% formate], [DETA + 1 wt% oxalate] and [DETA + 1 wt% acetate] systems recorded an average corrosion rates of 30 µm/yr, 19 µm/yr, 12 µm/yr and 22 µm/yr respectively. Within the margins of error there is not much of a difference in the corrosion rates for the first week, save the oxalate outlier at just 12 µm/yr. So in effect for the first week, the four different systems acted like the same homogenous corrosive medium. The reason behind this is hard to deduce but the same for the first week on stream trend was noticed in earlier work (Hayfron-Benjamin 2012) which was conducted under similar conditions but with a different amine system, being MEA. In that earlier work, [MEA + 1 wt% oxalate] medium had the highest

corrosion rate at 0.0255 mm/yr, followed by the [MEA] and [MEA + 1 wt% acetate] at 0.0208 mm/yr and 0.0162 respectively. The least corrosive after 160 hrs in the 135°C in the thermostat was formic acid at 0.0116 mm/yr. Careful inspection of the rates in just a week reveal that the different set-up do not differ by much.

So after 1 week of experiment neither a conclusion can be drawn nor a trend deduced by observing the samples (Hayfron-Benjamin 2012). This is in line with accepted standards like what such as the fact that ASTM standards predict saying “short-time tests can give misleading results on alloys that form passive films, such as stainless steel” (ASTM 2004; Hayfron-Benjamin 2012).

In subsequent weeks, after the baseline week (week number 1), the acetic and oxalic acid systems present a clear picture that contrast with the other two remaining systems as can be seen in figures 8-2, 8-3, 8-4 below. In all the cases presented in the figures, the difference between the least and most corrosive medium is quite high and in some cases by multiplicative factors ranging between 4 and 7. That is if one takes corrosion rates after 360 hours (corresponds to week 2), both the oxalate and acetate medium are more than 5 times as corrosive as either the formate or the DETA set-ups. In weeks 4 and 5 (please refer to figures 8-3 and 8-4) below the [DETA + 1wt% acetate] system corresponded to an average corrosion rate of 25  $\mu\text{m}/\text{yr}$  and 22  $\mu\text{m}/\text{yr}$  respectively and these rates as compared to say the [DETA] system at 2.5  $\mu\text{m}/\text{yr}$  is more than by a factor of 10. This proves the extreme corrosive behavior of heat stable salts which find their way into CO<sub>2</sub> amine treatment systems. The exact role of the HSS anions in solution and how they accelerate corrosion has been dealt in the theory portion of this thesis (chapter 5, section 5.4.2)

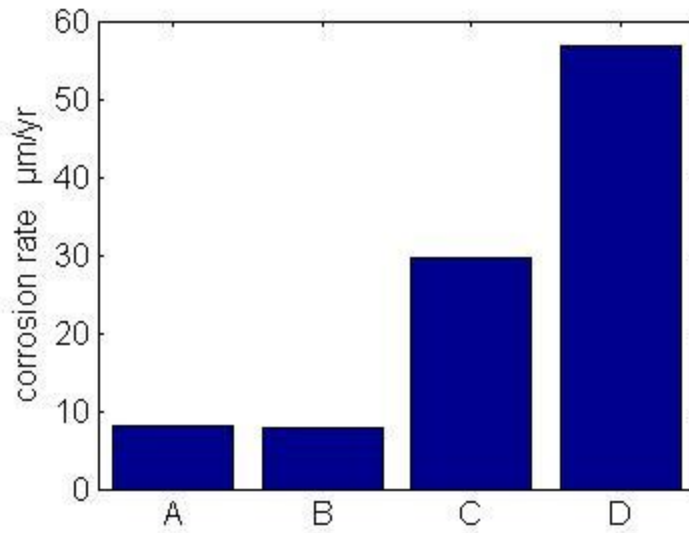


**Figure 8-2.** Week 2 corrosion rates and various systems- A = DETA, B = formate, C = oxalate, D = acetate

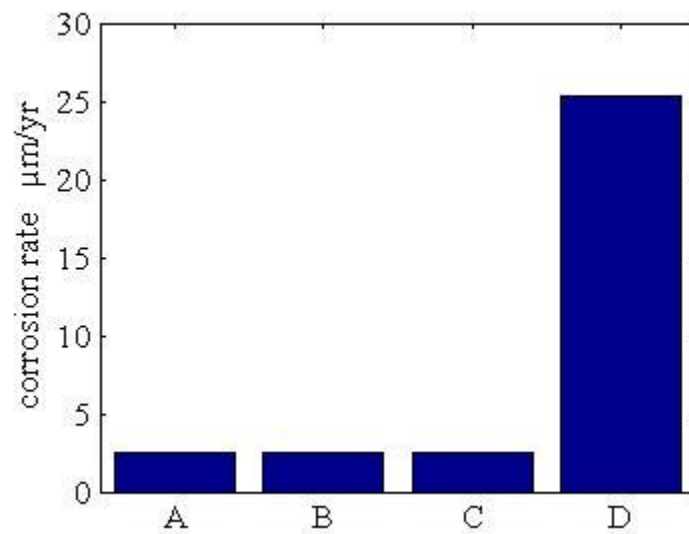


**Figure 8-3.** Week 4 corrosion rates and various systems- A = DETA, B = formate, C = oxalate, D = acetate

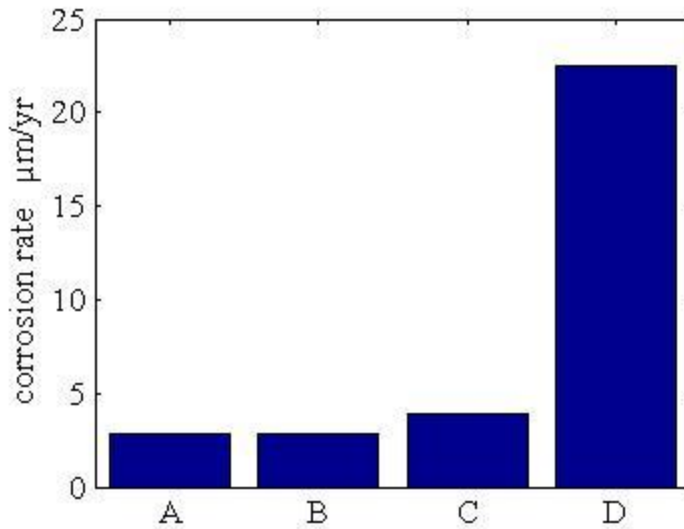
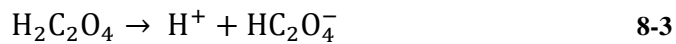


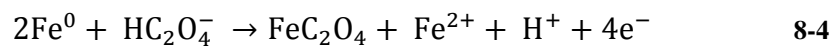
**Figure 8-4.** Week 5 corrosion rates and various systems- A = DETA, B = formate, C = oxalate, D = acetate

Possible mechanisms for the corrosion from oxalic and acetic acid can be explained by the following reactions which “suggests that the presence of oxalate enhanced the rates of oxidation (iron dissolution) and the reduction of oxidizing agents“, (Tanthapanichakoon, Veawab et al. 2006) as well as the fact that cathodic reaction involving oxalic acid proceeds with hydrogen evolution (Wiersma and Mickalonis 2008). A plausible mechanism has been suggested by Wiersma and Mickalonis (Wiersma and Mickalonis 2008):

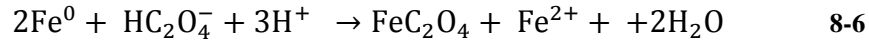
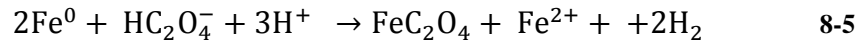
Oxalic acid dissociates into the hydrogen-oxalate ( $\text{HC}_2\text{O}_4^-$ ) species and hydrogen cation.



By nature corrosion can be categorized as an electrochemical process (anodic and cathodic reactions), with metal dissolution (anodic) and oxidizer reduction as the cathodic reaction (Veawab, Tontiwachwuthikul et al. 1999). The hydrogen-oxalate species then participates in the metal dissolution reaction as shown in equation 8-4:



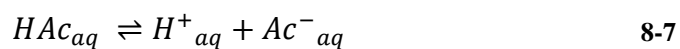
Depending on the presence of either O<sub>2</sub> or H<sub>2</sub>, two distinct cathodic reactions can proceed which produces two new overall corrosion reactions as shown below:



From the above ferrous species reacts further to form ferrous hydroxide (rust), further oxidation to ferric oxide (rust) and the observance of a yellowish species found on oxalic acid systems (FeC<sub>2</sub>O<sub>4</sub>•2H<sub>2</sub>O, a metal surface passivizing species).

In all the figures it can be seen that the amine type system itself has an effect on corrosion though not on the same scale as the highly corrosive oxalic and acetic acids. This observation is expected since numerous works have reported of the corrosive behavior of CO<sub>2</sub> loaded MEA among the amine-based systems on stainless and carbon steel (Veawab, Tontiwachwuthikul et al. 1999; Gao, Wang et al. 2012).

In a similar fashion mechanisms by which acetate anions causes corrosion has been dealt with by a number of authors in a particular recent (this year 2013) work Thu Tran et al. (Thu Tran, Bruce Brown et al. 2013) investigated the mechanism for acetic acid corrosion of mild steel. It was found that acetic acid is recognized as an important factor in mild steel corrosion and like carbonic acid (the source being CO<sub>2</sub> dissolved in aqueous solutions), acetic acid also partially dissociates, is a function of pH and the solution temperature (Thu Tran, Bruce Brown et al. 2013). But acetic acid is the stronger of the two weak acids (pKa 4.76 vs. 6.35 at 25°C), and hence in CO<sub>2</sub> dissolved amine systems, acetic acid becomes the main source of hydrogen ions when the concentration of each acid is the same (Thu Tran, Bruce Brown et al. 2013). Two dominant mechanisms have been proposed for acetate ion and corrosion: direct reduction and buffering effect mechanisms.



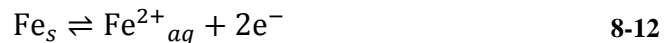
The effect of the acetate ions is to accelerate the cathodic hydrogen evolution reaction thereby increasing the corrosion current and hence corrosion rates at the anode (metal dissolution):



In the direct reduction approach (Thu Tran, Bruce Brown et al. 2013) the acid is reduced at the metal surface according to reaction (equation 8-11 below), in addition to the reduction of hydrogen ions typical for all acids (cathodic reduction reaction) as shown in reaction 8-10.



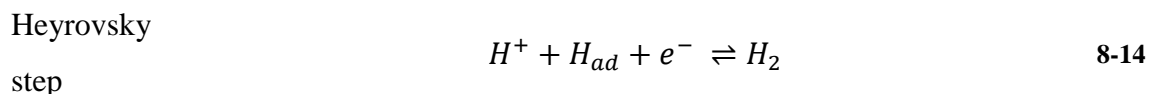
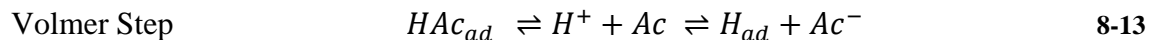
The anodic reaction that occurs at the same time at the metal surface is the dissolution of iron as shown equation 8-12 and this is done to balance the charge:



The additional reactions at the cathode accounts for an increased corrosion current  $i_{corr}$  at the anode causing greater dissolution of the Fe and hence a corresponding greater corrosion rates.

In the competing mechanisms put forward illustrated by the buffering effect (Thu Tran, Bruce Brown et al. 2013), acetic acid acts as the only source of ions and hence there is no reduction of the acid as shown in equation 8-11 above and the main reduction of hydrogen ions is the only surface reaction but then the role of acetic acid is to act as a “buffer,” which provides more hydrogen ions when the latter are consumed by the corrosion reaction at the surface as shown in reaction 8-13.

The surface adsorption and dissociation to produce  $H^+$  ions have been proposed by Amry (J. Amri, E. Gulbrandsen et al. 2011; Thu Tran, Bruce Brown et al. 2013) using the Volmer-Heyrovsky steps:



So in short, if direct reduction of acetic acid occurs at the surface, the corrosion rate will keep increasing with the increasing acetic acid concentration at the same pH, irrespective of the controlling step (charge or mass transfer control) (Thu Tran, Bruce Brown et al. 2013).

However, if the buffering effect mechanisms prevails the corrosion rate will stop increasing beyond a certain acetic acid concentration, when the control shifts from mass transfer to charge transfer control (Thu Tran, Bruce Brown et al. 2013). In essence regardless of the prevailing mechanisms, acetic acid is known to cause considerable damage to steel materials as this work also showed.

After longer exposure to the various acids, 357, 524, 669 and 750 hours, it can be seen from the scatter diagram (figure 8-5) of the various systems above, that the corrosion rates of oxalic acid remains steady after a slight increase from week 1 and week 2. As previously mentioned, the acetate solutions hit a high of 56.72  $\mu\text{m}/\text{yr}$  after just 357 hours on stream but then steadily become stable in the subsequent weeks. The reason for the high corrosion rate after the second week can be attributed to the fact that the thermal degradation of diethylenetriamine –  $\text{CO}_2$  systems has been reported by Davis to be rapid and results in having only 6% DETA left after 4 weeks at 135°C (Davis 2009). There is no data in the open literature of the time profile of thermal degradation of diethylenetriamine and hence no definitive conclusion can be drawn about when most of the DETA degraded in the Swagelok cylinders and as such attach an explanation to the observed corrosion trends in diethylenetriamine. Coupled with weight loss of solutions due to evaporation and other experimental control problems speculation could be made about the sharp drop for the acetate corrosion rates (from 56  $\mu\text{m}/\text{yr}$  at 357 hours to a mere 1.5

$\mu\text{m}/\text{yr}$  a week later). In fact in that situation it was found out that there were none of the [DETA+ 1 wt% acetate] solution and hence could explain why there was hardly any corrosion. The overall trend corresponds well with a similar set-up in a previous work (Hayfron-Benjamin 2012).

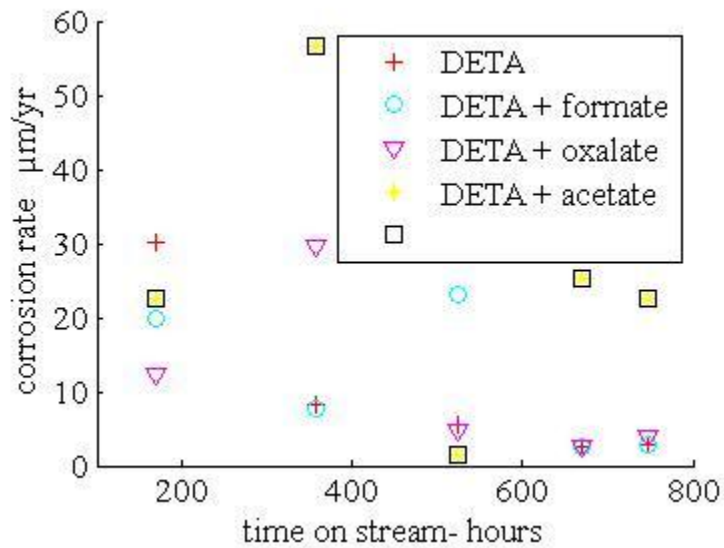


**Figure 8-5.** Corrosion trend for all systems for 5-week time period

To interpret the coupon weight loss data in a different perspective, a look at how corrosion rates increased or decreased was done with having week number 1 as the baseline. In this approach one can assess the slow down in corrosion rates with time in the Swagelok<sup>®</sup> 1.0 set-up.

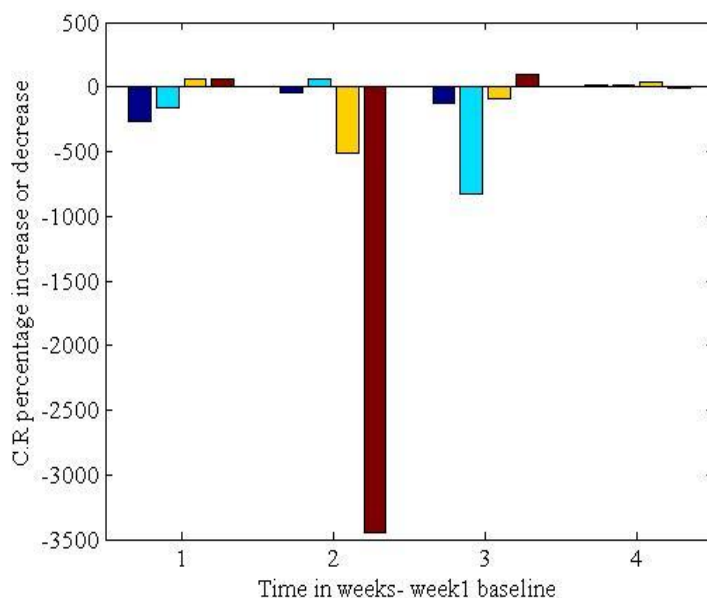


**Figure 8-6.** Baseline (DETA) % change in corrosion rates comparison

The massive (as much as 3500 % decrease) slow down in the corrosion rate as recorded after weeks 3 and 4 on stream can attributed to the deposition of corrosion products on the surface of the specimen. It can also be deduced (Hayfron-Benjamin 2012) that after longer exposure at such high temperatures (135°C), coupled with great mass loss of solution, the viscosity of the solutions will increase, leading to decrease in mobility of the ions (Singh and Mukherjee 2010) responsible for the cathodic and anodic reactions that lead to corrosion. For example acetic acid has been reported to have remarkably decreased corrosion rates in SS41 type meta (Sekine and Senoo 1984). The data for figure 8-6 above can be seen in Table 8-1:

**Table 8-1.** Percentage change in corrosion rates of all systems per week 1

% increase /decrease on the first week data					average
t/hrs	357.8333333	524.8333	669.2	746.75	
[DETA]	-266.078537	-46.2933	-122.749	11.04347	-106.019
[DETA + 1.00wt% formate]	-	66.32971	-828.881	11.16711	-226.596
[DETA + 1.00wt% oxalate]	58.09922548	-515.894	-91.252	35.87246	-128.294
[DETA + 1.00wt% acetate]	60.16662697	-3449.12	93.67881	-12.4415	-826.928

From the above table all the four systems experienced a remarkable decrease in average corrosion rates after the baseline week 1. After the first week, [DETA + 1.00 wt% acetate] enjoyed an increase of 60% in corrosion rate and this carried on till week 4 with 93% rise except the outlier in week number 2. Some of these observations could be due to a number of factors such as solution loss, thermal degradation of diethylenetriamine, deposition of iron carbonate systems that all impede and retard corrosion. Finally to present a contrast between the various acid systems as compared to only the DETA-CO<sub>2</sub> system, a comparison is made to generate what is termed as the relative corrosion rates. The result is as shown in figure 8-7 below.

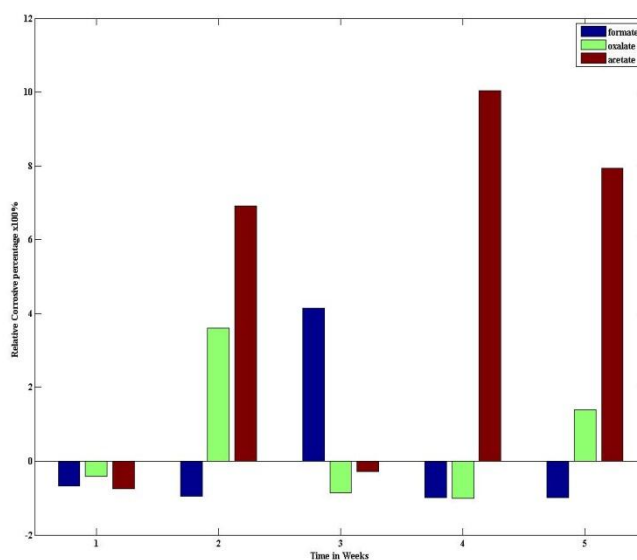
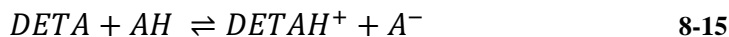


**Figure 8-7.** Relative corrosion rates, compared to DETA system

The relative corrosive term helps to have an idea about the impact of HSS anions in DETA –CO<sub>2</sub> systems. As has been explored in the theory section (chapter 5), the role of heat stable salts (HSS) has widely been documented that they worsen the corrosion problems. These salts act as precursors of corrosive agents for plant equipment corrosion. The figure 8-7 then simply shows that in the presence of formate, oxalate and acetate ions in diethylenetriamine-CO<sub>2</sub> solution, has a varying impact on the corrosion rate. Taking the acetate system for example, shows that from week 2 till the end of the experiment, acetic acid can be said to anywhere between 6-11 times as corrosive as only the DETA system. Similar conclusions can be drawn from the oxalate system.

The presence of formate species in DETA however can not be said to enhance corrosion, since most of its impact factors are in the negative as shown in the graph. The observed high corrosion rates due to the presence of HSS species can be explained by the fact that, these acids react with the amine by proton transfer (Veldman 2000) according to the following chemical equations:



Corrosion reaction (A.L. Kohl 1997; DeHart 1999):



The fact is that amine pH is greater than the pKa of these organic acids as well as the fact that in concentration terms (DETA = 2.5M, the amines concentration far exceeds those of the acids. The consequence is that equilibrium shifts to the right and the acids stay in the neutralized heat stable form (Veldman 2000). Therefore by increasing CO<sub>2</sub> loadings, pH is decreased and in addition under thermal regeneration of amines in the stripper, the acids in the heat stable form becomes volatile. This volatility coupled with hot temperatures, aqueous environment leads to very corrosive conditions.

In a previous work (Hayfron-Benjamin 2012), it was shown that indeed the presence of the acids of the HSS results in significantly high corrosion rates of stainless steel 316L as compared to the corrosive effect of only amine solutions. This information about the role of heat stable salts (HSS) can be useful in the design phase of a carbon capture and storage plant where material selection is an important stage of the process.

A snapshot of all measurements in all four systems: [DETA], [DETA + 1.00wt% formate], [DETA + 1.00wt% oxalate] and [DETA + 1.00wt% acetate] is as shown in figure 8-8. This figure includes all parallel systems that were run. The issue of reproducibility of results will shortly be discussed in conjunction with an earlier work (Hayfron-Benjamin 2012) that was done with MEA.

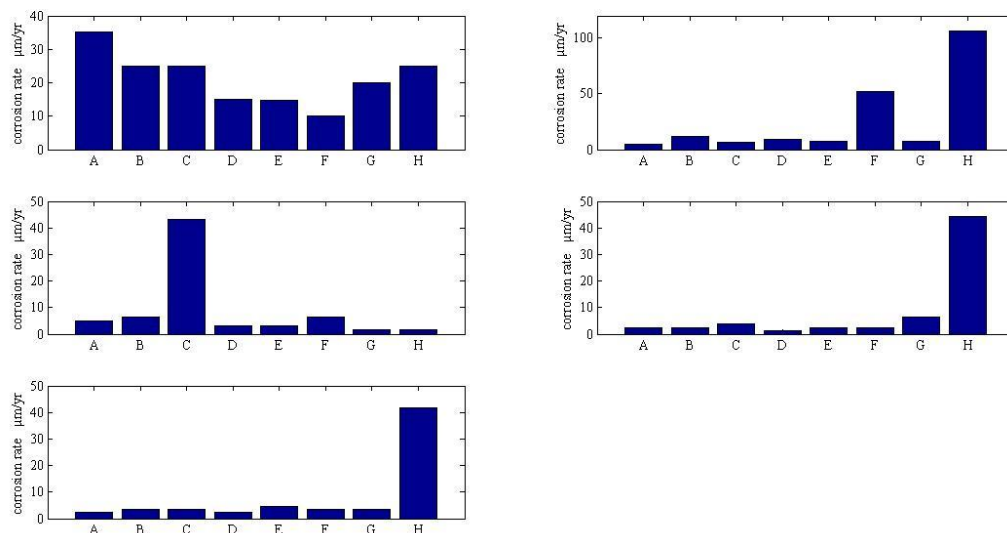


**Figure 8-8.** Snapshot of corrosion rates of all systems including parallel samples. A, B = DETA; C, D = formate; E, F = oxalate; G, H = acetate

### 8.1.1.1 MEA and DETA Corrosion Comparisons

In order to have an overall assessment of the corrosivity of diethylenetriamine in CO<sub>2</sub> environment, it is important to place DETA in line with how other amine-based CO<sub>2</sub> systems affect metal degradation. Monoethanolamine (MEA) has been the benchmark solvent for use in CCS plants worldwide for decades (Eirik F. da Silva ; F.C. Risenfeld and Blohm 1950; L.D. Polderman, C.P. Dillon et al. 1955; Aboudheir, Tontiwachwuthikul et al. 2003; Alie, Backham et al. 2005; Tanthapanichakoon, Veawab et al. 2006; Davis and Rochelle 2009; Edali, Aboudheir et al. 2009; Kittel, Idem et al. 2009; Tavera-Valero and Svendsen 2011; Vevelstad, Eide-Haugmo et al. 2011) and studies has shown that it is in combination with heat stable salts produced as a result of solvent degradation, that impacts heavily in terms of corrosion on plant material and most of the studies have focused on MEA corrosion on carbon steel (Peberé, Duprat et al. 1988; L. G. S. Gray, B. G. Anderson et al. 1990; Nesic, Drazic et al. 1996; Nesic, Postlethwaite et al. 1996; Rooney, DuPart et al. 1997; Veawab, Tontiwachwuthikul et al. 1999; Pletcher and Garsany 2003; Wiersma and Mickalonis 2008; Kladkaew, Idem et al. 2009; Kladkaew, Idem et al. 2009; Gao, Wang et al. 2012) and lately some on stainless steel (Wegrelius, Falkenberg et al. 1999; Olsson and Landolt 2003; Z.F. Yin, X.Z. Wang et al. 2010; Tavera-Valero and Svendsen

2011; Hayfron-Benjamin 2012). Diethylenetriamine (DETA) has been reported by plant operators to be highly corrosive (Rochelle 2013; Svendsen 2013) and intuitively because of its polyamine structure, with high CO<sub>2</sub> absorption capabilities and rapid thermal degradation (Davis 2009), it will be expected that DETA will be more corrosive than MEA under similar plant operating conditions. The only problem with this assessment is that there is hardly any data in the open literature to back it up. This work is one of the early if not the first to examine how diethylenetriamine-CO<sub>2</sub> systems corrode stainless steel material.

A simple comparison of corrosion rates of MEA and DETA on stainless steel is shown in the figures 8-9 and 8-10 below. The first diagram (figure 8-9), which shows acetic acid corrosion in both amine solvents (MEA and DETA) over a 5 week experimental period at 135°C with an identical loading of  $\alpha = 0.4$ . The figure shows that on average the 1 wt% acetate solution in DETA has a higher corrosivity towards stainless steel than its counterpart in MEA and for the overall corrosion comparison for the 2-3 week window of experiment when the diethylenetriamine has not completely degraded, MEA has a better corrosion resistance capabilities than DETA. Figure 8-9 might lead one to conclude without further inspection that MEA is more corrosive than DETA. This diagram is taken from the average corrosion data of all four systems (oxalate, amine only, formate and acetate) and their combination skews the representation. For example for system to system corrosion rates comparison, in MEA + acetate, there was a reported rate of 0.45 mpy (Hayfron-Benjamin 2012) after 2 weeks on stream and in DETA + acetate, the rate was 4.2 mpy. The difference is clear and wide rate differences were noted for the experimental times. Of course over the longer period of time MEA proved to be more corrosive than DETA and the reason simply being that DETA after close the 3 week on stream degrades almost completely and will thus have no effect on corrosion. The detailed weight loss procedure and numbers and corrosion rates for all the systems can be found in Appendix A1 attached to this work.

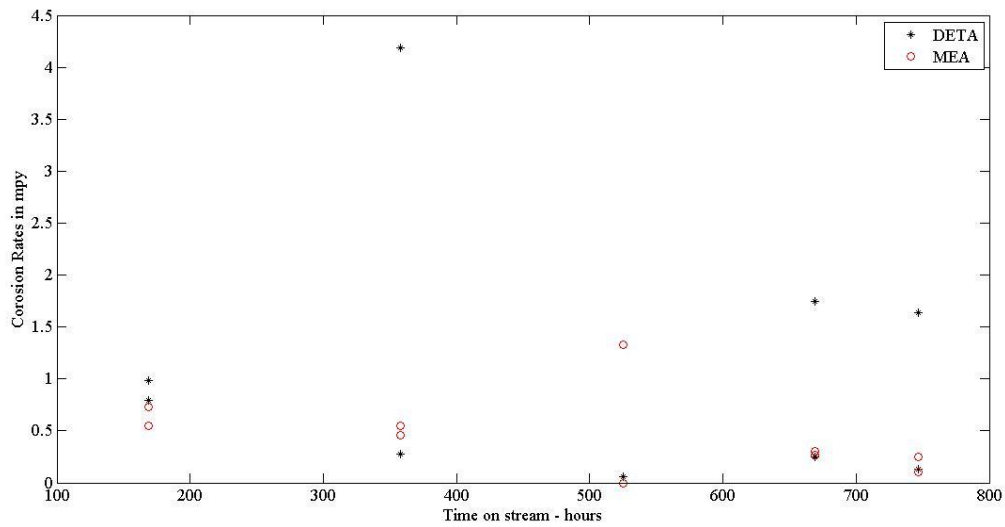


**Figure 8-9.** MEA and DETA acetic acid system corrosion rates comparison

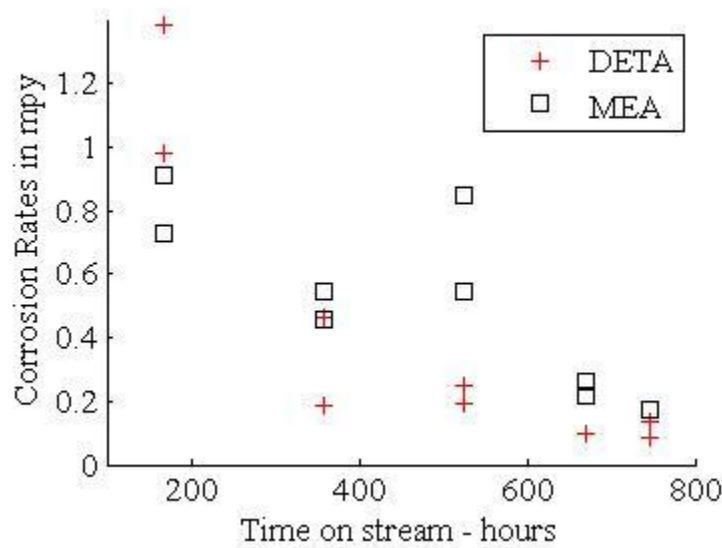


**Figure 8-10.** MEA and DETA corrosion rates

### 8.1.2 Swagelok® 2.0

The intuition that higher loadings of CO<sub>2</sub> in the DETA-H<sub>2</sub>O-degradation products systems will result in higher corrosion rates was not realized. This intuition is based on the fact that at higher  $\alpha$  values, the carbonate ion species will abound and since it is an oxidizing species will accelerate

the corrosion rates as has been pointed out thoroughly in the theory section (chapter 5). The reason for the comparatively low corrosion rates for the second-run could be attributed to a number of factors.

First, experimental control over the metal cylinder was difficult to achieve, the cylinders had been re-used for at least 3 years plus, and the condition at the higher temperature and pressures is simply not conducive to have a proper control over the conditions. The leakage problems, even though a mechanical torque tool was employed persisted and evaporation of solution as well.

The second and more scientific reason for the results as-is is that a higher loadings ( $\alpha = \max$  for DETA in Swagelok® 2.0) the concentration of  $\text{CO}_3^{2-}$  increases as compared to say  $\alpha = 1.2$  which was used for Swagelok® 1.0. This increase in  $\text{CO}_3^{2-}$  increases the ionic product of  $(\text{Fe}^{2+})(\text{CO}_3^{2-})$  and if this value exceeds the solubility constant  $K_{\text{sp}}(\text{FeCO}_3)$  beyond the saturation point, the surface of the metal is covered with layer of ferrous carbonate which will slow down corrosion. Nescic et al. (Srdjan Nescic, Dusan Sormaz et al. 2008) stated that “ferrous carbonate layer can slow down the corrosion process by presenting a diffusion barrier for the species involved in the corrosion process and thereby changing the conditions at the steel surface and that for high precipitation rates, and low corrosion rates, a dense and protective ferrous carbonate layer is obtained”. This is what is suspected to have happened, because of the abundance of carbonate species in the maximum loading in DETA.

The third reason for the results in this run, was that the specimen weight was low to begin with (average 1.6g) and the analytical balance used to measure all the weight were not sensitive as compared to say higher weights for Swagelok® 1.0 (average weight 8 g). This meant that for small changes in the weight loss of the specimen there were errors in reading it from the scales. For example from the corrosion tables attached to the appendix A1 (Swagelok® 2.0) the highest weight loss recorded was 0.002g and within the margins of errors (cleaning, drying etc.), the uncertainty could be quite high.

Finally even though the experiment under this weight-loss type run was fraught with problems, it nevertheless revealed some interesting observations like the fact that there was hardly any difference of the effect of wt% of the heat stable salts (oxalate, acetate, formate) on the overall corrosion rates. Meaning for both 1wt% and 2wt% loadings into the DETA systems, the rates

hardly changed. Also acetic acid systems recorded the highest corrosion rates at 0.0274 mm/yr after a week on stream. The rest of the results can be seen the appendix A1.

## 8.2 Solution Analysis

### 8.2.1 ICP-MS

To determine and quantify corrosion accurately, the use of precise and powerful analytical techniques is required. In this experiment the Inductively Coupled Mass Spectrometry (ICP-MS) was used for elemental determinations. In the solution of the corroded DETA-CO<sub>2</sub>- degraded products systems some ions of elements such as Fe, Cr, Mn, Ni and Mo are naturally expected to be in the solution. These elements are the alloying composition of stainless steel 316. The motivation for quantifying the ions in corrosion solution is to first to be able to reach a conclusion about whether selective de-alloying of stainless steel occurs in DETA-CO<sub>2</sub>- degraded products systems and secondly to verify that corrosion has taken place. The presence in significant amount of the ions of the alloy making up the composition of the stainless steel proves that the metal degradation has taken place at the anode and hence corrosion can with confidence and precision be said to have taken place. Of the metal alloys of stainless steel, the following elements were tested: Fe, Cr, Mn, Ni and Mo. These make up the significant portion of the metal composition as shown in table 8-2 below. Because of the scope of resources available and also detection limits capabilities, the smaller composition elements such as C, Si were excluded from the ICP testing.

**Table 8-2** Nominal elemental wt% composition

<b>element</b>	C	Si	Mn	Cr	Ni	Mo	Fe
<b>weight(%)</b>	0.06	0.47	1.74	17.0	11.0	2.2	balance

Table 8-2 and 8-3 show the raw absolute amounts and the calculated relative wt% compositions of the various elements in the different systems.

All analysis has a reported uncertainty of 10%, and also the analyses are controlled against reference material SPS-SW2 Batch 119 “Elements in Surface waters”.

Looking at the total concentrations of the various elements, iron, chromium, nickel, manganese and molybdenum, it can be seen that a sizeable amount of metal ions were in the corrosion solution. In total for the entire DETA set-up over the course of 5 weeks, 48,830 mg/Lm were obtained. Of this amount just under 50% was obtained in just the first 3 weeks and this invariably coincided with the highest rates of corrosion as explained earlier with regards to DETA solvent degradation. Considering the [DETA + acetate] systems, for the element Fe, Iron metal ions showed a consistent high values ranging from a low of 160mg/L (week 3) and higher values of 7300 mg/L to 9000mg/L for weeks 5 and 4 respectively. These numbers correlate well with the corrosion rates obtained via the weight loss method. For example for week 3 with a low iron concentration of only 160mg/L, results and calculations showed a extremely low rate of only 1.6  $\mu\text{m}/\text{yr}$  whereas on the contrary for weeks 4 and 5, the high iron concentrations in solutions of 9000mg/L, 7300 mg/L corresponded to higher rates of 44  $\mu\text{m}/\text{yr}$  and 41 $\mu\text{m}/\text{yr}$  respectively. So in effect what was calculated via weight loss was further validated by the HR-ICPMS technique. The iron concentrations for DETA systems as obtained in this work are similar to those obtained by Ingvid (Eide-Haugmo 2011) who reported that after 5 weeks of testing various amine under similar conditions as this work (135°C) iron concentrations in DETA were in the range of 7.6 to  $2.1 * 10^6 \mu\text{g}/\text{L}$ . The next in concentration levels in solution were Chromium > Nickel > Molybednum and Manganese in that order. Typical values can be verified in table 8-3.

Additional corrosion due to these metal ions in solutions was explained by Dingman et al. (Dingman, Allen et al. 1966) and also Ingvid (Eide-Haugmo 2011) who stated that the amine, diethylenetriamine (DETA) acts a chelating agent in hot solution, thereby creating iron chelates. Since  $\text{CO}_2$  is present as carbonic acid, iron bicarbonates are formed. Next the amine structure forms chelates with the Iron, thereby freeing the carbonate oxidizing agents for further corrosion. Figures 8-11 to 8-16 summarize all that has been said above and each week for experiment, the absolute amount of metals ions in solutions has been plotted on a horizontal bar chart using MATLAB.

**Table 8-3** ICP-MS absolute values of ions in corrosion solution

ICP-MS absolute values mg/L							
Week #	Test Specimens	Chromium	Manganese	Iron	Nickel	Molybdenum	Total mg/L
1	[DETA]_1	109.550	9.721	484.909	86.232	15.285	705.697
	[DETA + 1.00wt% formate]_3	79.834	8.329	420.224	62.614	12.045	583.046
	[DETA + 1.00wt% oxalate]_5	93.277	6.784	365.750	57.755	11.306	534.872
	[DETA + 1.00wt% acetate]_7	88.718	8.182	384.035	56.029	11.252	548.216
2	[DETA]_9	114.488	12.257	507.834	54.697	12.538	701.815
	[DETA + 1.00wt% formate]_12	95.208	8.952	527.134	66.416	12.433	710.144
	[DETA + 1.00wt% oxalate]_14	1425.854	133.082	6067.694	1007.789	180.358	8814.776
	[DETA + 1.00wt% acetate]_16	1436.752	125.428	6127.745	956.419	182.484	8828.827
3	[DETA]_17	44.478	5.723	203.383	16.320	5.123	275.028
	[DETA + 1.00wt% formate]_20	78.588	8.494	384.789	34.692	7.855	514.418
	[DETA + 1.00wt% oxalate]_21	152.494	5.665	283.642	26.166	7.276	475.244
	[DETA + 1.00wt% acetate]_24	74.778	2.774	161.469	19.411	6.216	264.648
4	[DETA]_26	39.739	4.900	253.595	43.078	5.558	346.870
	[DETA + 1.00wt% formate]_28	60.127	6.564	238.501	23.475	6.541	335.209
	[DETA + 1.00wt% oxalate]_30	57.620	6.962	384.627	65.692	8.560	523.460
	[DETA + 1.00wt% acetate]_32	1524.203	189.729	9006.220	1540.184	251.432	12511.770
5	[DETA]_34	98.108	12.482	643.558	54.090	10.897	819.136
	[DETA + 1.00wt% formate]_36	34.306	7.070	247.496	55.547	5.592	350.010
	[DETA + 1.00wt% oxalate]_37	79.114	7.565	412.910	49.780	8.922	558.291
	[DETA + 1.00wt% acetate]_40	1269.272	170.765	7290.522	1481.268	216.857	10428.680

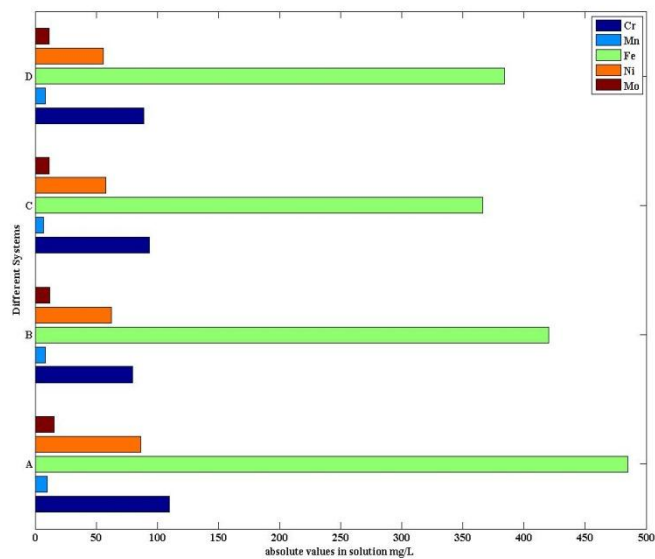


Figure 8-11. ICP-MS absolute values (mg/L) of ions in corrosion solution for Week 1

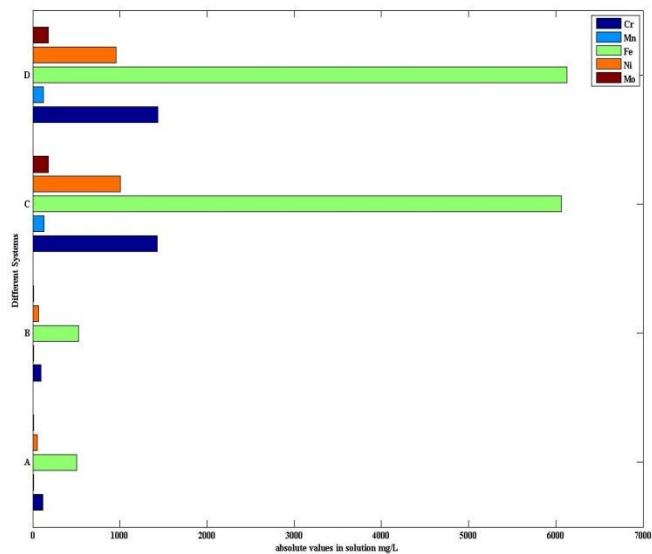
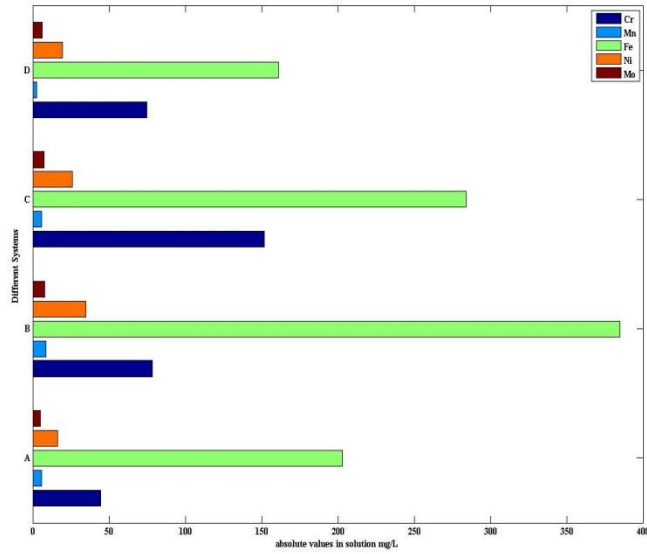
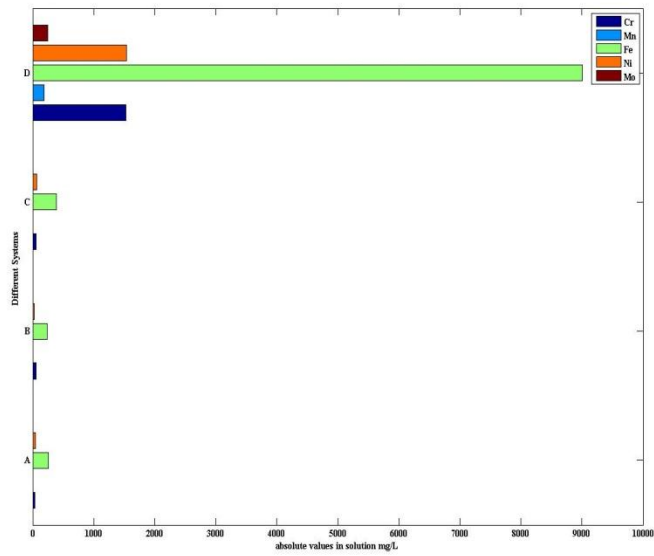


Figure 8-12. ICP-MS absolute values (mg/L) of ions in corrosion solution for Week 2



**Figure 8-13.** ICP-MS absolute values (mg/L) of ions in corrosion solution for Week 3



**Figure 8-14.** ICP-MS absolute values (mg/L) of ions in corrosion solution for Week 4

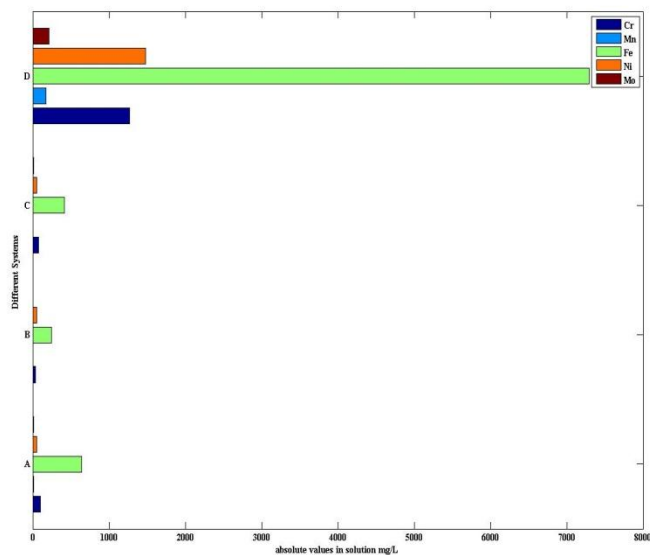


**Figure 8-15.** ICP-MS absolute values (mg/L) of ions in corrosion solution for Week 5

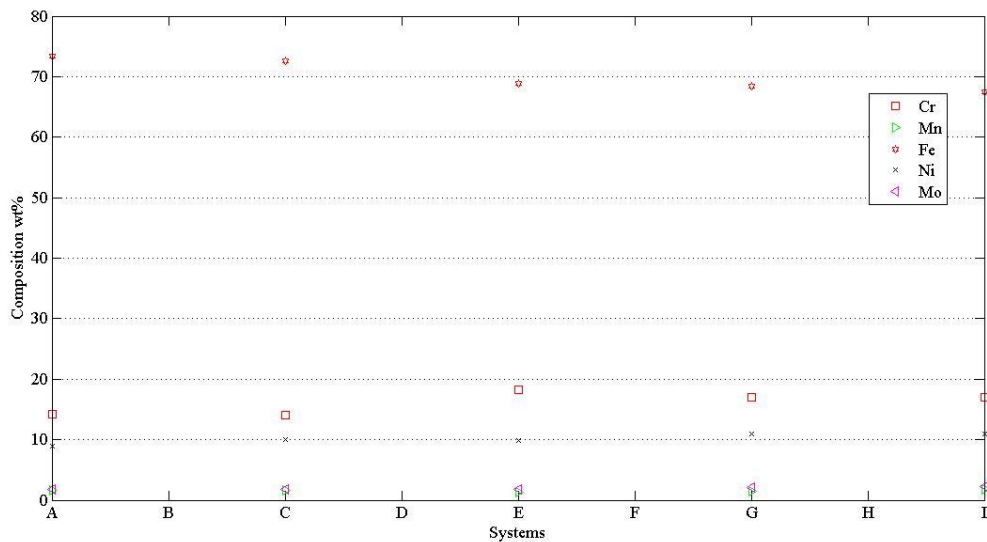


**Figure 8-16.** Overall ICP results composition wt% of various ions for whole 5 week period

Another information that can be gleaned from the metal ions in solution analysis is the concept of dealloying. In other words, does diethylenetriamine-CO<sub>2</sub> systems have a particular preference for any of the elements in stainless steel? To answer that question the nominal composition of the

specimen was compared to the wt % composition of metal ions in corrosion solution. Any appreciable dip in trends will indicate that one metal was leached in preference to the other. The pre-corrosion nominal wt% of stainless steel 316L is as shown in table 8-4 below:

**Table 8-4** Nominal percentage weight composition of stainless steel 316L

Element	Cr	Mn	Fe	Ni	Mo
wt %	17	1.74	~67.53	11	2.2

The overall trend as shown in figure 8-17 did not point to any particular element as being highly corroded than others. In this figure the nominal wt % composition of each element was plotted with the average values for each system and the two sets of data showed no appreciable deviation. For example Fe and Cr were comparable to their nominal figures with the exception of small deviations in [DETA + 1 wt% formate systems] which can be seen in that figure. And going from system to system a smooth trend for each element can be obtained. The as obtained various spectra from the high resolution- inductively coupled plasma mass spectrometry (HR-ICPMS) can be seen in figures 8-18 and 8-19.

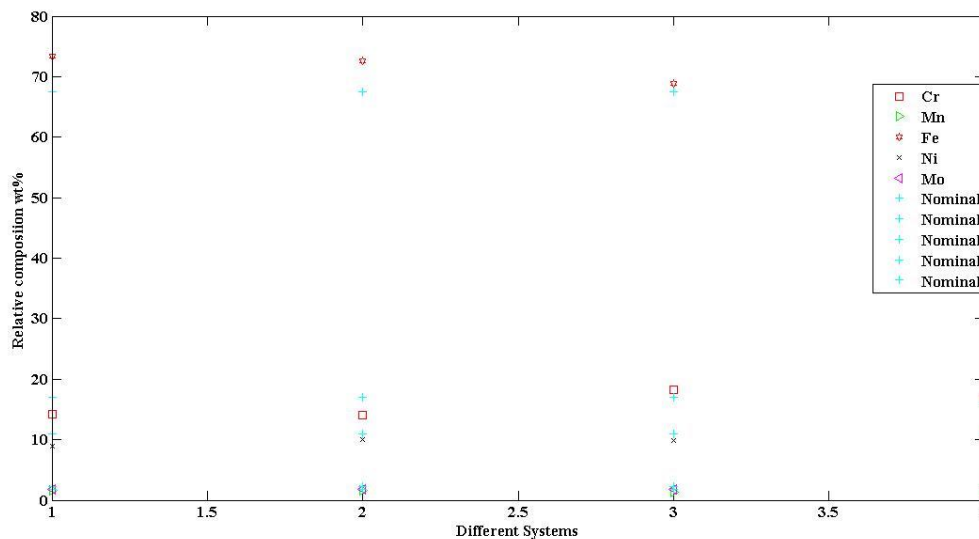


**Figure 8-17.** Composition wt% compared to nominal values (system 1 = DETA, system 2 = oxalate, system 3 = formate, system 4 = acetate)

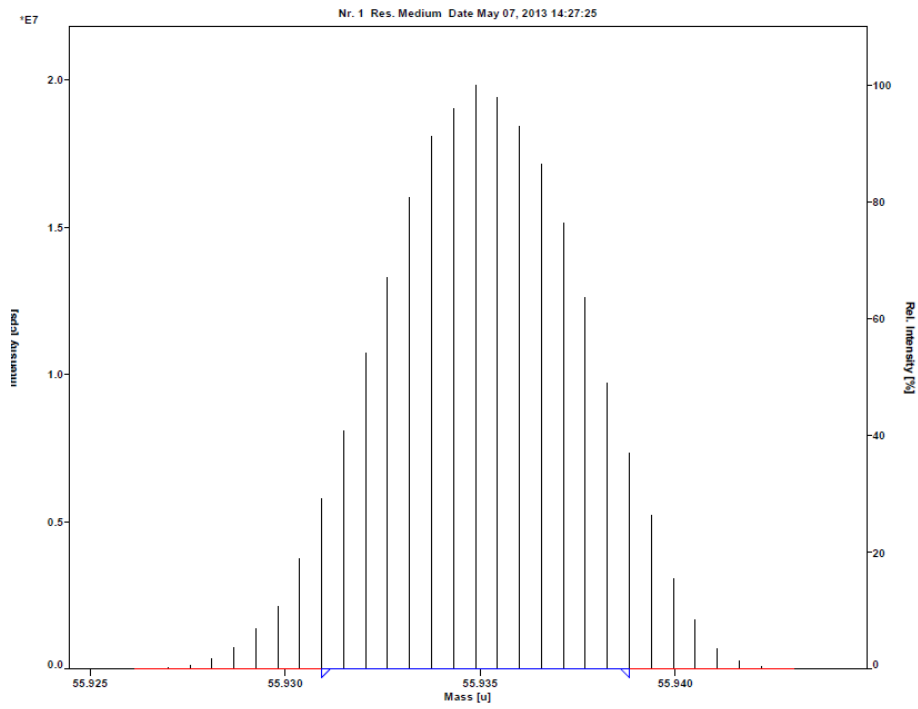


**Figure 8-18.** Fe spectrum as obtained by (HR-ICPMS)

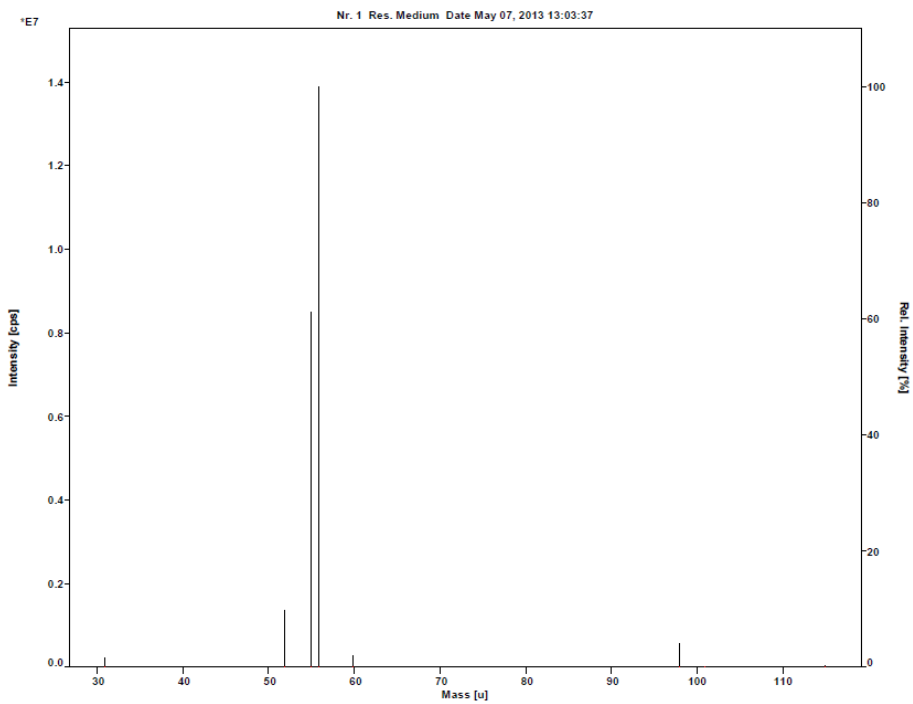


**Figure 8-19.** Total spectra of all ions as-obtained via (HR-ICPMS)

### 8.3 Amine and CO<sub>2</sub> analysis

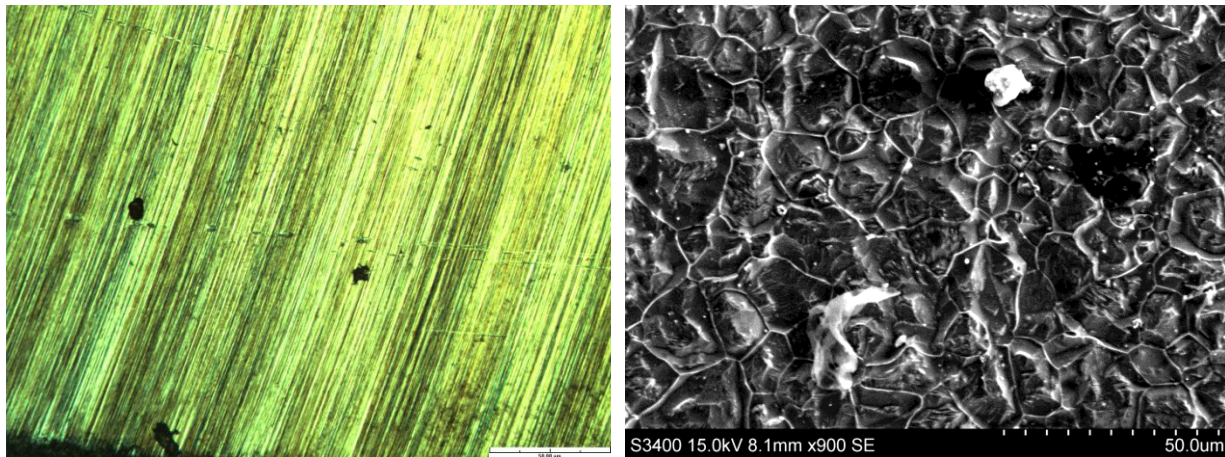
In order to test what the effects of the thermal conditions (135°C) have on the stability and concentration profile of the diethylenetriamine and CO<sub>2</sub>, a pre- and post- experiment solution analysis were done on all samples. For the DETA systems, the pre-experiment showed that for a loading of  $\alpha = 1.2$  (total alkalinity), the amine concentration can be reported to be 6.561 mol/kg and since diethylenetriamine has three (3) amine groups the effective amine concentration is 2.187 mol/kg with a deviation of 0.18% (parallel samples run) and for the CO<sub>2</sub> analysis the result was 2.657 mol/kg with a deviation in parallel samples of only 1.47%. Post-experiment analysis showed an interesting trend in the CO<sub>2</sub> content. For the 5 weeks that samples were on stream the following are the results of the CO<sub>2</sub> (mol/kg): 0.8662, 0.6314, 0.5954, 0.3806, 0.3951. It shows that after just a week on stream the CO<sub>2</sub> content decreased by as much as 70% and after the stretch of the experiment, there was hardly any CO<sub>2</sub> left. This makes sense because in normal CO<sub>2</sub> capture conditions (high temperature and pressures), CO<sub>2</sub> is meant to be separated from the amine solvent and subsequently sequestered for storage downstream.

The post-experiment amine analysis showed that the concentration of amine stabilized around 2.5 mol/kg for the first 3 weeks but then for the remaining weeks data outliers of over 6mol/kg were obtained. No concrete explanation could be attributed to the sudden change in the amine concentration, but possible reasons could be due to the complex presence of corrosion ions in solution (Fe<sup>2+</sup>, Cr<sup>2+</sup> and chelations), thermal degradation products, and a host of other issues. These, were though beyond the scope of this work. Further work could look at why this happened. No attempt was made to compare the amine and CO<sub>2</sub> concentrations in the other systems: oxalic, acetic and formic, the reason being that with the presence of the heat stable salts, the chemistry becomes complex and an attempt to investigate will take away the aim of this work and that is to simply characterize corrosion in diethylenetriamine-CO<sub>2</sub>-degradation products systems. Further details of pre- and post- amine and CO<sub>2</sub> analyses can be found in the appendix A2.

## 8.4 SEM and EDS Analysis

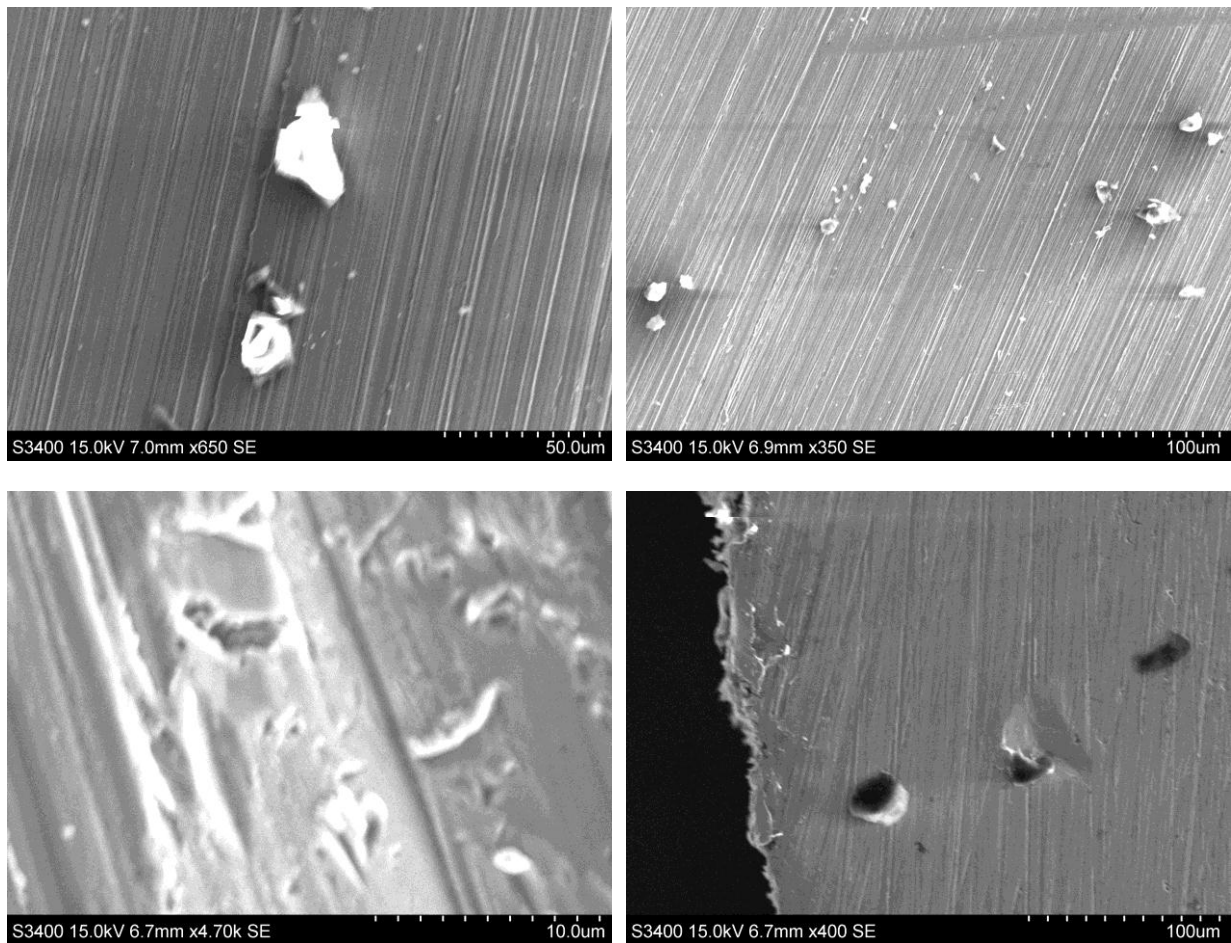
### 8.4.1 SEM

It is a recommended practice to use surface investigative techniques as per ASTM G1-03 (ASTM 2011) in order to characterize corrosion products on the surfaces of metals in general, stainless steel 316L included. In this work, for the weight loss based experiments representative samples (as is and after washing) were taken to the scanning electron microscopy (SEM) lab for surface characterization. Characterization of corrosion surfaces reveals the metal structure in terms of grain boundaries, phase boundaries, determination of the extent and form of the corrosive attack and differentiating the type of corrosion: pitting, uniform, crevice, and erosion corrosion (M.R. Louthan 1986). A Hitachi S-3400N SEM was used, with key parameters such as voltage 15.0kV, probe and emission currents of 30.9  $\mu\text{A}$  and 88.0  $\mu\text{A}$  respectively. The high resolution images thus obtained were in the range of 5 – 200  $\mu\text{m}$  as the images in the ensuing paragraphs under this section will reveal. It is noteworthy that one of the key constraints of an earlier work on corrosion of stainless steel with MEA (Hayfron-Benjamin 2012) was that even though corrosion was quantified via weight loss methods, the surface morphologies obtained with a simple optical microscope( Microfire Optronics<sup>®</sup>) with low resolution power was quite poor to say the least. An example of one of the best images taken in that work is as shown in figure 8-20 (left) below. Apart from showing possible corrosion pitting, the presence of corrosion products can hardly be identified. However the image on the right of figure 8-20 shows an SEM image of a corroded sample of the experiment Swagelok<sup>®</sup> 1.0, [DETA + 1.00wt% acetate],  $\alpha = 1.2$  (amine alkalinity) on stream at 135°C for a total time of 669 hours. In contrast with that obtained from a simple microscope, the SEM image shows deposition of corrosion products in the form of small crystalline globules (sandy crystals) or as fine plates (flowery structures).



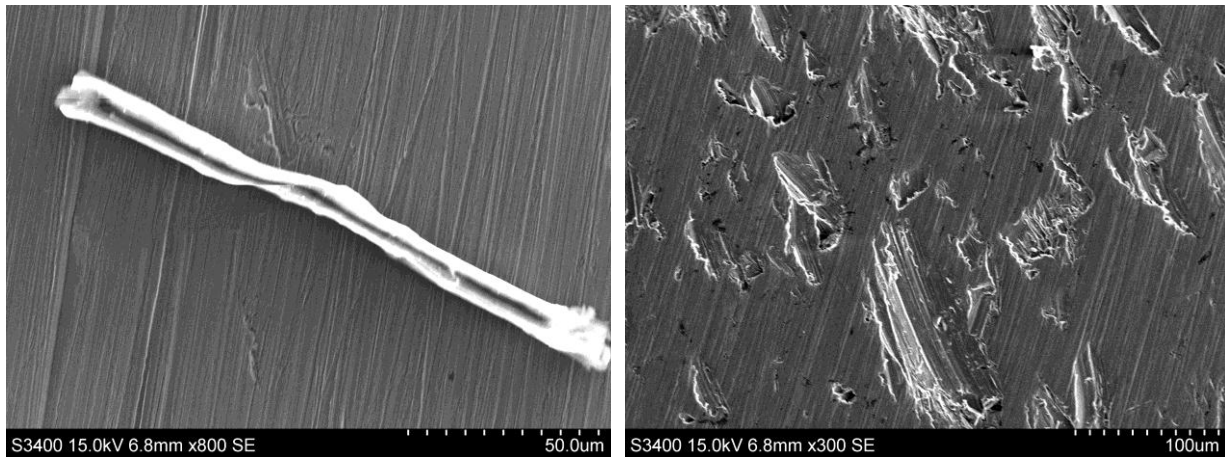
**Figure 8-20.** Contrast between optical microscope image (to the left) and the SEM image (to the right) showing deposition of corrosion products

Figure 8-21 shows the surface images of different samples in different DETA systems, the images were the SEM with as low as 5  $\mu\text{m}$  and high as 200  $\mu\text{m}$  resolution power. In figure 8-21 (top left) a stainless steel specimen  $\alpha = 1.5$  (amine alkalinity), 236 hours on stream and only in DETA solution can be seen to have small scattered corrosion products on the surfaces. The distinct grinding marks which were undertaken before the experiments can be seen in the background.



**Figure 8-21.** SEM images showing features on specimens (grinding marks, cracks, pits and deposition of corrosion products)

Similar surface characterization can be seen from figure 8-21 (top right) for the 2 wt% acetic acid sample, with  $\alpha = 1.5$  (amine alkalinity), 236 hours on stream. In this figure the increased littered products are clearly seen as well as the deformed surface of the metal. Oxalate and formate systems also produced some high quality images displaying corrosion products shapes such as the cylindrically-shaped product found on the oxalate specimen in figure 8-22 (left), features such as cracking, deformed surfaces and pitting as displayed in figure 8-22 (right).



**Figure 8-22.** Oxalate system features after 236 hours as obtained by SEM



**Figure 8-23.** SEM image of DETA systems after 405 hours looking like a human skull

The different shapes and morphologies thus obtained had to be compared with those in the open literature to make sure that precise identification procedure was being followed. The reason is that surface characterization like other branches of natural sciences can be tricky and if care is not taken wrong inferences and conclusions can be made.

Surface morphologies using tools like SEM has been carried out by a number of authors (A. Razvan and Raman. 1986; A. Raman, S. Nasrazadani et al. 1987; Kamimura, Yamashita et al. 2001; de la Fuente, Díaz et al. 2011; Gao, Wang et al. 2012) and the images obtained had features common structures described as flaky, crystalline (regular) structures such as  $\alpha$ -FeOOH and  $\gamma$ -FeOOH, amorphous-like phases ( $\text{Fe}_{3-x}\text{O}_4$  ( $\gamma$ - $\text{Fe}_2\text{O}_3$ )). The corrosion products indicated are all well documented regular main stay of rust found in corrosion environments.

In this work the as obtained figures below shows images obtained for various Swagelok<sup>®</sup> 1.0 corroded stainless steel specimens. The [DETA + 1.00wt% acetate],  $\alpha = 1.2$  (amine alkalinity), 357 hours on stream which actually had the highest of all the recorded corrosion rate at a very high number of 106  $\mu\text{m}/\text{yr}$  or 4.19mpy, this sample's SEM images showed interesting features which were comparable to the work of de la Fuente (de la Fuente, Díaz et al. 2011). The features noted were the severe pitting at the edges of the sample (figure 8-24) together with flowery corrosion products, fine plates typical of lepidocrocite (figure 8-25), corrosion product in the shape of a cotton ball nestled in a corrosion pit feature (typical of goethite figure 8-26). Furthermore flaky, porous and layers of corrosion products can be seen in the SEM image of only DETA system can be seen in figure 8-27. Identified images of corrosion product taken from the open literature can be seen in figure 28, which shows similar results from this work.

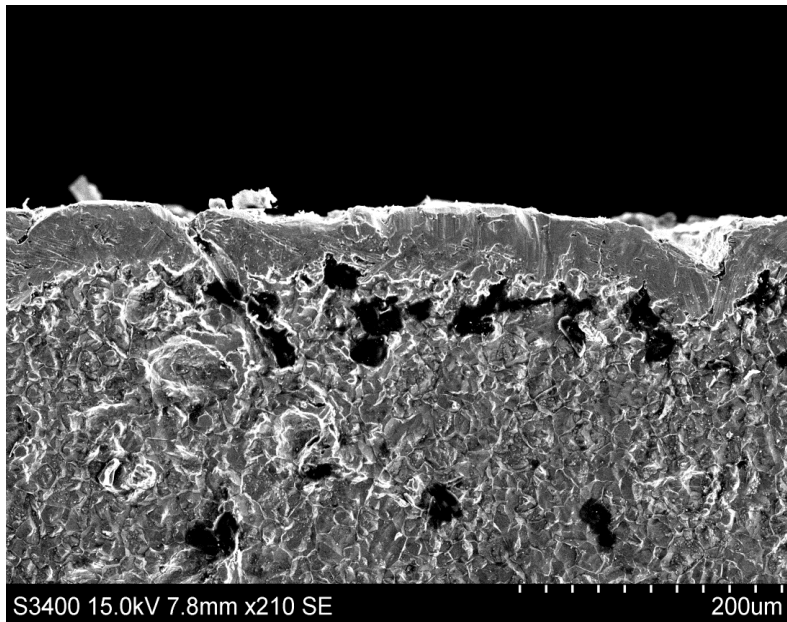


**Figure 8-24.** SEM revealing severe pitting on the edges of specimen



**Figure 8-25.** Lepidocrocite phase feature of corrosion products via SEM



**Figure 8-26.** SEM showing typical goethite phase of corrosion product

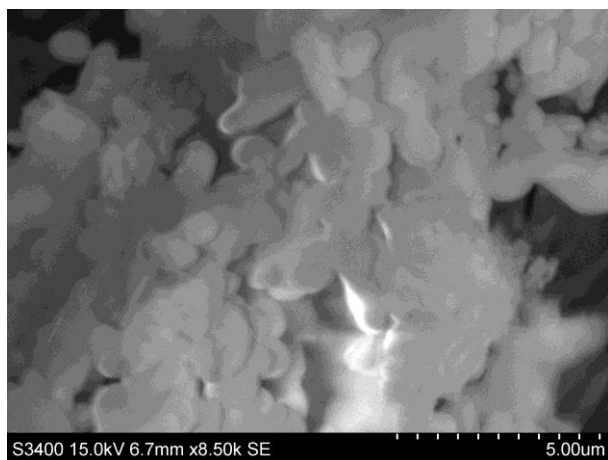
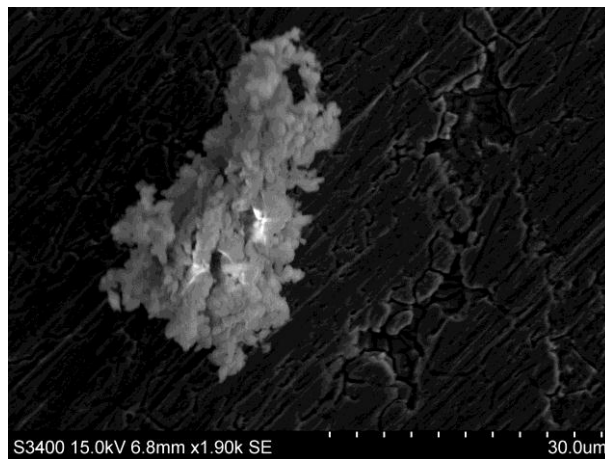
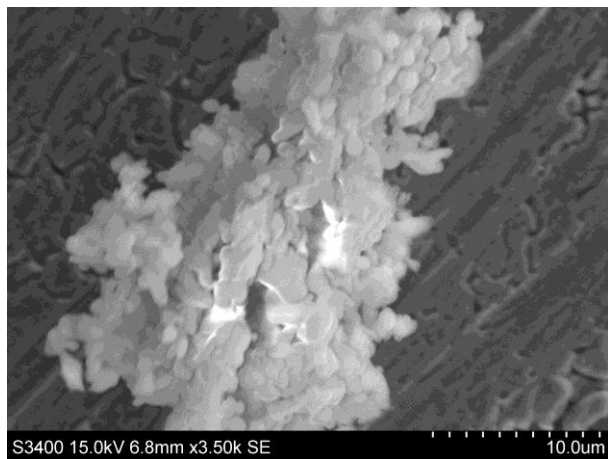


**Figure 8-27.** Flaky, porous and layers on metal surface as revealed by SEM

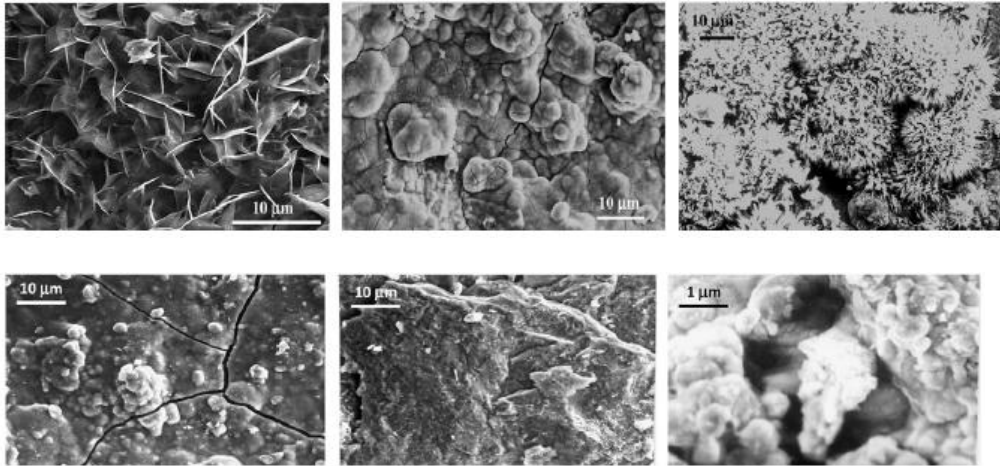


**Figure 8-28.** SEM images of corrosion on iron obtained in a different work found in the open literature (de la Fuente, Díaz et al. 2011)

#### 8.4.2 EDS

With the characterization of the likely corrosion products done, distribution and element identification in these products were done with the energy dispersive X-ray spectrometry (EDS). A simple diagram of the cross-section view can be seen in figure 8-29, which showed the following elements as being present, Fe, C, O and other usual elements present in rust formations. Extensive images as obtained from the EDS and SEM lab sessions are found in the appendices.

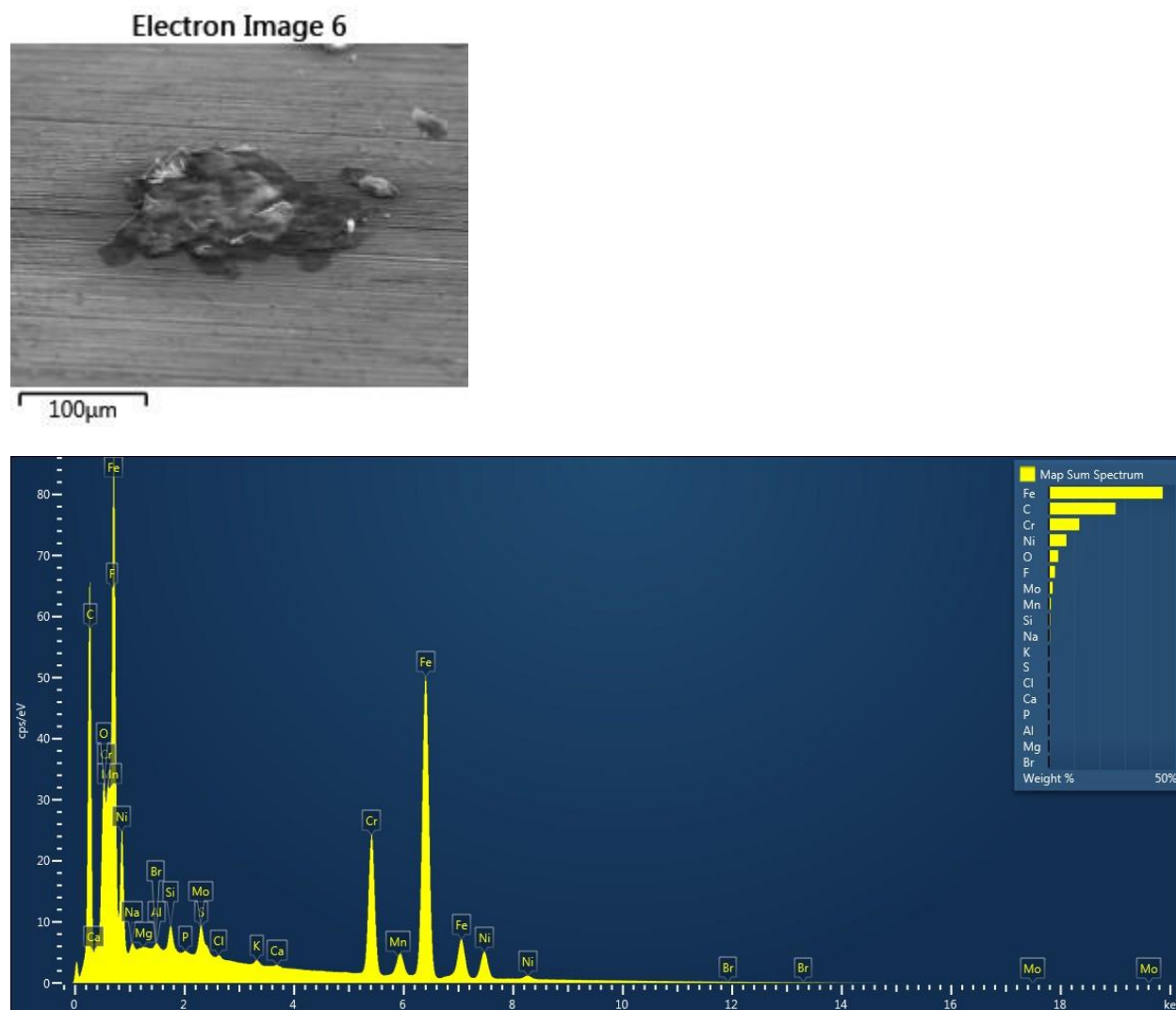


**Figure 8-29.** EDS image of a corrosion section showing the elemental map spectrum

### 8.5 EC-Autoclave Analysis

For the electrochemical experiments, the set-up was described in the experimental procedure (chapter 7) and it involves a three-electrode corrosion cell (Working, reference and auxiliary electrodes), a preloaded DETA and degradation products (formate, oxalate, acetate) electrolyte systems, and all of these coupled with an ACM® instruments potentiostat, which in turn is connected to a computer for data analysis. Prior to all experiments validation of the instruments per ASTM standard G5-13 (ASTM 2013) was done by measuring  $E_{corr}$  (rest potential) after about 55 min immersion of the reference electrode in the DETA solutions in the cell. Two electrochemical techniques were used Tafel plot and linear polarization resistance. For the

potentiodynamic (cyclic) sweep was started from -180mv to + 100mv about the rest potential. A scan rate of 50 mv/min, a half cycle, cell settle time (to give the working electrode, WE, a moment to adjust to the initial polarization) were entered in the parameters for the cycle sweep interface. Typically each sweep took, 5 minutes but repeated measurements (3-5 times) were made to improve reproducibility. A narrower sweep range of 20mv to + 20mv at a scan rate of 12 mv/min was applied to the LPR method. All measurements were taken over a span of approximately 48 hours, with intermittent reading of data.

Experimental data from both techniques were used to plot the graph of potential (E vs Ag/AgCl electrode) and log current density ( $i_{corr}$ ). Current densities are used because they simply describe the direct characteristics of interfacial properties of the stainless steel specimen (SS316L) but it should be noted that this over simplification does not account for localized corrosion. The reason is that if the specimen is modeled as both the anode and cathode, then the existence of pitting (which means that the anode area is much smaller than the cathode area) can not be adequately explained. But the point of the electrochemical testing in this work is to be able to measure uniform corrosion and so this model of using current densities should work fine.

For the Tafel plots, extrapolation of the E-log $i_{corr}$  and calculation of the Tafel slopes are then used to estimate the corrosion rates according to the following equations:

$$corrosion\ rate\left(\frac{mm}{year}\right) = \frac{3.3 * i_{corr} * E.W}{\rho} \quad 8-17$$

Where E.W = equivalent weight of test coupons

P = density of stainless steel 316L ( $g/cm^3$ )

$i_{corr}$  = corrosion current density ( $mAcm^{-2}$ )

The software that comes with the potentiostat and connected to the EC- Autoclave set-up, automatically calculates the corrosion rate based on the above principles, but for more accurate results, linear regression of data as-obtained is done.

For the linear polarization resistance, the following equations are used to compute the corrosion current and the equation 8-17 above is used to estimate the penetration rates.

$$i_{corr} = \frac{\beta}{R_p} \quad 8-18$$

$$\beta = \frac{\beta_a \beta_c}{2.3(\beta_a + \beta_c)} \quad 8-19$$

$$R_p = \frac{\Delta E}{\Delta i} \quad 8-20$$

Where  $\beta = Stern\ and\ Geary\ Constant$ ,

$\beta_a \beta_c = tafel\ slopes\ in\ the\ anodic\ and\ cathodic\ regions\ respectively$

$i_{corr} = corrosion\ current\ density$

$R_p = polarization\ resistance$

$\Delta E = change\ in\ potential\ on\ the\ LPR\ diagram$

$\Delta i = change\ in\ the\ current\ density\ on\ the\ LPR\ diagram.$

### 8.5.1 Tafel Plot Technique

In general stainless steel can exhibit active, passive and transpassive corrosion behavior, with the type of corroding electrolyte having an influence on it. For the Tafel cyclic sweep technique used in this work, all the 316L stainless steel were in the active region of metal dissolution and appreciable rates were measured. Table 8-5 summarizes all the electrochemical parameters and data which were obtained for the stainless steel 316L in various diethylenetriamine (DETA), and 2wt% (20,000ppm) of heat stable salts (oxalate, formate, and acetate) with CO<sub>2</sub> loadings of  $\alpha = 1.2$  and different temperatures of 135°C and 80°C. These temperatures represent those found in absorber and stripper sections of CO<sub>2</sub> absorption plant.

**Table 8-5** Key parameters and results from electrochemical testing (cyclic sweep) - DETA system at 135°C

Experimental conditions : DETA, 135° C, $\alpha = 1.2$						Corrosion rates				
Expt. Run	$E_{corr}/mV$	LPR/ $\Omega.cm^2$	$\beta_a$ (mV/dec)	$\beta_c$ (mV/dec)	$i_{corr}$ (mA/cm <sup>2</sup> )	mm/yr	mpy	Estimated $i_{corr}$	Estimated Potential (mV)	Time on stream/hrs
1	-783.66	271.435	839.906	44.831	0.068	0.873	34.35	0.070	-781.389	2
2	-845.85	1013.616	395.226	49.900	0.019	0.243	9.57	0.020	-845.852	13
3	-848.68	1002.857	396.243	52.960	0.020	0.259	10.20	0.020	-846.983	15
4	-851.16	1031.641	477.516	51.821	0.020	0.252	9.927	0.018	-852.858	18
5	-861.06	2196.855	448.275	48.907	0.009	0.112	4.398	0.009	-857.651	37
6	-861.38	1997.748	518.917	45.888	0.009	0.117	4.624			39

**Table 8-6** Key parameters and results from electrochemical testing (cyclic sweep) - DETA + 2 wt% oxalate system at 135°C

Experimental conditions : DETA + 2wt% oxalate, 135° C, $\alpha = 1.2$						Corrosion rates				
Expt. Run	$E_{corr}/mV$	LPR/ $\Omega.cm^2$	$\beta_a$ (mV/dec)	$\beta_c$ (mV/dec)	$i_{corr}$ (mA/cm <sup>2</sup> )	mm/yr	mpy	Estimated $i_{corr}$	Estimated Potential (mV)	Time on stream/hrs
1	-304.5	20.475	125.334	86.011	1.083	13.864	545.816	1.511	-299.170	2
2	-340.7	18.808	41.150	2.042	0.045	0.576	22.668			13
3	-341.9	18.610	252.225	136.771	2.072	26.520	1044.11 2			13
4	-306.2	17.168	111.142	107.127	1.381	17.683	696.180			14
5	-310.2	17.429	28.968	14.098	0.237	3.028	119.213	0.388	-308.774	14
6	-314.5	17.463	113.728	99.960	1.325	16.954	667.485	1.331	-314.490	15
7	-288.7	16.791	120.203	105.349	1.454	18.608	732.597	1.127	-288.291	22
8	-289.5	17.156	105.535	118.846	1.417	18.133	713.885			25
9	-296.4	22.337	25.250	17.796	0.203	2.601	102.397			26
10	-276.4	17.541	116.129	105.548	1.371	17.543	690.651	1.463	-276.395	37

**Table 8-7** Key parameters and results from electrochemical testing (cyclic sweep) - DETA + 2 wt% formate system at 135°C

Experimental conditions : DETA + 2wt% formate, 135° C, $\alpha = 1.2$						Corrosion rates				
Expt. Run	$E_{corr}/mV$	LPR/ $\Omega.cm^2$	$\beta_a$ (mV/dec)	$\beta_c$ (mV/dec)	$i_{corr}$ (mA/cm <sup>2</sup> )	mm/yr	mpy	Estimated $i_{corr}$	Estimated Potential (mV)	Time on stream/hrs
1	-718.6	165.376	843.723	49.423	0.123	1.571	61.856	0.127	-719.697	2
2	-738	211.734	590.507	48.121	0.091	1.170	46.044	0.091	-738.539	3
3	-746	245.698	589.616	46.893	0.077	0.984	38.737	0.074	-744.318	4
4	-747.74	305.649	593.936	49.466	0.065	0.831	32.733	0.061	-748.871	6
5	-749.4	272.012	395.206	51.142	0.072	0.926	36.475	0.069	-748.882	7
6	-752.9	321.340	476.402	49.964	0.061	0.783	30.834	0.060	-752.928	9
7	-761.1	390.309	809.316	45.144	0.048	0.610	24.003	0.052	-761.706	22

**Table 8-8** Key parameters and results from electrochemical testing (cyclic sweep) - DETA + 2wt% acetate system at 135°C

Experimental conditions : DETA + 2wt% acetate, 135 °C, $\alpha = 1.2$						Corrosion rates				
Expt. Run	$E_{corr}/mV$	LPR/ $\Omega \cdot cm^2$	$\beta_a$ (mV/dec)	$\beta_c$ (mV/dec)	$i_{corr}$ (mA/cm <sup>2</sup> )	mm/yr	mpy	Estimated $i_{corr}$	Estimated Potential (mV)	Time on stream/hrs
1	-773.1	422.524	513.001	54.380	0.051	0.648	25.497	0.049	-774.800	15.42
2	-771.8	555.533	498.286	46.457	0.033	0.426	16.760	0.035	-769.535	18
3	-769.07	570.536	494.066	49.093	0.034	0.436	17.149	0.036	-770.207	19
4	-770.8	514.238	614.883	47.292	0.037	0.475	18.711	0.040	-770.768	20
5	-737.6	82.351	321.821	41.058	0.192	2.461	96.879	0.182	-739.289	37
6	-740.4	82.351	541.264	15.430	0.079	1.014	39.914	0.066	-735.881	37

**Table 8-9** Key parameters and results from electrochemical testing (cyclic sweep) - DETA + 2 wt% oxalate system at 80°C

Experimental conditions : DETA + 2 wt% oxalate, 80° C, $\alpha = 1.2$						Corrosion rates				
Expt. Run	$E_{corr}/mV$	LPR/ $\Omega.cm^2$	$\beta_a$ (mV/dec)	$\beta_c$ (mV/dec)	$i_{corr}$ (mA/cm <sup>2</sup> )	mm/yr	mpy	Estimated $i_{corr}$	Estimated Potential (mV)	Time on stream/hrs
1	-550.17	579.205	625.783	52.973	0.037	0.469	18.475	3.402E-02	-553.580	2
2								5.806E-05	-519.014	5
3								6.163E-07	-472.709	7
4	-397.7	5.845E+05	812.308	2.783	2.06E-06	2.64E-05	0.00104			23
5	-383	9.916E+05	881.458	9.308	4.04E-06	5.17E-05	0.002035			26
6	-366.6	1.177E+06	804.693	79.951	2.69E-05	0.000343	0.01354			28

From table 8-9, a quick glance and comparison to table 8-8 reveals that at the higher temperatures, the corrosion current densities are much higher and these translate into greater corrosion rates. For example for the oxalate system, after 2 hours on stream and at the lower temperature of 80 °C,  $i_{corr} = 0.0366$  mA/cm<sup>2</sup> with a corrosion rate of 0.469 mm/yr. In contrast at the higher temperature of 135°C, a greater current is produced at the anode,  $i_{corr} = 1.0831$  mA/cm<sup>2</sup> and a corrosion rate of 13.863 mm/yr. The reason for higher rates at higher temperatures is connected to the kinetic and will be shortly explained under the effect of temperature section.

The Tafel plots and extrapolated corrosion rates for all four different systems are shown in figures: 8-30, 8-31, 8-32 and 8-34.

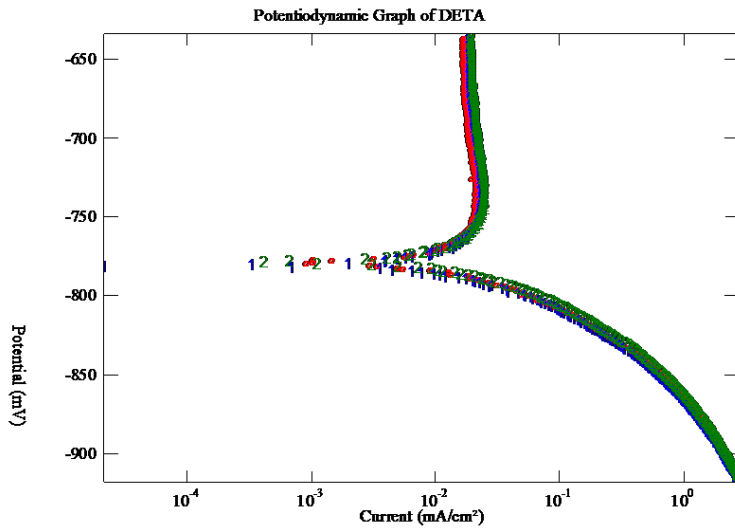


Figure 8-30. Tafel Plot extrapolation for DETA system

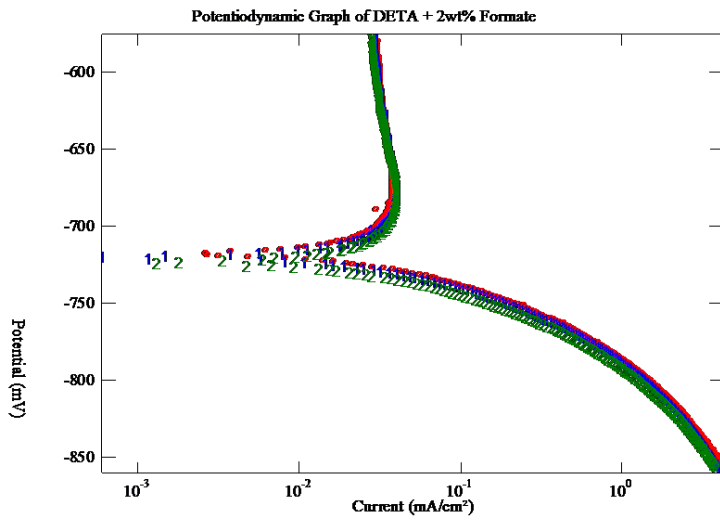


Figure 8-31. Tafel Plot extrapolation for DETA + 2wt% formate system

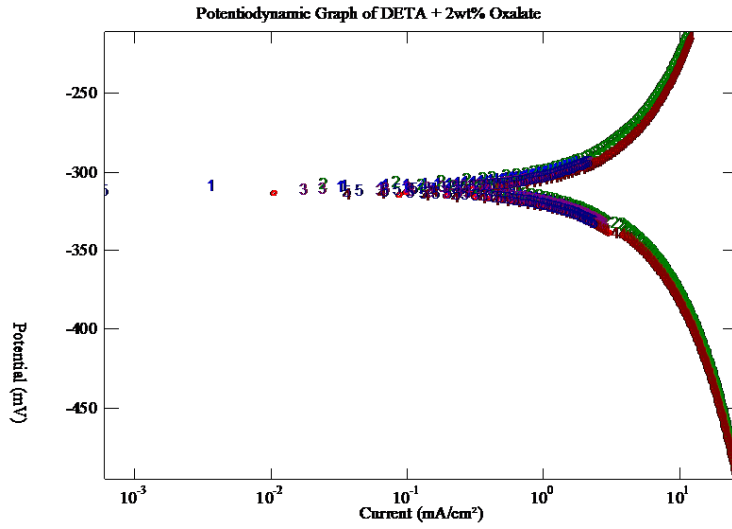


Figure 8-32. Tafel plot extrapolation for DETA + 2 wt% oxalate

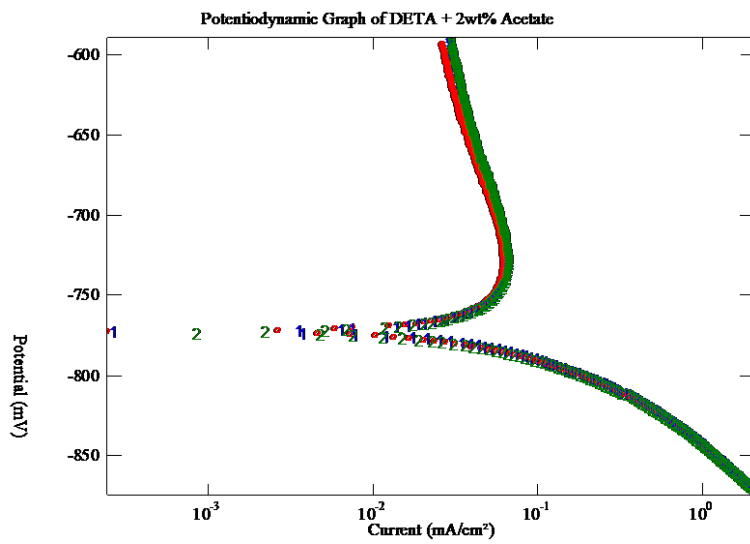
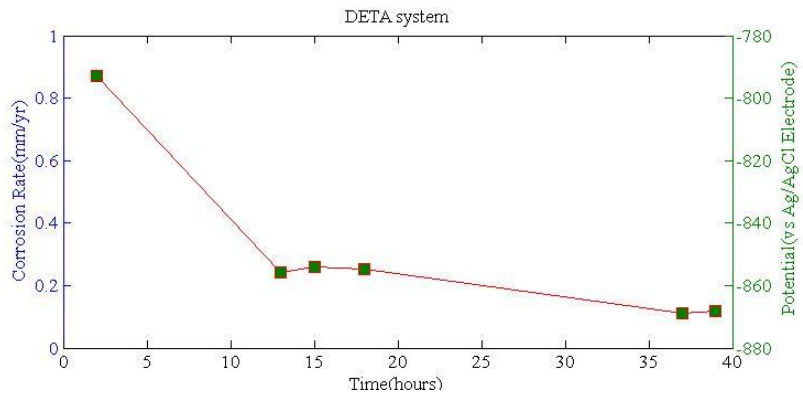


Figure 8-33. Tafel plot extrapolation for DETA + 2wt% acetate system

### 8.5.1.1 Effect of HSS in DETA systems

Overall, the oxalate systems were found to be the most corrosive in the DETA-CO<sub>2</sub> environment with a high of 26.52 mm/yr after only 13 hours on stream. At this rate, this corresponded to a relatively high current density  $i_{corr} = 2.0719095 \text{ mA/cm}^2$ , which in fact is double of the current at the beginning of the experiment. A look at the Tafel plot shown previously (figure 8-32) also reveals that the active anodic region lies in the region of higher current densities. High current densities, means that high current is flowing in the electrochemical cell and the anode reaction (dissolution of the metal) proceeds faster. In contrast with the other systems (no acid, formate and acetate), the anodic Tafel slopes ( $\beta_a$ ) of the oxalate was much smaller than the rest. For example, at the initiation of the experiment oxalate system had  $\beta_a = 125.3 \text{ mV/decade}$ , whereas the rest registered far above this value. The meaning being that the mechanism of iron dissolution in the presence of oxalate is altered due to the chelating effect (Tanthapanichakoon, Veawab et al. 2006). Also the mechanism of corrosion by oxalate systems was given earlier under the weight-loss method. For the DETA, acetate, formate set-ups, the likely reasons for the recorded lower corrosion rates could be due to the formation of possible passivating films. This is seen in their Tafel plots (figures: 8-30, 8-31, 8-33), where in the anodic regions, the current densities do not change (the curve is more steeper), this behavior indicates that passivation of the surface has occurred.

The additional effect of polarization on the surface behavior of the stainless steel specimen can be deduced by the changes in corrosion potential ( $E_{corr}$ ). For example from the graphs of all the systems as shown below in figures: 8-34, 8-35, 8-36, 8-37 and table 8-8 above it can be seen that the corrosion potential of DETA varied between - 861 to -785 mv, formate from -761 to -718 mv, oxalate from -304 to -276 mv and finally for the acetate from -740 to -773 mv. The implication of these changes is that for each time the polarization scan is done, the oxide layer is broken down and the systems do not have the ability to repassivate, meaning in corrosion in real process can be initiated by particles in the fluid flow removing some of the oxide layer (Kongstein 2010).



**Figure 8-34.** Corrosion rates, time and potential of DETA system

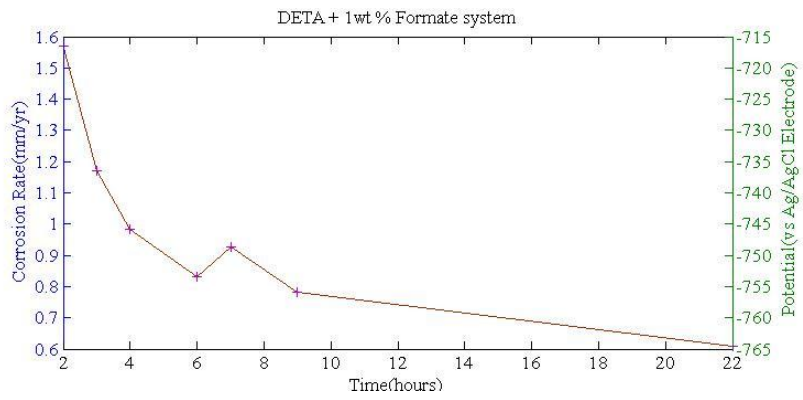


**Figure 8-35.** Corrosion rates, time and potential of DETA + 2 wt% formate system

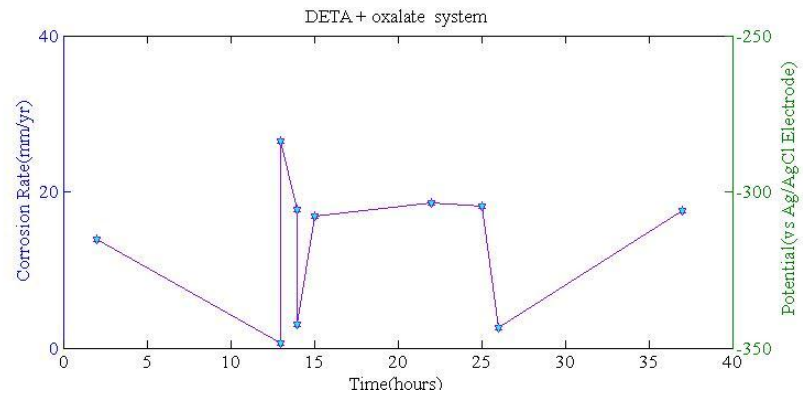


**Figure 8-36.** Corrosion rates, time and potential of DETA + 2wt% oxalate system

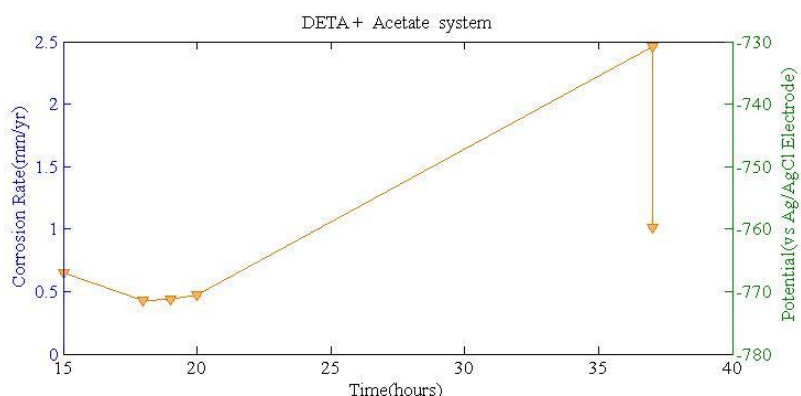


**Figure 8-37.** Corrosion rates, time and potential of DETA + 2wt% acetate system

An end of experiment comparison was done, that and analysis of results showed that DETA, formate, acetate and oxalate systems in increasing corrosion rate were the order for 135°C,  $\alpha = 1.2$  set-up used in this work. A graphical illustration can be seen in figure 8-38 and also a Tafel plot comparison seen in figure 8-39. The corrosion rate comparison has no acid DETA = 4.6 mpy < formate = 24.0 mpy < acetate = 39.9 mpy < oxalate = 690.7 mpy. In addition, the Tafel plot in figure 8-39, clearly shows the higher current densities for the oxalate system ( $E_{corr}$  in the region -300 mV), which lies far to the top right of the log current densities axis. The rest of the systems lies to the left of the 2wt% oxalate + DETA set-up. The corrosion rate of the no acid DETA = 0.87 mm/yr is comparable to a similar work done by Ole Kongstein (Kongstein 2010) under similar conditions which recorded a rate of 0.6 mm/yr.

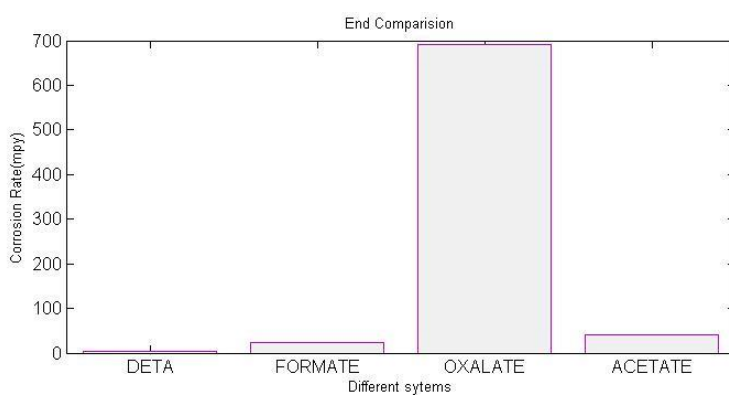


**Figure 8-38.** End of experiment overall corrosion rates comparisons

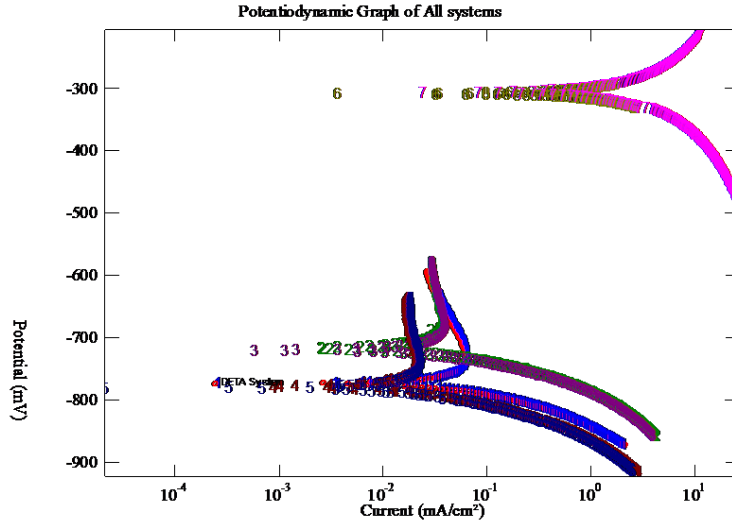


Figure 8-39. Superimposed potentiodynamic graph of all systems in Tafel polarization experiment

### 8.5.1.2 Effect of Temperature

To understand the effect of temperatures on corrosion rates in DETA-CO<sub>2</sub>-degradation products systems, similar electrochemical testing were done at 80°C and the resulting data was used to plot the Tafel plots as shown in figures 8-40, 8-41, 8-42 and 8-43 below. Typical values for the corrosion current densities show that they are of several orders below that of those obtained at 135°C thus representing lower corrosion rates. For example for the DETA containing no acid system, at 80°C a rate of only 4.587E-06 mm/yr compared to 0.872 mm/yr for that at 135°C. The reason for higher corrosion rates observed at higher temperatures can be explained by the reaction kinetics.

This phenomenon of increased corrosion rates with temperature could be explained by examining the two equations taking place in amine-CO<sub>2</sub> systems as shown below (Veawab, Tontiwachwuthikul et al. 1999). Dissociation of protonated amine:



Since temperature is an essential kinetic parameter in all absorption systems, an increase in temperature shifts the above equilibrium reactions resulting in greater amounts of  $H^+$  and  $HCO_3^-$  as explained by Rochelle and co-workers (Austgen, Rochelle et al. 1989). The increase in the above mentioned species results in more importantly disturbing the equilibrium of the metal dissolution and oxidizer reduction reactions which are the key reactions for corrosion and rust formation. So to restore equilibrium, more metal (iron) dissolves, generating more electrons for the cathodic reaction, which enhances the corrosion rate.

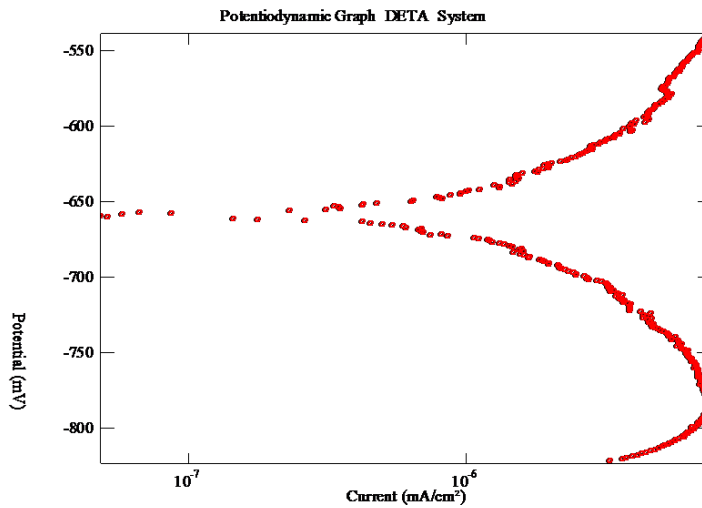


Figure 8-40. Tafel plot for 80°C experiment for DETA system

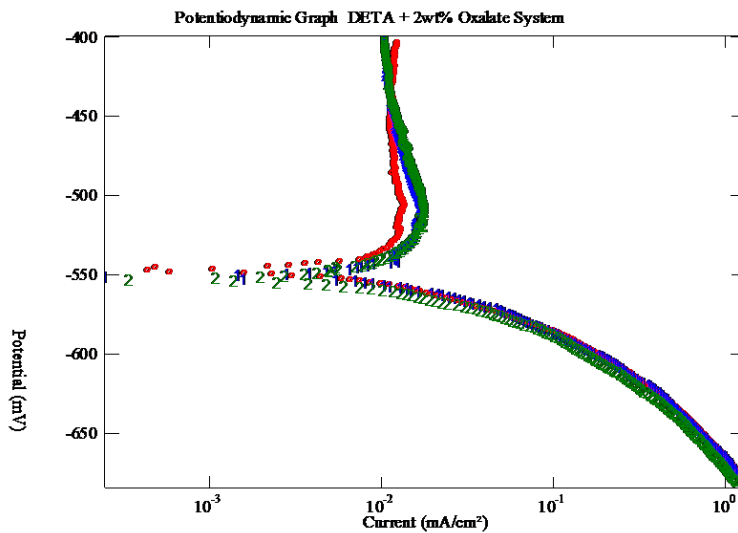
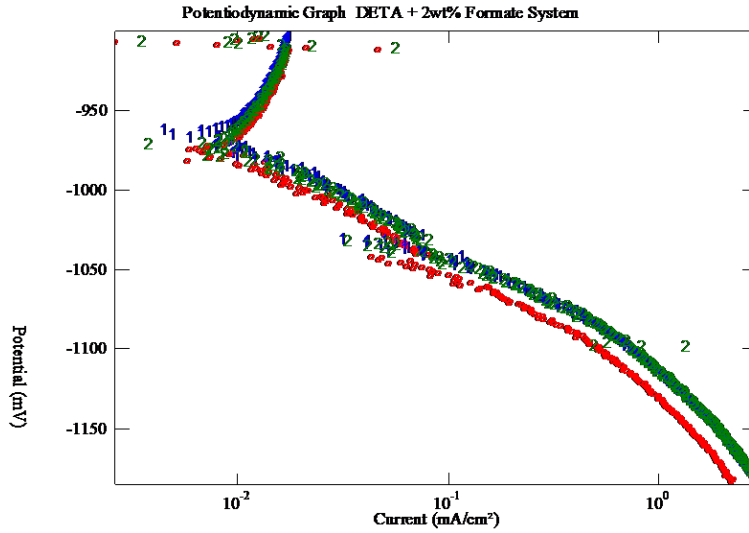
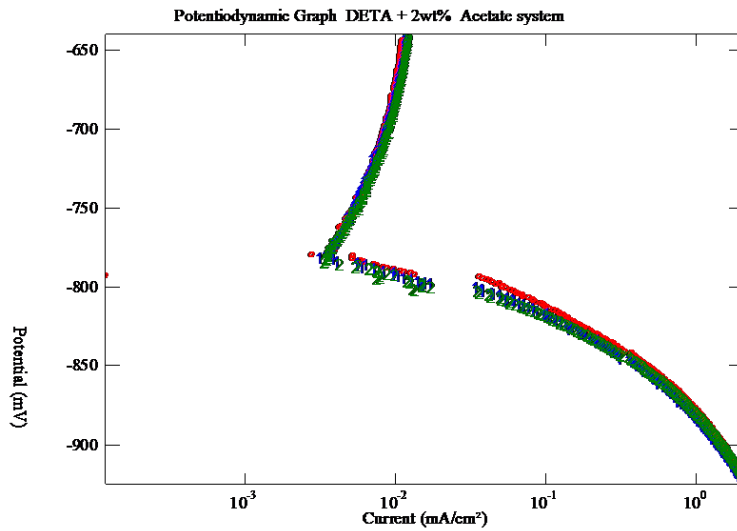


Figure 8-41. Tafel plot for 80°C experiment of DETA + 2wt% oxalate system



**Figure 8-42.** Tafel plot for 80°C experiment of DETA + 2wt% formate system



**Figure 8-43.** Tafel plot for 80°C experiment of DETA + 2wt% acetate system

Finally a comparison of all systems is shown in figure 8-44 and it shows that the DETA system containing no heat stable salts had the lowest corrosion current densities (lies far to the left on the axes) and hence low corrosion rates. The trend for the rest is similar to that obtained at 135°C with the notable exception of formate recording the highest rates. The flip in order of which heat stable salts is the most corrosive is not unusual in corrosion experiments. Consider for example the work of Nainar and Veawab (Nainar and Veawab 2009), which investigated the corrosion

effect of HSS species in MEA/PZ blends, at 80°C it was found out that the formate is the most corrosive compared to oxalate and acetate systems.

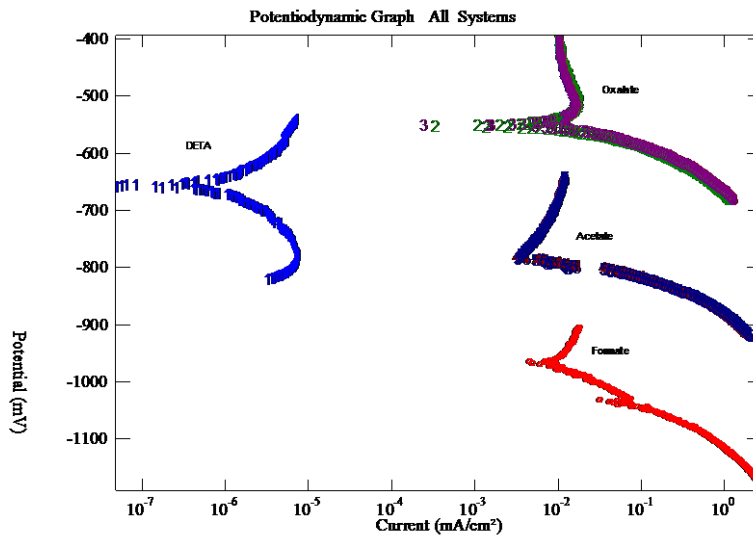


Figure 8-44. Overall Tafel plot for 80°C experiments

### 8.5.2 LPR Technique

Linear polarization resistance method was used as a complementary tool to compare corrosion rates. For the 2wt% oxalate plus DETA system, at 135°C, the results obtained were fairly comparable to those obtained via Tafel plot extrapolation as described above. A typical  $E-E_{corr}$  of the LPR is as shown in figure 8-45 below:

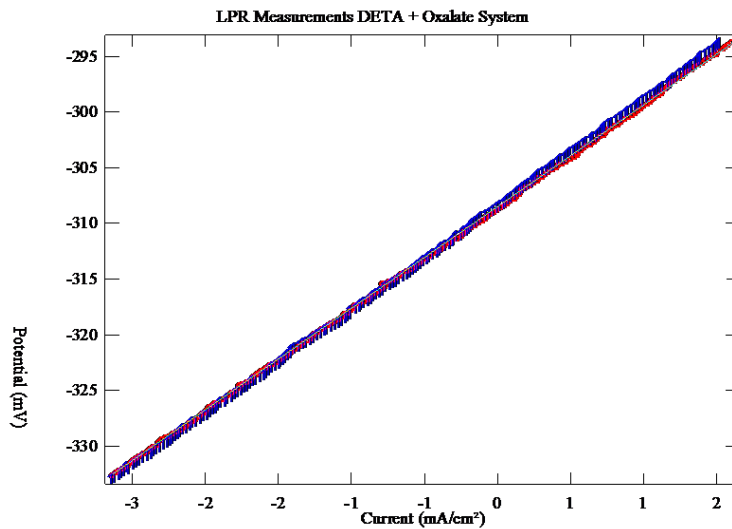
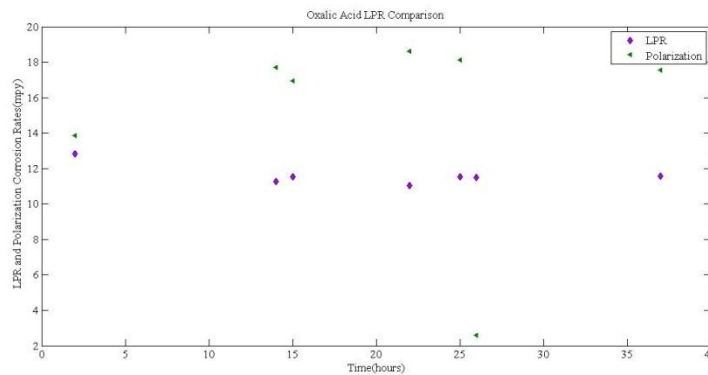
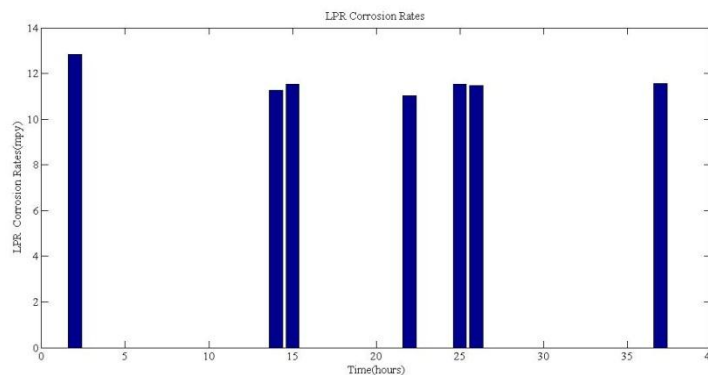


Figure 8-45. Linear polarization line for DETA + 2 wt% oxalate at 135°C

The figure shows a straight line plot which fits the ideal LPR diagram (ie. In theory a straight line plot is expected). The slope of the line in the figure gives the polarization resistance  $R_p$  ( $\Omega \cdot \text{cm}^2$ ). For the oxalate, an average of  $R_p = 20.175$  ( $\Omega \cdot \text{cm}^2$ ) was recorded and this gave on average corrosion currents  $i_{\text{corr}} = 0.967 \text{mA/cm}^2$  and thus an average corrosion rate of 11.604 mm/yr. A comparison of both techniques can be seen in figure 8-46 and a bar chart in figure 8-47 illustrates what has been stated under this sub-section. The discrepancy between the LPR method and the polarization technique can be attributed to errors in estimating the Stern and Geary constant  $\beta$ . For example in LPR method for the oxalate, the anode and cathode Tafel slope estimated was  $\beta_a = 410.6$  mV/decade and  $\beta_c = 49.8$  mV/decade respectively. In contrast that for cyclic polarization method yielded  $\beta_a = 111.11$  mV/decade and  $\beta_c = 107.1$  mV/decade respectively. The result is that LPR regression analysis gives a slightly lower corrosion current and as such lower corrosion rates.



**Figure 8-46.** Comparing LPR and Tafel Polarization results for oxalate system at 135°C



**Figure 8-47.** LPR corrosion rates trend over time for oxalate system

### 8.5.3 Pourbaix Diagrams

In corrosion studies, thermodynamic information cast into a potential- pH diagram is known as Pourbaix diagram. It is useful for knowing what kind of corrosion products will be possibly formed at a particular temperature, corrosion potential and pH. In this work, the pH of the corrosion systems were recorded as well as the  $E_{corr}$ . It has been stated that a Pourbaix diagram, or potential pH diagram, is a map of thermodynamic possibilities and can be seen as a map in the chemical space, summarizing thermodynamic information in a compact and at the same time useful way (Beveriskog and Puigdomenech 1996). The Pourbaix diagram consists of three regions of interest: immunity, passivity and corrosion. The various regions can be seen in figure 8-48 below for iron. The middle to top left where iron ions can be found is the corrosion region. The location the formation of  $Fe_2O_3$  and  $Fe_3O_4$  species is considered the passivity zone. The information in the diagrams can be beneficially used to control corrosion of pure metals in the aqueous environment that is by altering the pH and potential to the regions of immunity and passivation, corrosion can be controlled (uobabylon 2013). The theory behind these potential – pH diagrams was covered in the theory chapter of this work.

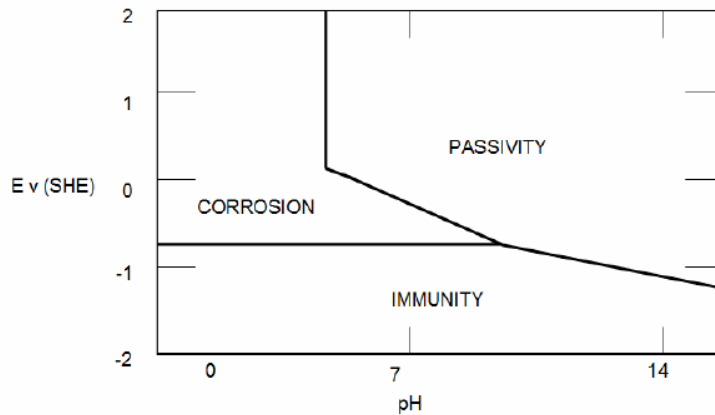


**Figure 8-48.** Schematic Pourbaix diagram with regions of corrosion, immunity and passivity (uobabylon 2013)

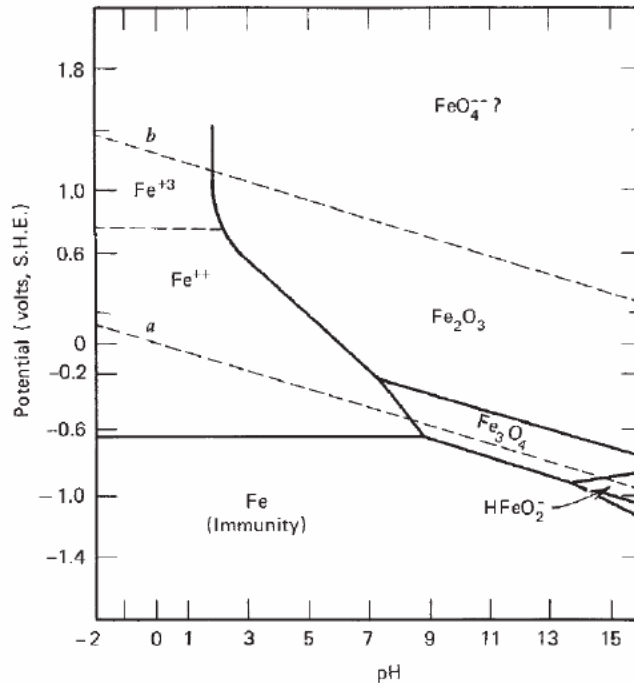


**Figure 8-49.** Pourbaix diagram for Iron in water at ambient conditions (uobabylon 2013)

The elements of interest for possible corrosion products will be iron, chromium and nickel. These alloying elements of stainless steel 316L form the bulk of the specimen and so possible corrosion products of these will be a useful insight into DETA-CO<sub>2</sub>-degradation products corrosion of stainless steel 316L .

From the electrochemical analysis data, for example for the most corrosive system, DETA + 2 wt% acetate, at room temperature, with a pH = 7.5 and a corrosion potential of  $E_{corr} = -574$  mV (vs. SHE- standard hydrogen electrode). Using these numbers and referring it to the Pourbaix diagram for Iron in figure 8-49 above, it can clearly be seen that the region will be in the corrosion zone, where the formation of Fe<sup>2+</sup> will dominate the reaction and this corresponded well with the weight loss approach and electrochemical analysis done for this work. A slight increase in pH of the DETA corrosive medium will put the iron in the passive region where it reacts to form the passivating layers Fe<sub>2</sub>O<sub>3</sub> and Fe<sub>3</sub>O<sub>4</sub>. Similar analysis can be done for all the systems where corrosion was substantially recorded. The Pourbaix for Ni and Cr are also shown in figures 8-50 and 8-51. For chromium ions (Cr<sup>2+</sup>), sometimes it has been reported to be stable

in solutions and formed chelates in amine or amino acids and can thus be used to explain the fact that corrosion is observed for stainless steel in these solutions (Kongstein 2010).

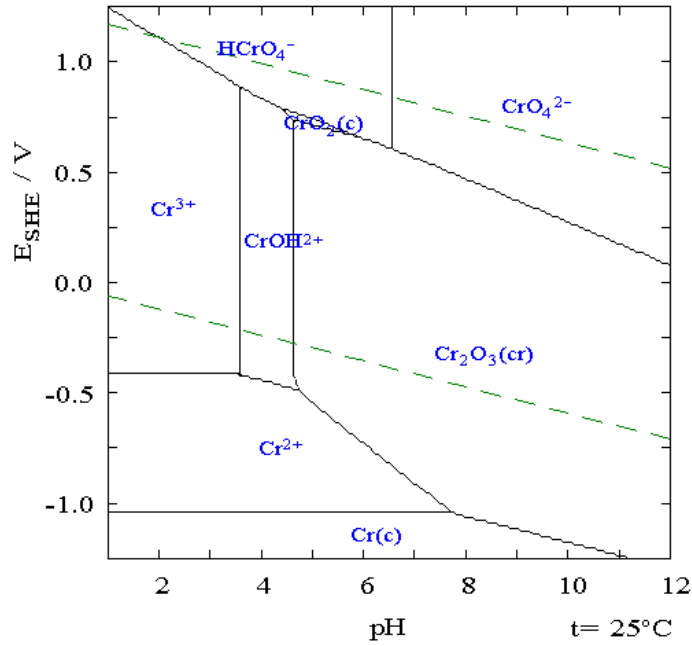


Figure 8-50. Pourbaix diagram for Cr in salt solution at ambient conditions (Kongstein 2010)

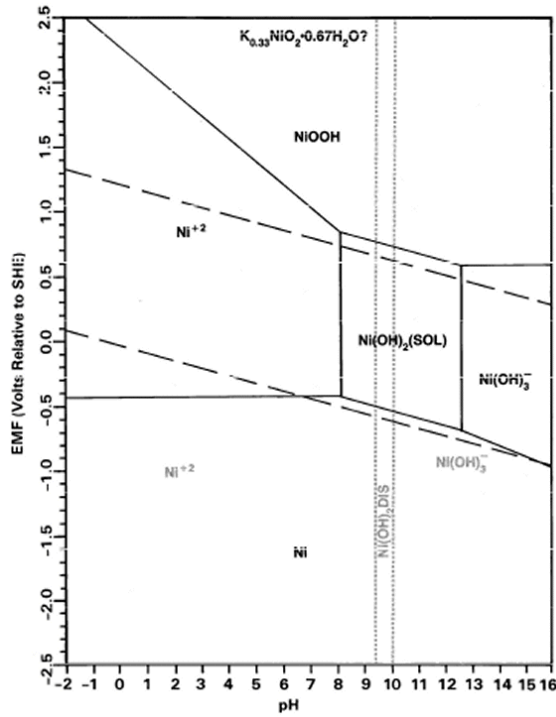


Figure 8-51. Pourbaix diagram for Nickel in solution at ambient conditions (CORWIKI 2008)

## 8.6 Uncertainties in the Result

A number of uncertainties could be associated and hence reported. The cylinders used had been earlier on reused several times. This led to the issue of contamination of solutions that were put in it and it could have affected the results. One major issue however with the Swagelok caps, and the cylinder was that despite following laid down procedure for cap tightening, massive amount of leakages occurred.

The containers were kept in an upright position and not stirred thereby introducing the possibility of the occurrence of concentration profile, which then mean that different parts of the metal could be exposed to different concentration of amines and acids and hence the corrosion rate might not be uniform and reproducibility of results become difficult.

Also the condition of the stainless steel as received from the fine mechanics shop has some surface deformations. In addition surface preparation prior to the experiment involves using silicon carbide paper (for wet grinding) or hydrochloric acid (chemical cleaning). All these could affect the surface morphologies and introduce pockets of deformations that could find its way into the overall corrosion.

The mass balances used in the Lab could have introduced a number of uncertainties in the results obtained. With an accuracy of  $\pm 0.001g$  as well as measuring the mass of over 80 specimens a number of times and over, various degrees of errors must have crept into the result obtained in.

For the electrochemical experiments, especially the LPR, the scan rate choice ultimately introduces errors and bias in the polarization and evaluation of the corrosion current density (through the Stern-Geary equation (this was covered in the methodology chapter 6 section 6.3.2).

## **Chapter 9 Introductory Modeling Approach**

### **9.0 Introduction**

Corrosion causes considerable damages in the process industries as has been highlighted in the beginning chapter of this work. Therefore, any means to be able to manage and predict corrosion is of immense help and from this need arises corrosion modeling. The aim is to be able to close to accurately predict when and what extent corrosion can have on materials used in the process industries. The problem however is that in the open literature the knowledge of corrosion prediction is limited especially for the amine solution corrosion (Ameerudeen Najumudeena, Amornvadee Veawab et al. 2012). With the exception of a mechanistic model by Najumudeen et al. (Ameerudeen Najumudeena, Amornvadee Veawab et al. 2012) and an open source model by (Srdjan Nestic, Dusan Sormaz et al. 2008) most of the models are commercially made and hence proprietary products. This makes it hard to add further developments on earlier models and thus hampering efforts to study the fundamental processes underlining corrosion at least for in the open literature. The point of this chapter is not to develop a radically new approach to corrosion modeling but rather to summarize the key points of a few of the open source models available (Nordsveen, Nešić et al. 2003; Ameerudeen Najumudeena, Amornvadee Veawab et al. 2012) and to lay the foundation for future work on specifically diethylenetriamine-CO<sub>2</sub> corrosion predictions in stripper operating conditions (135°C). This knowledge should enable corrosion engineers and scientists to build entry level corrosion simulation and prediction (Srdjan Nestic, Dusan Sormaz et al. 2008).

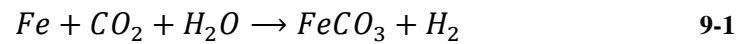
### **9.1 Chemistry of Corrosion**

#### **9.1.1 Thermodynamic equilibrium Considerations**

In order to fully develop a model, a broad understanding of chemistry of corrosion in the corrosive medium is required. The aim is to be able have a complete speciation of moieties in solution and use existing sub-models to cast reactions into mathematical equations and then numerical methods are used to calculate key parameters such as concentration of species in

solution, corrosion currents, from which corrosion rates can be derived. In other words find the equilibrium constants (K) of the key reactions and use these constants to help find the rate constants (k). Once the rate equations can be fully accounted for (corrosion rates found via kinetics not thermodynamics), numerical methods can be used to solve the equations and corrosion rates can be predicted. The most commonly used systems for corrosion modeling are the aqueous CO<sub>2</sub> corrosion and amine –CO<sub>2</sub> corrosion environments.

Aqueous CO<sub>2</sub> corrosion can be thought of as a function of the following parts: chemical, electrochemical and transport processes and the overall reaction is as shown below:



CO<sub>2</sub> solubility modeling via vapor-liquid-equilibrium (VLE) is required in order to know the concentration of CO<sub>2</sub> species in solution via dissolution of carbon dioxide:



From Henry's law and assuming ideal conditions, once the partial pressure of CO<sub>2</sub>(P<sub>CO<sub>2</sub></sub>) is known the concentration c<sub>CO<sub>2</sub></sub> in solution can be predicted :

$$H_{sol(CO_2)} = \frac{1}{K_{sol(CO_2)}} = \frac{P_{CO_2}}{c_{CO_2}} \quad 9-3$$

For DETA, the work done by Ardi Hartono (Hartono 2009) on solubility measurements were performed for different DETA concentrations, temperatures, or DETA loaded with CO<sub>2</sub>. This approach used the Deshmukh-Mater model which was implemented to the DETA-H<sub>2</sub>O-CO<sub>2</sub> system at 2.5 M for predicting the CO<sub>2</sub> partial pressure against loading at different temperatures and from such models the P<sub>CO<sub>2</sub></sub> as shown in the equation 9-3 above can be obtained especially for higher loadings in DETA such as α = 1.2 and at 120°C.

Next reaction is the formation of weak acid (carbonic acid)  $H_2CO_3$  according to the  $CO_2$  hydration equation:

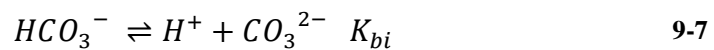


If infinite dilution is assumed, then the concentration of water remains constant and therefore the equilibrium reaction constant  $K_{hyd}$  is as obtained:

$$K_{hyd} = \frac{c_{H_2CO_3}}{c_{CO_2}} \quad 9-5$$

With  $c_{CO_2}$  known and  $K_{hyd}$  taken from the literature for temperature range (20-100°C) (Palmer and Van Eldik 1983) and extrapolation can be done for 120°C and more  $K_{hyd} = 2.58 * 10^{-3}$ , then  $c_{H_2CO_3}$  can thus be obtained.

The carbonic acid formed partially dissociates to form first, bicarbonate ( $HCO_3^-$ ) and carbonate ( $CO_3^{2-}$ ) and  $H^+$  according to the following equations:



The equilibrium constants given by the following equations:

$$K_{ca} = \frac{c_{H^+} c_{HCO_3^-}}{c_{H_2CO_3}} \quad 9-8$$

$$K_{bi} = \frac{c_{H^+} c_{CO_3^{2-}}}{c_{HCO_3^-}} \quad 9-9$$

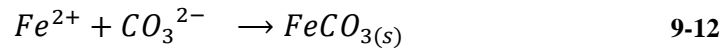
These equilibrium constants can be calculated as a function of temperature  $T$  and ionic strength  $I$  (J. Oddo and Tomson 1982):

$$K_{ca} = 387.6 * 10^{-(6.41-1.594*10^{-3}T_f+8.52*10^{-6}T_f^2-3.07*10^{-5}pCO_2*14.5-0.4772*I^{0.5}+0.118*I)} \quad \mathbf{9-10}$$

$$K_{bi} = 10^{-(10.61-4.97*10^{-3}T_f+1.331*10^{-5}T_f^2-2.624*10^{-5}pCO_2*14.5-1.166*I^{0.5}+0.3466*I)} \quad \mathbf{9-11}$$

Note that  $c_{H^+}$  can be obtained by knowing the pH value (a possible input into the model).

The formation of surface films significantly alters the rate of electrochemical reactions and corrosion rates (Nordsveen, Nešić et al. 2003) and hence their presence should be taken into account. For  $CO_2$  corrosion the following reaction accounts for the formation of surface films and occurs when the concentration of  $Fe^{2+}$  and  $CO_3^{2-}$  exceed the solubility limit (ionic product  $c_{Fe^{2+}}c_{CO_3^{2-}} > K_{sp(FeCO_3)}$  )



This reaction becomes important in the case of DETA- $CO_2$  corrosion since it is reported that above  $60^\circ C$  and supersaturation ( $S = \frac{c_{Fe^{2+}}c_{CO_3^{2-}}}{K_{sp(FeCO_3)}}$  ) surface films become appreciable and hence necessary to include in the model (Nordsveen, Nešić et al. 2003).

$FeCO_3$  precipitation is very difficult to model but two models in the literature have been proposed that can be included in any corrosion prediction model. The first one is according to Johnson and Tomson (M.L. Johnson and M.B. Tomson 1991):

$$R_{FeCO_3} = A * e^{54.8 - \frac{123.0kJ}{RT} * \frac{mol}{}} * K_{sp} * (S^{\frac{1}{2}} - 1)^2 \quad \mathbf{9-13}$$

The second model according to van Hunnik (E.W.J. van Hunnik, B.F.M. Pots et al. 1996):

$$R_{FeCO_3} = A * e^{52.4 - \frac{123.0kJ}{RT} * \frac{mol}{mol}} * K_{sp} * (S - 1)(1 - S^{-1}) \quad 9-14$$

Where the rate of precipitation is given by the expressions shown above, A is the surface area available for precipitation per unit volume. The Ksp can be taken from the literature such as the IUPAC model based on the ionic strength and temperature.

$$K_{sp(FeCO_3)} = 10^{-59.3498 - 0.041377 * T_k - \frac{2.1963}{T_k} + 24.5724 * \log T_k + 2.518 * I^{0.5} - 0.657 * I} \quad 9-15$$

For entry level simulations and modeling the presence of precipitation films can be ignored, though not accurate, it gives a simple model in the end and from which adjustments can be made later on.

### 9.1.2 Electrochemical Reactions

Moving to the surface of the steel in solution where the following key reactions take place, some at the anode and cathode (since corrosion is an electrochemical reaction at the core). The point of electrochemical reactions speciation is to be able to establish a charge balance and from which the corrosion current density ( $i_{corr}$ ) can be calculated. Knowledge of  $i_{corr}$  is then used to estimate the corrosion rates.

At the anode iron dissolution dominates according to the following:



This reaction has a rate which is dependent on the pH of the solution, for The reaction is pH dependent in acidic solutions with a reaction order with respect to  $OH^-$  between 1 and 2, decreasing toward 1 and 0 at  $pH > 4$ , which is the typical range for  $CO_2$  corrosion. Measured Tafel slopes are typically 30-80 mV (Srdjan Netic, Dusan Sormaz et al. 2008). From experience using DETA in this work, typical pH ranges are beyond 7 and as such a rate reaction order with respect to  $OH^-$  should have value between 1 to 0 and further experimental validation is needed to

frame the reaction rate equation more applicable to diethylenetriamine-CO<sub>2</sub> corrosion environment.

From the cathode, increasing hydrogen evolution is responsible for the increase in flow of cathodic current which in turn increases the dissolution of ion at the anode. The evolution reaction is as shown below:



This reaction is in the regime of mass transfer limit (diffusion control) for certain pH. For strong acidic environments (pH<4) Nesic et al. (Srdjan Nesic, Dusan Sormaz et al. 2008) reports that the reaction is limited by the rate at which  $H^+$  ions are transported from the bulk solution to the steel surface (mass transfer limitation). In  $CO_2$  solutions where typically pH>4, this limiting flux would be small and therefore it is the presence  $H_2CO_3$  which enables hydrogen evolution at a much higher rate. So for DETA corrosion  $H_2CO_3$  presence will be the key to  $H_2$  evolution at the cathode. Thus the following  $H_2CO_3$  (direct reduction of carbonic acid and  $HCO_3^-$  (direct reduction of bicarbonate ion – pH >5) reactions are key at the cathode as well:

Direct carbonic acid reduction (De Waard and Milliams 1975; E. Eriksrud and Søntvedt 1984; L. G. S. Gray, B. G. Anderson et al. 1989):



Direct bicarbonate ion reduction (L. G. S. Gray, B. G. Anderson et al. 1990):



The bicarbonate in reduction which could be applicable to DETA systems because for the pH specification, however has not been thoroughly validated with experimental data since the reaction mechanism can hardly be distinguished from that of the carbonic and  $H^+$  reactions shown above and hence this reaction can be ignored in a potential model.

In CO<sub>2</sub> capture plants the presence of traces of oxygen in the flue gas can affect corrosion as well the role of water in aqueous amine CO<sub>2</sub> corrosion. The role of water (hydrogen evolution by direct reduction of H<sub>2</sub>O) is important mainly for P<sub>CO2</sub> << 1 bar and pH > 5.

The O<sub>2</sub> reduction at the cathode is another key reaction:

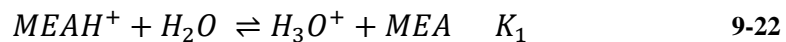


Hydrogen evolution:

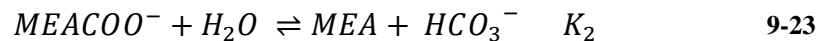


Finally for amine environments the following reactions are important to take into account and the equilibrium constants could be determined via the Kent-Eisenberg (K-E) model where the unity activity coefficients of all chemical species are assumed, and the rigorous electrolyte nonrandom two-liquid (NRTL) model where the activity coefficients can be determined from species interactions. The following are the chemical reactions used in both K-E and NRTL models for MEA as Nujameend and Veawab (Ameerudeen Najumudeena, Amornvadee Veawab et al. 2012) did for corrosion prediction in MEA solutions. This can be adapted for DETA solutions since the additional sources of H<sub>2</sub>O and H<sup>+</sup> affect the overall mass balance for these species in question:

Dissociation of protonated MEA:



Reversion of MEA Carbamate:



The above electrochemical processes can then be quantified using the well established electrochemical theory (Srdjan Nestic, Dusan Sormaz et al. 2008) according to the Faraday's law for computing current density(A/m<sup>2</sup>):

$$i = nF\mathfrak{R} \quad 9-24$$

Where  $\mathfrak{R}$  is the rate of electrochemical reactions (kmol/(m<sup>2</sup>s), F is the Faraday's constant and n is number of moles of electrons used in the reaction.

In order to establish a current density balance, the individual exchange current densities of the key electrochemical reactions are needed. These current densities are found from electrochemical theory and to be precise the fundamental exponential rate equation of electrochemistry that relates the current density (i) to the potential at the metal surface (E) (Nordsveen, Nešić et al. 2003):

$$i = \pm i_o * 10^{\pm \frac{E_{corr} - E_{rev}}{b}} \quad 9-25$$

Where  $E_{corr}$  is the so-called corrosion or rest potential,  $i_o$  is the exchange current density,  $E_{rev}$  is the reversible potential, b = Tafel slope.  $i_o$  and  $E_{rev}$  are non linear functions of the surface concentration of species involved in a particular reaction as will be shown later in this chapter. All three parameters are functions of temperature.

So for the key reactions: iron dissolution at the anode, cathodic reactions of hydronium, water, O<sub>2</sub> and carbonic acid reduction; a particular exchange current density ( $i_o$ ) is obtained and from a charge balance shown in equation 9-26 below, the corrosion potential can be calculated. Once  $E_{corr}$  is known the current density can be calculated and the particular rate equation also computed via equation 9-24 above (Nordsveen, Nešić et al. 2003) :

$$\sum_1^{n_a} i_a = \sum_1^{n_c} i_c \quad 9-26$$

Where  $n_a$ ,  $n_c$  are the total number of anodic and cathodic reactions respectively.

Or in the case of a potential DETA-CO<sub>2</sub> corrosion where the following species have been identified (H<sup>+</sup>, Fe<sup>2+</sup>, H<sub>2</sub>CO<sub>3</sub>, H<sub>2</sub>O and O<sub>2</sub>) the charge balance becomes:

$$i_{c(H^+)} + i_{c(H_2CO_3)} + i_{c(O_2)} + i_{c(H_2O)} = i_{a(Fe^{2+})} \quad 9-27$$

The individual exchange current densities and their temperature dependence correlation can be found in the literature (Srdjan Nestic, Dusan Sormaz et al. 2008) but an example for Fe at the anode is given by (Srdjan Nestic, Dusan Sormaz et al. 2008):

$$i_{\alpha(Fe)} = i_{o(Fe)} * 10^{\frac{E_{corr} - E_{rev(Fe)}}{b_{c(Fe)}}} \quad \mathbf{9-28}$$

$$i_{o(Fe)} = i_{o(Fe)}^{ref} * e^{\frac{-\Delta H_{Fe}}{R} \left( \frac{1}{T_c + 273.15} - \frac{1}{T_{c,ref} + 273.15} \right)} \quad \mathbf{9-29}$$

And the tafel slope for the anodic iron dissolution is given:

$$b_{\alpha(Fe)} = \frac{2.303 * R(T_c + 273.15)}{1.5 * F} \quad \mathbf{9-30}$$

It should be noted that in the computation of each exchange current and Tafel slopes, a knowledge of whether the reaction is under charge transfer control or mass transfer control will determine the kinds of extra parameters such as mass transfer coefficients etc. that will be needed to be introduced. For example for the reduction of hydronium, the reaction can either be under charge transfer or mass transfer and as such the overall current density will be the sum of the current due either transfer control:

$$\frac{1}{i_{c(H^+)}} = \frac{1}{i_{\alpha(H^+)}} + \frac{1}{i_{lim}^d(H^+)} \quad \mathbf{9-31}$$

Where charge transfer current density is given by:

$$i_{\alpha(H^+)} = i_{o(H^+)} * 10^{\frac{E_{corr} - E_{rev(H^+)}}{b_{c(H^+)}}} \quad \mathbf{9-32}$$

And the limiting mass transfer current density is related to the rate of transport of  $H^+$  ions from the bulk of the solution through the boundary layer to the steel surface (Srdjan Nestic, Dusan Sormaz et al. 2008):

$$i_{\text{lim}(H^+)}^d = k_{m(H^+)} F c_{H^+} \quad \mathbf{9-33}$$

The mass transfer coefficient  $k_{m(H^+)}$  has to be calculated via the transport processes speciation and governing equations.

### 9.1.3 Transport Processes

Species in solution can be adequately described and accounted for by constructing governing conservation equations for the transport of all species. For uniform corrosion, Nordsveen, Nestic et al. (Nordsveen, Nešić et al. 2003), argue that a one-dimensional computational domain is sufficient, stretching from the steel surface through the pores of a surface film and the mass-transfer boundary layer, ending in the bulk of the solution. Turbulent flow field can be assumed for the bulk solution, turbulent sub-layer whereas for the sub-layer close to the metal surface and in the pores of the film, transport of species is under molecular transport (diffusion) control.

The reason for taking into account the transport of species at the surface into account is that the corrosion process creates an established concentration gradient leading to molecular diffusion and hence affecting the rate of reactions of the electrochemical process (corrosion). Therefore to capture the role of turbulence, the concept of mass transfer coefficient  $k_m$  for the species in solution must be defined for a particular flow geometry regime; either by the straight pipe correlation of Berger and Hau (Berger and Hau 1977)

$$Sh_p = 0.0165 * Re^{0.86} * Sc^{0.33} \quad \mathbf{9-34}$$

or the rotating cylinder correlation by Eisenberg et al. (Eisenberg, Tobias et al. 1954):

$$Sh_r = 0.0791 * Re^{0.7} * Sc^{0.356} \quad \mathbf{9-35}$$

To calculate the rate of reactions and concentrations of the electrochemical species and reaction, a governing conservation (mass balance) is needed and this is valid for the liquid boundary layer (Newman 1991) and the porous film (Bear 1972) and provided as (Nordsveen, Nešić et al. 2003):

$$\left\{ \frac{\partial \varepsilon c_j}{\partial t} \right\}_{accumulation} = - \left\{ \frac{\partial (\mathcal{K} N_j)}{\partial X} \right\}_{net \ flux} + \{ \varepsilon \mathfrak{R}_j \}_{source \ or \ sink \ due \ to \ chemical \ reaction} \quad 9-36$$

Where  $c_j$  is the concentration of species  $j$ ,  $\varepsilon$ ,  $\mathcal{K}$ , are the volumetric porosity and surface permeability of the film respectively,  $t$  is the time,  $X$  is the spatial coordinates,  $N_j$  is the flux of species  $j$  and  $\mathfrak{R}_j$  is source or sink of species  $j$  due to chemical reactions which the species takes part.

To evaluate the net flux term, the following equation is used :

$$N_j = - \left\{ D_j \frac{\partial c_j}{\partial X} \right\} - \left\{ z_j u_j F c_j \frac{\partial \phi}{\partial X} \right\} + \{ c_j v \} \quad 9-37$$

The first term on the right in equation 9-37 above is the diffusion terms, where  $D_j$  is the molecular diffusion coefficient of species  $j$ ,  $z_j$  is the electrical charge of species  $j$ ,  $u_j$  is the mobility of species  $j$ ,  $F$  being the Faraday's constant,  $v$  is the characteristic and  $\phi$  is the electric potential in the solution.

The details about the evaluation of the molecular diffusion coefficients, electric potential and Faraday's constants can be found in the literature and handbooks on chemistry and physics as outlined by (Nordsveen, Nešić et al. 2003).

Numerical methods (which will not be described here) are then used to solve the governing equations with appropriate boundary conditions.

Hence by knowing the concentrations of all species in solution, the corrosion rates and current density ( $i_{corr} = i_{o(Fe)}$ ) the corrosion rate can be calculated by the usual Faraday's Law

$$CR = \frac{i_{corr} M_{Fe}}{\rho_{Fe} n F}$$

9-38

## 9.2. Conclusion

The model can then be validated against experimental data and the appropriate optimization done. It should be reiterated that the steps discussed above in this chapter is not meant to convey the impression that the author came up with all the modeling equations but rather this is a summary of a few of the open sources models that can be used as a springboard for future work in creating realistic and mechanistic corrosion prediction models, especially for amine solutions commonly encountered in CO<sub>2</sub> capture plants and which have been known to produce corrosion causing downtime, economic losses and in some cases injury and death to plant personnel. The model summarized in this chapter is also simple, it does not account for the presence of acetic acid (HAc) and other heat stable salts. Including these species makes the modeling complex and solving these equations demands a large computational time. Hence all deficiencies and loopholes in the described model above are that of this author and not the referenced authors.

The concluding chapter (following this chapter) summarizes all the results and interpretations carried out for the diethylenetriamine-CO<sub>2</sub>-degradation products experiments and the recommendations for future work will expand on what modeling aspect that will be needed done in order to have a full characterization of DETA-CO<sub>2</sub> corrosion on stainless steel.

## Chapter 10 Conclusion and Recommendations

### 10.1 Summary

The concept of global climate change that has been observed and currently on-going has necessitated the development of carbon capture and storage (CCS) technology. The goal of CCS is to be able to capture and store safely the main constituent of greenhouse gas CO<sub>2</sub>. In this work, the various aspects of the CO<sub>2</sub> capture and the deployment of the CCS technology has been reviewed from multiple references in the literature. The main objective though of this thesis was to look at one important aspect of the value chain of CCS technology: corrosion. The value chain of carbon capture and storage (CCS) technology stretches from the absorption stage (flue gases containing the CO<sub>2</sub>) using amine to the storage in safe sites via transport pipelines. Corrosion however cuts across multiple facets of the value chain, it is the integrity of process equipment in the amine absorption plants and the steel pipelines which makes corrosion of great importance. The sole objective of this work was thus to investigate the characterization of corrosion on stainless steel 316L material in a diethylenetriamine-CO<sub>2</sub>-degradation products environment and characterization included an introductory modeling approach to predicting corrosion rates on stainless steel specimen in diethylenetriamine environment.

Corrosion characterization was achieved by investigating the corrosion rates as a function of the following parameters: diethylenetriamine concentration of 2.5M, loaded with CO<sub>2</sub> (i.e.  $\alpha = 1.2$  and max), degradation products representing heat stable salts (oxalic, formic and acetic acid), simulate process conditions, stripper conditions at 135°C, and absorber temperature of 80°C, Inductive Coupled Plasma-Mass Spectrometry (ICP-MS) for solution analysis, Surface Metallography analysis (using SEM and optical microscope), time (1-5 weeks- weight loss and 8 days- electrochemical techniques) and framing a physicochemical model of CO<sub>2</sub> corrosion of steel.

The methodology for achieving the corrosion characterization was weight-loss of coupons and polarization via electrochemical methods.

From the results the following conclusions can be drawn:

- 1) CO<sub>2</sub> pre-loaded diethylenetriamine caused extensive corrosion of stainless steel. Even though it has been reported by plant operators that DETA causes corrosion, the sure way to verify it is to conduct experiments and this work confirmed what has been experienced in the field.
- 2) The extent of corrosion varies with the presence of HSS species. So for example from the weight loss methods, it was found out that the acetic and oxalic acid systems present a clear picture that contrast with the other two remaining systems. In that after 360 hours (corresponds to week 2), both the oxalate and acetate medium are more than 5 times as corrosive as either the formate or the DETA set-ups. The acetate solutions hit a corrosion rate high of 56.72 μm/yr after just 357 hours on stream. The mechanisms for both oxalic and acetic acid is that acetate ions accelerate the cathodic hydrogen evolution reaction thereby increasing the corrosion current and hence corrosion rates at the anode (metal dissolution) whereas the presence of oxalate (HC<sub>2</sub>O<sub>4</sub><sup>-</sup>) species and hydrogen cation enhanced the rates of oxidation (iron dissolution) and the reduction of oxidizing agents. The order of corrosion rates is: [DETA + acetate] > [DETA + oxalate] > [DETA + formate], [DETA]. From the Tafel plot it was found out that oxalate systems were the most corrosive in the DETA-CO<sub>2</sub> environment with a high of 26.52 mm /yr after only 13 hours on stream. At this rate, this corresponded to a relatively high current density  $i_{corr} = 2.0719095 \text{ mA/cm}^2$
- 3) The operating temperature has a significant impact on the corrosion rates. Faster kinetics at higher temperatures results in the quick transport of corrosion species and hence higher corrosion rates. For example DETA containing no acid system, at 80°C has corrosion rate of only 4.587E-06 mm/yr compared to 0.872 mm/yr for that at 135°C. The same trend was observed for all the systems.
- 4) Corrosion solution analysis by ICP-MS revealed that there was not the phenomenon of selective corrosion of the elements contained in stainless steel. That is compared to their nominal weight percentage (wt%) composition, no significant changes were observed. A total concentration of 48,830 mg/L for all ions in solution was recorded. Iron (Fe) consistently showed high concentrations in solution with a range of a low of 160mg/L (week 3) and higher values of 7300 mg/L to 9000mg/L for weeks 5 and 4 respectively.

- 5) Due to the extreme operating conditions like high temperatures of 135°C, the CO<sub>2</sub>-loaded diethylenetriamine was suspected to have undergone degradation. This suspicion was proven by a correlation of the corrosion rate trends with time. That is after 3 weeks, corrosion rates decreased dramatically and from literature review it was confirmed that diethylenetriamine experiences over 90% amine loss (6% remaining) at 135°C for just a period of only 4 weeks on stream. A plausible reason for the drop in corrosion rates is that there were not any significant diethylenetriamine present during these periods where low corrosion rates were obtained.
- 6) Surface morphology of the stainless steel specimen done with the scanning electron microscopy (SEM) revealed that the following types of surface features: flaky, porous, flowery and layers of corrosion products, fine plates typical of lepidocrocite, cotton ball shaped features typical of goethites, and severe pitting at the edges of the sample. Energy dispersive X-ray spectra (EDS) identified the following elements as being present: Fe, C, O, Si, Ni, Mo and other elements present in rust formations.
- 7) Excessive CO<sub>2</sub> loadings, that is having an  $\alpha = \max$  can have the reverse effect (passivating) on the expected corrosion rates. For Swagelok<sup>®</sup> 2.0 with CO<sub>2</sub> loadings of  $\alpha = \max$ , it was concluded that the ionic product of the iron and carbonate species exceeded the solubility constant ( $K_{sp}$ ) and hence the formation of a dense ferrous carbonate layer inhibited corrosion and resulted in a lower than expected corrosion rates.
- 8) Post-experiment CO<sub>2</sub> analysis confirms that the CO<sub>2</sub> concentration (mol/kg) in the diethylenetriamine solution decreased remarkably. For the 5 weeks that samples were on stream the following are the results of the CO<sub>2</sub> (mol/kg): 0.8662, 0.6314, 0.5954, 0.3806, 0.3951. It shows that after just a week on stream the CO<sub>2</sub> content decreased by as much as 70% and after the whole stretch of the experiment, there was hardly any CO<sub>2</sub> left. This made sense because in normal CO<sub>2</sub> capture conditions (high temperature and pressures), CO<sub>2</sub> is meant to be separated from the amine solvent and subsequently sequestered for storage downstream. In contrast the amine concentration stabilized for the first 3 weeks but in subsequent weeks, no conclusive data could be obtained from the amine analysis technique.
- 9) Pourbaix –diagram thermodynamic inferences based on the measured pH values showed that DETA + 2 wt% acetate, at room temperature, with a pH = 7.5 and a

corrosion potential of  $E_{\text{corr}} = -574 \text{ mV (vs SHE)}$  for Fe diagram, the reactions will lie in the corrosion region, where the formation of  $\text{Fe}^{2+}$  in solution is thermodynamically favored. For chromium ions ( $\text{Cr}^{2+}$ ), it can be reported to be stable in diethylenetriamine solutions forming chelates in amine and can thus be used to explain the fact that corrosion is observed for stainless steel in these solutions.

- 10) For an entry level corrosion simulation and prediction, a simple mechanistic model was introduced and covered key reactions in corrosion of stainless steel in diethylenetriamine- $\text{CO}_2$ - $\text{H}_2\text{O}$  medium. The key reactions are: electrochemical reactions at the steel surface, diffusion of species to and from the bulk including diffusion through porous surface films, migration due to potential (electric field) gradients, surface film precipitations and the accompanying fluxes.

It can thus be concluded that even though diethylenetriamine (DETA), a three functional group amine known is known for its high absorption capacity and faster kinetics, in the presence of  $\text{CO}_2$  in varying loadings and heat stable salts (HSS), significant corrosion of stainless steel 316L (a likely construction material for a CCS absorption plant (stripper)) remains a drawback from the point of view of likely cost impacts (capital and operating expenses). Hence Proper characterization of corrosion of stainless steel, will improve the overall feasibility of adopting CCS technology on an industrial scale. In addition a more rigorous development of models for predicting corrosion rates in amine solvents at industrial conditions will be needed before any commercial scale deployment of CCS can be realized.

## 10.2 Recommendations and Future works

Corrosion studies of metals especially stainless steel will likely remain an important feature in the CCS technology deployment. From the experiences from this work it can be recommended that more experimental and theoretical works on corrosion of amines, on stainless steel be done. The literature abound with many work on corrosion of carbon steel due to the fact that carbon steel is cheaper than stainless steel but does not offer the same long term benefits as would stainless steel. By having more experiments, data comparisons can achieve a uniform view on what the mechanisms are in amine-stainless steel corrosion.

In addition a greater availability of experimental data improves the optimization of models that can be used to predict corrosion. Better testing of various correlations (equilibrium and rate expressions) can be developed to complement the existing modeling tools such as the thermodynamic NRTL or the Kent-Eisenberg (K-E) models.

Accurate identification of surface morphologies can be achieved using X-ray diffraction (XRD), and Raman spectroscopy. Also evidence of degradation products can be obtained by using GC-MS (gas chromatography mass spectrometry).

Finally the weakest link in this work on stainless steel corrosion in diethylenetriamine (DETA)-CO<sub>2</sub> and the presence of degradation products was found to be a lack of better control over experimental conditions. The Swagelok<sup>®</sup> metal cylinders used should be discarded for glass reactors that can withstand extreme conditions. The reason is that the cylinders are also made from stainless steel and interferences, leakages were likely to affect the overall confidence in the results.

## Bibliography

- A. Raman, S. Nasrazadani, et al. (1987). "Morphology of rust phases formed on weathering steels during outdoor atmospheric exposure in sheltered locations under the bridges." Prakt. Metallogr. **24**: 535.
- A. Raman, S. Nasrazadani, et al. (1987). "Morphology of rust phases formed on weathering steels during outdoor atmospheric exposure in open, bold locations." Prakt. Metallogr. **24**: 577–587.
- A. Razvan and A. Raman. (1986). "Morphology of rust phases formed on naturally weathered weathering steels in bridge spans." Prakt. Metallogr. **23**: 223-236.
- A.L. Kohl, R. B. N. (1997). Gas Purification. Texas, Gulf Publishing Company.
- Aboudheir, A., P. Tontiwachwuthikul, et al. (2003). "Kinetics of the reactive absorption of carbon dioxide in high CO<sub>2</sub>-loaded, concentrated aqueous monoethanolamine solutions." Chemical Engineering Science **58**(23–24): 5195-5210.
- Agarwal, A., L. T. Biegler, et al. (2009). "Superstructure-Based Optimal Synthesis of Pressure Swing Adsorption Cycles for Precombustion CO<sub>2</sub> Capture." Industrial & Engineering Chemistry Research **49**(11): 5066-5079.
- AkerCleanCarbon (2012). "TCM Construction." Aker Solutions.
- Alie, C., L. Backham, et al. (2005). "Simulation of CO<sub>2</sub> capture using MEA scrubbing: a flowsheet decomposition method." Energy Conversion and Management **46**(3): 475-487.
- Ameerudeen Najumudeena, Amornvadee Veawab, et al. (2012). Corrosion Prediction of Carbon Steel in MEA -based CO<sub>2</sub> Capture Process. GHGT-11. Kyoto, Japan.
- Armor, A. F. and G. T. Preston (1996). "The impact of fossil generation advances on the emissions of CO<sub>2</sub> in the United States." Energy Conversion and Management **37**(6–8): 671-677.
- ASTM (2004). (G31-72) Standard Practice for Laboratory Immersion Corrosion Testing of Metals.

ASTM (2005). ASTM G46-94(2005) " Standard Guide for Examination and Evaluation of Pitting Corrosion". West Conshohocken, PA, ASTM International.

ASTM (2011). G1-03(2011) Standard Practice for Preparing, Cleaning, and Evaluating Corrosion Test Specimens.

ASTM (2013). Standard Reference Test Method for Making Potentiodynamic Anodic Polarization Measurements. West Conshohocken, PA, ASTM International.

Austgen, D. M., G. T. Rochelle, et al. (1989). "Model of vapor-liquid equilibria for aqueous acid gas-alkanolamine systems using the electrolyte-NRTL equation." Industrial & Engineering Chemistry Research **28**(7): 1060-1073.

B. Metz, O. Davidson, et al. (2006). IPCC Special Report of Carbon Dioxide Capture and Storage. Prepared by Working Group III of the Intergovernmental Panel on Climate Change. . Cambridge, Great Britain, New York, NY, USA 2005., Cambridge University Press.

Bailey, D., W. and P. Feron, H.M. (2005). "Capture post-combustion." Oil & Gas Science and Technology - Rev. IFP **60**(3): 461-474.

Bear, J. (1972). Dynamics of Fluids in Porous Media. Dover Publications. New York.

Bello, A. and R. O. Idem (2005). "Pathways for the Formation of Products of the Oxidative Degradation of CO<sub>2</sub>-Loaded Concentrated Aqueous Monoethanolamine Solutions during CO<sub>2</sub> Absorption from Flue Gases." Industrial & Engineering Chemistry Research **44**(4): 945-969.

Berger, F. P. and K. F. F. L. Hau (1977). "Mass transfer in turbulent pipe flow measured by the electrochemical method." International Journal of Heat and Mass Transfer **20**(11): 1185-1194.

Beverkog, B. and I. Puigdomenech (1996). "Revised pourbaix diagrams for iron at 25–300 °C." Corrosion Science **38**(12): 2121-2135.

Bhattacharyya, D., R. Turton, et al. (2010). "Steady-State Simulation and Optimization of an Integrated Gasification Combined Cycle Power Plant with CO<sub>2</sub> Capture." Industrial & Engineering Chemistry Research **50**(3): 1674-1690.

Billingham, M. A., C. H. Lee, et al. (2011). "Corrosion and materials selection issues in carbon capture plants." Energy Procedia **4**(0): 2020-2027.

Bockris, J. O. M., D. Drazic, et al. (1961). "The electrode kinetics of the deposition and dissolution of iron." Electrochimica Acta **4**(2-4): 325-361.

Caplow, M. (1968). "Kinetics of carbamate formation and breakdown." Journal of the American Chemical Society **90**(24): 6795-6803.

Chalmers, H. and J. Gibbins (2007). "Initial evaluation of the impact of post-combustion capture of carbon dioxide on supercritical pulverised coal power plant part load performance." Fuel **86**(14): 2109-2123.

Charles M. Blair Jr (1949). Process for Preventing Corrosion ad Corrosion Inhibitors. U. S. P. Office. United States of America, Petrolite Corporation Ltd. **2,598,213**: 6.

Cindra Fonseca, M. P., I. N. Bastos, et al. (2007). "Rust formed on cannons of XVIII century under two environment conditions." Corrosion Science **49**(4): 1949-1962.

CORWIKI (2008). "Potential-pH Diagrams." from [http://www.argentumsolutions.com/wiki/en/Potential-pH\\_Diagrams](http://www.argentumsolutions.com/wiki/en/Potential-pH_Diagrams).

Crooks, J. E. and J. P. Donnellan (1989). "Kinetics and mechanism of the reaction between carbon dioxide and amines in aqueous solution." Journal of the Chemical Society, Perkin Transactions 2 **0**(4): 331-333.

da Silva, E. F. and H. F. Svendsen (2004). "Ab Initio Study of the Reaction of Carbamate Formation from CO<sub>2</sub> and Alkanolamines." Industrial & Engineering Chemistry Research **43**(13): 3413-3418.

Danckwerts, P. V. (1979). "The reaction of CO<sub>2</sub> with ethanolamines." Chemical Engineering Science **34**(4): 443-446.

Danckwerts PV, M. K. (1967). "The absorption of carbon dioxide into aqueous amine solutions and the effects of catalysis. ." Trans. Inst. Chem. Eng. **45**, T32.

Davis, J. and G. Rochelle (2009). "Thermal degradation of monoethanolamine at stripper conditions." Energy Procedia **1**(1): 327-333.

Davis, J. D. (2009). Thermal Degradation of Aqueous Amines Used for Carbon Dioxide Capture. McKetta Department of Chemical Engineering. Austin- Texas, USA, The University of Texas at Austin. **Doctor of Philosophy**.

de Brito, M. H., U. von Stockar, et al. (1994). "Effective Mass-Transfer Area in a Pilot Plant Column Equipped with Structured Packings and with Ceramic Rings." Industrial & Engineering Chemistry Research **33**(3): 647-656.

de la Fuente, D., I. Díaz, et al. (2011). "Long-term atmospheric corrosion of mild steel." Corrosion Science **53**(2): 604-617.

De Waard, C. and D. E. Milliams (1975). "Carbonic Acid Corrosion of Steel." Corrosion **31**(5): 177-181.

DeHart, T. R. H., D. A.; Mariz, C. L.; McCullough, J. G. (1999). Solving corrosion problems at the NEA Bellingham Massachusetts carbon dioxide recovery plant. . NACE International Conference Corrosion '99. San Antonio, USA.

Delahay, P. (1952). "Implications of the Kinetics of Ionic Dissociation with Regard to Some Electrochemical Processes—Application to Polarography." Journal of the American Chemical Society **74**(14): 3497-3500.

DepartmentofEnergy (1993). Department of Energy Fundamentals Handbook Chemistry Module 2 : Corrosion. Washington D.C., USA, US Department of Energy.

Dingman, J. C., D. L. Allen, et al. (1966). "Minimize corrosion in MEA units." Hydrocarbon Processing **45**(9): 285-290.

DOE (2004). Applications of Gasification – Coal-to-Hydrogen Process Description. D. o. Energy.

Duda, Y., R. Govea-Rueda, et al. (2005). "Corrosion Inhibitors: Design, Performance, and Computer Simulations." The Journal of Physical Chemistry B **109**(47): 22674-22684.

Dugstad, A. (2006). Fundamental Aspects of CO<sub>2</sub> Metal Loss Corrosion - Part 1: Mechanism, NACE International.

DuPart, M. S. B., T. R.; Edwards, D. J. (1993). Understanding corrosion in alkanolamine gas treating plants (parts 1, 2). *Hydrocarbon Process*: 75 - 80.

E. Eriksrud and T. Søntvedt (1984). Effect of Flow on CO<sub>2</sub> Corrosion Rates in Real and Synthetic Formation Waters. *Advances in CO<sub>2</sub> Corrosion: Proceedings of the Corrosion /83 Symposium on CO<sub>2</sub> Corrosion in the Oil and Gas Industry*, Houston, TX, NACE.

E. Heitz, R. H. a. A. R. (1992). Corrosion Science : an experimental approach. .

E.W.J. van Hunnik, B.F.M. Pots, et al. (1996). paper no.6 : The Formation of Protective FeCO<sub>3</sub> Corrosion Product Layers in CO<sub>2</sub> Corrosion. CORROSION/96. Houston, TX, NACE.

Edali, M., A. Aboudheir, et al. (2009). "Kinetics of carbon dioxide absorption into mixed aqueous solutions of MDEA and MEA using a laminar jet apparatus and a numerically solved 2D absorption rate/kinetics model." International Journal of Greenhouse Gas Control **3**(5): 550-560.

EEA (2000). Annual Greenhouse Emissions by Sector. E. D. f. G. A. Research, European Environment Agency.

Ehmke, E. F. (1975). "Corrosion Correlations with Ammonia and Hydrogen Sulfide in Air Coolers." Material Performance : NACE **14**(7): 20.

Eide-Haugmo, I. (2011). Environmental impacts and aspects of absorbents used for CO<sub>2</sub> capture. . Faculty of Natural Science and Technology , Department of Chemical Engineering. Trondheim, Norway, NTNU. **Doctoral theses**

Eirik F. da Silva, H. L., Aslak Einbu, Adreas Grimstedvt, Kai Vernstad, Solrun Johanne Vevelstad, Hallvard F. Svendsen and Kolbjorn Zahlsten Understanding MEA degradation in post-combustion CO<sub>2</sub> capture. Trondheim, Norway, SINTEF Materials and Chemistry, NTNU

Eisenberg, M., C. W. Tobias, et al. (1954). "Ionic Mass Transfer and Concentration Polarization at Rotating Electrodes." Journal of The Electrochemical Society **101**(6): 306-320.

EPA (2012). Inventory of U.S. Greenhouse Gas Emissions and Sinks 1990-2010.

Epp, B., H. Fahlenkamp, et al. (2011). "Degradation of solutions of monoethanolamine, diglycolamine and potassium glycinate in view of tail-end CO<sub>2</sub> absorption." Energy Procedia **4**(0): 75-80.

F.C. Risenfeld and C. L. Blohm (1950). "Corrosion Problems in Gas Purification Units Employing MEA Solutions." Pet. Ref **29**(4): 141.

Freeman, S. A. and G. T. Rochelle (2012). "Thermal Degradation of Aqueous Piperazine for CO<sub>2</sub> Capture. 1. Effect of Process Conditions and Comparison of Thermal Stability of CO<sub>2</sub> Capture Amines." Industrial & Engineering Chemistry Research **51**(22): 7719-7725.

Gao, J., S. Wang, et al. (2012). "Corrosion Behavior of Carbon Steel at Typical Positions of an Amine-Based CO<sub>2</sub> Capture Pilot Plant." Industrial & Engineering Chemistry Research **51**(19): 6714-6721.

Geers, L. F. G., A. van de Runstraat, et al. (2011). "Development of an Online Monitoring Method of a CO<sub>2</sub> Capture Process." Industrial & Engineering Chemistry Research **50**(15): 9175-9180.

George, K. S. and S. Nešić (2007). "Investigation of Carbon Dioxide Corrosion of Mild Steel in the Presence of Acetic Acid—Part 1: Basic Mechanisms." Corrosion **63**(2): 178-186.

Grimstvedt, A. and W. He (2008). Corrosion Experiments in Amine Solutions. Trondheim-Norway, SINTEF Materials and Chemistry.

Gutzeit, J. and J. M. Johnson (1993). Corros. Inhibitor Sci. Technol. NACE **4**(1).

Haimour, N., A. Bidarian, et al. (1987). "Kinetics of the reaction between carbon dioxide and methyldiethanolamine." Chemical Engineering Science **42**(6): 1393-1398.

Han, J.-H. and I.-B. Lee (2012). "Multiperiod Stochastic Optimization Model for Carbon Capture and Storage Infrastructure under Uncertainty in CO<sub>2</sub> Emissions, Product Prices, and Operating Costs." Industrial & Engineering Chemistry Research **51**(35): 11445-11457.

Hartono, A. (2009). Characterization of diethylenetriamine (DETA) as absorbent for CO<sub>2</sub>. Faculty of Natural Sciences and Technology , Chemical Engineering Department. Trondheim - Norway, Norwegian University of Science and Technology. **philosophiae doctor(pHD)**.

- Hartono, A., E. F. da Silva, et al. (2006). "Qualitative Determination of Species in DETA–H<sub>2</sub>O–CO<sub>2</sub> System Using <sup>13</sup>C NMR Spectra." Industrial & Engineering Chemistry Research **46**(1): 249-254.
- Hartono, A., E. F. da Silva, et al. (2009). "Kinetics of carbon dioxide absorption in aqueous solution of diethylenetriamine (DETA)." Chemical Engineering Science **64**(14): 3205-3213.
- Hartono, A., O. Juliussen, et al. (2008). "Solubility of N<sub>2</sub>O in Aqueous Solution of Diethylenetriamine." Journal of Chemical & Engineering Data **53**(11): 2696-2700.
- Hartono, A. and H. F. Svendsen (2009). "Density, viscosity, and excess properties of aqueous solution of diethylenetriamine (DETA)." The Journal of Chemical Thermodynamics **41**(9): 973-979.
- Hartono, A. and H. F. Svendsen (2009). "Kinetics reaction of primary and secondary amine group in aqueous solution of diethylenetriamine (DETA) with carbon dioxide." Energy Procedia **1**(1): 853-859.
- Hasan, M. M. F., R. C. Baliban, et al. (2012). "Modeling, Simulation, and Optimization of Postcombustion CO<sub>2</sub> Capture for Variable Feed Concentration and Flow Rate. 1. Chemical Absorption and Membrane Processes." Industrial & Engineering Chemistry Research **51**(48): 15642-15664.
- Hasan, M. M. F., R. C. Baliban, et al. (2012). "Modeling, Simulation, and Optimization of Postcombustion CO<sub>2</sub> Capture for Variable Feed Concentration and Flow Rate. 2. Pressure Swing Adsorption and Vacuum Swing Adsorption Processes." Industrial & Engineering Chemistry Research **51**(48): 15665-15682.
- Haupt, S. and H. H. Strehblow (1995). "A combined surface analytical and electrochemical study of the formation of passive layers on FeCr alloys in 0.5 M H<sub>2</sub>SO<sub>4</sub>." Corrosion Science **37**(1): 43-54.
- Hayfron-Benjamin, E. (2012). Corrosion Effects on Industrial Grade Metals: Stainless Steel A316, caused by Degradation Products of Amine based Solvents. Trondheim- Norway, Norwegian University of Science and Technology.
- Herzog, H. (1993). The Capture, Utilization and Disposal of Carbon Dioxide from Fossil Fuel-Fired Power Plants, Department of Energy Technical Report DOE/ER-30194.

Ho, M. T., G. W. Allinson, et al. (2008). "Reducing the Cost of CO<sub>2</sub> Capture from Flue Gases Using Pressure Swing Adsorption." Industrial & Engineering Chemistry Research **47**(14): 4883-4890.

Hoppe, H. W., S. Haupt, et al. (1994). "Combined surface analytical and electrochemical study of the formation of passive layers on Fe/Cr alloys in 1 M NaOH." Surface and Interface Analysis **21**(8): 514-525.

Hsu Ch Fau - Chu, H., C. M. Chu H Fau - Cho, et al. "Absorption and reaction kinetics of amines and ammonia solutions with carbon dioxide in flue gas." (1096-2247 (Print)).

INER RAS. -M. (2001). Emission of greenhouse gases by energy complex of Russia for the period up to 2020., EUF of RAO "EES Rossii".

J. Amri, E. Gulbrandsen, et al. (2011). Role of acetic acid in CO<sub>2</sub> top of the line corrosion of carbon steel, paper no. 11329. CORROSION/11. Houston, TX, NACE.

J. Blamey, N. H. Florin, et al. (2009). "Calcium Looping Research." Imperial College of London.

J. Oddo and M. Tomson (1982). Simplified calculation of CaCO<sub>3</sub> saturation at high temperatures and pressures in brine solutions. SPE of AIME Richardson, TX, Society of Petroleum Engineers: 1583 - 1590.

Jassim, M. S. and G. T. Rochelle (2005). "Innovative Absorber/Stripper Configurations for CO<sub>2</sub> Capture by Aqueous Monoethanolamine." Industrial & Engineering Chemistry Research **45**(8): 2465-2472.

Jenna Worley and S. Kvech. 2013, from <http://www.webapps.cee.vt.edu/ewr/environmental/teach/smprimer/icpms/icpms.htm>.

John, F. and J. E. Jacobsen (1993). "Global Climate Change and Sustainable Development." Air & Waste **43**(9): 1202-1212.

John. Marion, Nsakala. ya Nsakala, et al. (2001). Controlling Power Plant CO<sub>2</sub> Emissions: A long Range View. U. S. DOE.

Jones, I. S. F. (2011). Engineering Strategies for Greenhouse Gas Mitigation Cambridge University Press.

Jovancicevic, V., P. Prince, et al. (1998). Inhibition of CO<sub>2</sub> Corrosion of Mild Steel by Imidazolines and Their Precursors, NACE International.

Kamimura, T., M. Yamashita, et al. (2001). "Correlation between Corrosion Rate and Composition of Crystalline Corrosion Products Formed on Weathering Steels." Journal of the Japan Institute of Metals **65**(10): 922-928.

Kittel, J., R. Idem, et al. (2009). "Corrosion in MEA units for CO<sub>2</sub> capture: Pilot plant studies." Energy Procedia **1**(1): 791-797.

Kladkaew, N., R. Idem, et al. (2009). "Corrosion Behavior of Carbon Steel in the Monoethanolamine–H<sub>2</sub>O–CO<sub>2</sub>–O<sub>2</sub>–SO<sub>2</sub> System." Industrial & Engineering Chemistry Research **48**(19): 8913-8919.

Kladkaew, N., R. Idem, et al. (2009). "Corrosion Behavior of Carbon Steel in the Monoethanolamine–H<sub>2</sub>O–CO<sub>2</sub>–O<sub>2</sub>–SO<sub>2</sub> System: Products, Reaction Pathways, and Kinetics." Industrial & Engineering Chemistry Research **48**(23): 10169-10179.

Knuutila, H. (2012). TKP 4535 Gas Purification and Absorption. Trondheim, Norway, Norwegian University of Science and Technology(NTNU).

Kohl, A. L. R., F. C. (1985). Gas Purification. Houston, USA, Gulf Publishing.

Kongstein, O. E. (2010). Carbon Lean Energy Operation(CLEO): Corrosion Test Method and Results. Trondheim, Norway, SINTEF.

L. G. S. Gray, B. G. Anderson, et al. (1989). paper no. 464: Mechanism of Carbon Steel Corrosion in Brines Containing Dissolved Carbon Dioxide at pH 4. Corrosion/89. Houston, TX, NACE International.

L. G. S. Gray, B. G. Anderson, et al. (1990). Effect of pH and Temperature on the Mechanism of Carbon Steel Corrosion by Aqueous Carbon Dioxide. CORROSION/90, paper no. 40. Houston, TX, NACE International.

L. G. S. Gray, B. G. Anderson, et al. (1990). paper no. 40 : Effect of pH and Temperature on the Mechanism of Carbon Steel Corrosion by Aqueous Carbon Dioxide. Corrosion/90. Houston, TX, NACE International.

L. Wegrelius and I. Olefjord (1993). 12th International Corrosion Congress NACE. Houston, TX, NACE. **5B**: 3887.

L.D. Polderman, C.P. Dillon, et al. (1955). "Degradation of MEA in Natural Gas Treating Service." Oil & Gas Journal.

Lin, Y.-J., T.-H. Pan, et al. (2010). "Plantwide Control of CO<sub>2</sub> Capture by Absorption and Stripping Using Monoethanolamine Solution." Industrial & Engineering Chemistry Research **50**(3): 1338-1345.

Littel, R. J., W. P. M. Van Swaaij, et al. (1990). "Kinetics of Carbon Dioxide with tertiary Amines in aqueous solution." AIChE Journal **36**(11): 1633-1640.

Littel, R. J., G. F. Versteeg, et al. (1992). "Kinetics of CO<sub>2</sub> with primary and secondary amines in aqueous solutions—I. Zwitterion deprotonation kinetics for DEA and DIPA in aqueous blends of alkanolamines." Chemical Engineering Science **47**(8): 2027-2035.

Liu, X., S. Chen, et al. (2006). "Protection of iron corrosion by stearic acid and stearic imidazoline self-assembled monolayers." Applied Surface Science **253**(2): 814-820.

Liu, Z., L. Wang, et al. (2012). "Onsite CO<sub>2</sub> Capture from Flue Gas by an Adsorption Process in a Coal-Fired Power Plant." Industrial & Engineering Chemistry Research **51**(21): 7355-7363.

Lloyd, D. K. and M. Lipow (1984). *Reliability: Management, Methods and Mathematics*. The American Society for Quality Control. Milwaukee, Wisc.

M.L. Johnson and M.B. Tomson (1991). paper no. 268 : Ferrous Carbonate Precipitation Kinetics and Its Impact on CO<sub>2</sub> Corrosion. CORROSION/91. Houston, TX, NACE.

M.R. Louthan, J. (1986). Optical Metallography, ASM International.

MacDowell, N., N. Florin, et al. (2010). "An overview of CO<sub>2</sub> capture technologies." Energy & Environmental Science **3**(11): 1645-1669.

Mariz, C. L., T. R. DeHart, et al. (1999). Solving Corrosion Problems at the NEA Bellingham, Massachusetts Carbon Dioxide Recovery Plant, NACE International.

Martin, S., H. Lepaumier, et al. (2012). "New Amines for CO<sub>2</sub> Capture. IV. Degradation, Corrosion, and Quantitative Structure Property Relationship Model." Industrial & Engineering Chemistry Research **51**(18): 6283-6289.

Mattsson, E. (1989). Basic Corrosion Technology for Scientists and Engineers.

Maurice, V., W. P. Yang, et al. (1998). "X-Ray Photoelectron Spectroscopy and Scanning Tunneling Microscopy Study of Passive Films Formed on (100) Fe-18Cr-13Ni Single-Crystal Surfaces." Journal of The Electrochemical Society **145**(3): 909-920.

Meng, H., S. Zhang, et al. (2008). "Removal of heat stable salts from aqueous solutions of N-methyldiethanolamine using a specially designed three-compartment configuration electro dialyzer." Journal of Membrane Science **322**(2): 436-440.

MetrohmAutoLab. Retrieved 5/21/2013, 2013, from <http://www.metrohm-autolab.co.uk/Downloads/Apl017.pdf>.

MettlerToledo (2013). "Basics of Titration." 2013, from [http://cn.mt.com/dam/Analytical/Titration/TI-Application/51725228\\_Basics\\_of\\_Titration\\_Broch\\_e.pdf](http://cn.mt.com/dam/Analytical/Titration/TI-Application/51725228_Basics_of_Titration_Broch_e.pdf).

Moiseeva, L. S. and N. S. Rashevskaya (2002). "Effect of pH Value on Corrosion Behavior of Steel in CO<sub>2</sub>-containing Aqueous Media." Russian Journal of Applied Chemistry **75**(10): 1625-1633.

Nainar, M. and A. Veawab (2009). "Corrosion in CO<sub>2</sub> capture unit using MEA-piperazine blends." Energy Procedia **1**(1): 231-235.

Nesic, S., D. Drazic, et al. (1996). Electrochemical Properties of Iron Dissolution in the Presence of CO<sub>2</sub> - Basics Revisited, NACE International.

Nesic, S., J. Postlethwaite, et al. (1996). "An Electrochemical Model for Prediction of Corrosion of Mild Steel in Aqueous Carbon Dioxide Solutions." Corrosion **52**(04).

Newman, J. S. (1991). Electrochemical Systems. Englewood Cliffs, NJ, Prentice Hall.

Nordsveen, M., S. Nešić, et al. (2003). "A Mechanistic Model for Carbon Dioxide Corrosion of Mild Steel in the Presence of Protective Iron Carbonate Films—Part 1: Theory and Verification." Corrosion **59**(5): 443-456.

Ogundele, G. I. and W. E. White (1987). "Observations on the Influences of Dissolved Hydrocarbon Gases and Variable Water Chemistries on Corrosion of an API-L80 Steel." Corrosion **43**(11): 665-673.

Olsson, C. O. A. and D. Landolt (2003). "Passive films on stainless steels—chemistry, structure and growth." Electrochimica Acta **48**(9): 1093-1104.

PaceTechnologies (2013). "Introduction to Metallography." 2013, from [www.metallographic.com](http://www.metallographic.com).

Palmer, D. A. and R. Van Eldik (1983). "The chemistry of metal carbonate and carbon dioxide complexes." Chemical Reviews **83**(6): 651-731.

Pebere, N., M. Duprat, et al. (1988). "Corrosion inhibition study of a carbon steel in acidic media containing hydrogen sulphide and organic surfactants." Journal of Applied Electrochemistry **18**(2): 225-231.

Pletcher, D. and Y. Garsany (2003). The Role of Acetate in CO<sub>2</sub> Corrosion of Carbon Steel - Studies Related to Oilfield Conditions, NACE International.

R.T. Watson, H.Rodhe, et al. (1990). Greenhouse gases and Aerosols. Climate Change, The IPCC Scientific Assessment. J.T. Houghton, G.J. Jenkins and J. J. Ephraums. Cambridge, UK., Cambridge University Press.

R.T. Watson, L.G.Meira Filho, et al. (1992). Greenhouse Gases: Sources and Sinks. Climate Change 1992: The Supplementary Report to the IPCC Scientific Assessment. J.T. Houghton, B.A. Callander and S.K. Varney. Cambridge, Great Britain, New York, NY, USA, and Victoria , Australia, Cambridge University Press.

Raman, A., S. Nasrazadani, et al. (1989). "Morphology of rust phases formed on weathering steels in various laboratory corrosion tests." Metallography **22**(1): 79-96.

Raman, A., A. Razvan, et al. (1986). "Characteristics of the Rust from Weathering Steels in Louisiana Bridge Spans." Corrosion **42**(8): 447-455.

Roberge, P. R. (2000). Handbook of Corrosion Engineering. Hightstown, New Jersey, USA, McGraw Hill.

Rochelle, G. (2013). DETA corrosivity. E. Hayfron-Benjamin. Trondheim TCCS- 7 Conference.

Rogner, H.-H., D. Zhou, et al. (2007). Introduction Climate Change 2007: Mitigation of Climate Change. B. Metz, O.R. Davidson, P.R. Bosch, R. Dave and L. A. M. (eds). Cambridge, United Kingdom and New York, NY, USA., Cambridge University Press.

Rooney, P. C., M. S. DuPart, et al. (1997). "Effect of heat stable salts on MDEA solution corrosivity: Part 2." Journal Name: Hydrocarbon Processing; Journal Volume: 76; Journal Issue: 4; Other Information: PBD: Apr 1997; Medium: X; Size: pp. 65-71.

S. Turgoose, R. A. C. and, et al. Modelling of Electrode Processes and Surface Chemistry in Carbon Dioxide Containing Solutions. Computer Modelling In Corrosion, Raymon S. Munn and ASTM Publishing. **Code Number 04-011540-27.**

S.F Bosen and S. A. Bedell (2004). The relevance of bicine in the corrosion of amine gas treating plants. Corrosion 2004: NACE International Annual Conference and Exposition. New Orleans, LA, USA, NACE International.

S.Nesic (2004). A Critical Review of CO<sub>2</sub> Corrosion Modelling in the Oil and Gas Industry. 10th Middle East Corrosion Conference.

S.W. Dean, D. Knotkova, et al. (2010). International Atmospheric Exposure Program: Summary of Results. West Conshohocken, PA, ASTM.

Saiwan, C., T. Supap, et al. (2011). "Part 3: Corrosion and prevention in post-combustion CO<sub>2</sub> capture systems." Carbon Management **2(6)**: 659-675.

Schmitt, G. and A. O. Saleh (2000). Evaluation of Environmentally Friendly Corrosion Inhibitors for Sour Service, NACE International.

Sekine, I. and K. Senoo (1984). "The corrosion behaviour of SS 41 steel in formic and acetic acids." Corrosion Science **24(5)**: 439-448.

Singh, S. K. and A. K. Mukherjee (2010). "Kinetics of Mild Steel Corrosion in Aqueous Acetic Acid Solutions." Journal of Materials Science & Technology **26**(3): 264-269.

Srdjan Nestic, Dusan Sormaz, et al. (2008). FREECORP - Corrosion Prediction background pdf and Software Copyright GNU. Ohio, USA, Institute for Corrosion and Multiphase Technology, Ohio State University.

Stangeland, R. S. a. A. ( September 2009). Amines Used in CO<sub>2</sub> Capture – Health and Environmental Impacts, The Bellona Foundation.

Steven J. Suess (2006). "Recognition and Analysis of Corrosion Failure Mechanisms." Journal on Systemics, Cybernetics and Informatics **4**: 73-79.

Suda, T., M. Iijima, et al. (1997). "Countercurrent absorption of CO<sub>2</sub> in a real flue gas into aqueous alkanolamine solutions in a wetted wall column." Environmental Progress **16**(3): 200-207.

Sun, Y., K. George, et al. (2003). The Effect of Cl<sup>-</sup> and Acetic Acid on Localized CO<sub>2</sub> Corrosion in Wet Gas Flow, NACE International.

Supap, T., R. Idem, et al. (2011). "Mechanism of formation of heat stable salts (HSSs) and their roles in further degradation of monoethanolamine during CO<sub>2</sub> capture from flue gas streams." Energy Procedia **4**(0): 591-598.

Supap, T., R. Idem, et al. (2009). "Kinetics of sulfur dioxide- and oxygen-induced degradation of aqueous monoethanolamine solution during CO<sub>2</sub> absorption from power plant flue gas streams." International Journal of Greenhouse Gas Control **3**(2): 133-142.

Svendsen, H. (2013). DETA Pilot Plant Campaign. E. Hayfron-Benjamin. NTNU , Trondheim.

Svendsen, H. F. (2012). TKP 4535 Gas Purification and Absorption. Department of Chemical Engineering. N. U. o. S. a. Technology. Trondheim - Norway, Faculty of Natural Sciences.

Svendsen, H. F., E. T. Hessen, et al. (2011). "Carbon dioxide capture by absorption, challenges and possibilities." Chemical Engineering Journal **171**(3): 718-724.

Tanthapanichakoon, W. and A. Veawab (2003). Heat Stable Salts and Corrosivity in Amine Treating Units. Greenhouse Gas Control Technologies - 6th International Conference. J. Gale and Y. Kaya. Oxford, Pergamon: 1591-1594.

Tanthapanichakoon, W., A. Veawab, et al. (2006). "Electrochemical Investigation on the Effect of Heat-stable Salts on Corrosion in CO<sub>2</sub> Capture Plants Using Aqueous Solution of MEA." Industrial & Engineering Chemistry Research **45**(8): 2586-2593.

Tavera-Valero, N. and H. Svendsen (2011). Effect of MEA Degradation Products on Corrosion of Stainless Steel in CO<sub>2</sub> Capture Units, Department of Chemical Engineering, Norwegian University of Science and Technology, N-7491 Trondheim, Norway.

Thu Tran, Bruce Brown, et al. (2013). Investigation of the Mechanism for Acetic Acid Corrosion of Mild Steel. Corrosion 2013. Orlando, Florida, USA, NACE International

Tontiwachwuthikul, P., A. Meisen, et al. (1992). "CO<sub>2</sub> absorption by NaOH, monoethanolamine and 2-amino-2-methyl-1-propanol solutions in a packed column." Chemical Engineering Science **47**(2): 381-390.

uobabylon (2013). "Pourbaix Diagrams." from [http://www.uobabylon.edu.iq/eprints/publication\\_12\\_18276\\_228.pdf](http://www.uobabylon.edu.iq/eprints/publication_12_18276_228.pdf).

Veawab, A. and A. Aroonwilas (2002). "Identification of oxidizing agents in aqueous amine-CO<sub>2</sub> systems using a mechanistic corrosion model." Corrosion Science **44**(5): 967-987.

Veawab, A., P. Tontiwachwuthikul, et al. (1999). "Corrosion Behavior of Carbon Steel in the CO<sub>2</sub> Absorption Process Using Aqueous Amine Solutions." Industrial & Engineering Chemistry Research **38**(10): 3917-3924.

Veldman, R. R. (2000). Alkanolamine Solution Corrosion Mechanisms and Inhibition From Heat Stable Salts and CO<sub>2</sub>. Corrosion2000, NACE International.

Verma, N. and A. Verma (2009). "Amine system problems arising from heat stable salts and solutions to improve system performance." Fuel Processing Technology **90**(4): 483-489.

Vevelstad, S. J., I. Eide-Haugmo, et al. (2011). "Degradation of MEA; a theoretical study." Energy Procedia **4**(0): 1608-1615.

Wegrelius, L., F. Falkenberg, et al. (1999). "Passivation of Stainless Steels in Hydrochloric Acid." Journal of The Electrochemical Society **146**(4): 1397-1406.

Wiersma, B. J. and J. I. Mickalonis (2008). Electrochemical Studies on the Corrosion of Carbon Steel in Oxalic acid cleaning solutions. NACE International Corrosion 2008.

Wolf, R. E. (2005). "What is ICP-MS? ... and more importantly, what can it do?". 2013, from <http://crustal.usgs.gov/laboratories/icpms/intro.html>.

Wonder, D. K., Balke R.J., et al. (1959). An approach to Monoethanolamine Solution Control: Chemical Analysis and its Interpretation. Proceedings of the Laurance Reid Gas Conditioning Conference.

Yamashita, M., H. Miyuki, et al. (1994). "The long term growth of the protective rust layer formed on weathering steel by atmospheric corrosion during a quarter of a century." Corrosion Science **36**(2): 283-299.

Z.F. Yin, X.Z. Wang, et al. (2010). "Characterization of Corrosion Product Layers from CO<sub>2</sub> Corrosion of 13Cr Stainless Steel in Simulated Oilfield Solution." Journal of Materials Engineering and Performance **20**: 1330-1335.

Zhang, X., F. Wang, et al. (2001). "Study of the inhibition mechanism of imidazoline amide on CO<sub>2</sub> corrosion of Armco iron." Corrosion Science **43**(8): 1417-1431.

# Appendices

## Appendix AI – Corrosion Tables and Results

Table AI- 1 (Swagelok 1.0)

Project  
Number # 34037300

Sample ID Cataloging Corrosion  
Experiment @135°C  
Start : Thursday 7  
February 2013

Legend  
**NO** - No Acid  
**FA** - Formic Acid  
**AA** - Acetic Acid  
Diethylenetriamine(DETA)  
**OA**- Oxalic Acid

End Week #	ID	Metal specimen				Empty cylinder(+caps)	Cylinder + Solution+ Metal		weight loss	weight loss procedure			weight loss	LOWEST WEIGHT LOSS corrosion rate(mm/yr)
		Mass/g	Dimension(mm)				Before	After		1	2	3		
1 Start : 08.55  12/02/13 - 19/02/13  stop: 09.45	NO1	8.054	87.87	5.91	1.85	170.30	189.852	188.113	1.739	8.050	8.050	8.047	0.007	0.035095896
	NO2	8.144	87.86	5.92	1.87	170.62	190.276	188.214	2.062	8.140	8.139	8.139	0.005	0.024971314
	FA3	8.174	87.93	5.92	1.89	170.43	190.058	185.681	4.377	8.170	8.170	8.169	0.005	0.024883092
	FA4	8.144	87.94	5.89	1.87	170.21	189.912	187.867	2.045	8.143	8.142	8.141	0.003	0.015026638
	OA5	8.136	87.93	5.94	1.95	170.05	189.764	188.530	1.234	8.134	8.133	8.133	0.003	0.014772217
	OA6	8.059	87.88	5.86	1.86	170.27	189.869	189.151	0.718	8.058	8.057	8.057	0.002	0.010077797
	AA7	8.128	87.88	5.89	1.84	170.41	190.126	189.510	0.616	8.126	8.125	8.124	0.004	0.020131892
	AA8	8.159	87.88	5.88	1.88	170.48	190.003	188.550	1.453	8.157	8.157	8.154	0.005	0.025060825
2 start: 09.00  12/02/13 - 27/02/13  stop: 06.50	NO9	8.142	87.93	5.90	1.89	170.66	188.620	184.410	4.210	8.140	8.141	8.140	0.002	0.004708271
	NO10	8.153	87.87	5.90	1.94	171.14	190.860	188.294	2.566	8.149	8.148	8.148	0.005	0.011700015
	FA11	8.164	97.89	5.91	1.91	170.59	190.394	185.254	5.140	8.162	8.161	8.161	0.003	0.006285886
	FA12	8.149	87.83	5.91	1.93	171.01	190.809	185.634	5.175	8.145	8.146	8.145	0.004	0.009365059
	OA13	8.121	87.86	5.85	1.88	171.13	190.826	185.425	5.401	8.119	8.119	8.118	0.003	0.007123925
	OA14	8.064	87.96	5.86	1.87	171.33	190.918	190.382	0.536	8.043	8.043	8.042	0.022	0.052182888
	AA15	8.155	87.99	5.91	1.91	169.84	189.646	184.286	5.360	8.153	8.153	8.152	0.003	0.007029258
	AA16	8.153	87.89	5.91	1.85	171.17	190.898	190.549	0.349	8.109	8.109	8.108	0.045	0.106425151

<b>3</b> start: 10.15  12/02/13 - 6/03/13  stop: 07.05	NO17	8.121	87.86	5.92	1.87	170.78	190.386	184.822	5.564	8.120	8.120	8.118	0.003	0.004819805	
	NO18	8.163	87.91	5.91	1.91	170.84	189.859	184.552	5.307	8.160	8.160	8.159	0.004	0.006396212	
	FA19	8.145	87.85	5.92	1.89	171.09	190.465	189.839	0.626	8.119	8.119	8.118	0.027	0.043266371	
	FA20	8.101	87.88	5.91	1.87	170.89	190.271	184.715	5.556	8.100	8.100	8.099	0.002	0.003216586	
	OA21	8.157	87.87	5.89	1.86	170.91	190.615	185.212	5.403	8.157	8.156	8.155	0.002	0.003229691	
	OA22	8.134	87.88	5.94	1.88	170.88	190.489	187.525	2.964	8.131	8.131	8.130	0.004	0.00639969	
	AA23	8.146	87.84	5.94	1.91	169.80	189.207	183.762	5.445	8.145	8.145	8.145	0.001	0.001594242	
	AA24	8.135	87.84	5.90	1.91	170.44	190.048	184.734	5.314	8.134	8.134	8.134	0.001	0.001602453	
	<b>4</b> start: 10.23  12/02/2013 - 12/03/13  stop: 07.35	NO25	8.163	87.84	5.91	1.89	170.05	189.818	184.362	5.456	8.161	8.161	8.161	0.002	0.00251706
NO26		8.127	87.92	5.92	1.87	170.49	190.133	184.670	5.463	8.125	8.126	8.125	0.002	0.00251821	
FA27		8.163	87.93	5.91	1.95	170.62	189.756	182.414	7.342	8.160	8.161	8.160	0.003	0.003741209	
FA28		8.135	87.90	5.94	1.83	170.48	190.216	184.560	5.656	8.134	8.134	8.134	0.001	0.001262982	
OA29		8.151	87.86	5.95	1.88	170.32	189.908	184.225	5.683	8.149	8.149	8.149	0.002	0.002506919	
OA30		8.118	87.92	5.89	1.87	169.94	189.483	184.358	5.125	8.116	8.117	8.116	0.002	0.002527998	
AA31		8.147	87.83	5.87	1.89	170.08	190.381	189.206	1.175	8.142	8.142	8.142	0.005	0.006326023	
AA32		8.131	87.90	5.87	1.89	170.56	190.502	188.724	1.778	8.096	8.098	8.096	0.035	0.044245088	
<b>5</b> start: 11.15  12/02/2013 - 15/03/13  stop: 14:00	NO33	8.145	87.86	5.97	1.91	169.63	189.263	183.747	5.516	8.145	8.145	8.144	8.143	0.001	0.001115914
	NO34	8.112	87.85	5.87	1.83	170.66	190.537	184.967	5.570	8.110	8.109	8.109	8.109	0.003	0.003428543
	FA35	8.130	87.93	5.90	1.91	169.96	189.622	184.322	5.300	8.128	8.128	8.127	8.127	0.003	0.003375089
	FA36	8.161	87.86	5.91	1.88	170.62	190.357	184.610	5.747	8.160	8.159	8.159	8.159	0.002	0.002258174
	OA37	8.153	87.87	5.94	1.90	170.67	190.203	184.977	5.226	8.151	8.150	8.149	8.149	0.004	0.004486297
	OA38	8.049	87.85	5.92	1.92	170.18	189.874	184.102	5.772	8.047	8.047	8.046	8.046	0.003	0.003365115
	AA39	8.122	87.88	5.88	1.90	171.05	190.668	185.148	5.520	8.120	8.120	8.120	8.119	0.002	0.002260273
	AA40	8.055	87.91	5.92	1.90	169.85	189.786	189.218	0.568	8.019	8.019	8.019	8.018	0.036	0.040461142

Table A1- 2 (Swagelok 2.0)

Project Number  
# 34037300

Sample ID Cataloging Corrosion  
Experiment @135°C

Legend  
NO - No  
Acid

FA - Formic Acid

AA - Acetic Acid  
Diethylenetriamine(DETA )

Start : Friday 10 May 2013

OA- Oxalic Acid

End Week #- wt% composition	ID	Metal ID	Metal specime n Mass/g	Cylinder + Solution+ Metal		weight loss	weight loss procedure			weight loss	Corrosion rates(mm/yr)
				Before	After		1	2	3		
1-1wt%  Start : 10:30  10/05/13 - 20/05/13  stop: 09:45	NO1	1	1.637	185.370	177.216	8.154	1.637	1.637	1.635	0.002	0.0183
	NO2	2	1.657			0.000					0.0000
	FA3	3	1.642	185.700	180.275	5.425	1.643	1.641	1.641	0.001	0.0091
	FA4	4	1.649			0.000	1.650	1.648	1.647	0.002	0.0183
	OA5	5	1.645	185.762	180.300	5.462	1.646	1.644	1.643	0.002	0.0183
	OA6	6	1.660			0.000	1.661	1.660	1.660	0.000	0.0000
	AA7	7	1.655	185.820	180.253	5.567	1.655	1.654	1.652	0.003	0.0274
	AA8	8	1.651			0.000	1.652	1.650	1.649	0.002	0.0183
1- 2wt%  start: 10:30  10/05/13 - 20/05/13	NO9	17	1.648	187.155	185.625	1.530	1.650	1.648	1.648	0.000	0.0000
	NO10	18	1.656			0.000	1.656	1.655	1.655	0.001	0.0091
	FA11	19	1.654	186.800	185.076	1.724	1.656	1.655	1.655	-0.001	-0.0091
	FA12	20	1.662			0.000	1.661	1.661	1.661	0.001	0.0091
	OA13	2	1.654	186.697	180.587	6.110					0.0000

stop: 09:45	OA14	3	1.641			0.000	1.639	1.639	1.639		0.002	0.0183
	AA15	4	1.635	186.542	184.491	2.051						0.0000
	AA16	5	1.645			0.000	1.645	1.644	1.644		0.001	0.0091
start: 10:30  10/05/13 - 27/05/13	NO17	9	1.649	185.766	181.454	4.312	1.648	1.648			0.001	0.0054
	NO18	10	1.655			0.000	1.655	1.654			0.001	0.0054
	FA19	11	1.632	185.874	181.910	3.964	1.633	1.632			0.000	0.0000
	FA20	12	1.652			0.000	1.653	1.653			-0.001	-0.0054
	OA21	13	1.659	185.874	180.108	5.766	1.658	1.658			0.001	0.0054
	OA22	14	1.732			0.000	1.731	1.730			0.002	0.0108
	AA23	15	1.654	185.288	183.865	1.423	1.653	1.652			0.002	0.0108
	AA24	16	1.652			0.000	1.650	1.650			0.002	0.0108
start: 10:30  10/05/13 - 27/05/13	NO25	8	1.652	186.621	180.483	6.138	1.650	1.650			0.002	0.0108
	NO26	9	1.655			0.000	1.655	1.652			0.003	0.0162
	FA27	10	1.654	186.160	179.766	6.394	1.653	1.653			0.001	0.0054
	FA28	11	1.660			0.000	1.658	1.656			0.004	0.0216
	OA29	12	1.645	187.084	186.072	1.012	1.645	1.644			0.001	0.0054
	OA30	13	1.657			0.000	1.657	1.655			0.002	0.0108
	AA31	14	1.655	186.921	185.611	1.310	1.656	1.653			0.002	0.0108
	AA32	20	1.661			0.000	1.661	1.660			0.001	0.0054

## Appendix AII – Solution Preparations and Post-experiment Amine/CO<sub>2</sub> analysis

### Swagelok ® 1.0

Table AII-1

Preparation of DETA(25.56wt%/ 2.5M) samples 4/02/2013 Benjamin					
Diethylenetriamine(DETA)					
CAS#	111-40-0				
Supplier	Sigma-Aldrich				
Molecular wt	103.17	g/mol			
Product #	D93856	batch #			
Purity	>99,0%				
Molecular wt CO <sub>2</sub>	44.01	g/mol			
DETA(2.5M)					
Total Solution	996.83	g			
DETA(2.5M)	257.925	g	Actual weighted	257.95	g
DI water added	738.88	g			

Table AII-2

<b>CO<sub>2</sub> Loadings</b>							
$\alpha$	DETA solution(g)	DETA ((2.5M)/g)	Mol DETA	CO <sub>2</sub> needed(g)	Actual CO <sub>2</sub> loaded(g)		
1.5	497.81	127.239	1.2332	81.4162	84.31		
<b>CO<sub>2</sub> Analysis</b>	<b>after back dilution to 1.2</b>						
Blank HCL	9.916	g					
Blank NaOH	9.31	ml					
Sample	loading( $\alpha$ )	Sample weight(g)	HCl(g)	NaOH(ml)	CO <sub>2</sub> mole/kg	Average CO <sub>2</sub> (mol/kg)	% dev
A	1.2	0.532	45.01	16.234	2.6475	2.6566	-1.4657
B		0.536	45.184	15.774	2.6869		
		0.538	45.287	16.322	2.6355		
<b>Amine Analysis</b>							
Sample	25/10/2012 Benjamin loading( $\alpha$ )	Sample weight(g)	Amine (mol/kg)	Average Amine(mole/kg)		% dev	
A	0.4	0.296	6.5568	6.561		0.1971	
B		0.362	6.5439				
		0.275	6.5823				
<b>Titration Results</b>							
Average CO <sub>2</sub> (mol/kg)	Average Amine(mol/kg)	Calc. $\alpha$ Loadings					
2.6566	2.187	1.2147					

Table AII-3

Degradation Products loadings(1 wt%)						
Acid Type	Amount DETA(loaded)/g	Mole DETA	Mass CO <sub>2</sub> in soln(g)	Amt DETA unloaded(g)	Based on unloaded wt basis	
					1 wt% acid needed(g)	weighted acid in DETA(g)
only DETA	119.56	0.2545	13.6065	105.9534		
Oxalic Acid	125.49	0.2671	13.6065	111.8834	1.1188	1.16
Formic Acid	129.12	0.2748	13.6065	115.5134	1.1551	1.18
Acetic Acid	124.88	0.2658	13.6065	111.2734	1.1127	1.16

## Swagelok® 2.0

Table AII-4

<b>CO<sub>2</sub> Loadings</b>							
$\alpha$	DETA solution(g)	DETA ((2.5M)/g)	Mol DETA	CO <sub>2</sub> needed(g)	Actual CO <sub>2</sub> loaded(g)		
1.5	497.81	127.2385	1.2332	81.4156	84.31		
<b>CO<sub>2</sub> Analysis</b>							
Blank HCL	10.453	g					
Blank NaOH	6.206	ml					
Sample	loading( $\alpha$ )	Sample weight(g)	HCl(g)	NaOH(ml)	CO <sub>2</sub> mole/kg	Average CO <sub>2</sub> (mol/kg)	% dev
A	1.5	0.729	57.284	8.6	3.0478	3.0872	-1.4730
B		0.467	48.439	15.274	3.0961		
		0.506	50.762	15.026	3.1115		
		0.581	53.084	12.892	3.0933		
<b>Amine Analysis</b>							
Sample	18/04/2013 Benjamin loading( $\alpha$ )	Sample weight(g)	Amine (mol/kg)	Average Amine(mole/kg)	% deviation		
A	1.5	0.364	6.268	6.2478	0.239		
B		0.36	6.253				
		0.301	6.2469				
<b>Titration Results</b>		0.304	6.2233				

Average CO <sub>2</sub> (mol/kg)	Average Amine(mol/kg)	Calc. α Loadings
3.087221395	2.0826	1.48238807

Table AII-5

Degradation Products loadings (2 wt%)						
Acid Type	Amount DETA(loaded)/g	Mole DETA	Mass CO <sub>2</sub> in soln(g)	Amt DETA unloaded(g)	Based on unloaded wt basis	
					2 wt% acid needed(g)	weighted acid in DETA(g)
only DETA	586.68	1.2499	81.5495	505.1304		
Oxalic Acid	464.24	0.9891	64.5301	399.7098	7.9941	7.86
Formic Acid	512.07	1.0910	71.1786	440.8913	8.81782	8.93
Acetic Acid	528.64	1.1263	73.4818	455.1581	9.1031	9.25

Table AII- 6 Post experiment amine and CO<sub>2</sub> analysis

Sample ID Cataloging  
 Corrosion Experiment @135°C Legend  
 Start : Friday 22 NO - No  
 June 2013 Acid OA- Oxalic Acid

FA -  
 Formic  
 Acid AA - Acetic Acid  
 Diethylenetriamine(DETA)

SINTEF REGISTRERING			End Week #	Test Specimen ID	Post -expt Amine (mol/kg)		DETA				Post-expt CO2(mole/kg)	average	Post- expt alpha	
Rekv. no	Journal no	ID			1	2	3	4	amine(mol/kg)	sample wt				HCl(ml)
20130042	P13412	Week 1 NO1	1	NO1	7.2925	7.2279		2.5171						
20130042	P13413	Week NO2		NO2	7.8726	7.8117			0.3320	47.9780	40.9300	0.9154	0.8662	0.3637
20130042	P13414	Week FA3		FA3					0.3920	48.2210	40.8460	0.8170		
20130042	P13415	Week FA4		FA4	6.3643									
20130042	P13416	Week OA5		OA5	6.3077	6.2799								
20130042	P13417	Week OA6		OA6	5.4633	5.4294								
20130042	P13418	Week AA7		AA7	4.7124	4.7432								
20130042	P13419	Week AA8		AA8	6.1976	6.2500								
20130042	P13420	Week 2 NO9	2	NO9					0.5670	48.2500	40.3240	0.6134	0.6314	0.2328
20130042	P13421	Week NO10		NO10	7.8663	7.9449		2.6352	0.5140	48.2590	40.6140	0.6493		
20130042	P13422	Week FA11		FA11	15.6410	15.7621	15.7532	15.7796						
20130042	P13423	Week FA12		FA12	15.5024									
20130042	P13424	Week OA13		OA13	18.5268	18.5642	18.4980	18.4208						
20130042	P13425	Week OA14		OA14	4.8191	4.8512								
20130042	P13426	Week AA15		AA15	18.2777	18.1051	18.1955	18.2020						
20130042	P13427	Week AA16		AA16	3.9587	3.9157								
20130043	P13428	Week 3 NO17	3	NO17					0.4330	48.1970	42.3160	0.5671	0.5954	0.2002
20130043	P13429	Week NO18		NO18	10.1928	7.6533		2.9744	0.3280	48.1870	43.1260	0.6236		

20130043	P13430	Week FA19		FA19	4.5537	4.4895								
20130043	P13431	Week FA20		FA20										
20130043	P13432	Week OA21		OA21										
20130043	P13433	Week OA22		OA22	6.8647									
20130043	P13434	Week AA23		AA23	19.0179	18.8942	18.9282							
20130043	P13435	Week AA24		AA24	-	-	-	-	-	-	-	-	-	-
<b>20130043</b>	<b>P13436</b>	<b>Week 4 NO25</b>	<b>4</b>	<b>NO25</b>	<b>18.6990</b>	<b>18.7170</b>	<b>17.5956</b>		<b>6.1124</b>	<b>0.3550</b>	<b>48.3140</b>	<b>44.1700</b>	<b>0.4470</b>	<b>0.3806 0.0623</b>
<b>20130043</b>	<b>P13437</b>	<b>Week NO26</b>		<b>NO26</b>						<b>0.4030</b>	<b>48.2780</b>	<b>44.7760</b>	<b>0.3141</b>	
20130043	P13438	Week FA27		FA27										
20130043	P13439	Week FA28		FA28										
20130043	P13440	Week OA29		OA29	19.3992	19.1519	19.2100							
20130043	P13441	Week OA30		OA30										
20130043	P13442	Week AA31		AA31	4.8556	4.8258								
20130043	P13443	Week AA32		AA32	7.6992	11.9885								
<b>20130044</b>	<b>P13444</b>	<b>Week 5 NO33</b>	<b>5</b>	<b>NO33</b>	<b>18.9941</b>	<b>19.1753</b>			<b>6.3616</b>	<b>0.4480</b>	<b>48.2470</b>	<b>43.3840</b>	<b>0.4345</b>	<b>0.3951 0.0621</b>
<b>20130044</b>	<b>P13445</b>	<b>Week NO34</b>		<b>NO34</b>						<b>0.4080</b>	<b>48.3070</b>	<b>44.4340</b>	<b>0.3558</b>	
20130044	P13446	Week FA35		FA35	17.1615	17.1725								
20130044	P13447	Week FA36		FA36										
20130044	P13448	Week OA37		OA37	19.6399	19.3310								
20130044	P13449	Week OA38		OA38	19.6399	19.3310								
20130044	P13450	Week AA39		AA39	21.7845									
20130044	P13451	Week AA40		AA40	3.8557	3.8374								

Blank HCl    **10.448** g  
Blank  
NaOH        **9.478** ml

## Appendix AIII Electrochemical Experiment Data Oxalate system

File name	C:\Users\Benjamin\Documents\THESIS\DataNEW\135OA_4wt2%
Test type	Cyclic sweep
Instrument serial number	780
Physical channel	1
Sequence number	2
ZRA Number	n/a
Time and Date	5/6/2013 10:30
Data points	338
Area (cm <sup>2</sup> )	34
Rest Potential (mV)	-314.4904
Metal	Stainless Steel 316L
Metal factor	1280
LPR (Ohm.cm <sup>2</sup> )	17.463017
Ba (mV)	113.72788
Bc (mV)	99.95951
Icorr (mA/cm <sup>2</sup> )	1.32454
Corrosion Rate (mm/year)	16.954112
Corrosion rate (mils/yr)	667.48471
Intercept (mA/cm <sup>2</sup> )	0.7779734
Intercept corrosion rate (mm/year)	9.95806
Intercept corrosion rate (mils/yr)	392.0496
IR Compensation value (Ohm.cm <sup>2</sup> )	N/A
Start Potential	-180 mV
Reverse Potential	100 mV
Sweep Rate	50 mV/min
Cycles	0.5
Readings Per Test	Automatic
Gradual Sweep From Cell to Start Potential	No
Cell Settle Time	20 seconds

Oversample	On
Count Resistor At Start	Auto
Count Resistor During Test	Auto
Offset To Rest Potential	Yes
Current Limit	Off
Limit at	N/A
After Limit Reached	N/A

Current (mA/cm <sup>2</sup> )	Potential (mV)	Time (Sec)
-25.989005	-492.64588	0
-25.893193	-491.74959	0.9670003
-25.769732	-490.9547	1.9960004
-25.625705	-490.08915	2.963
-25.506913	-489.2223	3.9930004
-25.382495	-488.39639	4.96
-25.261395	-487.58892	5.9270003
-25.136762	-486.6766	6.957
-25.021868	-485.89587	7.9240002
-24.901685	-485.07122	8.9540005
-24.792993	-484.21722	9.921
-24.701993	-483.40584	10.95
-24.56717	-482.56083	11.918
-24.438246	-481.7705	12.947
-24.313546	-480.87794	13.914001
-24.198032	-480.08384	14.881
-24.071763	-479.18727	15.911001
-23.949349	-478.41646	16.878
-23.820492	-477.55343	17.908
-23.702175	-476.69836	18.875
-23.584792	-475.93407	19.904
-23.461635	-475.03433	20.872

-23.354728	-474.19053	21.901
-23.228331	-473.38535	22.868
-23.104218	-472.51942	23.835
-22.972735	-471.66482	24.865
-22.856598	-470.87957	25.832
-22.750551	-470.00182	26.862
-22.649273	-469.15979	27.829
-22.536043	-468.40067	28.858
-22.39551	-467.49134	29.826
-22.286497	-466.68578	30.855
-22.155155	-465.84878	31.822
-22.03393	-465.04942	32.79
-21.912643	-464.1746	33.819
-21.795819	-463.38735	34.786
-21.664682	-462.50825	35.816
-21.543908	-461.71368	36.783001
-21.412303	-460.92959	37.813
-21.29	-460.03247	38.780001
-21.177325	-459.19607	39.809
-21.050809	-458.30998	40.776
-20.934644	-457.54886	41.744
-20.809837	-456.68513	42.773
-20.68589	-455.87785	43.740001
-20.551188	-455.03405	44.77
-20.431323	-454.19477	45.737
-20.32362	-453.42144	46.767
-20.202927	-452.49376	47.734
-20.081908	-451.72616	48.763
-19.961658	-450.85022	49.73
-19.844077	-450.06842	50.698
-19.722474	-449.24428	51.727

-19.596414	-448.41199	52.694
-19.515595	-447.55473	53.724
-19.393231	-446.72174	54.691
-19.263539	-445.93947	55.721
-19.126918	-445.04574	56.688
-18.999884	-444.23394	57.717
-18.880161	-443.38917	58.685
-18.764446	-442.58854	59.652001
-18.646836	-441.72123	60.681
-18.525871	-440.93449	61.648
-18.395254	-440.07429	62.678
-18.267611	-439.23371	63.645
-18.146862	-438.3792	64.675
-18.035561	-437.59292	65.642
-17.903529	-436.78401	66.671
-17.780411	-435.93234	67.639
-17.689523	-435.10378	68.606
-17.56558	-434.28895	69.635
-17.443492	-433.40854	70.602
-17.32601	-432.62641	71.632
-17.208553	-431.78364	72.599
-17.085633	-430.96397	73.629001
-16.964002	-430.11253	74.596
-16.826125	-429.27199	75.625
-16.695497	-428.41213	76.593
-16.575148	-427.62203	77.56
-16.477562	-426.80423	78.589001
-16.350274	-425.94878	79.557
-16.227602	-425.14719	80.586
-16.10328	-424.32947	81.553
-15.988641	-423.4533	82.583

-15.867378	-422.65561	83.55
-15.754799	-421.83175	84.58
-15.615898	-421.00938	85.547
-15.50578	-420.1497	86.514
-15.380534	-419.31429	87.543
-15.258928	-418.44394	88.511
-15.130443	-417.6824	89.54
-15.014175	-416.83171	90.507
-14.907339	-416.03174	91.537
-14.770187	-415.10075	92.504
-14.659145	-414.34428	93.534
-14.540519	-413.56281	94.501
-14.431616	-412.71659	95.468
-14.301502	-411.84964	96.497
-14.195869	-411.02745	97.465
-14.080292	-410.23354	98.494
-13.959057	-409.34945	99.461
-13.83447	-408.56211	100.491
-13.708399	-407.64989	101.458
-13.600271	-406.90437	102.488
-13.484665	-405.99224	103.455
-13.367898	-405.20145	104.422
-13.236627	-404.34032	105.452
-13.123418	-403.58353	106.419
-13.006056	-402.75632	107.448
-12.891205	-401.88266	108.415
-12.773227	-401.03738	109.445
-12.634712	-400.2484	110.412
-12.516023	-399.40651	111.442
-12.394452	-398.60067	112.409
-12.271812	-397.74109	113.438

-12.142771	-396.92724	114.406
-12.023933	-396.08046	115.373
-11.911747	-395.21961	116.402
-11.83625	-394.43101	117.369
-11.692347	-393.62075	118.399
-11.571951	-392.76391	119.366
-11.463483	-391.91308	120.396
-11.3254	-391.1201	121.363
-11.198635	-390.29935	122.392
-11.07693	-389.40264	123.36
-10.981649	-388.71842	124.327
-10.860488	-387.77476	125.356
-10.740663	-386.9795	126.324
-10.5999	-386.16565	127.353
-10.476902	-385.33079	128.32
-10.358379	-384.47372	129.35
-10.236274	-383.63999	130.317
-10.111803	-382.83452	131.347
-9.992296	-381.99715	132.314
-9.8779154	-381.20692	133.343
-9.7493487	-380.26666	134.31
-9.6383173	-379.5577	135.278
-9.5323768	-378.671	136.307
-9.3998377	-377.87202	137.274
-9.2707046	-377.04107	138.304
-9.1406758	-376.20077	139.271
-9.0228717	-375.37146	140.301
-8.8999447	-374.51094	141.268
-8.7835496	-373.70258	142.297
-8.6546892	-372.92101	143.264
-8.5325127	-372.0774	144.232

-8.4232761	-371.19997	145.261
-8.30601	-370.43485	146.228
-8.1833028	-369.60074	147.258
-8.0669819	-368.7425	148.225
-7.9540457	-367.9872	149.255
-7.8348574	-367.11154	150.222
-7.7155946	-366.25904	151.189
-7.5944874	-365.45641	152.219
-7.4795793	-364.65584	153.186
-7.3568576	-363.7418	154.215
-7.2388587	-362.92893	155.182
-7.1279512	-362.14876	156.212
-7.0074741	-361.27604	157.179
-6.8935892	-360.55399	158.146
-6.7745141	-359.66478	159.176
-6.6484009	-358.87166	160.143
-6.5234062	-357.99922	161.173
-6.404048	-357.19031	162.14
-6.2917066	-356.40613	163.169
-6.1740158	-355.50453	164.136
-6.0999169	-354.75677	165.166
-5.9548488	-353.84996	166.133
-5.837689	-353.05921	167.1
-5.709271	-352.21639	168.13
-5.5892046	-351.46971	169.097
-5.4711633	-350.59074	170.127
-5.357643	-349.76045	171.094
-5.2276566	-348.88698	172.123
-5.0986863	-348.14342	173.091
-4.982493	-347.26748	174.12
-4.8723501	-346.5052	175.087

-4.7491931	-345.64906	176.117
-4.621993	-344.83227	177.084
-4.5145265	-344.01735	178.114
-4.3880274	-343.24147	179.081
-4.2700746	-342.42841	180.048
-4.1586183	-341.54353	181.077
-4.0439508	-340.73397	182.045
-3.9207903	-339.88621	183.074
-3.8028977	-339.03985	184.041
-3.0542262	-338.29894	185.149
-2.9420759	-337.40554	186.116
-2.8450502	-336.51419	187.146
-2.7350417	-335.70178	188.113
-2.6470128	-334.92091	189.08
-2.5431499	-334.12826	190.109
-2.4383528	-333.32219	191.077
-2.3452523	-332.47126	192.106
-2.2492475	-331.60334	193.073
-2.1539592	-330.86811	194.103
-2.052959	-330.01565	195.07
-1.9604356	-329.18638	196.1
-1.8618495	-328.33839	197.067
-1.7643587	-327.54993	198.034
-1.6686732	-326.74512	199.064
-1.5752834	-325.93663	200.031
-1.4815817	-325.11002	201.06
-1.3793439	-324.30902	202.027
-1.2813384	-323.54007	203.057
-1.1836333	-322.62501	204.024
-1.0897072	-321.88411	205.054
-0.9897003	-321.0349	206.021

-0.8966298	-320.2449	206.988
-0.790213	-319.41629	208.018
-0.6952966	-318.6601	208.985
-0.588108	-317.80811	210.014
-0.4815404	-316.98108	210.981
-0.3863844	-316.23747	212.011
-0.3147644	-315.34737	213.056
-0.1945594	-314.4904	214.086
-0.0869203	-313.66015	215.053
0.0104213	-312.83629	216.098
0.0970054	-311.98928	217.128
0.1982879	-311.12662	218.095
0.300216	-310.29381	219.202
0.3910028	-309.42151	220.169
0.4753856	-308.69229	221.199
0.5817234	-307.79991	222.166
0.6825695	-306.9937	223.196
0.7859777	-306.15601	224.163
0.8664637	-305.40457	225.13
0.9552126	-304.54349	226.16
1.0475932	-303.73952	227.127
1.1480665	-302.90951	228.156
1.2413619	-302.08821	229.124
1.3370213	-301.30212	230.153
1.4374031	-300.41212	231.12
1.5371197	-299.63842	232.15
1.6325343	-298.74809	233.117
1.7163084	-298.01245	234.084
1.8116413	-297.1686	235.114
1.9844471	-296.3827	236.159
2.0828465	-295.47896	237.188

2.1812391	-294.72319	238.156
2.2636388	-293.85112	239.185
2.3766086	-293.04426	240.152
2.4676291	-292.28891	241.182
2.5697474	-291.3929	242.149
2.6640235	-290.62251	243.116
2.765178	-289.7985	244.146
2.8683085	-288.98177	245.113
2.9701251	-288.11976	246.142
3.0627167	-287.28882	247.11
3.1593782	-286.50161	248.139
3.2661571	-285.58692	249.106
3.3597404	-284.83418	250.136
3.4656067	-283.98247	251.103
3.5452773	-283.14551	252.07
3.6518041	-282.31131	253.1
3.7608335	-281.51298	254.067
3.8639181	-280.6587	255.097
3.9664475	-279.86655	256.064
4.0653909	-279.01991	257.093
4.1579083	-278.13103	258.06
4.2506676	-277.41621	259.09
4.3562366	-276.47525	260.057
4.4570957	-275.71678	261.087
4.5570314	-274.85286	262.054
4.6525535	-274.03962	263.021
4.7499627	-273.22749	264.051
4.8488477	-272.3632	265.018
4.9507868	-271.54609	266.047
5.0529467	-270.78921	267.014
5.1491722	-269.8516	268.044

5.2318976	-269.02276	269.011
5.3379576	-268.21375	270.041
5.4393287	-267.35878	271.008
5.5405536	-266.55019	271.975
5.6394667	-265.73085	273.005
5.7329591	-264.91504	273.972
5.8409328	-264.04902	275.001
5.9427298	-263.26522	275.969
6.0369971	-262.37573	276.998
6.1388819	-261.61647	277.965
6.2302835	-260.69209	278.995
6.3400155	-259.88994	279.962
6.4335049	-259.07231	280.929
6.5343083	-258.21715	281.959
6.6422614	-257.39823	282.926
6.7429744	-256.53873	283.955
6.8490658	-255.71329	284.923
6.9461135	-254.93921	285.952
7.0504273	-254.00748	286.919
7.1487051	-253.23825	287.949
7.2468082	-252.3707	288.916
7.3265332	-251.58415	289.883
7.4164531	-250.7322	290.913
7.5260346	-249.90442	291.88
7.6276096	-249.05378	292.91
7.7333068	-248.20798	293.877
7.8355058	-247.49506	294.844
7.9439604	-246.58922	295.873
8.0468742	-245.77286	296.841
8.1321872	-244.96316	297.87
8.2106702	-244.04376	298.837

8.3208464	-243.24556	299.867
8.4280337	-242.46106	300.834
8.5186212	-241.61866	301.864
8.622234	-240.72801	302.831
8.7199756	-239.89995	303.86
8.8254933	-239.08596	304.827
8.9214829	-238.2662	305.795
9.024035	-237.39455	306.824
9.122709	-236.56617	307.791
9.222544	-235.69326	308.821
9.325956	-234.88956	309.788
9.411595	-234.10422	310.818
9.525085	-233.19964	311.785
9.620414	-232.42142	312.814
9.722572	-231.51866	313.781
9.819955	-230.74635	314.749
9.926885	-229.82645	315.778
10.02716	-229.07837	316.745
10.128084	-228.20984	317.775
10.222435	-227.42314	318.742
10.311966	-226.63631	319.772
10.415401	-225.70406	320.739
10.504992	-224.88462	321.768
10.61606	-224.11493	322.736
10.724278	-223.20677	323.703
10.832212	-222.39264	324.732
10.929822	-221.57856	325.699
11.028419	-220.70639	326.729
11.122267	-219.92943	327.696
11.219756	-219.04036	328.726
11.318328	-218.27258	329.693

11.413873	-217.36278	330.722
11.517471	-216.53869	331.69
11.6122	-215.78935	332.657
11.701652	-214.88458	333.686
11.794663	-214.08005	334.653
		335.355

## Appendix IV CORROSION GLOSSARY

**activation:** The changing of a passive surface of a metal to a chemically active state.

**active:** The negative direction of electrode potential. [Also used to describe corrosion and its associated potential range when an electrode potential is more negative than an adjacent depressed corrosion-rate (passive) range.]

**anode:** The electrode of an electrolytic cell at which oxidation is the principal reaction. (Electrons flow away from the anode in the external circuit. It is usually the electrode where corrosion occurs and metal ions enter solution.)

**anodic polarization:** The change of the electrode potential in the noble (positive) direction due to current flow.

**austenite:** A solid solution of one or more elements in face-centered cubic iron. Unless otherwise designated (such as nickel austenite), the solute is generally assumed to be carbon.

**austenitic:** The name given to the face-centered cubic (FCC) crystal structure of ferrous metals. Ordinary iron and steel has this structure at elevated temperatures; certain stainless steels (300 series) also have this structure at room temperature.

**auxiliary electrode:** The electrode in an electrochemical cell that is used to transfer current to or from a test electrode, usually made of non-corroding material.

**buffer:** A chemical substance which stabilizes pH values in solutions.

**calomel electrode:** An electrode widely used as a reference electrode of known potential in electrometric measurement of acidity and alkalinity, corrosion studies, voltammetry, and measurement of the potentials of other electrodes.

**cathode:** The electrode of an electrolytic cell at which reduction is the principal reaction. Electrons flow toward the cathode in the external circuit.

**cathodic corrosion:** Corrosion of a metal when it is a cathode. (This usually happens to metals because of a rise in pH at the cathode or as a result of the formation of hydrides.)

**cathodic polarization:** A change in the electrode potential in the active (negative) direction as a result of current flow.

**cathodic reaction:** Electrode reaction equivalent to a transfer of negative charge from the electronic to the ionic conductor. A cathodic reaction is a reduction process.

**chelate:** A molecular structure in which a heterocyclic ring can be formed by the unshared electrons of neighboring atoms or a coordination compound in which a heterocyclic ring is formed by a metal bound to two atoms of the associated ligand.

**chelating agent:** A chemical compound sometimes fed to water to tie up undesirable metal ions, keep them in solution, and eliminate or reduce their normal effects.

**chelation:** The process of forming complex chemical compounds in which certain metal ions are bound into stable ring structures, keeping the ions in solution and eliminating or reducing their normal (and often undesirable) effects.

**chemical potential:** In a thermodynamic system with several constituents, the rate of change of the Gibbs function of the system with respect to the change in the number of moles of a particular constituent.

**corrosion:** A chemical or electrochemical reaction between a material, usually a metal, and its environment that produces a deterioration of the material and its properties.

**corrosion potential:** The potential of a corroding surface in an electrolyte relative to that of a reference electrode measured under open-circuit conditions.

**corrosion product:** A substance formed as a result of corrosion.

**corrosion rate:** The amount of corrosion occurring per unit time (for example, mass change per unit area per unit time, penetration per unit time).

**corrosion resistance:** The ability of a metal to withstand corrosion in a given corrosion system.

**corrosivity:** The tendency of an environment to cause corrosion in a given corrosion system.

**crevice corrosion:** Localized corrosion of a metal surface at or immediately adjacent to an area that is shielded from full exposure to the environment because of close proximity between the metal and the surface of another material.

**current density:** The electric current to or from a unit area of an electrode surface.

**dolomite:** A specific form of limestone containing chemically equivalent concentrations of calcium and magnesium carbonates; the term is sometimes applied to limestone with compositions similar to that of true dolomite.

**downtime:** The amount of time a piece of equipment is not operational.

**electrochemical cell:** An electrochemical system consisting of an anode and a cathode in metallic contact and immersed in an electrolyte. (The anode and cathode may be different metals or dissimilar areas on the same metal surface.)

**electrochemical impedance spectroscopy (EIS):** The frequency-dependent, complex-valued proportionality factor,  $E/I$ , between the applied potential (or current) and the response current (or potential) in an electrochemical cell. This factor becomes the impedance when the perturbation and response are related linearly (the factor value is independent of the perturbation magnitude) and the response is caused only by the perturbation. The value may be related to the corrosion rate when the measurement is made at the corrosion potential.

**electrochemical potential (electrochemical tension):** The partial derivative of the total electrochemical free energy of the system with respect to the number of moles of the constituent in a solution when all other factors are constant. (It is analogous to the chemical potential of the constituent, except that it includes the electrical as well as the chemical contributions to the free energy.)

**electrode potential:** The potential of an electrode in an electrolyte as measured against a reference electrode. (The electrode potential does not include any resistance losses in potential in either the solution or the external circuit. It represents the reversible work to move a unit charge from the electrode surface through the solution to the reference electrode.)

**electrolyte:** A nonmetallic substance that carries an electric current, or a substance which, when dissolved in water, separates into ions which can carry an electric current.

**electrolytic cell:** An assembly, consisting of a vessel, electrodes, and an electrolyte, in which electrolysis can be carried out.

**electrolytic cleaning:** A process of removing soil, scale, or corrosion products from a metal surface by subjecting it as an electrode to an electric current in an electrolytic bath.

**equilibrium:** The state in which the action of multiple forces produces a steady balance.

**equilibrium (reversible) potential:** The potential of an electrode in an electrolytic solution when the forward rate of a given reaction is exactly equal to the reverse rate. (The equilibrium potential can be defined only with respect to a specific electrochemical reaction.)

**equilibrium reaction:** A chemical reaction which proceeds primarily in one direction until the concentrations of reactants and products reach an equilibrium.

**equivalent weight:** The weight in grams of an element, compound, or ion which would react with or replace 1 g of hydrogen; the molecular weight in grams divided by the valence.

**erosion:** The progressive loss of material from a solid surface as a result of mechanical interaction between that surface and a fluid, a multicomponent fluid, or solid particles carried with the fluid.

**erosion-corrosion:** A conjoint action involving corrosion and erosion in the presence of a moving corrosive fluid; it leads to the accelerated loss of material.

**ferrite:** A solid solution of one or more elements in body-centered cubic iron. Unless otherwise designated (for instance, as chromium ferrite), the solute is generally assumed to be carbon. On some equilibrium diagrams, there are two ferrite regions separated by an austenite area. The lower area is alpha ferrite; the upper, delta ferrite. If there is no designation, alpha ferrite is assumed.

**ferritic:** Pertaining to the body-centered cubic (BCC) crystal structure of many ferrous (iron-based) metals.

**fouling:** The accumulation of refuse in gas passages or on heat-absorbing surfaces, resulting in undesirable restriction to the flow of gas or heat.

**free corrosion potential:** Corrosion potential in the absence of net electric current flowing to or from the metal surface.

**gage pressure:** The pressure above atmospheric pressure.

**general corrosion:** A form of deterioration that is distributed more or less uniformly over a surface; see uniform corrosion.

**Gibbs free energy:** Thermodynamic function; also called free energy, free enthalpy, or Gibbs function.

**grain boundary:** A narrow zone in a metal corresponding to the transition from one crystallographic orientation to another, thus separating one grain from another, with the atoms in each grain arranged in an orderly pattern; the irregular junction of two adjacent grains.

**incubation period:** A period prior to the detection of corrosion during which the metal is in contact with a corrodent.

**inhibitor:** A chemical substance or combination of substances that, when present in the proper concentration and forms in the environment, prevents or reduces corrosion.

**intergranular corrosion:** Preferential corrosion at or adjacent to the grain boundaries of a metal or alloy.

**Luggin probe or Luggin-Haber capillary:** A device used in measuring the potential of an electrode with a significant current density imposed on its surface. (The probe minimizes the IR drop that would otherwise be included in the measurement without significantly disturbing the current distribution on the specimen.)

**noble:** The positive (increasingly oxidizing) direction of electrode potential.

**noble metal:** A metal with a standard electrode potential that is more noble (positive) than that of hydrogen.

**noble potential:** A potential more cathodic (positive) than the standard hydrogen potential.

**open-circuit potential:** The potential of an electrode measured with respect to a reference electrode or another electrode when no current flows to or from it.

**overvoltage:** The change in potential of an electrode from its equilibrium or steady-state value when current is applied.

**passivation:** The process in metal corrosion by which metals become passive.

**passivator:** A type of inhibitor which appreciably changes the potential of a metal to a more noble (positive) value.

**passive:** The state of a metal surface characterized by low corrosion rates in a potential region that is strongly oxidizing for the metal.

**passive-active cell:** A corrosion cell in which the anode is a metal in the active state and the cathode is the same metal in the passive state.

**passivity:** A condition in which a piece of metal, because of an impervious covering of oxide or other compound, has a potential that is much more positive than that of the metal in the active state.

**pickle:** A solution or process used to loosen or remove corrosion products such as scale or tarnish.

**pickling:** Removing surface oxides from metals by chemical or electrochemical reaction.

**pitting:** Corrosion of a metal surface, confined to a point or small area, that takes the form of cavities.

**pK:** The reciprocal of the logarithm of the ionization constant of a chemical compound.

**polarization:** The change from the open-circuit electrode potential as the result of the passage of current.

**polarization curve:** A plot of current density versus electrode potential for a specific electrode-electrolyte combination.

**polarization resistance:** The slope ( $dE/di$ ) at the corrosion potential of a potential ( $E$ ) versus current density ( $i$ ) curve. It is inversely proportional to the corrosion current density when the polarization resistance technique is applicable. The term is also used to describe the method of measuring corrosion rates using this slope.

**potentiodynamic (potentiokinetic):** A technique wherein the potential of an electrode with respect to a reference electrode is varied at a selected rate by application of a current through the electrolyte.

**potentiostat:** An instrument for automatically maintaining an electrode in an electrolyte at a constant potential or controlled potentials with respect to a suitable reference electrode.

**potentiostatic:** The technique for maintaining a constant electrode potential.

**Pourbaix diagram (potential-pH diagram):** A graphical representation showing regions of thermodynamic stability of species in metal–water electrolyte systems.

**reference electrode:** A nonpolarizable electrode with a known and highly reproducible potential.

**standard electrode potential:** The reversible potential for an electrode process when all products and reactions are at unit activity on a scale in which the potential for the standard hydrogen half cell is zero.

**Tafel slope:** The slope of the straight-line portion of a polarization curve, usually occurring at more than 50 mV from the open-circuit potential, when the curve is presented in a semilogarithmic plot in terms of volts per logarithmic cycle of current density (commonly referred to as volts per decade).

**thermocouple:** A device for measuring temperatures, consisting of lengths of two dissimilar metals or alloys that are electrically joined at one end and connected to a voltage-measuring instrument at the other end. When one junction is hotter than the other, a thermal electromotive force is produced that is roughly proportional to the difference in temperature between the hot and cold junctions.

**titration:** An analytical process in which a standard solution in a calibrated vessel is added to a measured volume of sample until an endpoint, such as a color change, is reached. From the volume of the sample and the volume of standard solution used, the concentration of a specific material may be calculated.

**transpassive region:** The region of an anodic polarization curve, noble to and above the passive potential range, in which there is a significant increase in current density (increased metal dissolution) as the potential becomes more positive (noble).

**transpassive state:** A state of anodically passivated metal characterized by a considerable increase in the corrosion current, in the absence of pitting, when the potential is increased.

**turbulent flow:** A type of flow characterized by crosscurrents and eddies. Turbulence may be caused by surface roughness or protrusions in pipes, bends and fittings, changes in channel size, or excessive flow rates; turbulence significantly increases pressure drops. Contrast laminar flow.

**uniform corrosion:** Corrosion that proceeds at about the same rate at all points on a metal surface.

**working electrode:** The test or specimen electrode in an electrochemical cell.